ZooKeys 1016: 1–48 (2021)
doi: 10.3897/zookeys.1016.59617
https://zookeys.pensoft.net

RESEARCH ARTICLE

A peer-reviewed open-access journal
ZooKeys
Launched to accelerate biodiversity research

Revision and description of six species of *Choeradoplana* (Platyhelminthes, Tricladida), with an emendation to the genus

Domingo Lago-Barcia[1,2], Marcos Santos Silva[1], Fernando Carbayo[1,2,3]

1 *Laboratório de Ecologia e Evolução, Escola de Artes, Ciências e Humanidades (EACH), Universidade de São Paulo (USP), Av. Arlindo Bettio, 1000, São Paulo, SP, 03828-000, Brazil* **2** *Departamento de Zoologia, Instituto de Biociências, Universidade de São Paulo (USP), Rua do Matão, Tv. 14, 321, São Paulo, SP, 05508-090, Brazil* **3** *Programa de Pós-Graduação em Sistemática, Taxonomia Animal e Biodiversidade, Museu de Zoologia, Universidade de São Paulo, São Paulo, SP, Brazil*

Corresponding author: Domingo Lago-Barcia (domingo.lagobarcia@gmail.com)

Academic editor: D. Gibson | Received 20 October 2020 | Accepted 29 December 2020 | Published 11 February 2021

http://zoobank.org/133ADA73-102F-422D-8D6C-BD27A01F1551

Citation: Lago-Barcia D, Silva MS, Carbayo F (2021) Revision and description of six species of *Choeradoplana* (Platyhelminthes, Tricladida), with an emendation to the genus. ZooKeys 1016: 1–48. https://doi.org/10.3897/zookeys.1016.59617

Abstract

Living representatives of the Neotropical genus *Choeradoplana* Graff, 1896 (Geoplaninae, Tricladida, Platyhelminthes) are easily recognized by the typical shape of the head which is laterally expanded, rolled-up, and ventrally provided with two glandular cushions. In this study, the morphology and phylogeny (cytochrome C oxidase subunit I gene) of several species of land planarians are taxonomically investigated. Four of the six species studied are new to science, namely: *Ch. eudoxiae* Silva & Carbayo, **sp. nov.**, *Ch. claudioi* Lago-Barcia & Carbayo, **sp. nov.**, *Ch. onae* Lago-Barcia & Carbayo, **sp. nov.**, and *Ch. riutortae* Lago-Barcia & Carbayo, **sp. nov.** The species *Choeradoplana albonigra* and *Ch. eudoxiae* deviate from the usual body shape pattern in that the head does not present lateral expansions nor glandular cushions, becoming indistinguishable from its sister genus *Cephaloflexa*. *Pseudogeoplana tristriata* (Schultze & Müller, 1857) is also redescribed from a newly collected specimen and was discovered to be a member of *Choeradoplana*. Graff (1899) also studied another specimen that was considered to be conspecific with *P. tristriata*; however, in this new it is concluded that it is not conspecific but rather a new species. The name *Pseudogeoplana aevipandemiae* Lago-Barcia & Carbayo, **sp. nov.** is suggested for Graff's specimen.

Keywords

COI, flatworms, Geoplaninae, land planarians, rolled up, taxonomy

Introduction

Members of the Neotropical land planarians genera *Choeradoplana* and *Cephaloflexa* (Platyhelminthes: Geoplanidae: Geoplaninae) can be easily ascribed to either genus based on the head shape, which is characteristically kept rolled up backwards in both genera. The two genera can be distinguished from each other in that the cephalic region in *Choeradoplana* is laterally expanded and ventrally provided with two glandular cushions separated by a longitudinal groove, whereas the cephalic region in *Cephaloflexa* is ventrally concave and the anterior third of the body becomes thinner very gradually.

In a recent multi-gene phylogenetic analysis of the Geoplaninae, representatives of a species preliminarily ascribed in the field to *Cephaloflexa* turned out to be nested in the *Choeradoplana* clade (Carbayo et al. 2013); therefore, the authors transferred it to that genus and the species is currently named *Choeradoplana albonigra* (Riester, 1938). However, the authors did not provide any morphological evidence.

In this paper, we describe or redescribe six species of Brazilian land planarians of the genus *Choeradoplana*. The external aspect of two of these species is similar to that of *Cephaloflexa*, namely the above-mentioned *C. albonigra*, and a new species described herein. We also studied a greenish individual recently collected and identified it as *Pseudogeoplana tristriata* (Schultze & Müller, 1857). The remaining four species were also collected recently and are new to science. We sequenced a fragment of the cytochrome C oxidase subunit I gene (COI) of each specimen to infer the phylogenetic relationships of the species treated herein, and the other representatives of the genus available in the GenBank.

Materials and methods

Molecular analysis

Each specimen was divided into two tissue portions, one for histology and one DNA extraction, respectively (see also section below 'Morphological analysis'). Animal tissue destined for molecular studies was fixed in absolute ethanol and preserved at -20 °C. Genomic DNA was extracted using a standard ammonium acetate extraction protocol modified from Miller et al. (1988). The mitochondrial cytochrome oxidase I gene (COI) was amplified using the primers BarS (Álvarez-Presas et al. 2011), Flatworm-COIF (Sunnucks et al. 2006), and FlatwormCOIR (Lázaro et al. 2009). Standard PCR reactions were performed using Go Taq DNA polymerase (Promega) in a total volume of 25 µl, which included 0.5 ml of each primer (10 mM) and 2 ml of template DNA. PCR conditions for the COI gene consisted of an initial denaturation at 98 °C for 3 min, followed by 35 cycles of denaturation at 98 °C for 10 sec, annealing at 45 °C for 30 sec, end extension at 72 °C for 1 min, and a final extension at 72 °C for 5 min. Amplification products (~ 750 bp) were purified using ExoSAP-IT (Affymetrix, OH) before sequencing both strands on a 3730 DNA Analyzer (Thermo Fisher Scientific).

DNA sequence data were edited using BioEdit 5.0.9 (Hall 1999) and aligned using the online version of the Mafft v7 software program (Katoh et al. 2019) using the G-INS-i algorithm. The sequences of the mitochondrial COI gene reported in this paper were deposited in the NCBI/GenBank data libraries under accession numbers MW127833-MW127842 and MW148795.

The phylogenetic analysis included the newly obtained partial nucleotide sequences for the COI gene (Table 1), and additional sequences of the 12 species of *Choeradoplana* available in the NCBI/GenBank data libraries (Table 1) (Álvarez-Presas et al. 2011; Carbayo et al. 2013; Álvarez-Presas et al. 2014; Lemos et al. 2014; Carbayo et al. 2018). Two sequences belonging to the genus *Matuxia* (Carbayo et al. 2013) were selected as the outgroup (Table 1). PartitionFinder2 ver. 2.1.1 software (Lanfear et al. 2016) on XSEDE (CIPRES Gateway to Science (Miller et al. 2010) was used to discover the partitions and the evolutionary model which best fit the nucleotide dataset under the Akaike Information Criterion corrected (AICc) (Hurvich and Tsai 1989). We estimated the phylogenetic relationships with a Bayesian Inference (BI) obtained using MrBayes v. 3.2.7 (Ronquist et al. 2012). The Markov chain Monte Carlo search was run up to 10,000,000 generations and stoprule activated to stopval = 0.01. Samples were taken every 10,000 generations, discarding the first 25% trees as burn-in, after which the chain reached stationarity, which ensured that the average split frequencies between the runs were less than 1%. Maximum Likelihood (ML) was implemented in RaxML 7.2.+ software (Stamatakis 2006) available on the CIPRES Science Gateway platform (Miller et al. 2010). Bootstrap support values (Felsenstein 1985) were obtained from 10,000 replicates in ML analyses. The final trees were viewed and edited on the FigTree v. 1.4.2 software program (http://tree.bio.ed.ac.uk/software/figtree/).

Morphological analysis

All specimens included in this study (except for the holotype SMF No. 702, *Ch. albonigra*) (Table 1) were collected between May 2008 and January 2010 from conservation areas located in the southern region of the Atlantic Forest. Specimens were manually collected during daylight hours from under rocks, fallen leaves, and logs, and during nighttime hours when the animals are more active. Slides of the holotype of *Ch. albonigra* were obtained on loan from the Museum der Senckenbergischen Naturforschenden Gesellschaft in Frankfurt (**SMF**).

The flatworms were examined and photographed in vivo before being killed with boiling water. Tissue portions destined for histology were fixed in 10% formaldehyde and preserved in 80% ethanol. Color descriptions of the body of living and preserved specimens follow the online palette RAL colors (RAL gemeinnützige GmbH, available at https://www.ral-farben.de/uebersicht-ral-classic-farben.html?&L=1). Body portions were progressively dehydrated in an ascending series of ethanol and cleared in clove oil. Eye distribution was assessed from specimens cleared in clove oil. Body portions were subsequently embedded in Paraplast Tissue Embedding Medium and the resulting blocks were sectioned at 5–7 μm intervals using a retracting rotary microtome. Rib-

Table 1. List of samples used in this study showing species name, field number, museum accession number, type specimen status, collection locality and date, and GenBank accession number.

Species	Field number	Accession number	Type specimen	Coll. locality in Brazil	Coll. date	GenBank acc. (COI)
Choeradoplana abaiba Carbayo et al., 2018	F3905	MZUSP PL 1170	–	Parque Estadual da Serra do Tabuleiro, SC	07/14/09	MF802634
	F3894	MZUSP PL 1169	–	Parque Estadual da Serra do Tabuleiro, SC	07/13/09	MF802633
	F3865	MZUSP PL 1167	–	Parque Estadual da Serra do Tabuleiro, SC	07/12/09	MF802631
	F3866	MZUSP PL 1168	–	Parque Estadual da Serra do Tabuleiro, SC	07/12/09	MF802632
	F3864	MZUSP PL 1166	Holotype	Parque Estadual da Serra do Tabuleiro, SC	07/12/09	MF802630
	F3312	MZUSP PL 509	Paratype	Parque Estadual da Serra do Tabuleiro, SC	01/17/09	MF802629
	F3270	MZUSP PL 505	–	Parque Estadual da Serra do Tabuleiro, SC	01/15/09	MF802628
	F3315	MZUSP PL 511	–	Parque Estadual da Serra do Tabuleiro, SC	01/17/09	HQ542891
Choeradoplana agua Carbayo et al., 2018	F2214	MZUSP PL 448	–	Parque Estadual do Desengano, RJ	03/19/08	MF802637
	F2205	MZUSP PL 446	Paratype	Parque Estadual do Desengano, RJ	03/18/08	MF802636
	F2204	MZUSP PL 445	Paratype	Parque Estadual do Desengano, RJ	03/18/08	MF802635
	F2205	MZUSP PL 446	Paratype	Parque Estadual do Desengano, RJ	03/18/08	KF971686
	F3952	MZUSP PL 619	Paratype	Parque Estadual do Desengano, RJ	08/09/08	KF971680
Choeradoplana albonigra (Riester, 1938)	SMF N°702	–	Holotype	Teresópolis, RJ	04/09/14	–
	F2313	MZUSP PL 1109	–	Reserva Biológica Augusto Ruschi, ES	26/05/08	KF971684
	F2391	MZUSP PL 1113	–	Reserva Biológica Augusto Ruschi, ES	27/05/08	KF971683
	F3991	MZUSP PL 2273	–	Parque Estadual do Desengano, RJ	08/10/09	–
	F4024	MZUSP PL 2152	–	Parque Estadual do Desengano, RJ	08/11/09	–
	F4031	MZUSP PL 2153	–	Parque Estadual do Desengano, RJ	08/11/09	–
	F4081	MZUSP PL 1083	–	Parque Estadual do Desengano, RJ	08/13/09	KC608327
Choeradoplana banga Carbayo & Froehlich, 2012	F3706	MZUSP PL 568	–	Parque Estadual da Cantareira, SP	04/19/09	MF802639
	F3006	MZUSP PL 1001	Paratype	Parque Estadual da Cantareira, SP	12/14/08	MF802638
	F2023	MZUSP PL 1000	Holotype	Parque Estadual da Cantareira, SP	01/30/08	KC608267
	F3011	MZUSP PL 1002	Paratype	Parque Estadual da Cantareira, SP	12/14/08	KC608301
Choeradoplana benyai Lemos & Leal-Zanchet, 2014	F3813	MZUSP PL 1165	–	Parque Estadual da Serra do Tabuleiro, SC	07/12/09	MF802641
	F3494	MZUSP PL 1163	–	Floresta Nacional de São Francisco de Paula, RS	01/28/09	MF802640
	-	MZU PL.00151	Paratype	Floresta Nacional de São Francisco de Paula, RS	03/21/10	KJ690049
Choeradoplana sp.	F2332	MZUSP PL 2276	–	Reserva Biológica Augusto Ruschi, ES	26/05/08	MW127841*
	F2390	MZUSP PL 1155	–	Reserva Biológica Augusto Ruschi, ES	27/05/08	MW127842*
Choeradoplana bocaina Carbayo & Froehlich, 2012	F2822	MZUSP PL 997	Holotype	Parque Nacional da Serra da Bocaina, SP	09/08/09	KC608288
	F2104	MZUSP PL 999	Paratype	Parque Nacional da Serra da Bocaina, SP	02/10/08	KC608273
	F2803	MZUSP PL 998	Paratype	Parque Nacional da Serra da Bocaina, SP	09/07/08	KC608283
Choeradoplana claudioi sp. nov.	F2424	MZUSP PL 1156	Holotype	Reserva Biológica Augusto Ruschi, ES	28/05/08	MW127839*
	F2510	MZUSP PL 1157	Paratype	Reserva Biológica Augusto Ruschi, ES	29/05/08	MW127840*
Choeradoplana eudoxiae Silva & Carbayo, sp. nov.	F3417	MZUSP PL 2272	Holotype	Floresta Nacional de São Francisco de Paula, RS	01/22/09	–
Choeradoplana gladismarie Carbayo et al. 2013	F3802	MZUSP PL 1004	Paratype	Parque Estadual Intervales, SP	07/07/09	KC608326
	F3092	MZUSP PL 1003	Holotype	Parque Estadual Intervales, SP	12/12/08	KC608306
Choeradoplana iheringi Graff, 1899	F3465	MZUSP PL 537	–	Floresta Nacional de São Francisco de Paula, RS	01/25/09	MF802660
	F3454	MZUSP PL 535	–	Floresta Nacional de São Francisco de Paula, RS	01/25/09	MF802658
	F3447	MZUSP PL 531	–	Floresta Nacional de São Francisco de Paula, RS	01/25/09	MF802654

Species	Field number	Accession number	Type specimen	Coll. locality in Brazil	Coll. date	GenBank acc. (COI)
Choeradoplana iheringi Graff, 1899	F3430	MZUSP PL 528	–	Floresta Nacional de São Francisco de Paula, RS	01/23/09	MF802651
	F3409	MZUSP PL 524	–	Floresta Nacional de São Francisco de Paula, RS	01/22/09	MF802649
	-	MZU PL.00156	–	?		KJ690046
Choeradoplana marthae Froehlich, 1955	F2137	MZUSP PL 1153	–	Estação Biológica de Boraceia, SP	02/14/08	MF802665
Choeradoplana minima Lemos & Leal-Zanchet, 2014	-	MZU PL.00143	Paratype	Floresta Nacional de São Francisco de Paula, RS	02/25/10	KJ690052
	-	MZU PL.00145	Paratype	Floresta Nacional de São Francisco de Paula, RS	06/09/11	KJ690051
Choeradoplana onae Lago-Barcia & Carbayo, sp. nov.	F2230	MZUSP PL 2267	Paratype	Reserva Biologica de Ruschi, SP	05/24/08	MW127834*
	F2235	MZUSP PL 2277	–	Reserva Biologica de Ruschi, SP	05/24/08	MW127837*
	F2281	MZUSP PL 2268	Paratype	Reserva Biologica de Ruschi, SP	26/05/08	MW127836*
	F2310	MZUSP PL 2269	Paratype	Reserva Biologica de Ruschi, SP	26/05/08	MW127838*
	F2414	MZUSP PL 2270	Holotype	Reserva Biologica de Ruschi, SP	27/05/08	MW127835*
	F2311	MZUSP PL 1108	–	Reserva Biologica de Ruschi, SP	26/05/08	KF971685
Choeradoplana pucupucu Carbayo et al., 2018	F2844	MZUSP PL 541	Holotype	Parque Nacional da Serra da Bocaina, SP	09/01/08	MF802666
	F2840	MZUSP PL 540	Paratype	Parque Nacional da Serra da Bocaina, SP	09/20/08	KC608293
Choeradoplana riutortae Lago-Barcia & Carbayo, sp. nov.	F4217	MZUSP PL 1174	Paratype	Parque Nacional da Serra dos Orgãos, RJ	01/06/10	MW148795 *
	F4218	MZUSP PL 2274	Holotype	Parque Nacional da Serra dos Orgãos, RJ	01/06/10	–
	F4261	MZUSP PL 2275	Paratype	Parque Nacional da Serra dos Orgãos, RJ	01/08/10	–
Choeradoplana tristriata (Schultze & Müller, 1857)	F3226	MZUSP PL 2271	–	Parque Estadual da Serra do Tabuleiro, SC	01/11/09	MW127833*
Matuxia matuta (Froehlich, 1955)	F2184	MZUSP PL 1021	–	Parque Estadual do Desengano, RJ	03/17/08	KC608276
	F2187	MZUSP PL 1022	–	Parque Estadual do Desengano, RJ	03/17/08	KC608277
Choeradoplana sp. (in Álvarez-Presas et al. 2014)	F4063	MZUSP PL 636	–	Parque Estadual do Desengano, RJ	08/12/09	KF971679

bons of embedding medium were affixed with albumin-glycerol (1:1) on glass slides placed on a hot plate and stained with the method Mallory-Heidenhain as modified by Cason (1950). Reconstructions of the copulatory apparatus were carried out from the histological sections using a camera lucida attached to a microscope. The relative thickness of cutaneous musculature was measured as a value relative to the body height in sections of the pre-pharyngeal region; space between normal and sunken longitudinal cutaneous layers was excluded from measurement. Specimens are deposited in the Museu de Zoologia da Universidade de São Paulo (**MZUSP**).

Results

Molecular results

Tissue of the only *Ch. eudoxiae* Silva & Carbayo, sp. nov. individual was depleted during attempts to sequence it. COI sequences were obtained from the remaining ten specimens representing the three other new species, and *Ch. tristriata* and *Ch. albonigra*. Sequence alignments resulted in a matrix with 54 terminals and 679 base pairs.

PartitionFinder indicated two partitions (first and second codon positions and third codon position), each with a different evolutionary model, with the TIM substitution model having gamma-distributed rate variations across sites and a proportion of invariable sites (TIM + I+ G) for the first and second codons, and a GTR substitution model with gamma-distributed rate variation across sites and a proportion of invariable sites (GTR + I + G) for the third codon partition.

Phylogenetic analyses under the two optimality criteria (BI and ML) retrieved the genus *Choeradoplana* and all morphological species as monophyletic with high posterior probabilities and bootstrap value, respectively (Fig. 1). Nonetheless, the internal morphology of MZUSP PL 1108 and MZUSP PL 2277 could not be assessed; these two specimens were nested in the clade of *Ch. onae* Lago-Barcia & Carbayo, sp. nov. The genus was split into two large clades in both trees composed of the same species, with high PP and bootstrap value. All species studied herein (with the exception of *Ch. eudoxiae* Silva & Carbayo, sp. nov.) are nested in one of these large clades, which includes species having an extrabulbar prostatic vesicle and lacking a penis papilla. However, independently from the optimality criteria applied, COI does not contain sufficient information to resolve the species interrelationships, thereby producing some polytomies and poorly supported clades.

Taxonomic accounts

Family Geoplanidae Stimpson, 1857
Subfamily Geoplaninae Stimpson, 1857
***Choeradoplana* Graff, 1896**

***Choeradoplana tristriata* (Schultze & Müller, 1857)**
Figures 1–5

Geoplana tristriata Schultze & Müller, 1857: 23.
Not *Geoplana tristriata* in Graff 1899: 327–328, 331, taf. V, figs 25, 26.
Pseudogeoplana tristriata: Ogren & Kawakatsu, 1990: 161.

Material examined. MZUSP 2271 (field code, F3226), sexually mature: Parque Estadual da Serra de Tabuleiro, State of Santa Catarina, Brazil (-27.94, -48.79). coll. F. Carbayo and co-workers, 11 January 2009; transverse sections of the cephalic region on 6 slides; horizontal sections of the portion behind the cephalic extremity on 4 slides; transverse sections of the pre-pharyngeal region on 6 slides; sagittal sections of the pharynx and copulatory apparatus on 17 slides.

Distribution. Municipality of Blumenau and Parque Estadual da Serra de Tabuleiro, State of Santa Catarina, Brazil.

Diagnosis. *Choeradoplana* species with yellow green background color, with three thin discontinuous longitudinal black lines; ventral side is zinc-yellow. Copulatory apparatus compact, without penis papilla; female atrium funnel-shaped.

Description. The preserved specimen measures 22 mm long and 2.5 mm wide (Fig. 2A). The body is slender and subcylindrical. The cephalic region is differentiated from the remaining body by means of a 'neck', laterally dilated and rolled up so that the ventral surface is provided with glandular cushions, and is facing out (Fig. 2B); the posterior extremity is pointed. The creeping sole is 90% of body width at the pre-pharyngeal region. The mouth is positioned at a distance from the anterior extremity equal to 60% of the body length, and the gonopore is at 74%.

The dorsal coloration consists of a yellow green (RAL 1018) background color, with three thin discontinuous longitudinal lines of small black spots. These spots are less concentrated in the median line (Fig. 2A). The ventral side is zinc yellow (RAL 1018), except for a silver grey (RAL 7001) spot on the glandular cushions (Fig. 2A).

The eyes are formed by one pigmented cup of 80 μm in diameter (Fig. 2C). There are no clear halos around them. Eyes are absent in the very anterior extremity of the body; at 1.5 mm behind the anterior tip the eyes are marginally distributed in a row of two or three eyes; 3.8 mm posterior to the anterior tip, the eyes are placed in a single marginal row which runs along the whole body until posterior extremity, with each eye at a distance of ~ 0.3 mm from each other (Fig. 2B).

Sensory pits are 25 μm deep (Fig. 2C, arrowhead), and are distributed ventro-laterally in a uniserial row between ~ 0.4 mm behind the anterior extremity to at least the ovarian level.

Numerous rhabditogen cells discharge through the glandular cushions of the cephalic region. These cells are scarce in the dorsal epidermis. Abundant erythrophil gland cells pierce the dorsal and marginal epithelium in the pre-pharyngeal region. The entire epithelium is additionally pierced by scarce gland cells of two types, producing cyanophil and xanthophil granules, respectively. No glandular margin.

The cutaneous musculature of the pre-pharyngeal region comprises a subepithelial circular muscle, followed by a diagonal layer with decussate fibers, and a longitudinal muscle organized in tight bundles (Figs 2D, 3A). This longitudinal muscle is 70 μm thick dorsally; it is ventrally divided into a 35 μm-thick muscle, organized in bundles with 4–8 fibers each, and a 50 μm-thick muscle sunken into the parenchyma consisting of scattered bundles with 5–12 fibers each (Fig. 3B). The thickness of the cutaneous muscle coat is 17% of the body height.

There are three parenchymal muscle layers in the pre-pharyngeal region (Fig. 3A, B): a well-developed dorsal layer of diagonal, decussate fibers (12–18 μm thick); a transverse supra-intestinal muscle (22–25 μm); and a transverse subintestinal muscle (30–35 μm).

The ventral longitudinal cutaneous muscle is modified into the retractor muscle in the cephalic region. This retractor muscle is delta-shaped in cross-section along 0.7 mm (or 3% of body length), starting 0.2 mm (or 1%) from the anterior extremity of the body (Fig. 3C), and its thickness is 24% of the height of the cephalic region. The dorsal decussate and subintestinal parenchymal muscles in this region are weak, whereas the supra-intestinal is strongly developed and mixed with dorso-ventral muscle fibers giving rise to the Muskelgeflecht or interwoven muscle, and is 75 μm in thickness.

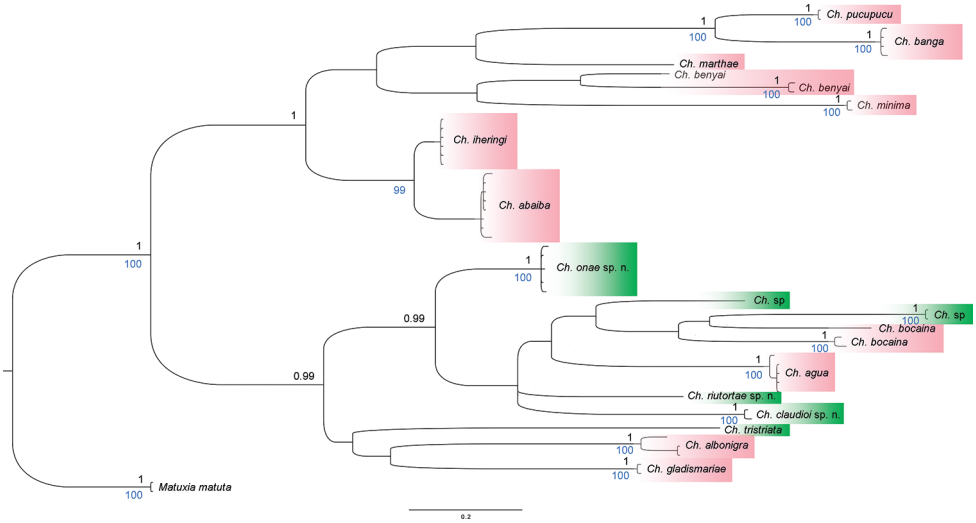

Figure 1. Phylogenetic tree of *Choeradoplana* obtained from the COI gene by Bayesian inference. Black numbers at the nodes correspond to the posterior probability (only values above 0.99 shown) and blue numbers to Bootstrap support in the tree by maximum likelihood (only values above 95% shown). See text for details.

A fourth subneural parenchymal muscle is present in the cephalic region, and is located beneath the central nerve system and above the retractor muscle. The paired glandular cushions are pierced by numerous rhabditogen cells. The arrangement of cutaneous and parenchymal muscles in the cephalic region and the glandular component of the cephalic cushions match those of the type species of the genus, *Choeradoplana iheringi* Graff, 1899.

The mouth is located in the middle of the pharyngeal pouch (Fig. 4A). It is a bell-shaped pharynx, with the dorsal insertion posterior to the ventral insertion ~ 45% of the pharyngeal length. An esophagus is not present. The pharyngeal pouch is lined with a non-ciliated, cuboidal-to-flat epithelium, underlain by a one-fiber thick layer of longitudinal muscle, followed by a 10 µm-thick layer of circular muscle. The outer pharyngeal epithelium is cuboidal, ciliated, underlain by a longitudinal muscle (7.5 µm thick), followed by a circular muscle (45 µm thick) with interspersed longitudinal fibers; the inner epithelium is flat, ciliated, underlain by a circular muscle (62 µm thick) with interspersed longitudinal fibers. Numerous erythrophil and xanthophil gland cells open and discharge their contents through the distal portion of the pharynx.

The testes are dorsal, located between the intestinal diverticula, with some of them reaching the parenchymal supra-intestinal transverse muscle (Figs 2D, 3A). The testes are arranged in two paramedian rows. They extend from 1 mm behind the level of the ovaries (30% of body length) to 1.2 mm from the root of the pharynx. Sperm ducts run straight and immediately above the subintestinal parenchymatic muscle. They distally penetrate the anterior region of the common muscle coat (Fig. 4B, C) to open into the proximal portion of the paired branches of the prostatic vesicle. The prostatic

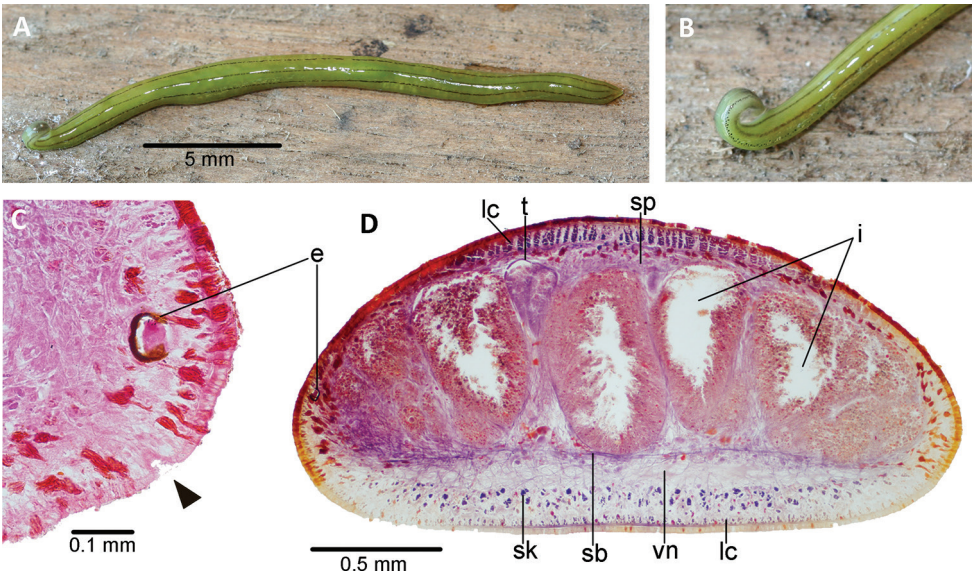

Figure 2. *Choeradoplana tristriata* (Schultze & Müller, 1857), specimen F3226 **A** dorsal view of the live specimen **B** lateral view of the anterior region of the live specimen **C** photomicrograph of a transverse section of the cephalic region, showing an eye and a sensory pit (arrowhead) **D** photomicrograph of a transverse section of the pre-pharyngeal region. Abbreviations: **cm** common muscle coat, **co** common glandular ovovitelline duct, **dd** decussate dorsal cutaneous muscles, **dm** diagonal decussate muscles, **e** eye, **ej** ejaculatory duct, **ep** esophagus, **er** erythrophil secretion, **fa** female atrium, **fd** female genital duct, **g** gonopore, **i** intestine, **lc** longitudinal cutaneous muscles, **ma** male genital atrium, **mk** Muskelgeflecht (Graff, 1899), **mo** mouth, **o** ovary, **ov** ovovitelline duct, **ph** pharyngeal pouch, **pp** penis papilla, **pv** prostatic vesicle, **px** pharynx, **rg** rhabditogen glands, **r** retractor muscle, **sb** subintestinal transverse muscles, **sd** sperm duct, **sg** shell glands, **sk** sunken longitudinal cutaneous muscles, **sm** spermatophore, **sn** subneural transverse muscles, **sp** supra-intestinal transverse muscles, **t** testis, **vi** vitellaria, **vn** ventral nerve plate.

vesicle consists of a proximal half of these paired branches and a distal unpaired half. This vesicle runs postero-dorsally to open into the dorso-anterior section of the male atrium. An ejaculatory duct and penis papilla are absent (Figs 4C, 5A). The penis bulb is thick and consists of numerous muscle fibers continuous with those underlying the epithelium of the male atrium. The prostatic vesicle is lined with a columnar-to-cuboidal epithelium, underlain by a thin longitudinal muscle (5 µm thick), followed by a 30 µm-thick circular muscle interspersed with longitudinal fibers. The paired portion of the prostatic vesicle receives abundant erythrophil and xanthophil granules from the respective gland cells, while the unpaired portion receives abundant cyanophil and xanthophil granules.

The male atrium is long and narrow with folded walls. The proximal third of the atrium runs postero-dorsally; distal two-thirds runs ventrally almost vertically above the gonopore canal. The atrium is lined by a cuboidal-non-ciliated epithelium, and underlain by an 80 µm-thick circular muscle with interspersed longitudinal fibers. The male atrium is 1.2× longer than the female atrium.

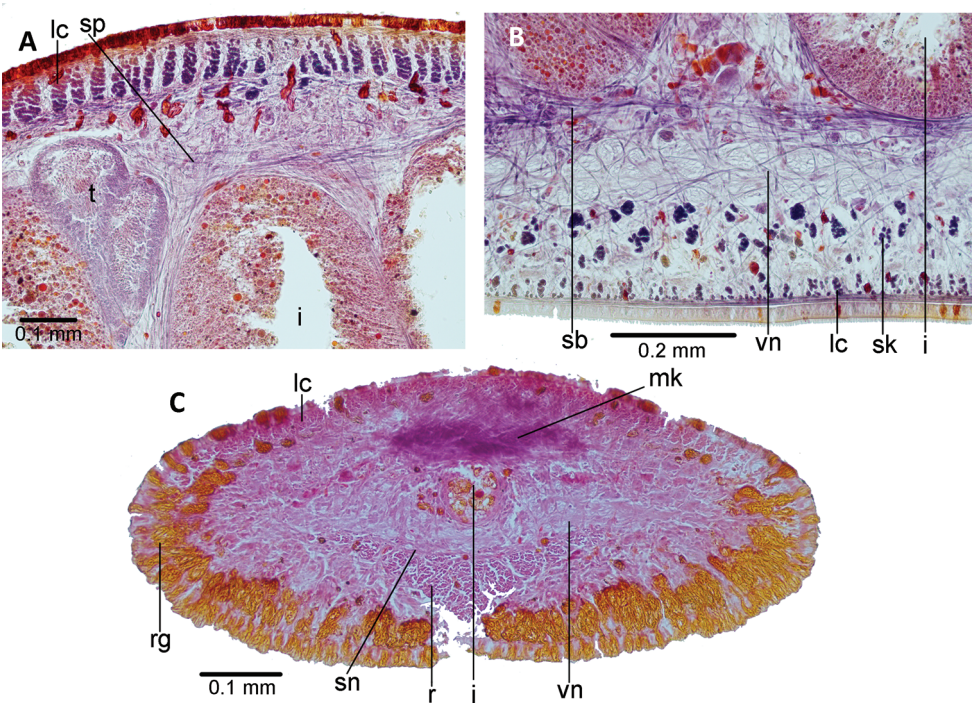

Figure 3. *Choeradoplana tristriata* (Schultze & Müller, 1857), specimen F3226. Photomicrographs of transverse sections **A** dorsal portion of the pre-pharyngeal region **B** ventral region of the pre-pharyngeal region **C** cephalic region. Abbreviations: **cm** common muscle coat, **co** common glandular ovovitelline duct, **dd** decussate dorsal cutaneous muscles, **dm** diagonal decussate muscles, **e** eye, **ej** ejaculatory duct, **ep** esophagus, **er** erythrophil secretion, **fa** female atrium, **fd** female genital duct, **g** gonopore, **i** intestine, **lc** longitudinal cutaneous muscles, **ma** male genital atrium, **mk** Muskelgeflecht (Graff, 1899), **mo** mouth, **o** ovary, **ov** ovovitelline duct, **ph** pharyngeal pouch, **pp** penis papilla, **pv** prostatic vesicle, **px** pharynx, **rg** rhabditogen glands, **r** retractor muscle, **sb** subintestinal transverse muscles, **sd** sperm duct, **sg** shell glands, **sk** sunken longitudinal cutaneous muscles, **sm** spermatophore, **sn** subneural transverse muscles, **sp** supra-intestinal transverse muscles, **t** testis, **vi** vitellaria, **vn** ventral nerve plate.

The ovaries are mature, ovoid, and 200 µm in length. They are located above the ventral nerve plate at a distance from the anterior body tip equal to 25% of its body length (5.5 mm from anterior tip). Ovovitelline ducts emerge from the dorso-lateral aspect of the ovaries, where-after they run backwards above the ventral nerve plate. The ducts bend medially, posteriorly to the female atrium, and subsequently ascend vertically and medially to communicate with each other above the postero-dorsal section of the female atrium (Fig. 5B). The ovovitelline ducts open directly into a very short female genital canal lined by a cuboidal ciliated epithelium. A small number of small shell gland cells can be spotted around the junction of the two ovovitelline ducts.

The female atrium is funnel-shaped, not folded, and lined by a ciliated columnar-to-cuboidal epithelium, which is surrounded by circular muscle fibers with interspersed longitudinal fibers. This muscle is continuous with the common muscle coat. Most of

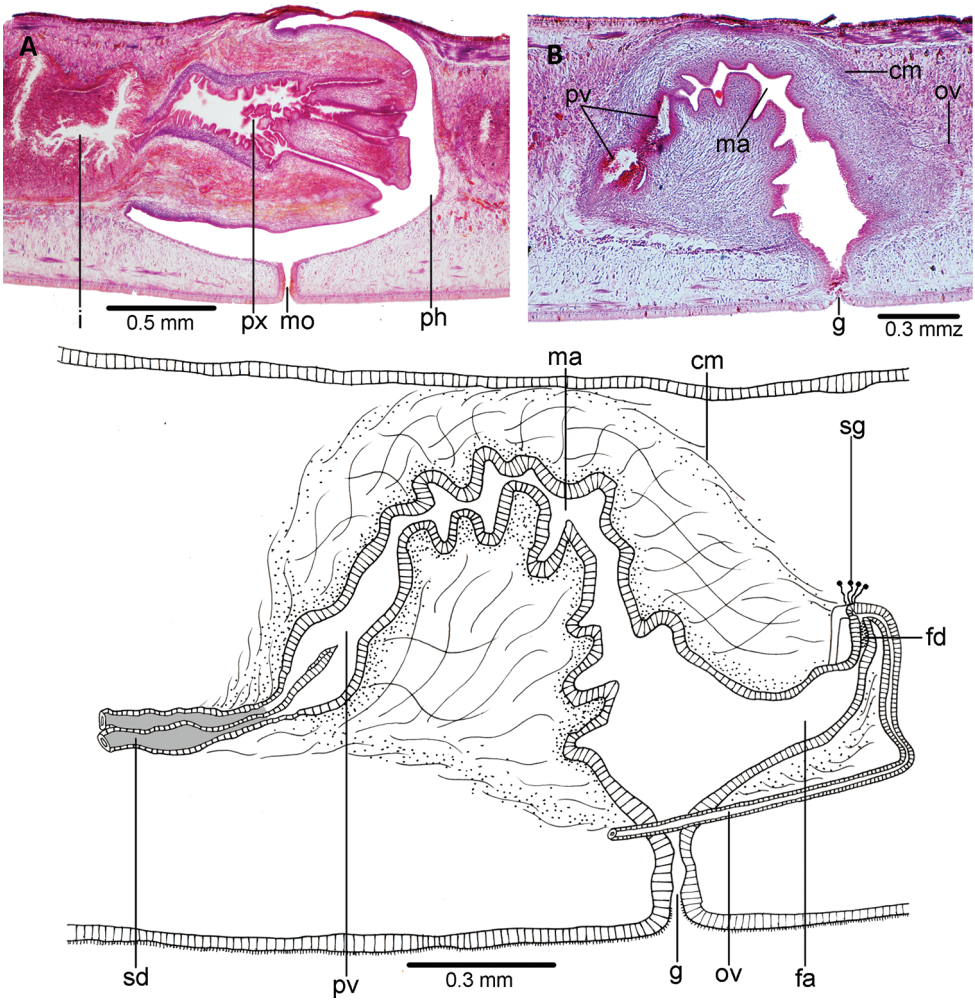

Figure 4. *Choeradoplana tristriata* (Schultze & Müller, 1857), specimen F3226 **A** photomicrograph of a sagittal section of the pharynx **B** photomicrograph of a sagittal section of the copulatory apparatus **C** diagrammatic representation of the copulatory apparatus. Abbreviations: **cm** common muscle coat, **co** common glandular ovovitelline duct, **dd** decussate dorsal cutaneous muscles, **dm** diagonal decussate muscles, **e** eye, **ej** ejaculatory duct, **ep** esophagus, **er** erythrophil secretion, **fa** female atrium, **fd** female genital duct, **g** gonopore, **i** intestine, **lc** longitudinal cutaneous muscles, **ma** male genital atrium, **mk** Muskelgeflecht (Graff, 1899), **mo** mouth, **o** ovary, **ov** ovovitelline duct, **ph** pharyngeal pouch, **pp** penis papilla, **pv** prostatic vesicle, **px** pharynx, **rg** rhabditogen glands, **r** retractor muscle, **sb** subintestinal transverse muscles, **sd** sperm duct, **sg** shell glands, **sk** sunken longitudinal cutaneous muscles, **sm** spermatophore, **sn** subneural transverse muscles, **sp** supra-intestinal transverse muscles, **t** testis, **vi** vitellaria, **vn** ventral nerve plate.

the abundant gland cells discharging into the female atrium have a fine granular xanthophil and erythrophil secretion. The length:height ratio of the copulatory apparatus enveloped by the common muscle coat is 1.4:1.

Remarks. On the identity of our specimen. Schultze and Müller (1857) described *Geoplana tristriata* from near Blumenau, in the State of Santa Catarina. The original description reads: "*Geoplana tristriata*, pale yellowish-green, with three narrow, dark, longitudinal lines on the back; belly paler. Greatest breadth at approx. the second third part of the length, where the mouth is situated. It likes to bend the head upwards. At the point of curvature on each side there is a closed packed group of eye-spots, which are continued in an irregular series to the posterior extremity. The anterior margin of the head appears to be destitute of eyes. Length 1 1/2 inch [38.1 mm]; breadth 1 1/2 line [3.81 mm]. Abundant."

There is no record of the deposition of the type series. It was probably not preserved. Our specimen was collected 115 km south from the type locality, and matches Schultze and Müller's species in all characteristics. The conspecificity of our specimen could be questioned since the copulatory apparatus is the most important organ assuring identification in triclads. However, this species combines a set of unusual features among Geoplanins: the color pattern of the body, the cephalic region bent to the dorsal side (actually only found in *Choeradoplana* and *Cephaloflexa* among Geoplaninae), and the absence of eyes in the very anterior tip of the body. Schultze and Müller's and our specimen sharing these uncommon attributes supports their conspecificity.

The species redescribed herein also matches all diagnostic characteristics of *Choeradoplana* and should therefore be transferred to this genus. The species is unique in the external aspect in that there are no other species of *Choeradoplana* with dorsal green color with three longitudinal dark stripes. Internally, *Choeradoplana bilix* Marcus, 1951; *Ch. crassiphalla* Negrete & Brusa, 2012; *Ch. langi* (Dendy, 1894); and *Ch. marthae* Froehlich, 1955 are similar to *Ch. tristriata* in the compact aspect of the copulatory apparatus, having a length:height ratio equivalent to 1.8:1 or less, as calculated in drawings (du Bois-Reymond Marcus 1951; Marcus 1951; Froehlich 1959; Negrete and Brusa 2012). However, *Ch. bilix*, *Ch. crassiphalla* and *Ch. marthae* possess a penis papilla (vs. absent in *Ch. tristriata*), and the female atrium of *Ch. langi* is a narrow canal (vs. a funnel-shaped cavity).

The identity of Graff's specimen and subsequent taxonomic actions. Herman von Ihering collected one specimen in Taquara, State of Rio Grande do Sul, Brazil, which he identified as a member of this species. Ihering sent it to Graff (1899), who endorsed his identification, but only provided a description of the external aspect. Froehlich (1959) disagreed with Ihering's identification because of the body shape, the relative position of the mouth, and the different width of the paramedian dorsal stripes. Froehlich concluded that both Schultze and Müller's and Graff's species remain obscure (Froehlich 1959), but did not propose taxonomic changes. Ogren and Kawakatsu (1990) considered Schultze and Müller's and Graff's specimens conspecific, and transferred the species to the *Pseudogeoplana* collective genus, which houses species lacking information about the internal organs, especially the copulatory apparatus. We agree with Froehlich's opinion that Graff's species is different from Schultze and Müller's species. Accordingly, we propose the name *Pseudogeoplana aevipandemiae*

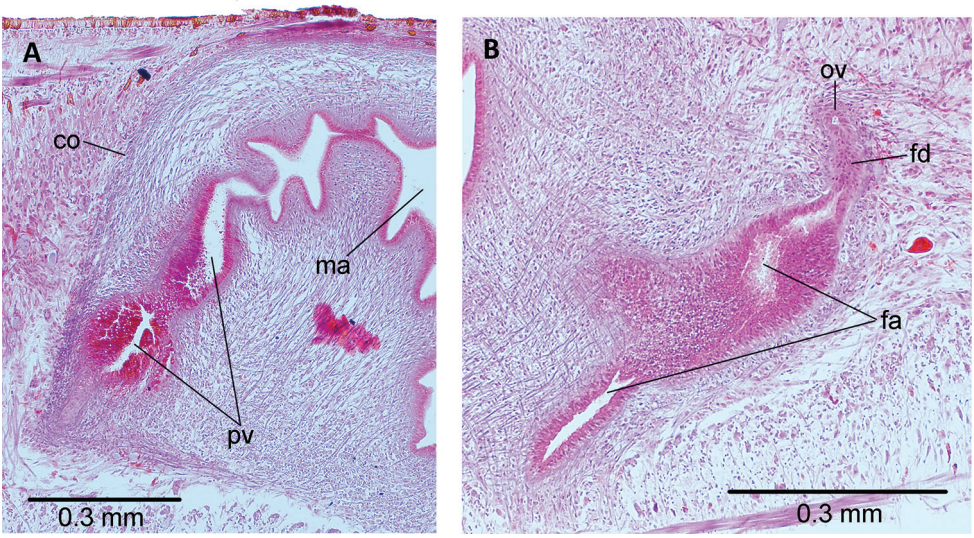

Figure 5. *Choeradoplana tristriata* (Schultze & Müller, 1857), specimen F3226. Photomicrographs of sagittal sections **A** prostatic vesicle and the male atrium **B** female atrium. Abbreviations: **cm** common muscle coat, **co** common glandular ovovitelline duct, **dd** decussate dorsal cutaneous muscles, **dm** diagonal decussate muscles, **e** eye, **ej** ejaculatory duct, **ep** esophagus, **er** erythrophil secretion, **fa** female atrium, **fd** female genital duct, **g** gonopore, **i** intestine, **lc** longitudinal cutaneous muscles, **ma** male genital atrium, **mk** Muskelgeflecht (Graff, 1899), **mo** mouth, **o** ovary, **ov** ovovitelline duct, **ph** pharyngeal pouch, **pp** penis papilla, **pv** prostatic vesicle, **px** pharynx, **rg** rhabditogen glands, **r** retractor muscle, **sb** subintestinal transverse muscles, **sd** sperm duct, **sg** shell glands, **sk** sunken longitudinal cutaneous muscles, **sm** spermatophore, **sn** subneural transverse muscles, **sp** supra-intestinal transverse muscles, **t** testis, **vi** vitellaria, **vn** ventral nerve plate.

Lago-Barcia & Carbayo, sp. nov. for Graff's species. The specific epithet means 'from the times of the pandemic'. The epithet alludes to the COVID-19 pandemic and is intended to keep the memory of the negative effects caused by the long months of closure of the laboratories for the conclusion of this paper.

We did not find Graff's specimen in the museums where part of this collection was disseminated (Naturhistorisches Museum, Basel; Museum of Natural History, Vienna; Senckenberg Museum, Frankfurt; Zoological Museum, Hamburg; Natural History Museum, London). Therefore, we consider Graff's specimen lost.

Choeradoplana albonigra **(Riester, 1938)**

Figures 6–9

Geoplana albonigra Riester, 1938: 7–9, figs 4, 5, 86, 87, taf. 1, fig. 2.
Notogynaphallia albonigra: Ogren & Kawakatsu, 1990: 140.
Choeradoplana albonigra: Carbayo et al., 2013: 514, 517.

Material examined. ***Holotype*** SMF N° 702, sexually mature: Teresópolis, Rio de Janeiro, Brazil, coll. E. Bresslau, April 9th, 1914; transverse sections of a body portion seemingly being close to the anterior tip of the body on 1 slide; sagittal sections of the pharynx and copulatory apparatus on 1 slide; anterior and posterior tips in Canada balsam on 1 slide.

Reserva Biológica Augusto Ruschi, municipality of Santa Teresa, State of Espírito Santo, Brazil. May 26–27th, 2008. **MZUSP PL 1109** (field code, F2313), only anterior half of the body collected: transverse sections of anterior extremity on 10 slides; sagittal sections of a portion behind anterior extremity on 5 slides; horizontal sections containing testes on 32 slides. **MZUSP PL 1113** (field code, F2391), sexually mature: transverse sections of anterior extremity on 9 slides; sagittal sections of ovaries and testes on 6 slides; sagittal sections of pharynx and copulatory apparatus on 11 slides.

Parque Estadual do Desengano, municipality of Santa Maria Madalena, State of Rio de Janeiro, Brazil. August 10–13th, 2009. **MZUSP PL 2273** (field code, F3991), juvenile: horizontal sections of anterior extremity on 3 slides. **MZUSP PL 2153** (field code, F4031), sexually mature: transverse sections of anterior extremity on 12 slides; horizontal sections of ovaries on 22 slides; transverse sections of pre-pharyngeal region on 4 slides; sagittal sections of pharynx and copulatory apparatus on 8 slides; horizontal sections of posterior extremity on 4 slides. **MZUSP PL 2152** (field code, F4024), sexually mature: horizontal sections of anterior extremity on 7 slides; sagittal sections of ovaries on 19 slides; horizontal sections of testes on 21 slides; transverse sections of pre-pharyngeal region on 9 slides; sagittal sections of pre-pharyngeal region on 12 slides; sagittal sections of copulatory apparatus on 12 slides. **MZUSP PL 1083** (field code, F4081), sexually mature: transverse sections of anterior extremity on 55 slides; sagittal sections of the ovaries on 25 slides; horizontal sections of testes on 9 slides; transverse sections of pre-pharyngeal region on 6 slides; sagittal sections of pharynx and copulatory apparatus on 38 slides; horizontal sections of posterior extremity on 24 slides.

Distribution. Reserva Biológica Augusto Ruschi, Santa Teresa, State of Espírito Santo; Parque Estadual do Desengano, Santa Maria Madalena, State of Rio de Janeiro; Municipality of Teresópolis, State of Rio de Janeiro, Brazil.

Diagnosis. *Choeradoplana* species with a white dorsum, covered by a wide median black band, darker at its margins; an additional thin black median stripe may be present. The anterior third of the body is progressively thinner towards the pointed tip; its extremity has no lateral dilations or "neck" differentiating the head from the body. The ventral side of the cephalic region is concave and without glandular cushions. The proximal third of the prostatic vesicle is extrabulbar. The copulatory apparatus is relatively long; penis papilla is absent, and the female atrium is approximately funnel-shaped.

Description. Living specimens range between 50–63 mm in length and 2–3 mm in width (n = 2). Preserved specimens range between 45–73 mm in length and 2–4 mm in width (n = 4). The body is slender and subcylindrical, with the anterior third becoming progressively thinner to the anterior tip. The anterior extremity is very thin

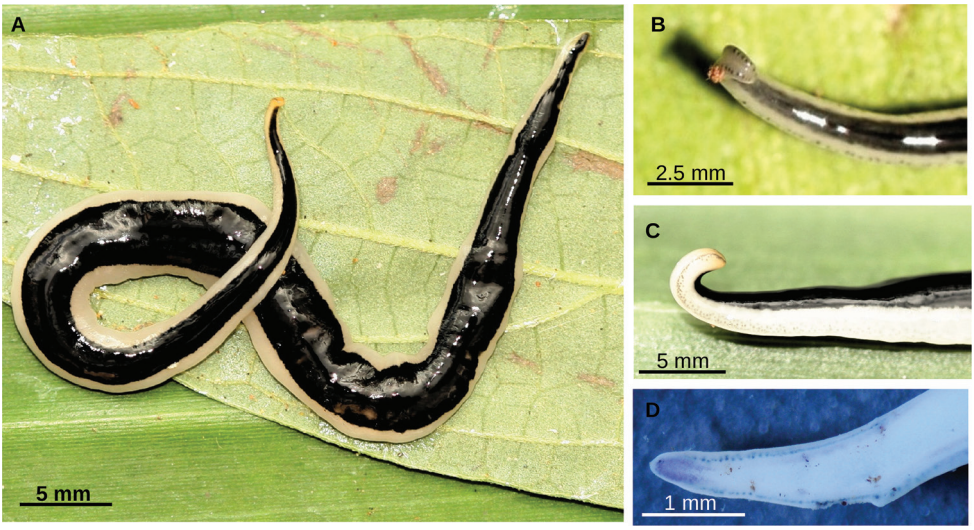

Figure 6. *Choeradoplana albonigra* (Riester, 1938) **A** habitus of living specimen F4024 in dorsal view **B** detail of anterior extremity of living specimen F2313 in dorsal view. Debris is glued on the body **C** detail of anterior extremity of living specimen F4024 in lateral view **D** detail of anterior extremity of preserved specimen F4031 in ventral view. Abbreviations: **cm** common muscle coat, **co** common glandular ovovitelline duct, **dd** decussate dorsal cutaneous muscles, **dm** diagonal decussate muscles, **e** eye, **ej** ejaculatory duct, **ep** esophagus, **er** erythrophil secretion, **fa** female atrium, **fd** female genital duct, **g** gonopore, **i** intestine, **lc** longitudinal cutaneous muscles, **ma** male genital atrium, **mk** Muskelgeflecht (Graff, 1899), **mo** mouth, **o** ovary, **ov** ovovitelline duct, **ph** pharyngeal pouch, **pp** penis papilla, **pv** prostatic vesicle, **px** pharynx, **rg** rhabditogen glands, **r** retractor muscle, **sb** subintestinal transverse muscles, **sd** sperm duct, **sg** shell glands, **sk** sunken longitudinal cutaneous muscles, **sm** spermatophore, **sn** subneural transverse muscles, **sp** supra-intestinal transverse muscles, **t** testis, **vi** vitellaria, **vn** ventral nerve plate.

and coiled up so that the ventral surface is facing out (Fig. 6A, B). The ventral side of the cephalic region is slightly concave with indistinct glandular cushions (Fig. 6B–D). The posterior extremity is pointed. The creeping sole is 80–86% of width in the prepharyngeal region (n = 3) (Fig. 7A). Its mouth is at a distance from the anterior extremity ranging between 50.9–64.4% of body length, gonopore at 63.2–75.3% (n = 3).

The background color of the body is traffic white (RAL 9016). It is dorsally covered by a wide graphite black (RAL 9011) band, darker at its margins, as wide as three-quarters of the body width, in the middle of which runs a thin jet black (RAL 9005) stripe which is not apparent in some individuals. Anterior and posterior extremities of the body are slightly orangish. The color has faded out in preserved specimens. The dorsal graphite black band in the body tips of the holotype split into two brownish stripes.

The eyes are of one-pigment cup type, 25–45 µm in diameter; with no clear halos. They are marginally distributed in an irregular row of 2–6 eyes, from the anterior tip of the body (Figs 6B, C, 7A), backwards to the posterior end. Anterior extremity devoid of eyes.

The sensory pits are 22–27 μm deep and ventro-laterally are distributed in a single row along approximately the anterior one-seventh of the body. The pits are absent at the very anterior tip of the body (300 μm).

Numerous rhabditogen cells open onto the dorsal surface of the body (Fig. 7B) in the pre-pharyngeal region and its margins; these margins are also pierced by scarce gland cells producing granular, erythrophil secretion. The ventral epithelium is pierced by scarce gland cells producing granular, xanthophil secretion, and abundant gland cells producing strong erythrophil secretion (Fig. 7C). There is no glandular margin.

The cutaneous musculature consists of a subepithelial circular muscle, followed by a diagonal layer with decussate fibers, and a strong longitudinal muscle organized in bundles (Fig. 7A–C). This longitudinal muscle is 81.2–175 μm thick dorsally; it is ventrally divided into a 37.5–50.0 μm-thick muscle, organized in bundles with 20–35 fibers each, and an equally thick muscle sunken into the parenchyma, and constituted by scattered bundles with 7–30 fibers each (Fig. 7B). A few dorsal longitudinal fibers are medially intermingled with those of the parenchymatic dorsal layer of diagonal decussate fibers. The thickness of the cutaneous muscle coat is 22–25% (n = 3) of the body height.

The pre-pharyngeal region, namely the dorsal decussate muscle (40–55 μm thick, n = 2), transverse supra-intestinal muscle (74–100 μm); and transverse subintestinal muscle (45–65 μm) (n = 2) (Fig. 7A–C).

The retractor muscle of the head is delta-shaped in a cross-section along 0.3 mm (or 0.5% of body length) from behind, 0.1 mm (or 0.15%) of the anterior extremity of the body (Fig. 7C), and its thickness equals 36% of the height of the cephalic region. The Muskelgeflecht is 18–25 μm thick (24% of body height). The subneural parenchymal muscle consists of a few scarce transverse fibers. The glandular cushions are composed of a relatively small quantity of rhabditogen cells (Fig. 7D–F).

The mouth is located at a distance from the anterior section of the pharyngeal pouch ranging between 55.1–78.9% (n = 4) (Fig. 8A). The pharynx is bell-shaped with dorsal insertion near the mouth level. An esophagus is absent. The outer epithelium of the pharynx is cuboidal, ciliated and underlain by a thin longitudinal muscle (3–5 μm); followed by a circular muscle (15–20 μm) with interspersed longitudinal fibers. The inner pharyngeal epithelium is ciliated, underlain by a circular muscle (50 μm thick; n = 3) with longitudinal fibers interspersed. There is abundant granular secretion of three types, cyanophil, erythrophil, and xanthophil, respectively, and pierce the distal pharyngeal epithelium.

The testes are dorsal, located under the supra-intestinal transverse muscle layer, partially placed between the intestinal diverticula. They extend from the level of the ovaries (a distance from the anterior extremity of the body equal to 27% of the body length) to nearly the root of pharynx (53% of the body length). Sperm ducts run immediately above the subintestinal muscle layer, dorsally and slightly laterally to the ovovitelline ducts. Distal portions of sperm ducts contain sperm, and are surrounded by a circular muscle. Sperm ducts communicate with the two roughly horizontal branches of the extrabulbar portion of the prostatic vesicle. These branches open later-

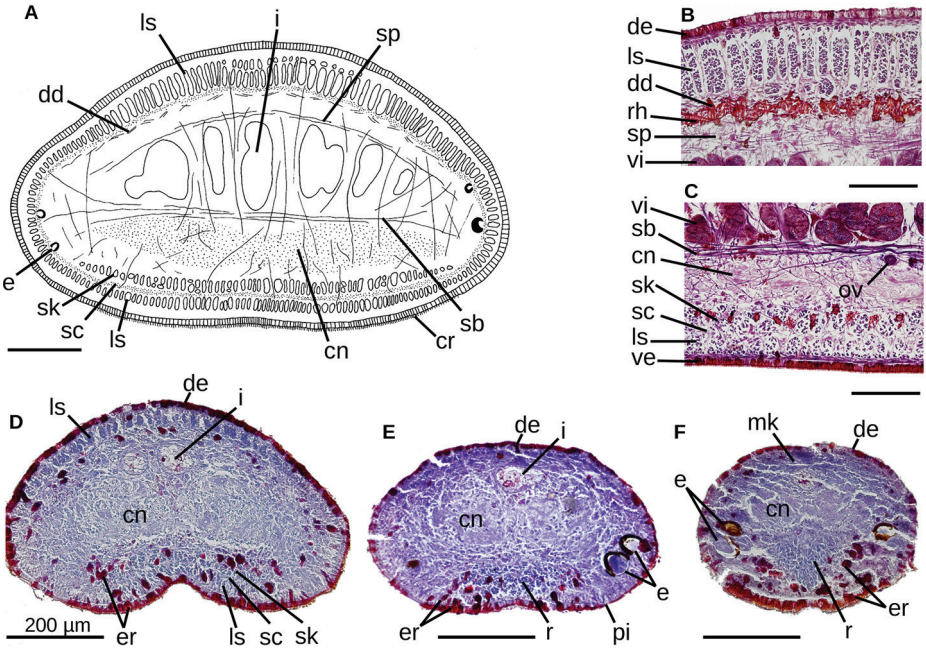

Figure 7. *Choeradoplana albonigra* (Riester, 1938) **A** diagrammatic transverse section of a portion, seemingly near the anterior extremity, of holotype. Photomicrographs of transverse sections (**B–F**) **B** dorsal epidermis in pre-pharyngeal region of specimen F4024 **C** ventral epidermis in pre-pharyngeal region of specimen F4024 **D–F** cephalic region of specimen F4081 at 1.2, 0.4, and 0.15 millimeters from anterior extremity of the body, respectively. Scale bar: 200 µm. Abbreviations: **cm** common muscle coat, **co** common glandular ovovitelline duct, **dd** decussate dorsal cutaneous muscles, **dm** diagonal decussate muscles, **e** eye, **ej** ejaculatory duct, **ep** esophagus, **er** erythrophil secretion, **fa** female atrium, **fd** female genital duct, **g** gonopore, **i** intestine, **lc** longitudinal cutaneous muscles, **ma** male genital atrium, **mk** Muskelgeflecht (Graff, 1899), **mo** mouth, **o** ovary, **ov** ovovitelline duct, **ph** pharyngeal pouch, **pp** penis papilla, **pv** prostatic vesicle, **px** pharynx, **rg** rhabditogen glands, **r** retractor muscle, **sb** subintestinal transverse muscles, **sd** sperm duct, **sg** shell glands, **sk** sunken longitudinal cutaneous muscles, **sm** spermatophore, **sn** subneural transverse muscles, **sp** supra-intestinal transverse muscles, **t** testis, **vi** vitellaria, **vn** ventral nerve plate.

ally into an irregular, pear-shaped cavity, which is located more or less under the anterior section of the penis bulb (Figs 8B, C, 9A–C). The prostatic vesicle continues as an almost vertical, tubular portion inside the very dense penis bulb to bend posteriorly towards a loose small ring-shaped horizontal fold (or 'small penis-shaped fold', after Riester 1938) which may be narrowed and elongated as a finger (Fig. 8B, arrow). This fold gives passage to the male atrium. The penis bulb is very thick and consists of very numerous muscle fibers which are continuous with those underlying the epithelium of the male atrium. There is no ejaculatory duct as a differentiated portion. The prostatic vesicle is lined with a columnar, ciliated epithelium. The very abundant secretions discharging into it are zoned along the prostatic vesicle: paired branches receive very fine granular erythrophil and pink-reddish staining secretion; the dilated portion takes gross granular erythrophil intensely reddish staining secretion; a proximal intrabulbar

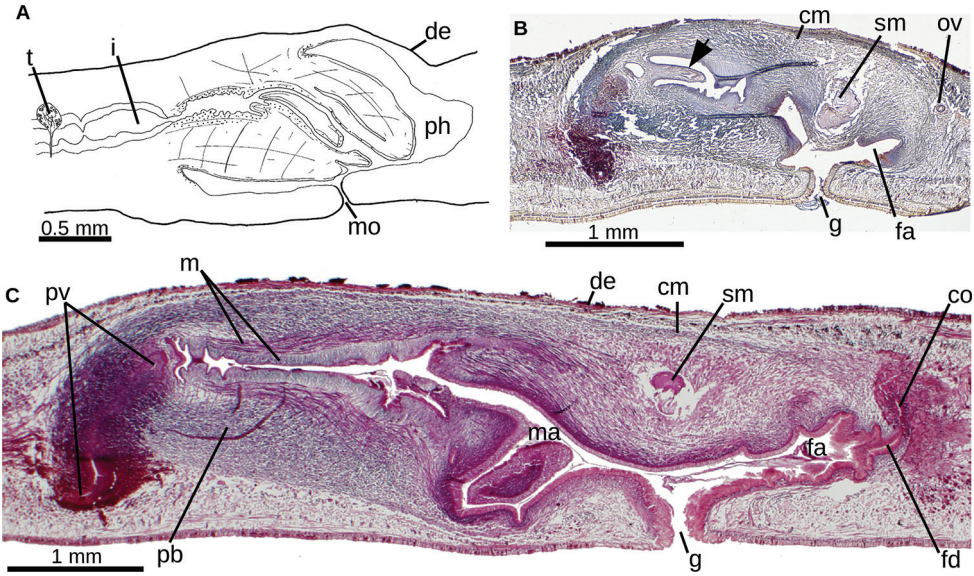

Figure 8. *Choeradoplana albonigra* (Riester, 1938) **A** diagrammatic representation of the pharynx from sagittal sections of holotype **B** sagittal section of the copulatory apparatus of specimen F2391; note the small finger-shaped fold of the male atrium (arrow) **C** photomicrograph of a sagittal section of the copulatory apparatus of specimen F4024. Abbreviations: **cm** common muscle coat, **co** common glandular ovovitelline duct, **dd** decussate dorsal cutaneous muscles, **dm** diagonal decussate muscles, **e** eye, **ej** ejaculatory duct, **ep** esophagus, **er** erythrophil secretion, **fa** female atrium, **fd** female genital duct, **g** gonopore, **i** intestine, **lc** longitudinal cutaneous muscles, **ma** male genital atrium, **mk** Muskelgeflecht (Graff, 1899), **mo** mouth, **o** ovary, **ov** ovovitelline duct, **ph** pharyngeal pouch, **pp** penis papilla, **pv** prostatic vesicle, **px** pharynx, **rg** rhabditogen glands, **r** retractor muscle, **sb** subintestinal transverse muscles, **sd** sperm duct, **sg** shell glands, **sk** sunken longitudinal cutaneous muscles, **sm** spermatophore, **sn** subneural transverse muscles, **sp** supra-intestinal transverse muscles, **t** testis, **vi** vitellaria, **vn** ventral nerve plate.

portion receives finely erythrophil secretion; the distal section takes both finely cyanophil granular secretion and xanthophil variously sized secretion granules (Fig. 9B). The extrabulbar portion is surrounded by interwoven muscle fibers, and the intrabulbar portion by a muscular layer of circular fibers interspersed with longitudinal ones, both portions are 20–35 µm thick. The loose small ring-shaped horizontal fold is lined with a 3–6 µm high non-ciliated epithelium and is surrounded by a few seemingly circular muscle fibers.

The proximal half of the male atrium is slightly folded and narrow. The distal half is ample and is narrowed distally by a large, dorsal fold extending through both the male and female atria. The stroma of this fold is strongly muscularized with longitudinal and oblique fibers. Additional lateral folds may be present in the distal half (Figs 8B, C, 9B).

The proximal half of the male atrium is lined with a 5 µm high non-ciliated, infranucleated epithelium which is pierced by scarce gland cells producing fine erythrophil granules, and by gland cells producing variously sized xanthophil granules. This epi-

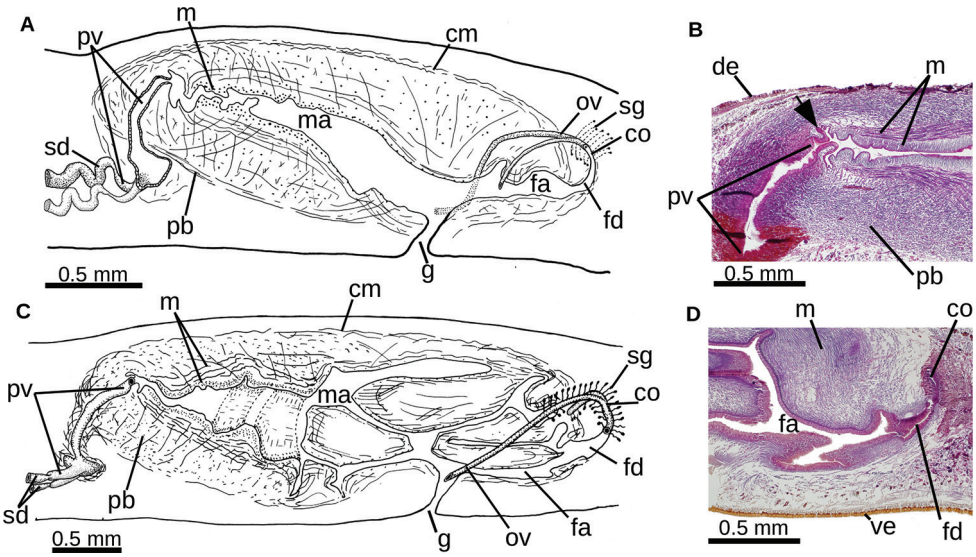

Figure 9. *Choeradoplana albonigra* (Riester, 1938) **A** diagrammatic reconstruction of copulatory apparatus of holotype from sagittal sections **B** photomicrograph of a sagittal section of the unpaired portion of the prostatic vesicle and proximal section of male atrium of specimen F4024. Arrow points the small ring-shaped horizontal fold communicating prostatic vesicle with male atrium **C** diagrammatic reconstruction of copulatory apparatus of specimen F4081 from sagittal sections **D** photomicrograph of a sagittal section of the female atrium of specimen F4081. Abbreviations: **cm** common muscle coat, **co** common glandular ovovitelline duct, **dd** decussate dorsal cutaneous muscles, **dm** diagonal decussate muscles, **e** eye, **ej** ejaculatory duct, **ep** esophagus, **er** erythrophil secretion, **fa** female atrium, **fd** female genital duct, **g** gonopore, **i** intestine, **lc** longitudinal cutaneous muscles, **ma** male genital atrium, **mk** Muskelgeflecht (Graff, 1899), **mo** mouth, **o** ovary, **ov** ovovitelline duct, **ph** pharyngeal pouch, **pp** penis papilla, **pv** prostatic vesicle, **px** pharynx, **rg** rhabditogen glands, **r** retractor muscle, **sb** subintestinal transverse muscles, **sd** sperm duct, **sg** shell glands, **sk** sunken longitudinal cutaneous muscles, **sm** spermatophore, **sn** subneural transverse muscles, **sp** supra-intestinal transverse muscles, **t** testis, **vi** vitellaria, **vn** ventral nerve plate.

thelium is surrounded by a 20–60 µm-thick dense muscle of very thin muscle fibers (2 µm); followed by a muscle (< 150 µm thick) of 4 µm-thick fibers. The distal half of the male atrium is lined with an epithelium which is pierced by gland cells producing erythrophil granules. An intensely reddish erythrophil is found beneath this epithelium secretion. The lining epithelium of the distal half of the male atrium is surrounded by a circular muscle (18–45 µm); followed by a longitudinal muscle (80–150 µm) (n = 3).

A spermatophore is in the stroma of the large dorsal fold leveled with the gonopore in three specimens (F2391, F4024, F4081) (Fig. 8B, C). The spermatophore is ovoid in shape, with approximately 150 µm in diameter, and seems to be constituted of a central mass of sperm partially surrounded by irregular strands of erythrophil granules. The biological meaning of the position of the spermatophore will be discussed elsewhere.

The ovaries are mature, very elongated, and club-shaped due to the dilated proximal extremity. The thin portion can be divided into smaller segments. The size of the

ovaries ranges between 700–1200 μm in length and 120–170 μm in width (n = 4). They are located above the ventral nerve plate, and at a distance from the anterior extremity equal to 27.1–31.3% of the body length (n = 2). Ovovitelline ducts emerge from the dorso-lateral aspect of the ovaries and run above the nerve plate. The proximal segment of the oviducts is dilated and contains sperm (n = 4). They ascend posteriorly and medially laterally to the female atrium, then unite dorsally to the common glandular ovovitelline duct (Fig. 9A–C). The distal portion of the oviducts is pierced by shell gland cells. The common glandular ovovitelline duct is downwards directed; it is continuous with a posteriorly and upward directed diverticulum of the female atrium, i.e., the female genital canal. The female atrium is roughly funnel-shaped, narrowed by a large dorsal fold continued with that of the male atrium. The female genital duct is lined with epithelial cells, with the apical portion containing fine erythrophil granules, and is surrounded by a thin layer of circular and longitudinal muscle fibers.

The female atrium is lined with a columnar, non-ciliated epithelium, and is pierced by two types of cells producing erythrophil and cyanophil granular secretions, respectively. The female atrium is as long as half the male atrium. The common muscular coat of the copulatory apparatus is composed of a weak layer of intermingled fibers; it is 20–40 μm thick in the anterior section, and thinner in the posterior section. The length:height ratio of the copulatory apparatus enveloped by the common muscle coat ranges between 3.0–3.5:1 (n = 5; mean 3.2:1).

Behavioral note. Creeping on the Petri dish, the animals sometimes rise up to three-quarters of the body from the substrate and swing to the sides as they would be searching for ground. When touched, they can react by tumbling. A similar behavior, named 'escape reaction', was observed for *Ch. marthae* by Froehlich (1959).

Remarks. This species was originally described as *Geoplana albonigra* Riester, 1938, from Teresópolis, State of Rio de Janeiro, Brazil. The external aspect and the internal morphology of the pharynx and copulatory apparatus were given in the original description. The species was later transferred to the recently proposed new genus *Notogynaphallia* Ogren & Kawakatsu, 1990, erected for species of Geoplaninae without penis papilla and dorsally located female genital canal. Based on morphological and molecular information, Carbayo et al. (2013) transferred the species to *Choeradoplana*, but they did not provide morphological evidence supporting that taxonomic decision.

On the identity of our specimens. Our specimens and the holotype of *Ch. albonigra* are much alike, with the exception of the size of the male and female atria. Whereas the male and female atria are relatively narrow in the holotype, these atria are higher in two out of four mature individuals. Differences of the same nature have been observed in other land planarians (e.g., *Pasipha pasipha* (Marcus, 1951); *Obama josefi* (Carbayo & Leal-Zanchet, 2001)), and this might be caused by different states of maturation of each specimen, albeit all being mature, or by the physiological state of the individuals such as a recent copulation, as seems to be the case of the specimens bearing a spermatophore.

The systematic position of Ch. albonigra. Riester described the species from a single individual and assigned the species to *Geoplana*. In Riester's description, there is no reference to the inner structures of the cephalic region, nor to the cutaneous

muscle coat. The cephalic region of the holotype is embedded in Canada balsam on a histological glass slide. Our study revealed a set of additional aspects, including the delta-shaped retractor muscle of the head and the in-sunk ventral longitudinal cutaneous muscle which only agree with *Choeradoplana*. Our molecular data also support this conclusion. However, *Ch. albonigra* deviates from the genus in the body shape, since its anterior third narrows progressively towards the anterior extremity, with the latter also lacking the typical glandular cushions of *Choeradoplana.* Accordingly, the diagnosis of the genus is revised below.

Choeradoplana eudoxiae **Silva & Carbayo, sp. nov.**
http://zoobank.org/51DD356F-96DA-43B7-B860-CE6C40B5405B
Figures 10–13

Material examined. ***Holotype*** MZUSP 2272 (field code, F3417), sexually mature: Floresta Nacional de São Francisco de Paula, State of Rio Grande do Sul, Brazil, (-29.43628, -50.37369). coll. F. Carbayo and co-workers, 22 January 2009; transverse sections of the cephalic region on 7 slides; horizontal sections of ovaries on 4 slides; transverse sections of the pre-pharyngeal region on 4 slides; sagittal sections of the pharynx and copulatory apparatus on 8 slides; the posterior extremity on 3 slides.

Distribution. Only known from the type locality, Floresta Nacional de São Francisco de Paula, State of Rio Grande do Sul, Brazil.

Etymology. The specific epithet pays homage to the late Prof. Eudóxia Maria Froehlich, 21 October 1928 – 26 September 2015, for her insightful life lessons and lasting contribution to the knowledge of the neotropical planarian fauna for 60 years.

Diagnosis. *Choeradoplana* species with pastel yellow back and brown fawn spots more concentrated in the paramedian region. Its anterior extremity has no lateral dilations or "neck" differentiating its head from its body. The ventral side of the cephalic region is concave, and without distinct glandular cushions. The extrabulbar portion of the prostatic vesicle has paired branches and an unpaired, roughly rounded section; the intrabulbar portion is a dilated vertical duct. Penis papilla is absent.

Description. The live holotype measured 38 mm in length, and 1.5 mm in width. Preserved, it measured 27.5 mm in length and 2 mm in width. Its body is slender and subcylindrical, with the anterior 1/8 becoming progressively thinner towards the anterior tip. The anterior extremity is rounded and the posterior is pointed. The dorsal side is convex, while the ventral side is slightly convex. The anteriormost body portion is approximately five millimeters long and rolled up so that the ventral side is facing upwards (Fig. 10A–C). This ventral surface is concave, without distinct glandular cushions. This ventral surface is flat in the preserved holotype. Its creeping sole is as wide as 75.5% of body width at the pre-pharyngeal region. Its mouth is 14.5 mm (52.7% of body length) from the anterior extremity, and the gonopore is 16.8 mm (61.1%).

The dorsum background color of the body is pastel yellow (RAL 1034) with fawn brown (RAL 8007) spots (Fig. 10A–C); these spots are more densely distributed in

the paramedian regions, some merged with each other. The ventral side is cream (Fig. 10D). The cephalic extremity is greyish dorsally and ventrally. The body color faded on the preserved holotype.

The eyes are one pigmented-cup type of 25–30 μm in diameter. There are no clear halos around them (Fig. 10C, D). Since the very anterior histological sections are lost, it could not be ascertained whether they occur in this body region. Posteriorly, the eyes are marginal along the body length.

Sensory pits are 17.0–22.5 μm deep, distributed ventro-laterally in a uniserial row from the anterior sections of the body (approximately 0.2 mm of the anteriormost body were lost) to 4.5 mm behind it.

Abundant rhabditogen cells open onto the dorsal surface of the body and its margins in the pre-pharyngeal region. The epithelium of the margins is also pierced by gland cells producing erythrophil granules (Fig. 11A, B). The ventral epithelium is pierced by three types of gland cells, namely scarce gland cells producing granules of dark, cyanophil secretion, gland cells producing cyanophil granules, and gland cells producing an erythrophil secretion. There is no glandular margin.

The cutaneous musculature consists of a subepithelial circular muscle, followed by a diagonal layer with decussate fibers, and a longitudinal muscle organized in bundles (Fig. 11A, B). This longitudinal muscle is 57.5 μm thick dorsally and arranged in bundles of 50–90 fibers each, whereas ventrally it is divided into a 30 μm-thick muscle of bundles (with 8–15 fibers each), and an insunk muscle with 70 μm-thick bundles (with 16–32 fibers each) (Fig. 11A). The thickness of the cutaneous muscle coat is 20% of the body height.

In the pre-pharyngeal region, the same parenchymal muscles as in *Ch. iheringi*, namely the dorsal decussate muscle (52–55 μm thick), transverse supra-intestinal muscle (20–22 μm); and transverse subintestinal muscle (12–15 μm) (Fig. 11A, B).

The muscle retractor of the head is delta-shaped in a cross-section along ~ 0.5 mm (or 1.8% of body length) starting from 0.1 mm behind the anterior extremity of the body (Fig. 11C, D), and its thickness equals 36% of the height of the cephalic region. The Muskelgeflecht is 32 μm thick (22% of body height). The subneural parenchymal muscle consists of a few transverse fibers. The glandular cushions are composed of a relatively small quantity of rhabditogen cells (Fig. 11C, D).

The central nervous system presents a ventral nerve plate (70–85 μm thick or 9–11% of body height) in the pre-pharyngeal region.

The mouth is located in the middle of the pharyngeal pouch (Fig. 12A). The pharynx is bell-shaped (Fig. 12B). An esophagus is absent. The outer pharyngeal epithelium is underlain by an 8 μm-thick longitudinal muscle, followed by a 15 μm-thick circular muscle. The inner pharyngeal epithelium is underlain by a circular muscle layer with longitudinal fibers interspersed (20 μm thick).

The testes are dorsal, 90–150 μm in diameter, located under the supra-intestinal transverse muscle layer, and partially placed between the intestinal diverticula. The anteriormost testes are located 0.9 mm anterior to the ovaries (or 21% of the body length); posteriormost near the root of the pharynx (49% of the body length). Sperm

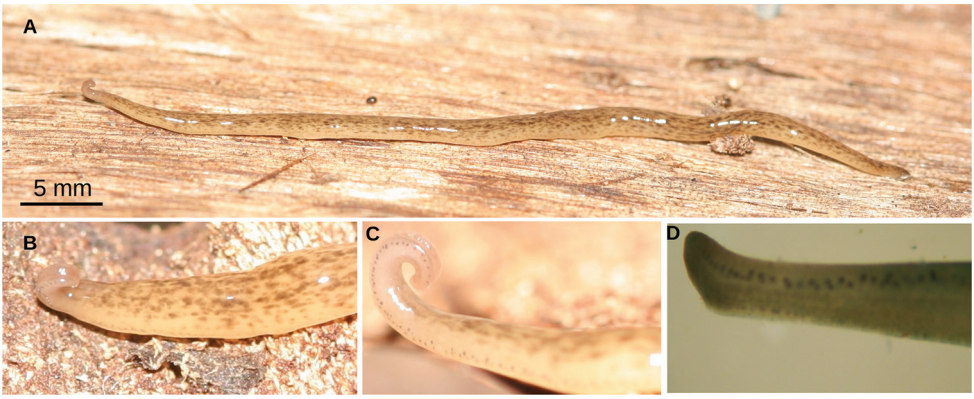

Figure 10. *Choeradoplana eudoxiae* Silva & Carbayo, sp. nov. Holotype **A** living animal in dorsal view **B, C** detail of anterior extremity in a dorsal view **D** detail of anterior extremity in ventro-lateral view in the preserved specimen. Abbreviations: **cm** common muscle coat, **co** common glandular ovovitelline duct, **dd** decussate dorsal cutaneous muscles, **dm** diagonal decussate muscles, **e** eye, **ej** ejaculatory duct, **ep** esophagus, **er** erythrophil secretion, **fa** female atrium, **fd** female genital duct, **g** gonopore, **i** intestine, **lc** longitudinal cutaneous muscles, **ma** male genital atrium, **mk** Muskelgeflecht (Graff, 1899), **mo** mouth, **o** ovary, **ov** ovovitelline duct, **ph** pharyngeal pouch, **pp** penis papilla, **pv** prostatic vesicle, **px** pharynx, **rg** rhabditogen glands, **r** retractor muscle, **sb** subintestinal transverse muscles, **sd** sperm duct, **sg** shell glands, **sk** sunken longitudinal cutaneous muscles, **sm** spermatophore, **sn** subneural transverse muscles, **sp** supra-intestinal transverse muscles, **t** testis, **vi** vitellaria, **vn** ventral nerve plate.

ducts run immediately above the subintestinal muscle layer, dorsally and slightly internal to the ovovitelline ducts. Distal portions of sperm ducts contain sperm and are surrounded by a 20 µm-thick circular muscle. These ducts communicate with the respective short branch of the prostatic vesicle (Fig. 12C, D). The paired branches run posteriorly. The extrabulbar portion of the prostatic vesicle consists of these paired branches and an unpaired, roughly rounded section with pleated wall receiving the branches. The intrabulbar portion of the prostatic vesicle is elongate and runs dorsally and posteriorly. The passage of the prostatic vesicle to the proximal region of the male atrium is narrowed by an annular fold (Fig. 12C, D). There is no ejaculatory duct, nor penis papilla. The penis bulb is very thick and consists of numerous muscle fibers which are continuous with those underlying the epithelium of the male atrium. The prostatic vesicle is lined with a columnar, ciliated epithelium underlain by a dense layer (20 µm thick) of interwoven circular and longitudinal muscle fibers. The epithelium of the diverticula and that of the anterior section of extrabulbar section of prostatic vesicle are pierced by numerous gland cells producing strong erythrophil (pinkish) granules. The epithelium of the posterior section of the extrabulbar portion is pierced by gland cells producing abundant erythrophil granules. Two types of gland cells pierce the epithelium of the intrabulbar portion of the vesicle; one type is very abundant, and produces cyanophil granules, while the second type produces erythrophil granules.

The male atrium is elongated. The proximal half is horizontal, slightly folded and narrow. The distal half is wider, and provided with two large transverse and oblique

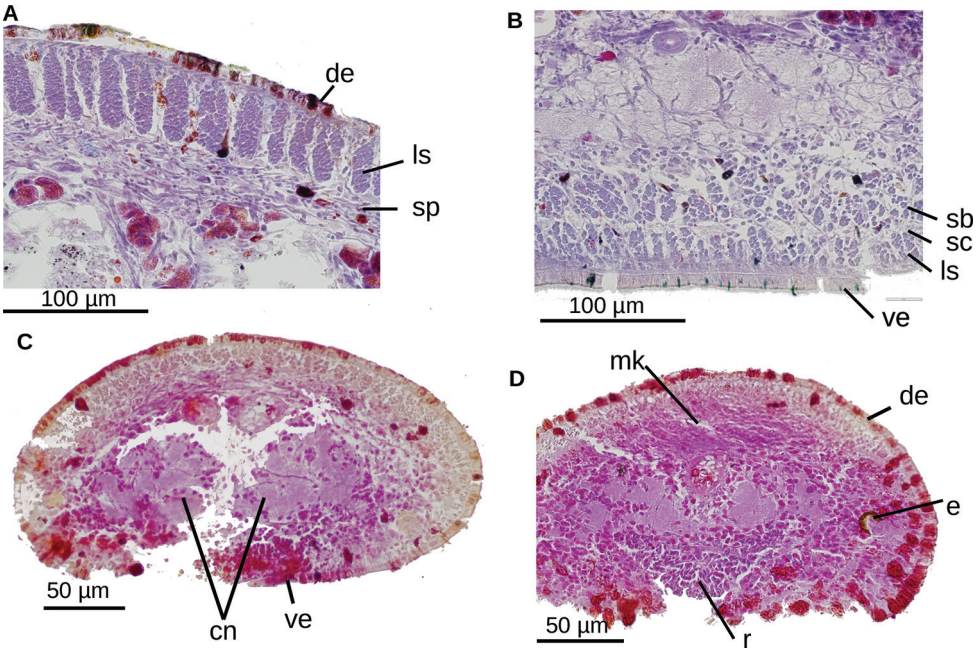

Figure 11. *Choeradoplana eudoxiae* Silva & Carbayo, sp. nov. Photomicrographs of transverse sections of the holotype **A** dorsal portion of the pre-pharyngeal region ofreion **B** ventral portion of the pre-pharyngeal region **C** anterior region at 0.1 mm from the anterior tip of the body. of the pre-pharyngeal region **D** anterior region at 0.5 mm from the anterior tip of the body. Abbreviations: **cm** common muscle coat, **co** common glandular ovovitelline duct, **dd** decussate dorsal cutaneous muscles, **dm** diagonal decussate muscles, **e** eye, **ej** ejaculatory duct, **ep** esophagus, **er** erythrophil secretion, **fa** female atrium, **fd** female genital duct, **g** gonopore, **i** intestine, **lc** longitudinal cutaneous muscles, **ma** male genital atrium, **mk** Muskelgeflecht (Graff, 1899), **mo** mouth, **o** ovary, **ov** ovovitelline duct, **ph** pharyngeal pouch, **pp** penis papilla, **pv** prostatic vesicle, **px** pharynx, **rg** rhabditogen glands, **r** retractor muscle, **sb** subintestinal transverse muscles, **sd** sperm duct, **sg** shell glands, **sk** sunken longitudinal cutaneous muscles, **sm** spermatophore, **sn** subneural transverse muscles, **sp** supra-intestinal transverse muscles, **t** testis, **vi** vitellaria, **vn** ventral nerve plate.

folds. The atrium is lined with a 7 µm high epithelium, and pierced by two types of gland cells producing erythrophil and cyanophil granules, respectively. The atrial epithelium is underlain by a 20 to 35 µm-thick circular muscle with longitudinal fibers intermingled (Figs 12D, 13A).

The ovaries are mature, rounded, ~ 100 µm in diameter. They are located 8.9 mm from the anterior extremity of the body (24.7 % of body length), and above the ventral nerve plate. The ovovitelline ducts emerge from the dorso-lateral aspect of the ovaries and run above the nerve plate; their proximal section contains sperm. Laterally to the female atrium, they rise posteriorly to unite dorsally to the common glandular ovovitelline duct (Fig. 13A, B). This common duct is located behind the female atrium, and runs downwards to open into a canalicular projection of the posterior section of the female atrium.

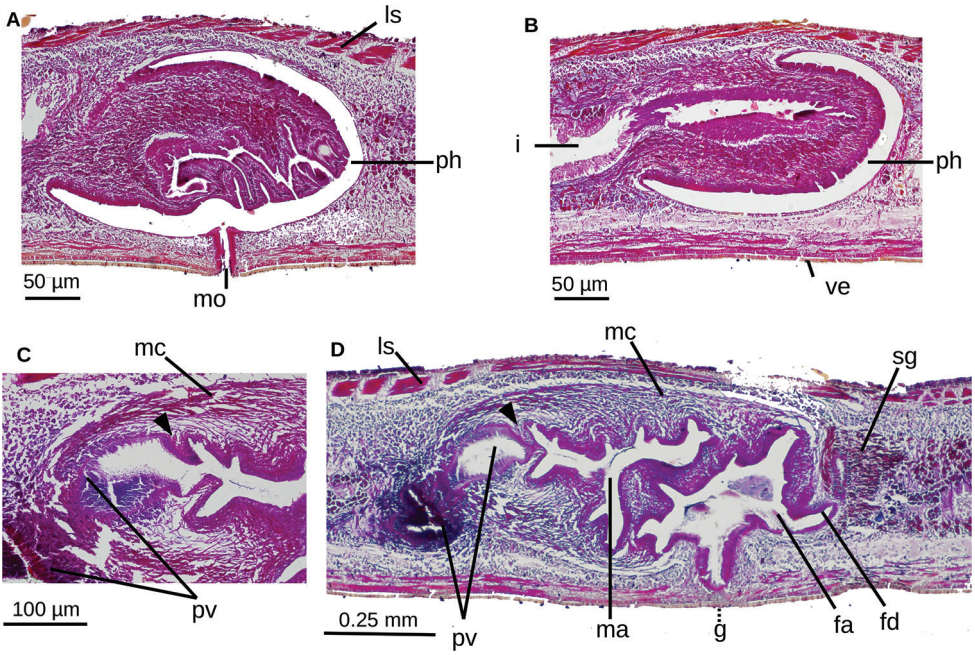

Figure 12. *Choeradoplana eudoxiae* Silva & Carbayo, sp. nov. Photomicrographs of sagittal sections of holotype **A, B** pharynx **C** prostatic vesicle and male atrium **D** copulatory apparatus. Abbreviations: **cm** common muscle coat, **co** common glandular ovovitelline duct, **dd** decussate dorsal cutaneous muscles, **dm** diagonal decussate muscles, **e** eye, **ej** ejaculatory duct, **ep** esophagus, **er** erythrophil secretion, **fa** female atrium, **fd** female genital duct, **g** gonopore, **i** intestine, **lc** longitudinal cutaneous muscles, **ma** male genital atrium, **mk** Muskelgeflecht (Graff, 1899), **mo** mouth, **o** ovary, **ov** ovovitelline duct, **ph** pharyngeal pouch, **pp** penis papilla, **pv** prostatic vesicle, **px** pharynx, **rg** rhabditogen glands, **r** retractor muscle, **sb** subintestinal transverse muscles, **sd** sperm duct, **sg** shell glands, **sk** sunken longitudinal cutaneous muscles, **sm** spermatophore, **sn** subneural transverse muscles, **sp** supra-intestinal transverse muscles, **t** testis, **vi** vitellaria, **vn** ventral nerve plate.

The female atrium is irregular, provided with two or three lateral and dorsal folds (Fig. 13). This atrium is as long as half the male atrium, and is lined with an 8–10 µm high epithelium, the cells of which are erythrophil in their subapical portion. This epithelium is pierced by gland cells producing cyanophil granules, and is underlain by a 10 µm-thick muscle of circular and longitudinal muscle fibers.

The common muscular coat is well developed and continuous with the penis bulb. This coat wraps the intrabulbar portion of the prostatic vesicle, and the male and female atria. The length:height ratio of the copulatory apparatus enveloped by the common muscle coat is 2.2:1.

Behavioral note. When touched with a finger on the posterior end, the animal reacted by rolling forward. Firstly, it lifted its posterior extremity forward to touch the ground at the level of the midbody so that the body forms a loop. Next, the loop moved forwards until the anterior third of the body detached from the ground, which

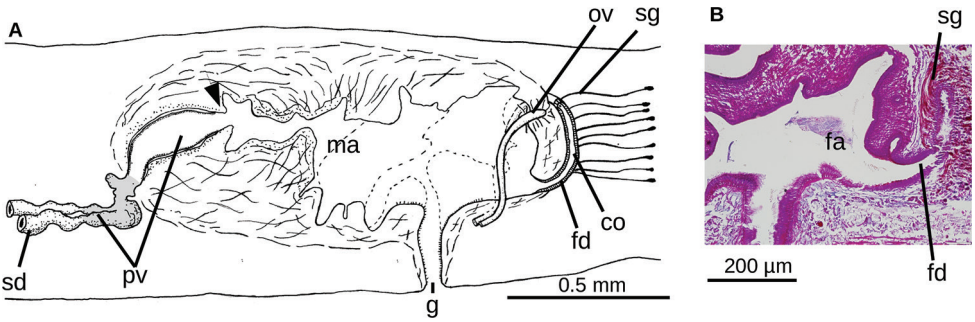

Figure 13. *Choeradoplana eudoxiae* Silva & Carbayo, sp. nov. Holotype **A** diagrammatic reconstruction of copulatory apparatus **B** photomicrograph of a sagittal section of the female atrium. Abbreviations: **cm** common muscle coat, **co** common glandular ovovitelline duct, **dd** decussate dorsal cutaneous muscles, **dm** diagonal decussate muscles, **e** eye, **ej** ejaculatory duct, **ep** esophagus, **er** erythrophil secretion, **fa** female atrium, **fd** female genital duct, **g** gonopore, **i** intestine, **lc** longitudinal cutaneous muscles, **ma** male genital atrium, **mk** Muskelgeflecht (Graff, 1899), **mo** mouth, **o** ovary, **ov** ovovitelline duct, **ph** pharyngeal pouch, **pp** penis papilla, **pv** prostatic vesicle, **px** pharynx, **rg** rhabditogen glands, **r** retractor muscle, **sb** subintestinal transverse muscles, **sd** sperm duct, **sg** shell glands, **sk** sunken longitudinal cutaneous muscles, **sm** spermatophore, **sn** subneural transverse muscles, **sp** supra-intestinal transverse muscles, **t** testis, **vi** vitellaria, **vn** ventral nerve plate.

subsequently lengthened and touched the substrate. By doing so, the animal moved forward a distance equivalent to half its body length in approximately one second. It then immediately repeated this whole movement repeatedly.

Remarks. The species described herein matches all diagnostic characteristics of *Choeradoplana*, except for the glandular cushions of the cephalic region, which are not developed. This is so notable that the species was initially assigned to *Cephaloflexa* upon examination of the live and preserved specimen. Regarding the body shape, *Cephaloflexa* is characterized by having "the anterior third very gradually narrowing, without constriction or widening and without grooves on the ventral surface. The anterior tip rolled upwards and is ventrally concave" (Carbayo and Leal-Zanchet 2003). *Ch. albonigra* is similar in this aspect to the genus *Cephaloflexa* and to *Ch. eudoxiae* Silva & Carbayo, sp. nov. Unfortunately, it was not possible to sequence DNA from the small tissue available of *Ch. eudoxiae* Silva & Carbayo, sp. nov., and the homology test of the particular body shape of these two species remains an open question.

The remaining diagnostic attributes of *Choeradoplana* are present in *Ch. eudoxiae* Silva & Carbayo, sp. nov., such as the ventral cutaneous longitudinal muscle partially sunken into the parenchyma; a retractor muscle of the cephalic extremity with a delta shape in transverse section; and a dorsal decussate parenchymatic muscle modified in the cephalic region into the Muskelgeflecht.

The body color of the *Ch. eudoxiae* Silva & Carbayo, sp. nov. resembles that of some congeners in the brownish background color with dark black or dark brown spots over it, namely *Choeradoplana abaiba* Carbayo et al., 2018, *Ch. agua* Carbayo et al., 2018, *Ch. banga* Carbayo & Froehlich, 2012, *Ch. benyai* Lemos & Leal-Zanchet,

2014, *Ch. bocaina* Carbayo & Froehlich, 2012, *Ch. cyanoatria* Iturralde & Leal-Zanchet, 2019, *Ch. longivesicula* Iturralde & Leal-Zanchet, 2019, *Ch. pucupucu* Carbayo et al., 2018, and the herein-described *Ch. onae* Lago-Barcia & Carbayo, sp. nov., *Ch. riutortae* Lago-Barcia & Carbayo, sp. nov. and *Ch. claudioi* Lago-Barcia & Carbayo, sp. nov. However, the general aspect of *Ch. eudoxiae* is lighter. Moreover, only *Ch. eudoxiae* Silva & Carbayo, sp. nov. and *Ch. albonigra* lack the cephalic glandular cushions among all species of the genus, with the latter having a different, black-striped dorsum.

With respect to the internal morphology, *Ch. eudoxiae* Silva & Carbayo, sp. nov. is similar to *Ch. albonigra*, *Ch. tristriata*, *Ch. bocaina*, *Ch. riutortae* Lago-Barcia & Carbayo, sp. nov., *Ch. claudioi* Lago-Barcia & Carbayo, sp. nov., and *Ch. onae* Lago-Barcia & Carbayo, sp. nov. in that the prostatic vesicle is extrabulbar and it is lacking a penis papilla. However, in the latter four species an extrabulbar portion of the prostatic vesicle is dish-shaped, whereas this organ is pear-shaped (in *Ch. eudoxiae* Silva & Carbayo, sp. nov.) or has two short tubular branches (branches (with a pear-shaped organ) *Ch. tristriata* (*paired tubes*) and *Ch. albonigra*). *Ch. eudoxiae* sp. nov. is distinguished from *Ch. tristriata* in the relatively compact copulatory apparatus of the latter, and from *Ch. albonigra* in that the copulatory apparatus in this species is relatively longer, the paired portions of the prostatic vesicle are shorter, and the common glandular ovovitelline duct is relatively shorter.

***Choeradoplana claudioi* Lago-Barcia & Carbayo, sp. nov.**
http://zoobank.org/375D0CE0-B9DF-4AA4-9DEA-1281AFB7BFDC
Figures 14, 15

Material examined. Both specimens were collected in Reserva Biológica Augusto Ruschi, Santa Teresa, State of Espírito Santo, Brazil (-19.8891, -40.5459) by F. Carbayo and co-workers, May 27–29th, 2008; ***Holotype*** **MZUSP PL 1156** (field code, F2424), sexually mature: transverse sections of the cephalic region on 6 slides; horizontal sections of a portion behind the cephalic region on 4 slides; sagittal sections of the ovarian region on 4 slides; transverse sections of the pre-pharyngeal region on 4 slides; sagittal sections of the pharynx and copulatory apparatus on 11 slides. ***Paratype*** **MZUSP PL 1157** (field code, F2510), sexually mature: sagittal sections of the pharynx and copulatory apparatus on 10 slides. The ovarian region was lost.

Distribution. Only known from the type locality, Reserva Biológica Augusto Ruschi, Santa Teresa, State of Espírito Santo, Brazil.

Etymology. The specific epithet honors Prof. Claudio Gilberto Froehlich for his contributions to the knowledge of the Neotropical land planarians.

Diagnosis. *Choeradoplana* species with a golden yellow background color, with scattered sepia brown speckles on the whole dorsal surface, except for the anterior, greyish extremity. The extrabulbar portion of the prostatic vesicle is dish-like. The female genital atrium is compressed dorso-ventrally and partially positioned below the distal section of the male atrium.

Description. Preserved specimens measure 24.0–36.5 mm in length and 2.5–3.0 mm in width (n = 2). The body is slender and subcylindrical. The cephalic region is differentiated from the remaining body by a 'neck', laterally dilated and rolled up so that the ventral surface provided with glandular cushions faces out; the posterior extremity is pointed. The creeping sole is as wide as 75% (F2424) of the body width at the pre-pharyngeal region. The mouth is positioned at a distance from the anterior extremity equal to 50% of the body length, and the gonopore is at 60%.

The dorsal coloration of the live specimens consists of a golden yellow (RAL 1004) background color, with scattered sepia brown (RAL 8014) speckles on the whole dorsal surface, except for the anterior, greyish extremity (Fig. 14A). The ventral coloration is golden yellow.

Its eyes are devoid of halos and are formed by a one-pigmented cup of 60 µm in diameter. Eyes are absent in the very anterior extremity of the body equivalent to more or less 1% of the body length. The eyes are distributed marginally in a row of two or three eyes along the first 4.5 mm (or 12% of body length), then they are arranged in a single marginal row until the posterior end.

The sensory pits are 15 µm deep, and are distributed ventro-laterally in a uniserial row, only starting at approximately the equivalent to 1% of body length. The ventral epithelium of the ovarian region was lost and sensory pits are absent in the pre-pharyngeal region.

The cutaneous musculature of the pre-pharyngeal region consists of a subepithelial circular muscle followed by a diagonal layer with decussate fibers, and a strong longitudinal muscle organized in bundles (Fig. 14B). This longitudinal muscle is 95 µm thick dorsally; it is ventrally divided into a 15 µm-thick muscle organized in bundles with 5–12 fibers each, and a 45 µm-thick muscle sunken into the parenchyma constituted of bundles with 6–17 fibers each. The thickness of the cutaneous muscle coat is 16% of the body height. (measurements from animal F2424 which has the best histological sections).

In the pre-pharyngeal region, a dorsal decussate muscle (25 µm thick), transverse supra-intestinal muscle (25 µm); and transverse subintestinal muscle (15 µm) (n = 1) (Fig. 14B).

The cutaneous and parenchymal musculature is organized in the cephalic region as in *Ch. iheringi*. The muscle retractor of the head is delta-shaped in a cross-section along 1.8 mm (or 5% of body length, F2424) from behind, 1.3 mm (or 4%, F2424) of the anterior extremity of the body (Fig. 14C), and its thickness equals 36% of the height of the cephalic region. The Muskelgeflecht is 190 µm thick (32% of body height). The subneural parenchymal muscle consists of scattered transverse fibers. The glandular cushions are composed of numerous rhabditogen cells (Fig. 14C).

The mouth is located in the middle of the pharyngeal pouch (Fig. 14D). The pharynx is cylindrical-to-bell-shaped, with its dorsal insertion approximately at the mouth level. An esophagus is absent. The pharyngeal pouch is lined with a non-ciliated, low epithelium underlain by a thin layer of circular muscle with interspersed longitudinal fibers (11–12 µm thick, n = 2). The outer pharyngeal epithelium is flat, ciliated and

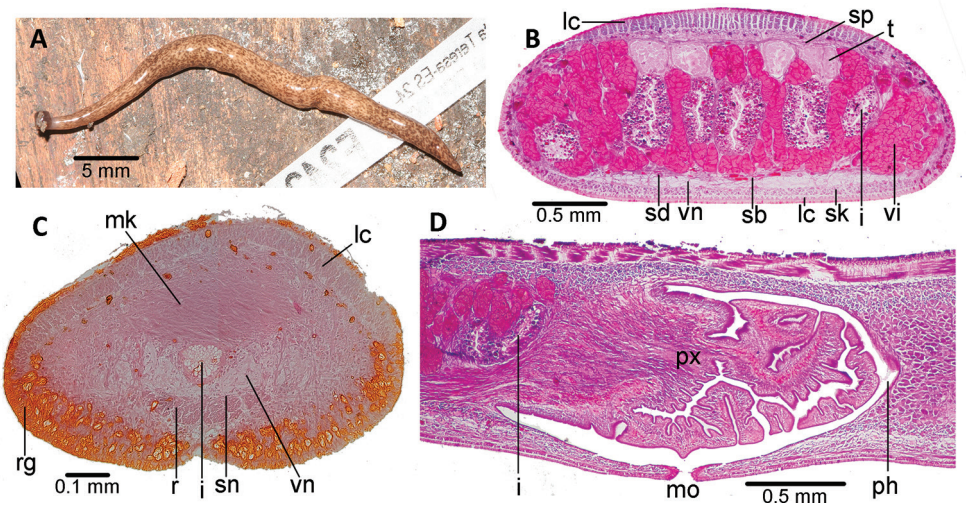

Figure 14. *Choeradoplana claudioi* Lago-Barcia & Carbayo, sp. nov., holotype **A** dorsal view of the creeping live animal **B** photomicrograph of a transverse section of the pre-pharyngeal region **C** photomicrograph of a transverse section of the cephalic region **D** photomicrograph of a sagittal section of the pharynx. Abbreviations: **cm** common muscle coat, **co** common glandular ovovitelline duct, **dd** decussate dorsal cutaneous muscles, **dm** diagonal decussate muscles, **e** eye, **ej** ejaculatory duct, **ep** esophagus, **er** erythrophil secretion, **fa** female atrium, **fd** female genital duct, **g** gonopore, **i** intestine, **lc** longitudinal cutaneous muscles, **ma** male genital atrium, **mk** Muskelgeflecht (Graff, 1899), **mo** mouth, **o** ovary, **ov** ovovitelline duct, **ph** pharyngeal pouch, **pp** penis papilla, **pv** prostatic vesicle, **px** pharynx, **rg** rhabditogen glands, **r** retractor muscle, **sb** subintestinal transverse muscles, **sd** sperm duct, **sg** shell glands, **sk** sunken longitudinal cutaneous muscles, **sm** spermatophore, **sn** subneural transverse muscles, **sp** supra-intestinal transverse muscles, **t** testis, **vi** vitellaria, **vn** ventral nerve plate.

underlain by circular muscle (40–48 µm thick, n = 2) with interspersed longitudinal fibers ectally. The inner pharyngeal epithelium is flat, ciliated, and underlain by a thin circular muscle (48–50 µm, n = 2). The pharynx presents numerous xanthophil, erythrophil and cyanophil gland cells.

The testes are mature, dorsal, arranged in four paramedian rows between the supra-intestinal transverse parenchymal muscle and the intestinal diverticula (Fig. 14B). They extend from the level of the ovaries (i.e., 7.7 mm behind the anterior extremity of the body, or 21% of body length, holotype) to the root of the pharynx (48%). Sperm ducts run immediately above the subintestinal parechymatic muscle layer. In their distal portion, they open into the respective branch of the prostatic vesicle (Fig. 15A–C). The prostatic vesicle is divided into two differentiated halves (Fig. 15A–D). The proximal half is extrabulbar and constituted by the two widened and rounded branches opening into a broadened, dish-shaped section located above the paired portion. The distal half is intrabulbar, dilated canal oriented dorso-posteriorly. The paired portion is lined with a cuboidal-to-columnar, ciliated epithelium, which is pierced by numerous gland cells producing fine erythrophil granules. The columnar epithelium of the dish-

shaped portion is pierced by very numerous gland cells producing erythrophil gross granules (1–2 μm); and by two types of scarce gland cells producing fine, erythrophil and xanthophil granules, respectively (Fig. 15D). The distal half is lined by a columnar, ciliated epithelium with a sinuous surface which is pierced by gland cells producing erythrophil granules along its whole length, and additionally a low number of gland cells producing xanthophil granules in its distal portion. The lining epithelium of the proximal half of the prostatic vesicle is coated by a 28–30 μm-thick (n = 2) circular muscle; the distal half is coated by a 1 μm-thick circular muscle, followed by a 22–25 μm-thick (n = 2) longitudinal muscle. The extrabulbar portion of the prostatic vesicle is coated by additional muscle fibers attaching it to the common muscle coat (Fig. 15A–C). The opening of the prostatic vesicle into the antero-dorsal region of the male atrium is wide, without an ejaculatory duct or penis papilla (Fig. 15A–C).

The male atrium is 5–6× longer than the female atrium, and divided into a dorsal, proximal narrow third, slightly folded, and a distal two-thirds portion with some smaller folds. A main, very large, oblique fold on each side of the body extends behind the gonopore level and over the female atrium (Fig. 15E). The male atrium is lined by a cuboidal, non-ciliated epithelium, and is underlain by a 30–60 μm-thick mixed layer of circular muscle with numerous interspersed longitudinal fibers (n = 2). The whole atrium receives two types of abundant gland cells producing erythrophil and cyanophil fine granules, respectively, and a third type of gland cells producing amorphous xanthophil secretion in the proximal third of the atrium.

The ovaries are mature, very elongated and placed above the ventral nerve plate at a distance from anterior tip of the body equal to 21% of body length (7.7 mm from anterior tip) (holotype). They present an anterior, ovoid section, 300 μm in length (F2424), and a posterior, 600 μm (F2424) long narrow section (Fig. 15E). Ovovitelline ducts emerge from the lateral aspect of the ovoid section of the ovaries and run ventrally. Lateral to the posterior section of the female atrium, the ovovitelline ducts run medially and dorsally, then unite posteriorly to the female atrium (Fig. 15C). The common glandular ovovitelline duct is 45–50 μm in length (n = 2) and runs ventro-anteriorly to communicate with the female genital canal. This canal runs slightly downwards and anteriorly, subsequently penetrates the common muscle coat to open into the female atrium. The female genital canal is lined by a cuboidal, ciliated epithelium.

The female atrium is dorso-ventrally compressed and wider towards the gonopore canal. It is placed below the posterior section of the male atrium (Fig. 15F), and is lined with a cuboidal non-ciliated epithelium. This epithelium is pierced by gland cells producing fine xanthophil granules. The lining epithelium of the female atrium is underlain by a 37 μm-thick layer of mixed circular and longitudinal muscle fibers (n = 2).

The common muscle coat is a very dense layer composed by variously oriented muscle fibers. The length:height ratio of the copulatory apparatus enveloped by the common muscle coat ranges between 2.5–2.8:1.

Remarks. *Ch. claudioi* Lago-Barcia & Carbayo, sp. nov. externally differs from most congeners in that the dorsum is composed of a light background color evenly covered with brown spots. However, this color pattern is so similar to *Ch. abaiba*, *Ch. agua*,

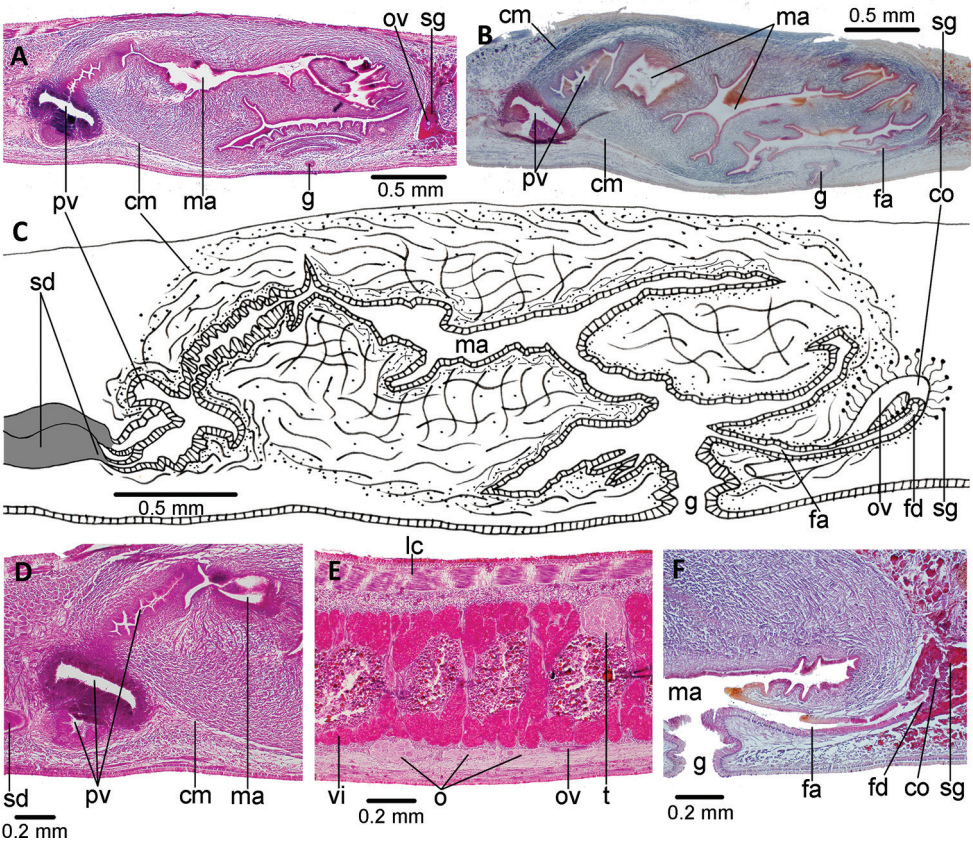

Figure 15. *Choeradoplana claudioi* Lago-Barcia & Carbayo, sp. nov. **A** photomicrograph of a sagittal section of the copulatory apparatus of holotype **B** photomicrograph of a sagittal section of the copulatory apparatus of paratype F2510 **C** diagrammatic representation of the copulatory apparatus of holotype **D** photomicrograph of a sagittal section of the prostatic vesicle of holotype **E** photomicrograph of a sagittal section of the ovarian region of holotype **F** photomicrograph of a sagittal section of the female atrium of holotype. Abbreviations: **cm** common muscle coat, **co** common glandular ovovitelline duct, **dd** decussate dorsal cutaneous muscles, **dm** diagonal decussate muscles, **e** eye, **ej** ejaculatory duct, **ep** esophagus, **er** erythrophil secretion, **fa** female atrium, **fd** female genital duct, **g** gonopore, **i** intestine, **lc** longitudinal cutaneous muscles, **ma** male genital atrium, **mk** Muskelgeflecht (Graff, 1899), **mo** mouth, **o** ovary, **ov** ovovitelline duct, **ph** pharyngeal pouch, **pp** penis papilla, **pv** prostatic vesicle, **px** pharynx, **rg** rhabditogen glands, **r** retractor muscle, **sb** subintestinal transverse muscles, **sd** sperm duct, **sg** shell glands, **sk** sunken longitudinal cutaneous muscles, **sm** spermatophore, **sn** subneural transverse muscles, **sp** supra-intestinal transverse muscles, **t** testis, **vi** vitellaria, **vn** ventral nerve plate.

Ch. banga, *Ch. iheringi*, and *Ch. pucupucu* that *Ch. claudioi* Lago-Barcia & Carbayo, sp. nov. cannot be confidently distinguished from them.

With respect to the internal morphology, *Ch. claudioi* Lago-Barcia & Carbayo, sp. nov. can be differentiated from most *Choeradoplana* species by the dish-shaped portion of the extrabulbar region of the prostatic vesicle. This attribute is only shared with *Ch. onae*

Lago-Barcia & Carbayo, sp. nov., *Ch. riutortae* Lago-Barcia & Carbayo, sp. nov., and *Ch. bocaina*. However, the female genital atrium is compressed dorso-ventrally and partially positioned below the distal section of the male atrium, which readily distinguishes *Ch. claudioi* Lago-Barcia & Carbayo, sp. nov. from these three other species.

Choeradoplana onae **Lago-Barcia & Carbayo, sp. nov.**

http://zoobank.org/0CBCD7FD-683B-4075-9D90-B3C62CB97631
Figures 16–18

Choeradoplana sp. in Álvarez-Presas et al. 2014.

Material examined. All specimens collected in the Reserva Biológica Augusto Ruschi, Santa Teresa, State of Espírito Santo, Brazil (-19.88, -40.54) by F. Carbayo and co-workers, 25–27 May 2008; ***Holotype*** **MZUSP PL 2270** (field code, F2414), transverse sections of the cephalic region on 8 slides; horizontal sections of the portion behind the cephalic region on 5 slides; sagittal sections of the ovarian region on 12 slides; horizontal sections of the testes on 10 slides; transverse sections of the pre-pharyngeal region on 9 slides; sagittal sections of the pharynx and copulatory apparatus on 12 slides; ***Paratype*** **MZUSP PL 2267** (field code, F2230), transverse sections of the cephalic region on 8 slides; sagittal sections of the pharynx and copulatory apparatus on 9 slides; ***Paratype*** **MZUSP PL 2268** (field code, F2281), sagittal sections of the pharynx and copulatory apparatus on 12 slides. ***Paratype*** **MZUSP PL** 2269 (field code, F2310), transverse sections of the cephalic region on 12 slides; horizontal sections of the ovarian region on 8 slides.

Distribution. Only known from the type locality, Reserva Biológica Augusto Ruschi, Santa Teresa, State of Espírito Santo, Brazil.

Etymology. The name *onae* is the affectionate nickname of the biologist Marta Álvarez-Presas (Bristol University). The specific epithet honors her for her contributions to understanding the systematics of free-living flatworms.

Diagnosis. *Choeradoplana* species with a light ivory background color and a wide sepia brown median band. The extrabulbar region of the prostatic vesicle has a dish-shaped portion. The copulatory apparatus is 3.8× longer than its height. The male atrium has 4–6 main folds.

Description. External aspect. Preserved specimens range between 41–44.5 mm in length and 3–4 mm (n = 4) in width. The body is slender and subcylindrical. The cephalic region is differentiated from the remaining body by a 'neck' and laterally dilated. This region is rolled up so that the ventral surface provided with two prominent glandular cushions is facing out when alive (Fig. 16A–C); the posterior extremity is pointed. The creeping sole is as wide as 85–87% of body width at the pre-pharyngeal region (n = 4). The mouth is positioned at a distance from the anterior extremity equal to 51% of body length, and the gonopore is 61% (paratype F2230).

The dorsal coloration of live specimens consists of a light ivory (RAL 1015) background color (Fig. 16A), covered on a wide median band with sepia brown pigment (RAL

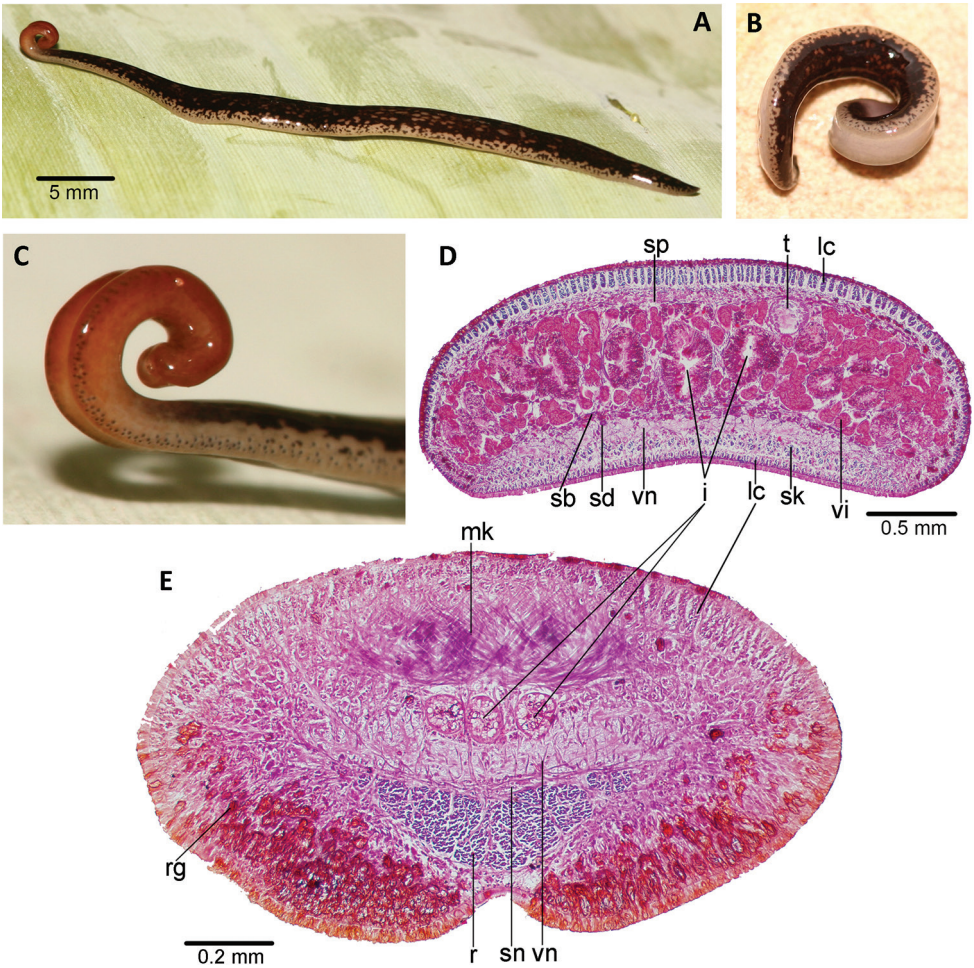

Figure 16. *Choeradoplana onae* Lago-Barcia & Carbayo, sp. nov. **A** dorsal view of the creeping live paratype F2230 **B** live paratype F2310 rolled up showing the ventral surface **C** lateral view of the cephalic region of live paratype F2230 **D** photomicrograph of a transverse section of the pre-pharyngeal region of holotype **E** photomicrograph of a transverse section of the cephalic region of holotype. Abbreviations: **cm** common muscle coat, **co** common glandular ovovitelline duct, **dd** decussate dorsal cutaneous muscles, **dm** diagonal decussate muscles, **e** eye, **ej** ejaculatory duct, **ep** esophagus, **er** erythrophil secretion, **fa** female atrium, **fd** female genital duct, **g** gonopore, **i** intestine, **lc** longitudinal cutaneous muscles, **ma** male genital atrium, **mk** Muskelgeflecht (Graff, 1899), **mo** mouth, **o** ovary, **ov** ovovitelline duct, **ph** pharyngeal pouch, **pp** penis papilla, **pv** prostatic vesicle, **px** pharynx, **rg** rhabditogen glands, **r** retractor muscle, **sb** subintestinal transverse muscles, **sd** sperm duct, **sg** shell glands, **sk** sunken longitudinal cutaneous muscles, **sm** spermatophore, **sn** subneural transverse muscles, **sp** supra-intestinal transverse muscles, **t** testis, **vi** vitellaria, **vn** ventral nerve plate.

8014), except for irregular clear spots with the background color exposed. The bordering line of the band merging with the background color on the sides is irregular with large sepia brown spots. The curled anterior extremity is red orange (RAL 2001). The ventral surface is red orange in the cephalic region, and light grey (RAL 7035) in the rest of body (Fig. 16B).

The eyes are devoid of halos, and formed by a one-pigmented cup of 60 µm in diameter. Eyes are absent in the very anterior extremity of the body equivalent to 1% of the body length (n = 1). Eyes behind the anterior tip are distributed marginally in a row of two or three eyes (Fig. 5C) and extend along the entire body until the posterior end.

Sensory pits are 20–25 µm deep in a uniserial ventro-lateral row, starting from 0.4 mm behind the anterior extremity, the equivalent of 1% body length to at least 80 mm from the anterior tip (20% of body length, n = 1).

Rhabditogen gland cells pierce the marginal epidermis in the pre-pharyngeal region. Erythrophil granules and scarce cyanophil granules are discharged through the entire epidermis. There is no glandular margin (Fig. 16D).

The cutaneous musculature consists of a subepithelial circular muscle, followed by a diagonal layer with decussate fibers, and a strong longitudinal muscle organized in bundles (Fig. 16D). This longitudinal muscle is 90–100 µm thick dorsally, and organized in tight bundles with > 32–60 fibers each; it is ventrally divided into a 30–32.5 µm-thick muscle organized in bundles with 5–11 fibers each, and a 75 µm-thick muscle sunken into the parenchyma, and constituted of bundles with 8–27 fibers each (Fig. 16D). The thickness of the cutaneous muscle coat is 18–20% (n = 4) of the body height.

In the pre-pharyngeal region, there are three parenchymal muscles, namely a dorsal decussate muscle (40–50 µm thick), a transverse supra-intestinal muscle (15 µm); and transverse subintestinal muscle (18–20 µm) (n = 4) (Fig. 16D).

The cutaneous and parenchymal musculature is organized in the cephalic region as in *Ch. iheringi*. The muscle retractor of the head is delta-shaped in a cross-section along 2.5 mm (or 6% of body length) from behind, 0.9 mm (or 2%) anterior extremity of the body (Fig. 16E), and its thickness equals 19% of the height of the cephalic region. The Muskelgeflecht is 160–180 µm thick (23% of body height). The subneural parenchymal muscle consists of a number of transverse fibers; this muscle is weak in the ovarian region. Glandular cushions are composed of numerous rhabditogen cells (Fig. 16E).

The mouth is located in the middle of the pharyngeal pouch (n = 4) (Fig. 17A, B). The pharynx is bell-shaped with its dorsal insertion at mouth level (n = 4). The esophagus is as long as 15% of the pharyngeal length. The pharyngeal pouch is lined with a non-ciliated, low epithelium underlain by a one-fiber thick longitudinal muscle followed by a 10 µm-thick circular muscle. The outer pharyngeal epithelium is flat, ciliated, and underlain by a 5 µm-thick longitudinal muscle followed by a 15 µm-thick circular muscle. The inner pharyngeal epithelium is flat and ciliated, and is underlain by a mixed circular muscle with longitudinal fibers (80 µm thick). The pharynx has numerous interspersed erythrophil and xanthophil gland cells.

The testes are mature, dorsally located under the supra-intestinal transverse parenchymal muscle, placed between the intestinal diverticula. They extend from 13.2 mm (32% of body length, holotype) from the anterior extremity to 0.2 mm of the root of the pharynx (63%, holotype). Sperm ducts bend dorsally and medially immediately above the subintestinal parechymatic muscle layer to open into the respective dilated

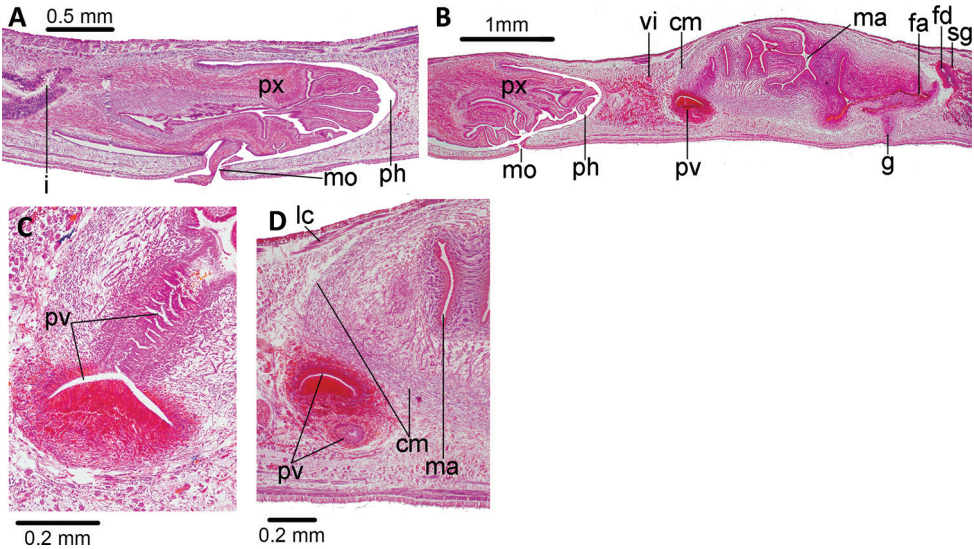

Figure 17. *Choeradoplana onae* Lago-Barcia & Carbayo, sp. nov. Photomicrographs of sagittal sections **A** pharynx of paratype F2230 **B** pharynx and copulatory apparatus of holotype **C** prostatic vesicle of paratype F2230 **D** prostatic vesicle of holotype. Abbreviations: **cm** common muscle coat, **co** common glandular ovovitelline duct, **dd** decussate dorsal cutaneous muscles, **dm** diagonal decussate muscles, **e** eye, **ej** ejaculatory duct, **ep** esophagus, **er** erythrophil secretion, **fa** female atrium, **fd** female genital duct, **g** gonopore, **i** intestine, **lc** longitudinal cutaneous muscles, **ma** male genital atrium, **mk** Muskelgeflecht (Graff, 1899), **mo** mouth, **o** ovary, **ov** ovovitelline duct, **ph** pharyngeal pouch, **pp** penis papilla, **pv** prostatic vesicle, **px** pharynx, **rg** rhabditogen glands, **r** retractor muscle, **sb** subintestinal transverse muscles, **sd** sperm duct, **sg** shell glands, **sk** sunken longitudinal cutaneous muscles, **sm** spermatophore, **sn** subneural transverse muscles, **sp** supra-intestinal transverse muscles, **t** testis, **vi** vitellaria, **vn** ventral nerve plate.

branch of the prostatic vesicle. The prostatic vesicle is divided into two halves (Fig. 17C). The anterior half is extrabulbar and proximally presents a dilated and paired tubular portion oriented vertically which opens into a broadened, dish-shaped section located above the paired portion. This proximal half is lined by a columnar-to-cuboidal epithelium that is pierced by gland cells producing xanthophil granules. These gland cells are much more abundant in the dish-shaped portion and present a strongly reddish appearance; the ventral face and the border of this dish-shaped section of the prostatic vesicle is also pierced by gland cells producing cyanophil granules. The distal half is an intrabulbar dilated canal oriented dorso-posteriorly. It is lined by a columnar epithelium with a sinuous surface that is pierced by gland cells producing cyanophil granules along its whole length and additionally gland cells producing xanthophil granules in its distal portion. The lining epithelium of the proximal half of prostatic vesicle is coated by an 18–20 µm-thick circular muscle layer, while it is coated by a 1 µm-thick circular muscle in the distal half, followed by a 15 µm-thick longitudinal muscle (n = 4). The extrabulbar portion of the prostatic vesicle is coated by additional muscle fibers attaching it to the common muscle coat (Fig. 17D). The opening of the

prostatic vesicle into the antero-dorsal region of the male atrium is wide, without an ejaculatory duct or penis papilla (Fig. 18A–C).

The male atrium is long, 5× as long as the female atrium, with the same height along its length and 4–6 large transverse folds narrowing its lumen. The male atrium is lined by a cuboidal, non-ciliated epithelium, and is underlain by a 40–70 μm-thick circular muscle with numerous interspersed longitudinal fibers (n = 4). The proximal two thirds of the atrium receive two types of abundant gland cells producing xanthophil and erythrophil granules, respectively, and a third type of scarce gland cells producing amorphous xanthophil secretion; the distal third of the male atrium receives abundant gland cells producing erythrophil granules. The sub-apical portion of the cells of the lining epithelium of this distal third contains xanthophil granules.

The ovaries are mature, ovoid, 250 μm in length, placed above the ventral nerve plate and at a distance from the anterior tip of the body equal to 28% of body length (11.8 mm from the anterior tip) (n = 1). Ovovitelline ducts emerge from the dorsolateral aspect of the ovaries and run ventrally. Ovovitelline ducts run medially and dorsally lateral to the posterior section of the female atrium, then unite above the postero-dorsal section of the female atrium (Fig. 18A–C). The common glandular ovovitelline duct length ranges between 25–150 μm in length (n = 4) and runs ventrally or ventro-posteriorly to communicate with the female genital canal. This canal runs downwards, and subsequently penetrates the common muscle coat to open into the posterior section of the female atrium. The genital canal is lined by a cuboidal, ciliated epithelium, and the sub-apical portion of its lining cells is stained reddish.

The female atrium is funnel-shaped, and is lined with a 50 μm high epithelium, which is pierced by gland cells producing fine erythrophil granules. The subapical portion of the lining cells contains xanthophil granules. The lining epithelium of the female atrium is underlain by a 1-fiber-thick longitudinal muscle, followed by a 10 μm-thick layer of decussate muscle fibers. Paratype F2281 presents a female atrium smaller than that of the remaining specimens and also bears a spermatophore at the entrance of the gonopore canal. This spermatophore is ovoid, and with approximately 100 μm in maximum diameter. It is constituted on an inner mass of sperm surrounded by a thin fibrous, erythrophil layer, external to which is a gross layer of xanthophil, granular secretion and a bluish fine granular secretion, each prevailing on one side of the spermatophore (Fig. 18D).

The common muscle coat is a very dense layer composed by variously oriented muscle fibers. The length:height ratio of the copulatory apparatus enveloped by the common muscle coat ranges between 2.5–3.3:1 (n = 3).

Remarks. The species described herein matches all diagnostic characteristics of *Choeradoplana*. As reported for *Ch. claudioi* Lago-Barcia & Carbayo, sp. nov., *Ch. onae* Lago-Barcia & Carbayo, sp. nov. only resembles *Ch. abaiba*, *Ch. agua*, *Ch. banga*, *Ch. iheringi*, *Ch. claudioi* Lago-Barcia & Carbayo, sp. nov., and *Ch. pucupucu* in the body color. The great similarity between them hinders confident identification. However, none of them present the prominent cushions found in this species with a red-orange color.

With respect to the internal morphology, *Ch. onae* Lago-Barcia & Carbayo, sp. nov. only compares with *Ch. riutortae* Lago-Barcia & Carbayo, sp. nov. and *Ch. bocai-*

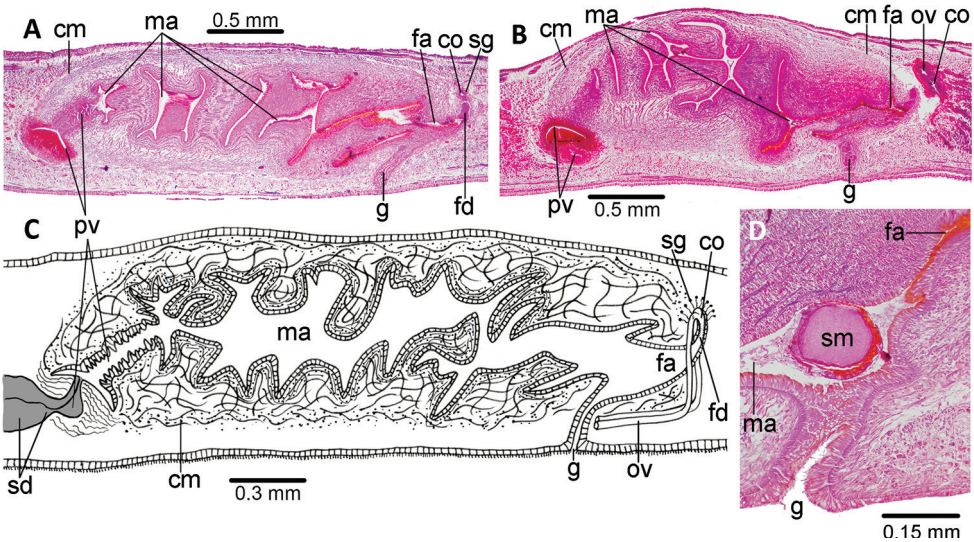

Figure 18. *Choeradoplana onae* Lago-Barcia & Carbayo, sp. nov. **A** photomicrograph of a sagittal section of the copulatory apparatus of paratype F2230 **B** photomicrograph of a sagittal section of the copulatory apparatus of holotype **C** diagrammatic representation of the copulatory apparatus of paratype F2230 **D** photomicrograph of a sagittal section of the entrance of the gonopore of paratype F2281 housing a spermatophore. Abbreviations: **cm** common muscle coat, **co** common glandular ovovitelline duct, **dd** decussate dorsal cutaneous muscles, **dm** diagonal decussate muscles, **e** eye, **ej** ejaculatory duct, **ep** esophagus, **er** erythrophil secretion, **fa** female atrium, **fd** female genital duct, **g** gonopore, **i** intestine, **lc** longitudinal cutaneous muscles, **ma** male genital atrium, **mk** Muskelgeflecht (Graff, 1899), **mo** mouth, **o** ovary, **ov** ovovitelline duct, **ph** pharyngeal pouch, **pp** penis papilla, **pv** prostatic vesicle, **px** pharynx, **rg** rhabditogen glands, **r** retractor muscle, **sb** subintestinal transverse muscles, **sd** sperm duct, **sg** shell glands, **sk** sunken longitudinal cutaneous muscles, **sm** spermatophore, **sn** subneural transverse muscles, **sp** supraintestinal transverse muscles, **t** testis, **vi** vitellaria, **vn** ventral nerve plate.

na in that they also present a dish-shaped prostatic vesicle. However, the length:height ratio of the copulatory apparatus in these species is 2.6:1 (vs. 3.8:1 in *Ch. onae* Lago-Barcia & Carbayo, sp. nov.); the male atrium:female atrium ratio in *Ch. bocaina* and *Ch. riutortae* Lago-Barcia & Carbayo, sp. nov. ratio ranges between 1:1–3:1 (Carbayo & E. M. Froehlich, 2012), whereas it is ~5:1 in *Ch. claudioi* Lago-Barcia & Carbayo, sp. nov. and *Ch. onae* Lago-Barcia & Carbayo, sp. nov., and the male atrium presents 1–2 large folds (vs. 4–6 in *Ch. onae* Lago-Barcia & Carbayo, sp. nov.).

Choeradoplana riutortae Lago-Barcia & Carbayo, sp. nov.

http://zoobank.org/DDF3C826-CC45-4D40-8438-602D8BC687CF
Figures 19–22

Material examined. All specimens were collected in the Parque Nacional da Serra dos Orgãos, Teresópolis, State of Rio de Janeiro, Brazil (-22.48, -43.06) by F. Carbayo and co-workers, January 6th, 2010. ***Holotype*** **MZUSP 2274** (field code, F4218), transverse

sections of the cephalic region on 5 slides; horizontal sections of the portion behind the cephalic region on 6 slides; sagittal sections of ovarian region on 6 slides; horizontal sections of the testes on 4 slides; transverse sections of the pre-pharyngeal region on 7 slides; sagittal sections of the pharynx and copulatory apparatus on 9 slides. ***Paratype* MZUSP PL 1174** (field code, F4217), transverse sections of the cephalic region on 9 slides; horizontal sections of the ovarian region on 7 slides; transverse sections of the pre-pharyngeal region on 8 slides; sagittal sections of the pharynx and copulatory apparatus on 12 slides. ***Paratype* MZUSP PL 2275** (field code, F4261), transverse sections of the pre-pharyngeal region on 16 slides; sagittal sections of the pharynx and copulatory apparatus on 27 slides.

Distribution. Only known from the type locality, Parque Nacional da Serra dos Orgãos, municipality of Teresópolis, State of Rio de Janeiro, Brazil.

Etymology. The specific epithet honors Prof. Marta Riutort for her contributions to understanding the evolution of flatworms.

Diagnosis. *Choeradoplana* species with a light ivory background color covered by numerous sepia brown spots except for the anterior extremity which is red orange. The ventral surface is pale orange in the cephalic region, and light grey in the rest of the body. Part of the longitudinal cutaneous musculature is sunken in the parenchyma of the ventral side. The prostatic vesicle has a paired extrabulbar dish-shaped portion, and an elongated intrabulbar portion with an irregular epithelium. It has a short copulatory apparatus (the length:height ratio of the copulatory apparatus is 2.6:1). The male atrium presents the same size as the female atrium.

Description. The preserved animals measure between 37–42 mm in length and 2.5–3 mm in width (n = 3). The body is slender and subcylindrical. The cephalic region is differentiated from the remaining body by a 'neck', laterally dilated and rolled up so that the ventral surface, provided with prominent glandular cushions, is facing out (Fig. 19A–C); the posterior extremity is pointed. The creeping sole is as wide as 72–75% of body width in the pre-pharyngeal region (n = 3). The mouth is positioned at a distance from the anterior extremity equal to 63–67% of body length, and the gonopore is 72–78% (n = 3).

The dorsal coloration in live specimens consists of a light ivory (RAL 1015) background color, with numerous sepia brown (RAL 8014) spots which are more (F4218) or less (F4217) merged with each other, with the latter situation presenting a somewhat homogeneous aspect. A midline with the background color may extend along the body length (paratype F4217) or is restricted to the anterior region of the body (paratype F4261). The spots extend to the body sides, where they are scattered so as to create an irregular bordering line, followed by the background color of the sides of the body. A curled anterior extremity is red orange (RAL 2001). The ventral surface is pale red orange in the cephalic region, and light grey (RAL 7035) in the rest of the body (Fig. 19B).

The eyes are formed by a one-pigmented cup of 46–50 μm in diameter. There are no halos around them. Eyes are absent in the very anterior extremity of the body equivalent to 1% of the body length (F4218). Eyes behind the anterior tip are distrib-

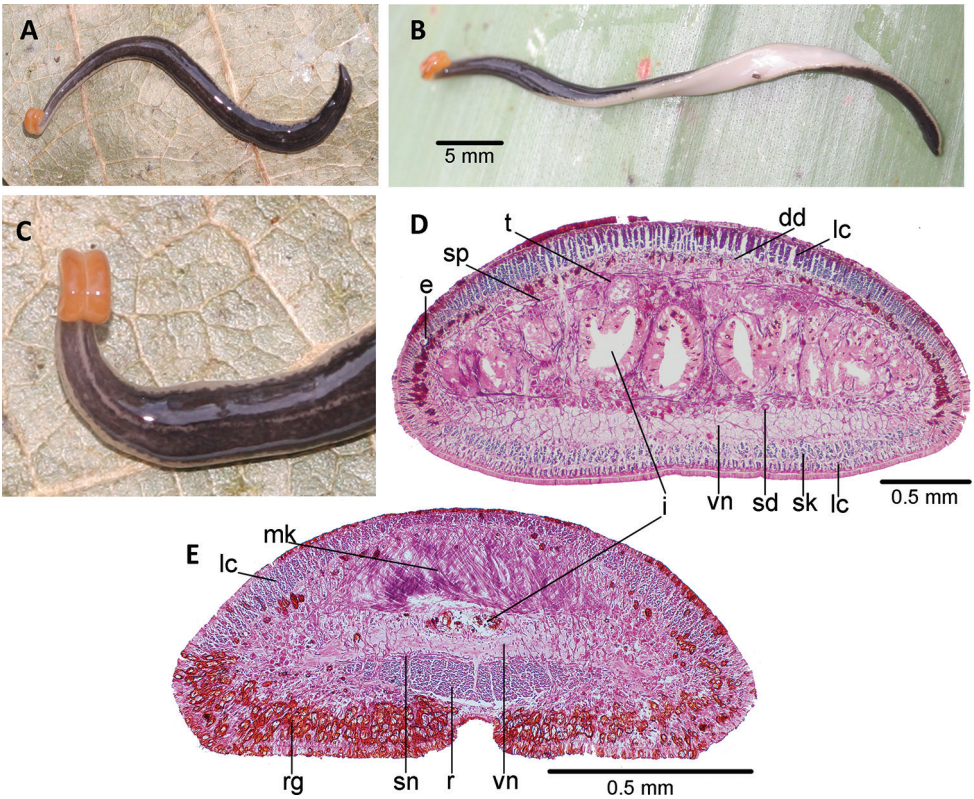

Figure 19. *Choeradoplana riutortae* Lago-Barcia & Carbayo, sp. nov. **A** dorsal view of the creeping live paratype F4217 **B** the live holotype twisted showing the ventral surface **C** dorsal view of the anterior region of paratype F4217 **D** photomicrograph of a transverse section of the pre-pharyngeal region of holotype **E** photomicrograph of a transverse section of the cephalic region of holotype. Abbreviations: **cm** common muscle coat, **co** common glandular ovovitelline duct, **dd** decussate dorsal cutaneous muscles, **dm** diagonal decussate muscles, **e** eye, **ej** ejaculatory duct, **ep** esophagus, **er** erythrophil secretion, **fa** female atrium, **fd** female genital duct, **g** gonopore, **i** intestine, **lc** longitudinal cutaneous muscles, **ma** male genital atrium, **mk** Muskelgeflecht (Graff, 1899), **mo** mouth, **o** ovary, **ov** ovovitelline duct, **ph** pharyngeal pouch, **pp** penis papilla, **pv** prostatic vesicle, **px** pharynx, **rg** rhabditogen glands, **r** retractor muscle, **sb** subintestinal transverse muscles, **sd** sperm duct, **sg** shell glands, **sk** sunken longitudinal cutaneous muscles, **sm** spermatophore, **sn** subneural transverse muscles, **sp** supra-intestinal transverse muscles, **t** testis, **vi** vitellaria, **vn** ventral nerve plate.

uted marginally in a row of two or three eyes and extend along the entire body until the posterior extremity.

Sensory pits are 15 µm deep, distributed ventro-laterally in a uniserial row initiating 0.3 mm behind the anterior extremity (the equivalent of 1% of the body length in paratype F4217), and from the very anterior tip in holotype.

In the pre-pharyngeal region, very abundant rhabditogen gland cells pierce the dorsal and marginal epidermis. These types of cells are scarce on the ventral epidermis;

instead, there are gland cells producing erythrophil granules and scarce gland cells secreting cyanophil granules. There is no glandular margin (Fig. 19D).

The cutaneous musculature of the pre-pharyngeal region consists of a subepithelial circular muscle, followed by a diagonal layer with decussate fibers, and a longitudinal muscle organized in bundles (Fig. 19D). This longitudinal muscle is 80–100 µm-thick dorsally and organized in tight bundles with approximately 60–110 fibers each; it is ventrally divided into a 28–30 µm-thick muscle organized in bundles with 10–27 fibers each, and a 55–65 µm-thick muscle sunken into the parenchyma and constituted of bundles with 18–40 fibers each (Fig. 19D). The thickness of the cutaneous muscle coat is 22–25% (n = 3) of the body height. There are three parenchymal muscles in the pre-pharyngeal region, namely a dorsal decussate muscle (46–50 µm thick), transverse supra-intestinal muscle (25–30 µm), and transverse subintestinal muscle (70–75 µm) (n = 3) (Fig. 19D).

The cutaneous and parenchymal musculature is organized in the cephalic region as in *Ch. iheringi*. A portion of the retractor muscle of the head is delta-shaped in a cross-section and ranges between 2–5 mm (or 5–14% of body length) from behind, 1–1.3 mm (2–3%) of the anterior extremity of the body (Fig. 19E), and its thickness equals 36% of the height of the cephalic region. The Muskelgeflecht is 200–210 µm thick (30% of body height). The subneural parenchymal muscle consists of transverse fibers. Glandular cushions are composed of very numerous rhabditogen cells and scarce gland cells produce erythrophil granules (Fig. 19E).

The mouth is located in the middle of the pharyngeal pouch (n = 3) (Fig. 20A). The pharynx is bell-shaped, and has its dorsal insertion shifted posteriorly with the equivalent to 44% of the pharynx length. The esophagus length is 20% of the pharyngeal length. The pharyngeal pouch is lined with a non-ciliated, low epithelium underlain by a one-fiber-thick layer of longitudinal muscle followed by 20 µm-thick layer of circular muscle. The outer pharyngeal epithelium is flat, ciliated, and underlain by a one-fiber-thick longitudinal muscle, followed by a 15 µm-thick muscle with some longitudinal fibers interspersed. The inner pharyngeal epithelium is flat, ciliated, and underlain by a mixed layer of circular muscle with longitudinal muscle (75 µm thick). The pharynx presents numerous erythrophil and xanthophil gland cells interspersed.

The testes are mature and dorsally located under the supra-intestinal transverse muscle layer, mostly placed between the intestinal diverticula. They extend from 12.7 mm (30% of body length, holotype) of the anterior extremity of the body to 0.5 mm before the root of the pharynx. Sperm ducts run immediately above the subintestinal parechymatic muscle layer. The sperm ducts bend dorsally close to the copulatory apparatus, and subsequently penetrate the ventral proximal region of the common muscle coat to open into the respective dilated branch of the prostatic vesicle (Fig. 20B). The prostatic vesicle is divided into two differentiated halves; the anterior half proximally presents a dilated and paired portion oriented vertically which opens into a broadened, dish-shaped section located above the paired portion (Figs 20B, 21A, B). This proximal half is extrabulbar and lined by a columnar-to-cuboidal epithelium which is pierced by gland cells producing xanthophil granules. These gland cells are much more abundant

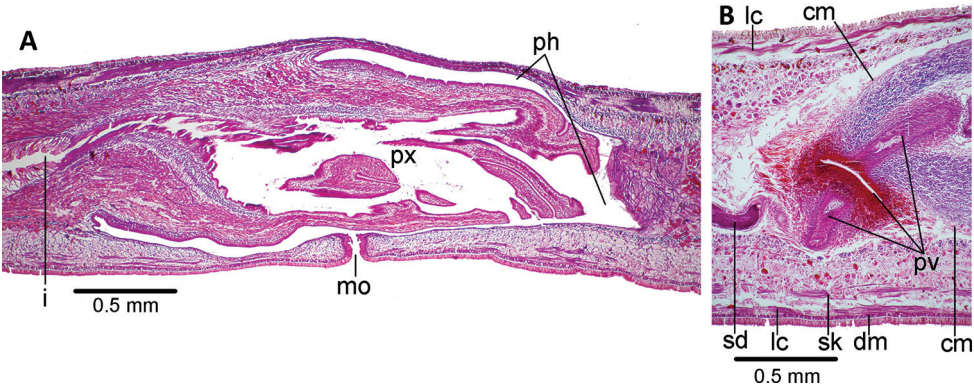

Figure 20. *Choeradoplana riutortae* Lago-Barcia & Carbayo, sp. nov., holotype. Photomicrographs of sagittal sections **A** pharynx **B** prostatic vesicle. Abbreviations: **cm** common muscle coat, **co** common glandular ovovitelline duct, **dd** decussate dorsal cutaneous muscles, **dm** diagonal decussate muscles, **e** eye, **ej** ejaculatory duct, **ep** esophagus, **er** erythrophil secretion, **fa** female atrium, **fd** female genital duct, **g** gonopore, **i** intestine, **lc** longitudinal cutaneous muscles, **ma** male genital atrium, **mk** Muskelgeflecht (Graff, 1899), **mo** mouth, **o** ovary, **ov** ovovitelline duct, **ph** pharyngeal pouch, **pp** penis papilla, **pv** prostatic vesicle, **px** pharynx, **rg** rhabditogen glands, **r** retractor muscle, **sb** subintestinal transverse muscles, **sd** sperm duct, **sg** shell glands, **sk** sunken longitudinal cutaneous muscles, **sm** spermatophore, **sn** subneural transverse muscles, **sp** supra-intestinal transverse muscles, **t** testis, **vi** vitellaria, **vn** ventral nerve plate.

in the dish-shaped portion, and present a reddish appearance; the border of this dish-shaped section of the prostatic vesicle is also pierced by gland cells producing cyanophil granules. The distal half is intrabulbar, and is a straight tube running postero-dorsally to open into the proximal region of the male atrium. This half is lined by a columnar epithelium with a sinuous surface which is pierced along its whole length by gland cells producing cyanophil granules; additionally, gland cells producing xanthophil granules pierce its distal portion. The lining epithelium of the proximal half of the prostatic vesicle is coated by a 20 µm-thick circular muscle; the distal half is coated by a 1 µm-thick circular muscle, followed by a 15 µm-thick longitudinal muscle. The male atrium is the same size as the female atrium, and is divided into a proximal, narrow half and a distal, dilated half with some small folds (Figs 21, 22).

The male atrium is lined by a cuboidal, non-ciliated epithelium, and underlain by a 45–80 µm-thick layer of circular muscle with numerous interspersed longitudinal fibers (n = 3). The proximal half of the atrium receives two types of gland cells, one producing erythrophil granules, and a second type of scarce gland cells producing xanthophil granules; the distal half of the male atrium receives abundant gland cells producing xanthophil granules and the sub-apical portion of the cells of the lining epithelium contains xanthophil granules. The extrabulbar portion of the prostatic vesicle is coated by additional muscle fibers attaching it to the common muscle coat (Figs 21, 22).

The ovaries are mature, ovoid, 190 µm in length, and placed above the ventral nerve plate, and at a distance from the anterior body tip equal to 27% of body length (11.5

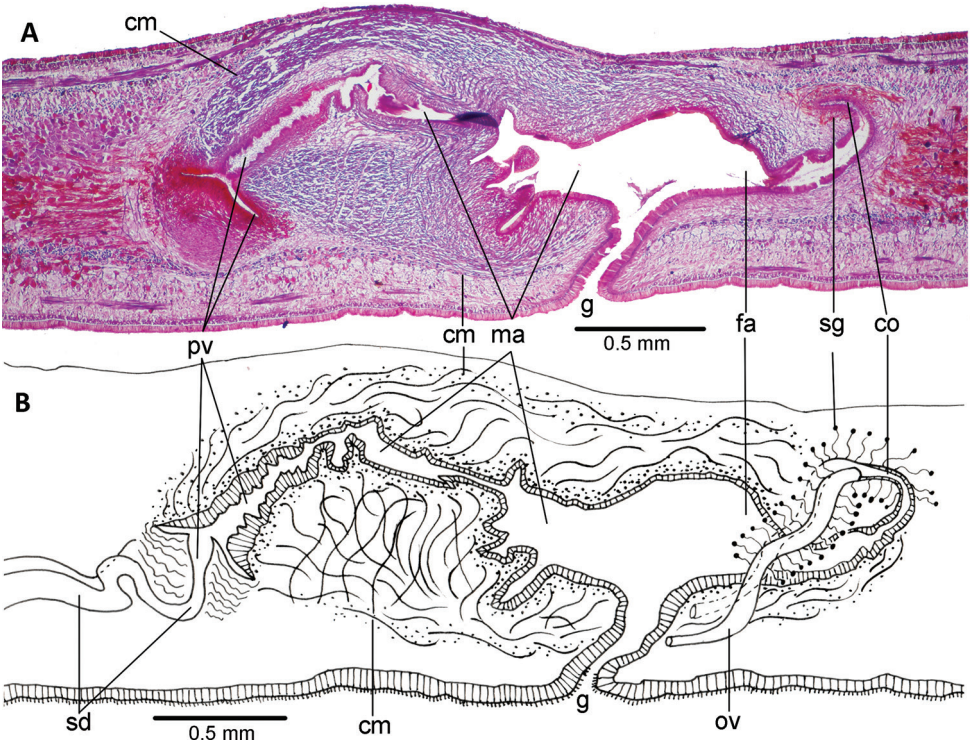

Figure 21. *Choeradoplana riutortae* Lago-Barcia & Carbayo, sp. nov., holotype **A** photomicrograph of a sagittal section of the copulatory apparatus **C** Diagrammatic representation of the copulatory apparatus. Abbreviations: **cm** common muscle coat, **co** common glandular ovovitelline duct, **dd** decussate dorsal cutaneous muscles, **dm** diagonal decussate muscles, **e** eye, **ej** ejaculatory duct, **ep** esophagus, **er** erythrophil secretion, **fa** female atrium, **fd** female genital duct, **g** gonopore, **i** intestine, **lc** longitudinal cutaneous muscles, **ma** male genital atrium, **mk** Muskelgeflecht (Graff, 1899), **mo** mouth, **o** ovary, **ov** ovovitelline duct, **ph** pharyngeal pouch, **pp** penis papilla, **pv** prostatic vesicle, **px** pharynx, **rg** rhabditogen glands, **r** retractor muscle, **sb** subintestinal transverse muscles, **sd** sperm duct, **sg** shell glands, **sk** sunken longitudinal cutaneous muscles, **sm** spermatophore, **sn** subneural transverse muscles, **sp** supra-intestinal transverse muscles, **t** testis, **vi** vitellaria, **vn** ventral nerve plate.

mm from anterior tip) (holotype). Ovovitelline ducts emerge from the dorso-lateral aspect of the ovaries and run above the ventral nerve plate. Lateral to the female atrium, the ovovitelline ducts bend medially and dorsally, then unite above the postero-dorsal section of the female atrium (Figs 21, 22). The common glandular ovovitelline duct is outside the common muscle coat, and runs posteriorly, progressively inclining to the ventral side to communicate with the posterior section of the female atrium.

The female atrium is divided into a dilated canal running ventro-anteriorly and outside the common muscle coat, and a distal, funnel-shaped half is widely communicated with the male atrium (Figs 21, 22). The female atrium is lined with a 35 µm high epithelium. This epithelium is pierced by gland cells producing fine erythrophil

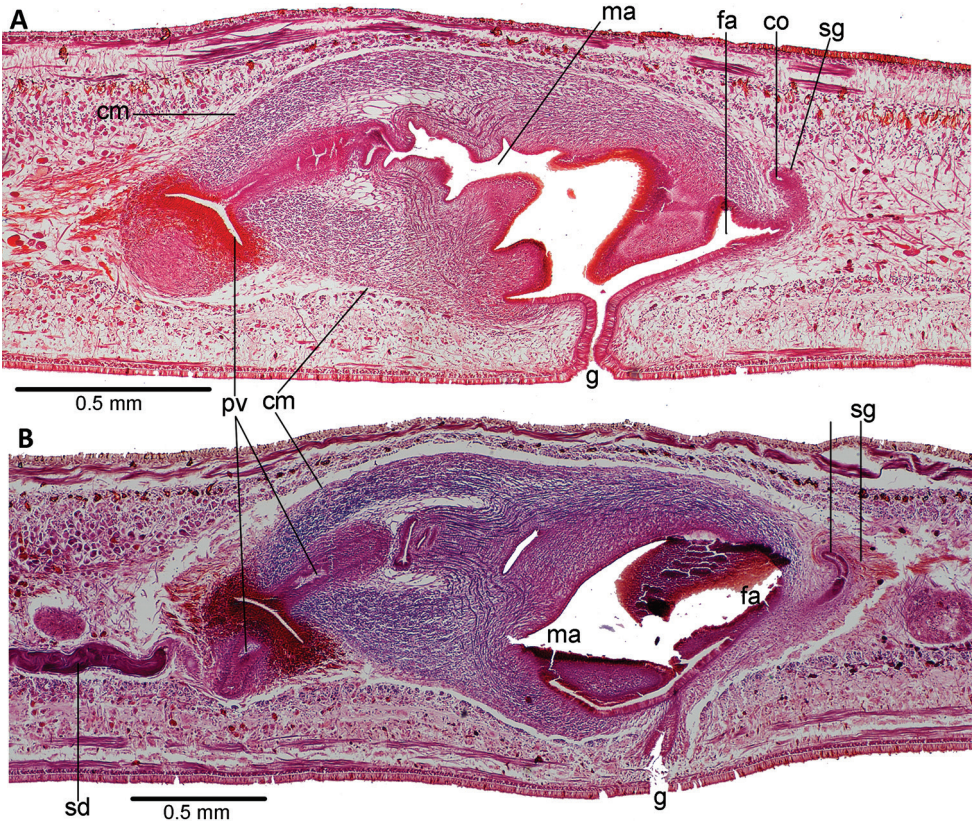

Figure 22. *Choeradoplana riutortae* Lago-Barcia & Carbayo, sp. nov. Photomicrographs of sagittal sections **A** copulatory apparatus of paratype F4217 **B** copulatory apparatus of paratype F4261. Abbreviations: **cm** common muscle coat, **co** common glandular ovovitelline duct, **dd** decussate dorsal cutaneous muscles, **dm** diagonal decussate muscles, **e** eye, **ej** ejaculatory duct, **ep** esophagus, **er** erythrophil secretion, **fa** female atrium, **fd** female genital duct, **g** gonopore, **i** intestine, **lc** longitudinal cutaneous muscles, **ma** male genital atrium, **mk** Muskelgeflecht (Graff, 1899), **mo** mouth, **o** ovary, **ov** ovovitelline duct, **ph** pharyngeal pouch, **pp** penis papilla, **pv** prostatic vesicle, **px** pharynx, **rg** rhabditogen glands, **r** retractor muscle, **sb** subintestinal transverse muscles, **sd** sperm duct, **sg** shell glands, **sk** sunken longitudinal cutaneous muscles, **sm** spermatophore, **sn** subneural transverse muscles, **sp** supra-intestinal transverse muscles, **t** testis, **vi** vitellaria, **vn** ventral nerve plate.

granules. The subapical portion of lining cells of the distal half of the atrium contains xanthophil granules. The lining epithelium of the female atrium is underlain by a layer of mixed circular and longitudinal fibers 10 µm high.

The common muscle coat is a very dense layer composed by densely packed muscle fibers variously oriented (Figs 21, 22). The length:height ratio of the copulatory apparatus enveloped by the common muscle coat ranges between 2.2–2.7:1 (n = 3).

Remarks. *Choeradoplana riutortae* Lago-Barcia & Carbayo, sp. nov. matches all diagnostic characteristics of *Choeradoplana*. The external dorsal coloration resembles

11 species inside the genus with the background color being brownish with dark black or dark brown spots over it, namely *Choeradoplana abaiba*, *Ch. agua*, *Ch. banga*, *Ch. benyai*, *Ch. bocaina*, *Ch. cyanoatria*, *Ch. longivesicula*, *Ch. pucupucu*, and the herein described *Ch. onae* Lago-Barcia & Carbayo, sp. nov., *Ch. eudoxiae* Silva & Carbayo, sp. nov. and *Ch. claudioi* Lago-Barcia & Carbayo, sp. nov. However, none of them present the prominent cushions found in this species, nor the conspicuous red-orange coloration of the cephalic region.

With respect to the internal morphology, *Ch. riutortae* Lago-Barcia & Carbayo, sp. nov. is only similar to *Ch. onae* Lago-Barcia & Carbayo, sp. nov., *Ch. bocaina* and *Ch. claudioi* Lago-Barcia & Carbayo, sp. nov. in that the extrabulbar section of the prostatic vesicle is dish-shaped. However, the female atrium in *Ch. claudioi* Lago-Barcia & Carbayo, sp. nov. is partially below the male one (vs. behind, in *Ch. riutortae* Lago-Barcia & Carbayo, sp. nov.), whereas the male atrium in *Ch. onae* Lago-Barcia & Carbayo, sp. nov. has the same height along its length, (vs. a proximal, narrow half, and a distal, widened half). Finally, the male atrium in *Ch. bocaina* is 3× as long as the female, whereas this ratio is 1.2 in *Ch. riutortae* Lago-Barcia & Carbayo, sp. nov.

Discussion

The monophyletic origin of the genus *Choeradoplana* was first demonstrated by Carbayo et al. (2013), and subsequently by Lemos et al. (2014) and Carbayo et al. (2018) with additional terminals and species. All species were recovered as monophyletic, perhaps with the exception of *Ch. bocaina*. The clade which includes the three type specimens of *Ch. bocaina* also houses two individuals not studied morphologically which were collected in the Reserva Biológica Augusto Ruschi, ES (500 km distance from the type locality). These two individuals are terminals with long internal branches. In agreement with this view, Carbayo et al. (2018) found uneven molecular delimitations of species depending on the method applied. Interestingly, although the species interrelationships are poorly supported, the species composition of the two large clades is similar to the phylogeny inferred from five mitochondrial and nuclear concatenated genes by Carbayo et al. (2018).

Choeradoplana is one among the few geoplanid genera which can be recognized through the body shape. The cephalic region in this genus is typically rolled up and the ventral surface of it is provided with glandular cushions, separated by a longitudinal groove. However, as shown above, the cephalic region of *Ch. albonigra* and *Ch. eudoxiae* Silva & Carbayo, sp. nov. lack the glandular cushions and it is not expanded laterally. In this respect, these two species cannot be distinguished from *Cephaloflexa*. Moreover, the anterior third of the body in *Ch. albonigra* narrows very gradually as in *Cephaloflexa*. Therefore, assignment to a genus must be based on internal aspects of these two species.

Another interesting observation is the distribution of the sensory pits. Following the diagnosis of *Choeradoplana*, these pits occur along a variable portion of the

anterior region of the body, but they are absent in the apex (a feature also shared with *Cephaloflexa*). However, sensory pits in *Ch. riutortae* Lago-Barcia & Carbayo, sp. nov. contour the anterior extremity in one of the two examined specimens. Since the sensory pits in the apex are not present in all specimens, it can be interpreted as a deviant individual situation.

The diagnosis of *Choeradoplana* was emended by Froehlich (1955), Ogren and Kawakatsu (1990), and Carbayo and Froehlich (2012) and as a consequence of the morphological variations reported in this paper, we propose to emend the genus as follows (emendation underlined):

Geoplaninae of elongated subcylindrical body. The cephalic region is kept rolled up and backwards; this region usually presents two glandular cushions, ventrally separated by a longitudinal groove. The cephalic region may be laterally dilated giving rise to a "neck" which differentiates this region from the remaining body. Eyes absent in the apex. Sensory pits absent in the apex. Broad creeping sole, more than one-third of body width. Strong cutaneous longitudinal muscles partially sunken into the parenchyma, exclusively ventrally or, more rarely, ventrally and dorsally too. Anteriorly all sunken ventral longitudinal fibers are medially concentrated, constituting the retractor unroller of the cephalic extremity. Bodies of rhabditogen cells located between the retractor and the epidermis. Common glandular ovovitelline duct approaching female genital canal dorsally from anterior direction, more rarely approaching behind the female atrium from the ventral direction.

Four of the six species studied in this paper (not *Ch. albonigra* and *Ch. eudoxiae* Silva & Carbayo, sp. nov.) present the external and internal characteristics of the genus *Choeradoplana*. The morphological diagnostic characteristics of this genus are remarkably heterogeneous in attributes found to be stable within other geoplanin genera. In addition to the variable shape of the cephalic region (discussed above), the longitudinal dorsal cutaneous musculature in *Choeradoplana* can be sunken (*Ch. gladismariae* Carbayo & Froehlich, 2012), a penis papilla can be present (*Ch. crassiphalla*, *Ch. benyai*, *Ch. marthae*), an inverted penis may also occur (*Ch. minima* Lemos & Leal-Zanchet, 2014), the prostatic vesicle may be intrabulbar (several species), the female genital canal can approach the female atrium behind it from the ventral direction (*Ch. banga*). Thus, we have increased the number of morphological variations seen in the genus in the present study, with the most remarkable being the ventral glandular cushions may be reduced or even absent, as in *Ch. albonigra* and *Ch. eudoxiae* Silva & Carbayo, sp. nov. and the anterior third of the body may become progressively thinner towards the anterior tip, as in *Ch. albonigra*. Therefore, one cannot trust the shape of the cephalic region for assigning a species with the head rolled-up to a genus. Instead, histological sections should be examined.

Despite the great variability in the diagnostic features, the genus can still be diagnosed by the following two exclusive attributes among Geoplanids: muscle retractor of the cephalic region delta-shaped in the cross-section and bodies of rhabditogen cells piercing the cephalic ventral epidermis are located between the retractor and the epidermis.

Acknowledgements

Dieter Fiege (Museum der Senckenbergischen Naturforschenden Gesellschaft in Frankfurt, Germany) kindly sent the holotype of *C. albonigra* on loan. ICMBio provided permit #11748-4 for the fieldwork. Ana Cristina Vasconcellos, Lucas Beltrami, and Geison Castro helped with histological sections. Marcus R. Hara and Fernando Portella de Luna Marques for their constructive comments on a previous version of the manuscript. Ana Laura Almeida is fully thanked for her help with molecular bench work. Ana María Rodríguez (University Carlos III de Madrid) is thanked for her help with the etymology, and Christopher Quinn for revision of the English text. DL-B thanks the Conselho Nacional de Desenvolvimento Científico e Tecnológico – CNPq (Proc. 152971/2016-5) for a PhD fellowship. São Paulo Research Foundation (FAPESP, Process # 2019/12357-7) provided financial support to FC. Ana Maria Leal-Zanchet and Hugh Jones are gratefully acknowledged for their revision of the manuscript.

References

Álvarez-Presas MA, Carbayo F, Rozas J, Riutort M (2011) Land planarians (Platyhelminthes) as a model organism for fine-scale phylogeographic studies: understanding patterns of biodiversity in the Brazilian Atlantic Forest hotspot. Journal of Evolutionary Biology 24: 887–896. https://doi.org/10.1111/j.1420-9101.2010.02220.x

Álvarez-Presas M, Sánchez-Gracia A, Carbayo F, Rozas J, Riutort M (2014) Insights into the origin and distribution of biodiversity in the Brazilian Atlantic forest hot spot: a statistical phylogeographic study using a low-dispersal organism. Heredity 112: 656–665. https://doi.org/10.1038/hdy.2014.3

Carbayo F, Leal-Zanchet AM (2001) A new species of terrestrial planarian (Platyhelminthes: Tricladida: Terricola) from South Brazil. Brazilian Journal of Biology 61: 1519–6984. https://doi.org/10.1590/S1519-69842001000300013

Carbayo F, Leal-Zanchet AM (2003) Two new genera of Geoplaninae (Terricola: Tricladida: Platyhelminthes) of Brazil in the light of cephalic apomorphies. Invertebrate Systematics 17(3): 449–468. https://doi.org/10.1017/S0952836901000401

Carbayo F, Froehlich EM (2012) Three new Brazilian species of the land planarian *Choeradoplana* (Platyhelminthes: Tricladida: Geoplaninae), and an emendation of the genus. Journal of Natural History 46(19–20): 1153–1177. https://doi.org/10.1080/00222933.2012.657699

Carbayo F, Álvarez-Presas M, Olivares CT, Marques FPL, Froehlich EM, Riutort M (2013) Molecular phylogeny of Geoplaninae (Platyhelminthes) challenges current classification: proposal of taxonomic actions. Zoologica Scripta 42(5): 508–528. https://doi.org/10.1111/zsc.12019

Carbayo F, Silva MS, Riutort M, Alvarez-Presas M (2018) Rolling into the deep of the land planarian genus *Choeradoplana* (Tricladida, Continenticola, Geoplanidae) taxonomy. Organisms Diversity & Evolution 18(2): 187–210. https://doi.org/10.1007/s13127-017-0352-4

Cason JE (1950) A rapid one-step Mallory-Heidenhain stain for connective tissue. Stain Technology 25(4): 225–226. https://doi.org/10.3109/10520295009110996

Dendy A (1894) Note on a new variety of Peripatus novae-zelandiae, Hutton. Transactions and Proceedings of the Royal Society of New Zealand 27: 190–191.

Du Bois-Reymond Marcus E (1951) On South American geoplanids. Boletim da Faculdade de Filosofia Ciências e Letras da Universidade de São Paulo, Série Zoologia 16: 217–255. https://doi.org/10.11606/issn.2526-4877.bsffclzoologia.1951.125222

Felsenstein J (1985) Confidence limits on phylogenies: an approach using the bootstrap. Evolution 39: 791–793. https://doi.org/10.1111/j.1558-5646.1985.tb00420.x

Froehlich CG (1955) Sobre morfologia e taxonomia das Geoplanidae. Boletim da Faculdade de Filosofia, Ciências e Letras. Série Zoologia 19: 195–279. https://doi.org/10.11606/issn.2526-3382.bffclzoologia.1954.120092

Froehlich CG (1959) On geoplanids from Brazil. Boletins da Faculdade de Filosofia, Ciências e Letras, Universidade de São Paulo, Série Zoologia 22: 201–265. https://doi.org/10.11606/issn.2526-3382.bffclzoologia.1959.120326

Graff L (1896) Ueber das System und die geographische Verbreitung der Landplanarien. Verhandlungen de Deutschen Zoologischen Gesellschaft 6: 75–93.

Graff LV (1899) Monographie der Turbellarien. II. Tricladida Terricola (Landplanarien). I–XII. Atlas von Achtundfünfzig Tafeln zur Monographie der Turbellarien II. Tricladida Terricola (Landplanarien). Pls I–LVIII. Wilhelm Engelmann, Leipzig, 574 pp.

Hall TA (1999) BioEdit: A User-Friendly Biological Sequence Alignment Editor and Analysis Program for Windows 95/98/NT. Nucleic Acids Symposium Series 41: 95–98.

Hurvich CM, Tsai C-L (1989) Regression and Time Series Model Selection in Small Samples. Biometrika 76: 297–307. https://doi.org/10.1093/biomet/76.2.297

Iturralde GG, Leal-Zanchet (2019) Why be original? Two new species of Choeradoplana resembling the type species of the genus in their external aspects (Platyhelminthes, Continenticola). ZooKeys 813(2): 1–19. https://doi.org/10.3897/zookeys.813.29565

Katoh K, Rozewicki J, Yamada KD (2019) MAFFT online service: Multiple sequence alignment, interactive sequence choice and visualization. Briefings in Bioinformatics 20(4): 1160–1166. https://doi.org/10.1093/bib/bbx108

Lanfear R, Frandsen PB, Wright AM, Senfeld T, Calcott B (2016) PartitionFinder 2: new methods for selecting partitioned models of evolution for molecular and morphological phylogenetic analyses. Molecular biology and evolution. https://doi.org/10.1093/molbev/msw260

Lázaro EM, Sluys R, Pala M, Stocchino GA, Baguñà J, Riutort M (2009) Molecular barcoding and phylogeography of sexual and asexual freshwater planarians of the genus *Dugesia* in the Western Mediterranean (Platyhelminthes, Tricladida, Dugesiidae). Molecular Phylogenetics and Evolution 52: 835–845. https://doi.org/10.1016/j.ympev.2009.04.022

Lemos VSA, Cauduro GPB, Valiati HV, Leal-Zanchet AM (2014) Phylogenetic relationships within the flatworm genus *Choeradoplana* Graff (Platyhelminthes: Tricladida) inferred from molecular data with the description of two new sympatric species from Araucaria moist forests. Invertebrate Systematics 28: 605–627. https://doi.org/10.1071/IS14003

Marcus E (1951) Turbellaria brasileiros (9). Boletim da Faculdade de Filosofia, Ciências e Letras da Universidade de São Paulo. Série Zoologia 16: 1–217. https://doi.org/10.11606/issn.2526-4877.bsffclzoologia.1951.125221

Miller SA, Dykes DD, Polesky HF (1988) A simple salting out procedure for extracting DNA from human nucleated cells. Nucleic Acids Research 16(3): e1215. https://doi.org/10.1093/nar/16.3.1215

Miller MA, Pfeiffer W, Schwartz T (2010) Creating the CIPRES Science Gateway for inference of large phylogenetic trees. In 2010 gateway computing environments workshop (GCE), 8 pp. https://doi.org/10.1109/GCE.2010.5676129

Negrete L, Brusa F (2012) *Choeradoplana crassiphalla* sp. nov. (Platyhelminthes: Tricladida: Geoplanidae): a new species of land planarian from the Atlantic Forest of Argentina. Studies on Neotropical Fauna and Environment 47: 227–237. https://doi.org/10.1080/01650521.2012.735071

Ogren RE, Kawakatsu M (1990) Index to the species of the family Geoplanidae (Turbellaria, Tricladida, Terricola) Part I: Geoplaninae. Bulletin of Fuji Women's College 28(1): 79–166.

Riester A (1938) Beiträge zur Geoplaniden-Fauna Brasiliens. Abhandlungen der Senkenbergischen naturforschenden Gesellschaft 441: 1–88.

Ronquist F, Teslenko M, van der Mark P, Ayres DL, Darling A, Höhna S, Larget B, Liu L, Suchard MA, Huelsenbeck JP (2012) MrBayes 3.2: Efficient Bayesian phylogenetic inference and model choice across a large model space. Systematic Biology 61: 539–542. https://doi.org/10.1093/sysbio/sys029

Schultze M, Müller F (1857) Beiträge zur Kenntnis der Landplanarien, nach Mittheilungen des Dr. Fritz Müller in Brasilien und nach eigenen Untersuchungen von Dr. Max Schultze. Abhandlungen der Naturforschenden Gesellschaft zu Halle 4: 61–74.

Spencer WB (1892) Land Planarians from Lord Howe Island. Part. 1. Descriptions of Species. Transactions R.S. Victoria 2: 42–51.

Stamatakis A (2006) RAxML-VI-HPC: maximum likelihood-based phylogenetic analyses with thousands of taxa and mixed models. Bioinformatics 22(21): 2688–2690. https://doi.org/10.1093/bioinformatics/btl446

Stimpson W (1857) Prodromus descriptionis animalium evertebratorum, etc. Proceedings of the Academy of Natural Sciences of Philadelphia 9: 19–14.

Sunnucks P, Blacket MJ, Taylor JM, Sands CJ, Ciavaglia SA, Garrick RC, Tait NN, Rowell DM, Pavlova A (2006) A tale of two flatties: different responses of two terrestrial flatworms to past environmental climatic fluctuations at Tallaganda in montane southeastern Australia. Molecular Ecology 15: 4513–4531. https://doi.org/10.1111/j.1365-294X.2006.03107.x

Winsor L (1991) A new genus and species of terrestrial flatworm from the central highlands of New Caledonia (Tricladida Terricola). Mémoires du Museum national d'histoire naturelle (Paris) 149: 19–30.

ZooKeys 1016: 49–61 (2021)
doi: 10.3897/zookeys.1016.55071
https://zookeys.pensoft.net

RESEARCH ARTICLE

A peer-reviewed open-access journal
ZooKeys
Launched to accelerate biodiversity research

Assessment of *Megadenus holothuricola* Rosén, 1910 (Eulimidae), an endoparasite of *Holothuria mexicana* Ludwig, 1875 (Holothuriidae) in the southern Gulf of Mexico and the description a new species

Norma Emilia González-Vallejo[1], Stephanie Amador-Carrillo[1]

1 *El Colegio de la Frontera Sur, Depto. Sistemática y Ecología Acuática, Av. Centenario km. 5.5 Chetumal, Quintana Roo, CP. 77014, Mexico*

Corresponding author: Norma Emilia González-Vallejo (negv0707@hotmail.com)

Academic editor: Eike Neubert | Received 3 June 2020 | Accepted 17 December 2020 | Published 11 February 2021

http://zoobank.org/E25A831E-CDAB-4060-9B5F-17C22EB3EFC4

Citation: González-Vallejo NE, Amador-Carrillo S (2021) Assessment of *Megadenus holothuricola* Rosén, 1910 (Eulimidae), an endoparasite of *Holothuria mexicana* Ludwig, 1875 (Holothuriidae) in the southern Gulf of Mexico and the description a new species. ZooKeys 1016: 49–61. https://doi.org/10.3897/zookeys.1016.55071

Abstract

As part of a study on holothurians from the southern Gulf of Mexico, some *Holothuria mexicana* Ludwig, 1875 were obtained for gut analysis. In two of them, a couple of eulimids were located inside the main tube of the respiratory tree. They were identified as *Megadenus holothuricola* Rosén, 1910, described from the Bahamas Islands, based on five specimens attached to the respiratory tree of *H. mexicana*. The original description was brief with few details, the type material is lost, and the species has not been found again. In this contribution, this species is confirmed for Campeche Bay, Mexico. The adult shell is globular to conical, transparent, thin, and fragile. *Megadenus smithi* **sp. nov.** from Palmyra Atoll, Central Pacific is described based on adult specimens. It differs from its congeneric species in its more robust shell, the pseudopallium does not cover the shell, and its short and contracted proboscis forms a thick disc. Further research on these eulimid parasites is now complicated in the southern Gulf of Mexico because of the holothurian population collapse due to over-exploitation of the fishery.

Keywords

Campeche, Eulimidae, gastropods, holothurians fishery, new species, Palmyra Atoll, symbiosis

Introduction

Eulimidae form a large group of parasitic snails infesting sea urchins, holothurians, starfish, and feather stars. Genera vary in their physical characteristics and lifestyle (Heller 2015). Some species live permanently attached to their echinoderm host; others attack their prey only temporarily and fall off if disturbed. Therefore, they are usually collected apart from their host, which thus may remain unknown (Warén 1984). However, many eulimid species are found to live on the body surface like ectoparasites, or as endoparasites especially in holothurians, accomplished by a series of morphological and anatomical changes (Nekhaev 2016; González-Vallejo 2018; Souza et al. 2018).

Our knowledge of marine parasites is fragmentary. This observation, especially in the case of invertebrate hosts, is probably caused by their low occurrence rates (Boxshall 2020). In Mexico, there are no records so far for eulimid endoparasites in holothurians; one ectoparasitic species was reported as *Melanella intermedia* (Cantraine, 1835), originally described from the Mediterranean Sea, in the skin of *Holothuria* (*Halodeima*) *grisea* Selenka, 1867 and *Holothuria glaberrima* Selenka, 1867. Both holothurians were reported from Veracruz in the Gulf of Mexico (Caso 1968, 1971).

The fishery of holothurians has increased in Campeche Bay during the last eight years. As part of a study of their feeding habits, some holothurians were obtained. After examining the internal organs, several endoparasites were located attached to or immersed in the main tube of the respiratory tree of *Holothuria* (*Halodeima*) *mexicana* Ludwig, 1875. One of the endoparasitic species was identified as *Megadenus holothuricola* Rosén, 1910. This eulimid was found attached to the respiratory tree of *H. mexicana*. The type locality of this species is the Bahamas Islands; the type series contained five specimens, and the original shell description was brief with few details only. The type material is lost, and the species has not been found again (Warén 1984). The genus *Megadenus* Rosén, 1910 includes five species found all around the world, and all of them live in an endoparasitic relationship with holothurian species. The type species *M. holothuricola* was reported from *H. mexicana*; *M. voeltzkowi* Shepman & Nierstrasz, 1913 from *H.* (*Holothuria*) *pardalis?* Selenka, 1867 from Zanzibar, East Africa; *M. cantharelloides* Humphreys & Lützen, 1972 from *Stichopus chloronotus* Brandt, 1835 in Picard Island, Aldabra, Indian Ocean; *M. oneirophantae* Bouchet & Lützen, 1980 from *Oneirophanta mutabilis* Thèel, 1879 off W bay of Biscay, France and *M. atrae* Takano, Warén & Kano, 2017 from *H.* (*Halodeima*) *atra* Jaeger, 1833 from Japan, New Caledonia, India and Australia (see Table 1).

Rosén (1910) supplied a brief description of the shell of *M. holothuricola* as "conical, shiny, finely cross-striae, fragile, without an umbilicus, without an operculum, with six spiral turns, the first two very small". He mainly focused on describing the histology of the species (pls 1–4, figs 1–16) comparing the morphological differences of *M. holothuricola* with species from other genera such as *Stilifer* Broderip, 1832, *Mucronalia* Adams, 1860, *Pelseeneria* Koehler & Vaney, 1908, and *Turtonia* Rosén,

1910. Thus, the species' shell features remain ill-defined, which makes a detailed re-description necessary. In this work, we assess the endoparasitic relationship of *M. holothuricola* with *H. mexicana* in the Bay of Campeche, which also represents the first finding after the original description and the first record for this species from the Gulf of Mexico. Details of the shell and its variation are described, and information on the shells of sub-adults, juveniles, and larvae are provided, as well as comments on morphological features such as proboscis, mantle color, and egg capsules and supported by illustrations. Additionally, a new species is described from Palmyra Atoll, Central Pacific.

Materials and methods

One hundred holothurians were collected and donated by fisherman for gut-analyses and molecular studies. Holothurians were collected at 5 m depth in mixed sea grass meadows and sandy areas off the coast of Lerma (19°49.31'N, 90°36.51'W), Campeche Bay, Mexico, on 4 May 2012. Two species of holothurians were identified, *H. mexicana* and *H. floridana*; the identification was confirmed by molecular studies and the analysis of calcareous ossicles (following Amador-Carrillo 2014). The holothurians were all adults, 12–22 cm long, and were relaxed in freshwater to avoid evisceration. The holothurians were injected with a 4% formaldehyde solution in sea water and preserved in 70% ethanol. In the laboratory, holothurians were dissected using a sagittal cut, the visceral mass was removed, and placed in individual containers. Three specimens identified as *Megadenus* sp. were collected from Palmyra Atoll, Central Pacific by J. Smith, on 11 September 2011 attached to the cloaca of *H. atra* Jaeger, 1833, were studied and are described as a new species.

The Eulimidae were photographed with a stereomicroscope and a Cannon EOS T6i camera, mounted with an adapter into the ocular tube. Measurements were made with a micro ruler (mm). Digital plates were assembled with Adobe Photoshop CC. Holothurians and eulimids were deposited in the collections of El Colegio de la Frontera Sur (**ECOSUR**) Unidad Chetumal, Mexico.

Results

The endoparasite *M. holothuricola* was found in only two holothurians. In the first one, there were two adult specimens and one juvenile; all were immersed in the skin of the main tube of the respiratory tree (Fig. 1A). The second holothurian had two adult specimens and one juvenile attached in the same way as the previous specimen, but additionally there were four probosces, without shells or specimens (Fig. 2A). In total, there were three adults and three juveniles or sub-adults. The prevalence of the endoparasites in the host was 2% of the total holothurians examined.

Taxonomy

Class Gastropoda Cuvier, 1795
Order Littorinimorpha Golikov & Starobogatov, 1975
Familia Eulimidae Philippi, 1853

Genus *Megadenus* Rosén, 1910

Type species. *Megadenus holothuricola* Rosén, 1910:18 by monotypy.

Diagnosis. Shell conical to globular, translucent, colorless, sculpture of fine axial striae. Pseudopallium covers the shell or not; proboscis large or short forming a thick contracted disc; large pedal gland (Rosén 1910; Humphreys and Lützen 1972).

Remarks. *Megadenus* species are found in shallow waters in tropical or subtropical regions, especially as endoparasites of Aspidochirotida (Echinodermata, Holothuroidea); usually they live in the cloacal chamber or attached to the respiratory tree. *Megadenus oneirophantae* Bouchet & Lützen, 1980 is the only abyssal species (4796 m). Warén (1984) defined *Megadenus* as "shell fragile, globular, and at least lower part is covered by a big pseudopallium, has separate sexes, with smaller males and the animals live in the cloaca of holothurians." He also indicated there was no type material.

Megadenus holothuricola Rosén, 1910

Figs 1A–E, 2A–F

Megadenus holothuricola Rosén, 1910:18–49 pl. 1 figs 1, 2 (type locality: Bahamas Islands; Type material lost).

Specimens examined. four adult specimens ECOSUR-1386, two juveniles ECOSUR-1387 from Lerma, Campeche Bay, Gulf of Mexico.

Distribution. Bahamas and Lerma, Campeche, Mexico.

Description. ***Shell*** conical to globose, translucent, thin, fragile, sculpture consists of fine striations and growth scars from earlier positions of outer lip, two or three in random position per whorl. Adult size 4.0–5.5 mm long and 2.5–3.5 mm wide range (N = 6) (Fig. 1B, C); teleoconch 4–6 very convex whorls, body whorl comprising more than 50% of the total shell length, posterior whorls reduced in size, sutures well defined aperture broad, inner lip broken, rounded basally; outer lip thin, slightly convex in lateral view, no operculum or periostracum; protoconch mucronate, 1½ whorls, translucent, rounded apex; sub-adults shell globose, low spiral, 2½ whorls, 1.0–2.0 mm long, 1.0 mm wide; body whorl half as long as body and more globose than in adults.

Body fully retractable into shell, mantle light cream-colored, pseudopallium whitish to light yellow in color; short and rounded tentacles, eyes round, black at the base of each tentacle (Fig. 2D); foot reduced with a huge marginal gland of unknown

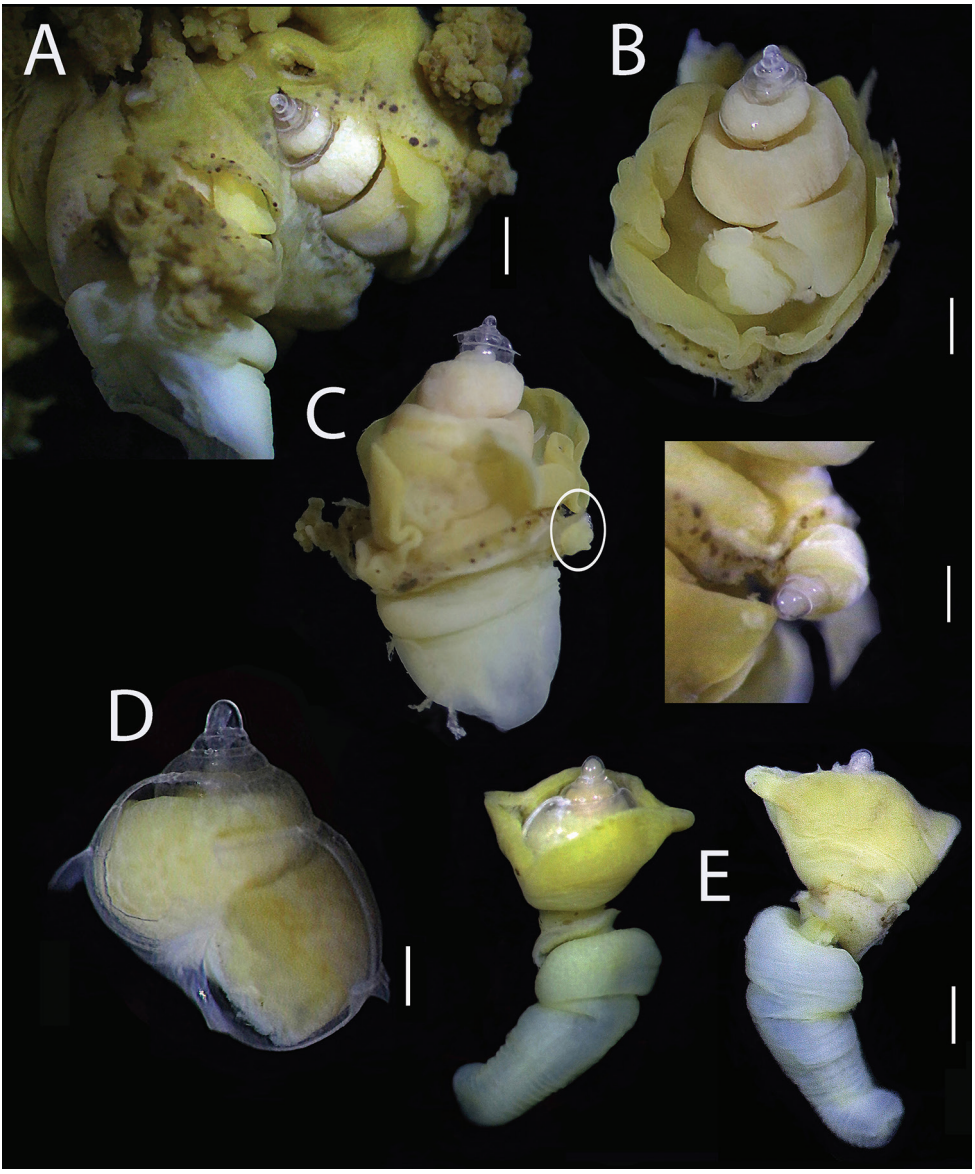

Figure 1. *Megadenus holothuricola* Rosén, 1910 **A** two adults between filaments of the respiratory tree **B, C** detached adult shells, SL = 5.5 mm and 4.5 mm; right side juvenile attached SL = 1.0 mm **D** broken adult shell SL = 2.5 mm **E** subadult SL = 2.0 mm with everted proboscis L = 2.5 mm. Scale bars: 1.6 mm (**A**); 1.8 mm (**B**); 1.4 mm (**C**); 0.2 mm (**D**); 1.1 mm (**E**).

function in dorsal position. The anterior region has two structures arising next to the mantle, the pseudopallium surrounding and partially covering the shell forming an extensive fold with pleated edges, and the proboscis. Epithelium fused with the holothurian respiratory tree; proboscis only partially fused with a part of the pseudopallium

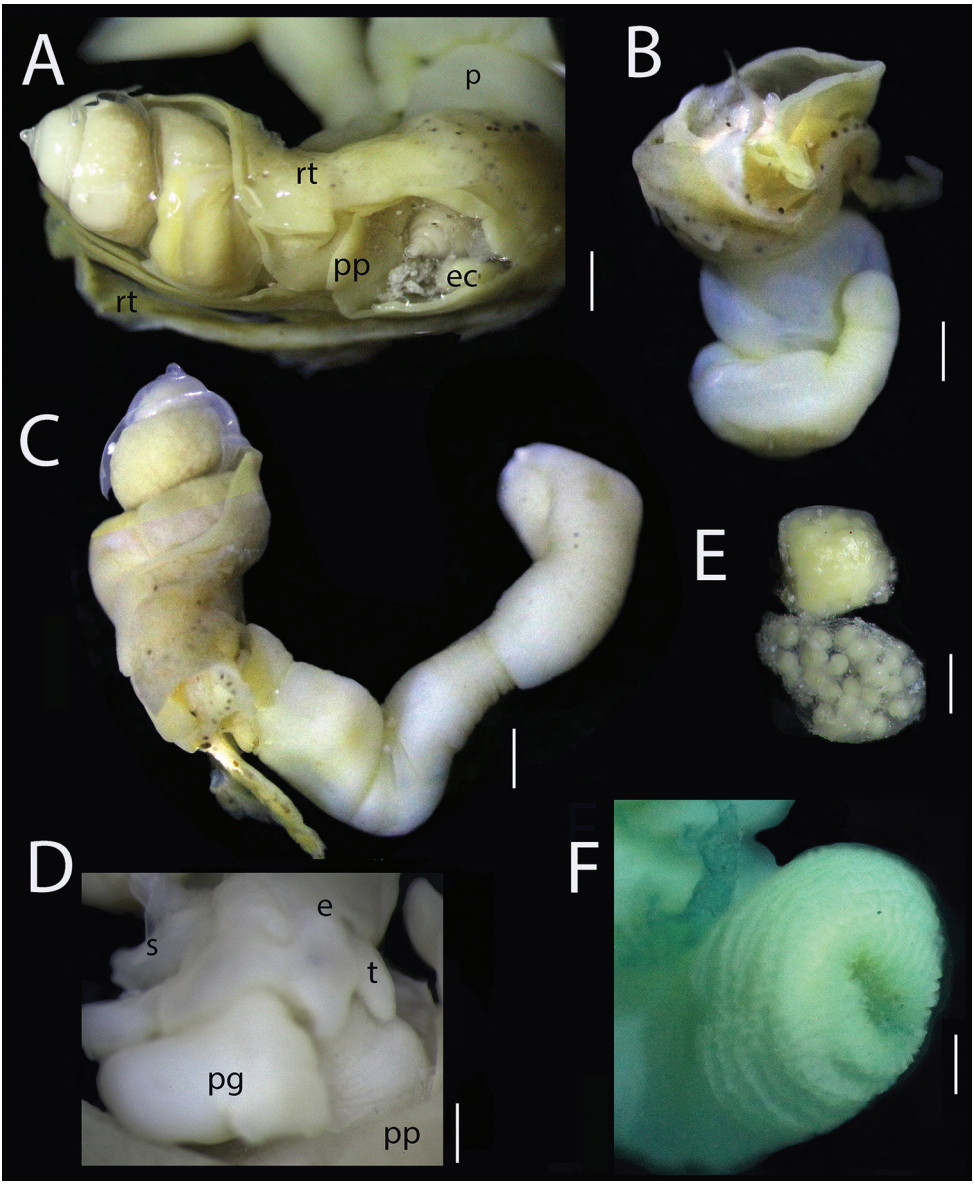

Figure 2. *Megadenus holothuricola* Rosén, 1910 **A** adults immersed in the main tube of the respiratory tree **B, C** two adults showing the mottled skin of the respiratory tree and the pseudopallium covering shell; proboscis slightly rolled, and another adult stretched to the maximum **D** cephalic view, 40× **E** two egg capsules, L = 2 mm **F** view of the distal part of an adult proboscis. Scale bars: 1.2 mm (**A**); 2.3 mm (**B**); 1.65 mm (**C**); 0.8 mm (**D**); 0.6 mm (**E**); 0.5 mm (**F**). Abbreviations: e: eyes; eg: egg capsules; p: proboscis; pg: pedal gland; pp: pseudopallium; rt: respiratory tree; s: shell; t: tentacle.

and foot, protruding from pseudopallium folds; in juveniles, pseudopallium covering lateral areas, leaving the apical teleoconch exposed; in 1 mm long juveniles, a small fold distinguishable (Figs 1E, 2C).

Proboscis funnel-shaped, forming a flexible, semi-transparent or white non-retractable tube (Fig. 2C); inside is a series of long and circular muscular packs giving it an elastic morphology and a rough outer cuticular surface; on the distal part is a series of papillae, allowing it to adhere like a suction cup to the epidermis of the host's respiratory tree (Fig. 2F). The proboscis size varies with total shell size: in adults, it is 3 × longer than the shell, 7.0 mm stretched to the maximum, in sub-adults or juveniles the proboscis is smaller and smoother (Fig. 2B, C).

Variations. The larval shell shows some intraspecific variations in adults. It is glassy, low, and rounded to mucronate. This seems to be related to the protection of the pseudopallium when it is immersed inside the respiratory tube. The juvenile develops the pseudopallium relatively early, when it has 1.5 whorls, and protects the shell from this stage onwards; at the same time, it is attached to an area of the host's skin respiratory tree (Fig. 1C, E).

Remarks. Inside the posterior whorls of the shell, all adults and subadults presented pink oocytes or germinal cells. Two oval-shaped egg capsules were found situated between the shell and the pseudopallial folds, in one specimen (Fig. 2A, E). Each capsule was transparent, 1.5 mm long × 1.0 mm wide, with 25–30 embryos in each. A juvenile was found strongly attached to the skin layer of the respiratory tube of the host, in the anterior area close to an adult eulimid (Fig. 1C). Shells were difficult to preserve complete due to their fragility.

Rosén (1910) illustrated an adult and its coiled proboscis. His figures 1 and 2, show an adult with the pseudopallium at the top, and the proboscis of another adult separated from the respiratory tree tube. Our results are similar. The shape and sculpture of our shells correspond to Rosén's original description; that is, a conical shape in pre-adults to globose shell, wider in the body whorl, two posterior smaller whorls, and with fine axial striations and continuous incremental growth lines in adults. The shells of *M. catharelloides* and *M. voeltzkowi* were described and illustrated, but subsequently destroyed to make histological cuts. In *M. holothuricola* there are no shells preserved as type material, hindering a better comparison, as noted by Warén (1984). However, shell shape of the pre-adults or juveniles of *M. holothuricola* resemble adults of *Monogamus minibulla* Olsson & McGinty, 1958 or juvenile specimens of *Pelseeneria* (Koehler & Vaney, 1908). Therefore, the morphological comparison of shells can be misleading, although these genera parasitize sea urchins (González-Vallejo 2008; Delongeville et al. 2011).

***Megadenus smithi* sp. nov.**
http://zoobank.org/B1F27E92-096F-4D99-8697-EBA5F1CDD2B2
Fig. 3A–D

Type material. ***Holotype*** (ECOSUR-0234) female; paratypes (ECOSUR-0235) two males, one juvenile from the type locality found attached in the cloacal chamber of *Holothuria* (*Halodeima*) *atra* Jaeger, 1833 collected on 11 September 2011 by J Smith.

Type locality. Palmyra Atoll, Central Pacific Ocean, shallow water in reef lagoon.

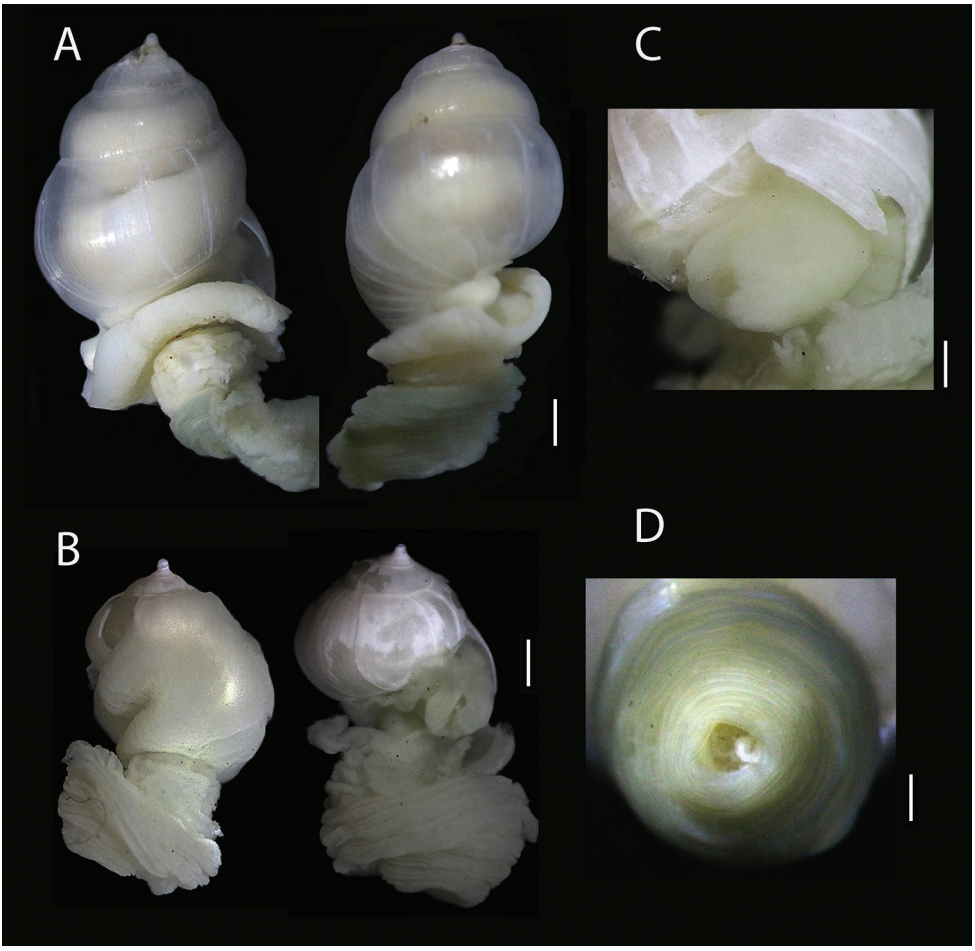

Figure 3. *Megadenus smithi* sp. nov. **A** holotype female in apertural and posterior views (ECOSUR-0234) SL = 6.5 mm × 4.0 mm wide **B** paratype male in apertural and lateral view, showing the tentacles SL = 4.0 mm. × 3.5 mm wide **C** pedal gland view **D** distal open proboscis view. Scale bars: 1.2 mm (**A**); 1.0 mm (**B**); 0.6 mm (**C**); 0.5 mm (**D**).

Etymology. This species is being named after the collector Mr. J. Smith, as a means of recognition, for his sampling efforts.

Distribution. Known only from the type locality.

Diagnosis. Female shell globose to conical, transparent, fragile, glassy, colorless, fine incremental axial stria; apex mucronate glassy white not tilt; proboscis slightly dark; large pedal gland.

Description. ***Shell*** globose, translucent, thin, fragile, colorless, smooth sculpture, with fine axial striae, several growth scars of earlier outer lip positions are irregularly spaced, suture impressed. Adult shell 6.5 mm long; 4.0 mm wide; body whorl 4.5 mm long (holotype Fig. 3A). Teleoconch 5.5 convex whorls, three flat, small post-larval whorls, the penultimate whorl 1.0 mm. Aperture broad, inner lip smooth, concave at

base, outer lip simple, slightly curved in most protruding part. Protoconch mucronate, two whorls, glassy white, no operculum or periostracum; sexually dimorphic, male with a penis behind the eye, female is 30% larger than male (Fig. 3B).

Soft tissues pale cream with reddish pigmentation, seen through transparent shell. Pseudopallium cauldron-shaped in sub-adults arising from the aperture and covering large part of shell, or short mantle folds not covering female shells, smooth. When skin was removed, a thick, rounded pedal gland was visible in the aperture (Fig. 3C). Head with a pair of thick long tentacles and black eyes; penis large, placed behind right eye in males. Proboscis slightly dark colored, retractile, separate from the pseudopallium by a deep constriction. Proboscis skin slightly contracted after fixation, forming a thick disc with the mouth distally (Fig. 3D), almost as long as whole specimen. No egg capsules or juveniles were found.

Remarks. The new species shares several shell and morphological traits with the other five congeneric species. A comparison of the most important structures, almost all based on the literature, is provided in Table 1. *Megadenus smithi* sp. nov. resembles *M. voeltzkowi* because both have a tall shell (6.5 mm), a swollen and more convex penultimate whorl than *M. holothuricola* and *M. atrae*. The protoconch in *M. holothuricola* is transparent, 1.5 whorls, and is slightly wider than high, while in *M. smithi* sp. nov. it is two whorls higher than wide much like in *M. cantharelloides*, *M. voeltzkowi*, and *M. atrae*. However, the latter has a slightly tilted protoconch axis. *Megadenus oneirophantae* has a long thin proboscis, the pseudopallium is missing, and the species exhibits a marked sexual dimorphism with a dwarf male.

Table 1. Comparison of the main character states separating the species of *Megadenus*. The information provided is based on literature (Schepman and Nierstrasz 1913; Humphreys and Lützen 1972; Bouchet and Lützen 1980; Takano et al. 2017). For *M. holothuricola* and *M. smithi* sp. nov. data obtained from specimens.

Species	Shell/size/sex	Pseudopallium	Proboscis	Host/attach site	Geographical distribution & depth
M. holothuricola Rosén, 1910	Globose to conical, thin, transparent, fine striae, 4.0–5.5 mm length × 2.0–1.5 mm width	Bowl-shaped with pleated margin	Funnel-shaped, white, flexible, rough cuticular surface; not retractable	*Holothuria mexicana* respiratory tree	Bahamas, Campeche Bay, shallow water
M. voeltzkowi Shepman & Nierstrasz, 1913	Ovoid transparent to whitish, slightly smooth 6.5 × 4 mm	Arises from folds of foot	Suction disc form, contracted and wrinkled	*Holothuria pardalis*? esophageal region	Zanzibar East Africa, shallow water?
M. cantharelloides Humphreys & Lützen, 1972	Cyrtoconoid and globose, transparent ♀ 5.7 × 4.5 mm	Bowl-shaped fold of tissue, more extensive in male than female	Chanterelle-shaped, darkened, contracted	*Stichopus chloronotus* intestine	Picard Island, Aldabra, India, shallow water
M. oneirophantae Bouchet & Lützen, 1980	Globose, vitreous ♀ 9.3 × 7.5 mm, ♂ 3.0 × 1.6 mm	Base partly covered by foot and its folds	Long, thin	*Oneirophanta mutabilis* within galls in intestine	Bay of Biscay, 4796 m abyssal depth
M. atrae Takano,Warén & Kano, 2017	Globose, pyriform to biconical, transparent to whitish ♀ 5.2 mm; ♂ 2.0–1.5 mm	Cauldron-shaped	Long, thickened at the middle into a collar-like	*Holothuria atra*, cloacal chamber and respiratory tree	Japan, New Caledonia, India Australia, tidal waters
M. smithi sp. nov.	Globose to biconical, transparent,finally axial striae ♀6.5 mm L ♂ 4.0 mm	In folds of foot and cauldron-shaped	Suction disc form, slightly dark colored retractable	*Holothuria atra* cloacal chamber	Palmyra Atoll, shallow water

Discussion

Megadenus holothuricola Rosén, 1910 was described from the Bahamas Islands, Caribbean, more than one hundred years ago. The low occurrence of finding this kind of endoparasites, 2% as in this study, had already been reported elsewhere: Jones and James (1969) reviewed 1,300 specimens of *H. atra* from the Gulf of Mannar, India, and found only eight holothurians with eulimids (0.6%), Humphreys and Lützen (1972) reviewed one holothurian containing only two eulimids, while Takano et al. (2017) reviewed 3,848 specimens of *H. atra*, and only 1.7% with the associated eulimid endoparasite.

Rosén (1910) illustrated a histological section of the proboscis of *M. holothuricola*, but, following Humphreys and Lützen (1976), he used confusing terminology, for example, a type of cell in the proboscis epithelium which was "neither ciliate nor glandular columnar cells produce cuticular process", and concluded "only *M. holothuricola* has a cuticular surface in the distal part of the proboscis". Checking the internal surface of the proboscis, we observed that the cuticular aspect as mentioned by Rosén is caused by inner muscles fibers. Size and retraction abilities of the proboscis differs among the species in the genus. He indicated that "the proboscis is larger in the female"; however, in our study all probosces observed were extended, none was retracted (Fig. 2C). The new species *M. smithi* has a short retracted disc, without papillae in the distal area, without differences in size between male and female specimens (Fig. 3A), but resembles a short, thick, retracted disc as figured for *M. voeltskowi* (Shepman & Nierstrasz, 1913: pl. 1, fig. 1), *M. cantharelloides* Humphreys & Lützen (1972: fig. 2A), and *M. atrae* Goto (2010: fig. 1D, E; Takano et al. 2017: fig. 1D, E). Apparently the differences in the shapes and lengths of the probosces between species are primarily related to the size of the adults or sub-adults, and secondly to the type of host organ it inhabits, which is usually the cloacal chamber or the respiratory tree.

Holothuria mexicana is the largest holothurian in the Gulf and Mexican Caribbean Sea, reaching up to 50 cm in length. The hindgut (cloaca) bears highly branched outgrowths that extend anteriorly, the respiratory trees. The function of the pair of respiratory trees is to take oxygen from the water, but at the same time they are excretory organs in combination with the intestine. Nitrogenous waste (ammonia) is carried by coelomocytes to the respiratory trees and released through pumping systems (Brusca and Brusca 1990). According to the above, *M. holothuricola* apparently does not cause any harm to the host and as Rosén (1910) reported, the proboscis floats freely in the body cavity of the holothurian, due to a circular perforation of the respiratory tree tubes that it had made previously. It may obtain food by extracting coelomocytes from the walls of the respiratory tree, or it traps organic microparticles. We observed that this species also lives attached to the outer wall of the intestine during the early stages of development; however, there is no information available on its food nor other activities.

An egg capsule was described and illustrated by Rosén (1910: 57, fig. 1): it is oval with a stalk and was attached to a male shell on a gelatinous mass; he did not mention how many capsules were in a clutch. In *M. holothuricola* from Lerma, two egg capsules each containing only 25–30 embryos were protected between the folds of the pseudo-

pallium and the teleoconch, but we suppose there were more, as in their congeners. The same form of protection was reported for *M. cantharelloides* with 26 egg capsules each containing 85–157 embryos, confirming a continuous production of embryos (Humphreys and Lützen 1972). For *M. atrae*, 11 egg capsules containing ca. 170 embryos in total at different stages of development with small degrees of sexual dimorphism were reported (Takano et al. 2017). The presence of sexual dimorphism was not confirmed in this study. Warén (1980) mentioned five sexual strategies in Eulimidae, and protandric hermaphrodites with environmental sex determination strategy (ESD) seem to be common. Adults of *M. holothuricola* were present in pairs, both shells were the same size, only one had egg capsules, but oocytes and germ cells could be observed in the posterior whorls in both specimens. It has been shown that *M. atra* is dimorphic, lives in pairs, and the sexes are separate with males being smaller than females (Takano et al. 2017), who assumed that the species of *Megadenus* follow the ESD strategy. In *Megadenus smithi* sp. nov. from Palmyra, a penis could be observed in the cephalic dorsal area. The specimen had a smaller shell and thus exhibits sexual dimorphism, which is part of the sexual strategy ESD. However, *M. holothuricola* may follow the simultaneous hermaphrodites strategy (SH) but it is difficult to fully confirm without either detailed growth and reproductive cycle or histological analysis.

Another pending question is how these endoparasites migrate from one to another holothurian. Juveniles were found attached to the pseudopallial wall of an adult specimen and was immersed in the same main respiratory tree tube of the host (Fig. 1C, white circle). This finding indicates a brief larval development and displacement of the juvenile within the same host specimen. For long-distance dispersal, the larvae perhaps use the water exchange currents produced in the cloaca by the holothurian (Humphreys and Lützen 1972), or they could be released during the periodical evisceration events of *Holothuria.* Evisceration may be caused by pollution, or as a defense mechanism. During this phenomenon, the cloaca is expelled as well as parts of the respiratory tree, the digestive system, and the gonads (Barnes 1984). In these cases, the juveniles would have the opportunity to find and colonize another host specimen.

Further research on this eulimid parasites is now compromised in the southern Gulf of Mexico, because the holothurian populations have collapsed due to over exploitation. This illegal practice has been interdicted by a law that prohibits the extraction of holothurians in the area (DOF 2013).

Acknowledgements

Unai Markaida helped by contacting the fishermen and provided lab facilities in ECOSUR-Campeche. Leslie Harris (LACM) kindly shared some specimens from Palmyra. Sergio Salazar and Alejandro Salazar González helped in the field for management and preservation of holothurians. Ryutaro Goto and anonymous reviewer and editor Eike Neubert are sincerely thanked for their helpful comments that have much improve this paper.

References

Amador-Carrillo SR (2014) Composición temporal de los hábitos alimenticios de *Holothuria* (*Halodeima*) *floridana* Pourtalès 1851 en Lerma, Campeche. Tesis Lic. Instituto Tecnológico de Chetumal, Chetumal, 74 pp.

Barnes RD (1984) Zoología de los invertebrados. Clase Holoturoidea. Ed. Interamericana, México, 1157 pp.

Bouchet P, Lützen J (1980) Deux gastéropodes parasites d´une holothurie élasipode. Bulletin du Museum National d´Historie Naturelle París, Série 2, Section A1: 59–75.

Boxshall GA (2020) Self-help for taxonomists: three things we must do for taxonomy to survive. Megataxa 39–42. https://doi.org/10.11646/megataxa.1.1.7

Brusca RC, Brusca GJ (1990) Phylum Echinodermata. In: Sinauer AD (Ed.) Invertebrates. Sinauer Association Press, Sunderland, 801–839.

Caso ME (1968) Contribuciones al estudio de los holoturoideos de México. Un caso de parasitismo de *Balcis intermedia* (Cantraine) sobre *Holothuria glaberrima* Selenka. Anales del Instituto de Biología UNAM, México, Serie Ciencias del Mar y Limnología 39(1): 31–40.

Caso ME (1971) Contribución al estudio de los holoturoideos de México. Morfología externa e interna y ecología de *Holothuria grisea* Selenka. Anales del Instituto de Biología UNAM, Serie Ciencias del Mar y Limnología 42(1): 31–40.

DOF (2013) Acuerdo por el que se modifica el Aviso por el que se da a conocer el establecimiento de épocas y zonas de veda para la pesca de diferentes especies de la fauna acuática en aguas de jurisdicción federal de los Estados Unidos Mexicanos, publicado el 16 de marzo de 1994, para establecer el periodo de veda para el pepino de mar en las aguas marinas colindantes con la Península de Yucatán. 25 April 2013, 3 pp. https://dof.gob.mx

Delongeville C, Scaillet R, Swinnen F (2011) Le genre *Pelseneeria* Koehler & Vaney, 1908 (Eulimidae) dans les eaux de la Péninsule Ibérique. Xenophora 136: 45–53. https://core.ac.uk/download/pdf/45440342.pdf

González Vallejo NE (2018) Revisión y aspectos ecológicos de la familia Eulimidae Philippi 1853 (Gasterópoda) de las costas del Pacífico oriental tropical y Atlántico mexicano. Tesis Doctorado, Posgrado Facultad de Ciencias Biológicas, Universidad Autónoma de Nuevo León, México, 257 pp. http://eprints.uanl.mx/16688/1/1080290320.pdf

González Vallejo NE (2008) Parasitism of *Monogamus minibulla* (Olsson & McGinty, 1958) (Gastropoda: Eulimidae) on the red sea-urchin *Echinometra lucunter* (Linnaeus, 1758) (Echinodermata: Echinometridae) on the Caribbean coast of Mexico. The Nautilus 122(3): 178–181.

Goto R (2010) First record of the genus *Megadenus* Rosén, 1910 (Gastropoda; Eulimidae) endoparasites of sea cucumbers from Japan. Venus 69(1–2): 81–83. https://www.jstage.jst.go.jp/article/venus/69/1-2/69_80/_pdf

Heller J (2015) Eulimoidea: Parasitic snails. In: Sea snails. A natural history. Springer, 169–173. [eBook] https://link.springer.com/content/pdf/10.1007/978-3-319-15452-7.pdf

Humphreys WF, Lützen J (1972) Studies on parasitic gastropods from echinoderms 1. On the structure and biology of the parasitic gastropod *Megadenus cantharelloides* n. sp. with comparisons on *Paramegadenus* n. g. Det Kongelliage Danske Videnskabernes Selskab Biologiske Skrifter 19: 1–27. [pls 1–4]

Jones S, James DB (1969) On a stiliferid gastropod parasitic in the cloacal chamber of *Holothuria atra* Jaeger. Proceedings of the Symposium on Mollusca, Marine Biological Association of India 3: 799–804. http://eprints.cmfri.org.in/2370/

Nekhaev IO (2016) A new species of endoparasitic mollusk from the Artic (Gastropoda: Eulimidae). Journal of Conchology 42(3): 73–78.

Rosén N (1910) Zur Kenntnis der parasitischen Schnecken. Lunds Universitets Arsskrift 6(4): 1–67. [+4 pls]

Schepman MM, Nierstrasz HF (1913) Parasitische und kommensalistische Mollusken aus Holothurien. Reise in Ostafrika in den Jahren 1903–1905 mit Mitteln der Hermann und Elise geb. Heckmann Wentzel-Stiftung ausgeführt von Professor Dr. Alfred Voeltzkow, Wissenschaftliche Ergebnisse 4: 383–416. https://doi.org/10.5962/bhl.title.13015

Souza LS, Rogers A, Hamel JF, Mercier A (2018) Eulimids (Gastropoda: Eulimidae) on the sea cucumber *Holothuria mexicana* (Ludwig 1875) (Holothuroidea: Holothuriidae) in Belize. Check List 14(5): 923–931. https://doi.org/10.15560/14.5.923

Takano T, Warén A, Kano Y (2017) *Megadenus atrae* n, sp. an endoparasitic eulimid gastropod (Mollusca) from the black sea cucumber *Holothuria atra* Jaeger (Aspidochirotida: Holothuriidae) in the Indo-West Pacific. Systematic Parasitology 94: 699–709. https://doi.org/10.1007/s11230-017-9731-7

Warén A (1980) Sexual strategies in Eulimidae (Prosobranchia). In: Ponder WF, Underwood AJ (Eds) Symposium on the biology and evolution in Mollusca. Journal of the Malacological Society of Australia 4(4): e231. https://doi.org/10.1080/00852988.1980.10673931

Warén A (1984) A generic revision of the family Eulimidae (Gastropoda, Prosobranchia). Journal of Molluscan Studies, Supplement 13: 1–96. https://doi.org/10.1093/mollus/49.Supplement_13.1

ZooKeys 1016: 63–76 (2021)
doi: 10.3897/zookeys.1016.61397
https://zookeys.pensoft.net

RESEARCH ARTICLE

A peer-reviewed open-access journal
ZooKeys
Launched to accelerate biodiversity research

Two new species of the genus *Anillinus* Casey (Coleoptera, Carabidae, Anillini) from the southern United States

Igor M. Sokolov[1]

1 *Systematic Entomology Laboratory, ARS, USDA, c/o Smithsonian P.O. Box 37012, National Museum of Natural History, Washington, DC 20013-7012, USA*

Corresponding author: Igor M. Sokolov (igor.sokolov@usda.gov)

Academic editor: B. Guéorguiev | Received 26 November 2020 | Accepted 7 January 2021 | Published 11 February 2021

http://zoobank.org/96F664E8-AE1D-4E3D-86E9-9DEDF4DCF6AA

Citation: Sokolov IM (2021) Two new species of the genus *Anillinus* Casey (Coleoptera, Carabidae, Anillini) from the southern United States. ZooKeys 1016: 63–76. https://doi.org/10.3897/zookeys.1016.61397

Abstract

Two new species of blind ground beetles are described from the southern United States. One species, *Anillinus relictus* **sp. nov.** (type locality: E of Oneonta, Blount County, Alabama), based on the structure of male genitalia, is similar to Texan *Anillinus*, in particular to the endogean *A. sinuatus* Jeannel. The second species, *A. felicianus* **sp. nov.** (type locality: 4 mi SW Jackson, West Feliciana Parish, Louisiana), is superficially similar to the endogean *A. sinuaticollis* Jeannel from Roane County, Tennessee, and represents the first record of the genus for the state of Louisiana. All species are illustrated with digital images of habitus, body parts, and male and female genitalia. Biogeographical and evolutionary implications of the new findings are discussed.

Keywords

Alabama, *Anillinus*, distribution, Louisiana, new species, soil fauna

Introduction

The genus *Anillinus* Casey, in spite of its wide range, remains one of the most incompletely known genera of carabid beetles in the United States. Litter, soil-dwelling or cavernicolous representatives of the genus inhabit a huge area from the Potomac River in the north to the Florida Panhandle in the south, and from eastern Texas in the west to

the Piedmont hills of North Carolina in the east (Bousquet 2012). Across this territory, the number of species recorded in neighboring states varies greatly, and the necklace of the Gulf States is exactly the region where the biodiversity of *Anillinus* changes from state to state rather unevenly and often unexpectedly. Moving from the west to the east, the number of species recorded to date starts from seven in Texas, then jumps down to zero in Louisiana and to one in Mississippi; thereafter, the number of species increases again to twelve in Alabama, and drops down to two in Georgia and Florida (Bousquet 2012; Sokolov et al. 2014; Sokolov 2020). Obviously, such an uneven distribution of anilline species across neighboring states may result from the interaction of natural ecological and historical factors. One more reason for the dramatic variation in the recorded numbers of species is insufficient sampling of representatives of the genus, which are hard to collect. Each discovery of a new species of *Anillinus* in the Gulf states adds to our knowledge of local faunas and brings us closer to understanding the roles of the aforementioned factors in shaping biodiversity on the lands bordering the Gulf of Mexico. Descriptions of two new species discovered in the Gulf states form the main content of this paper.

Material and methods

This study is based on examination of specimens of *Anillinus* either collected in Louisiana or originating from the late Tom C. Barr's collection of Anillini (now in the Carnegie Museum of Natural History, Pittsburgh, Pennsylvania, USA – **CMNH**). Type material of the newly described species is deposited in the National Museum of Natural History, Washington, DC (**NMNH**), in the CMNH, and in the Louisiana State Arthropod Museum (**LSAM**). Verbatim label data are given for the type specimens of the newly described species, with label breaks indicated by a backslash ("\").

Terms used in this paper follow Sokolov et al. (2014).

Extractions and processing of genitalia were made using the standard techniques described by Sokolov and Kavanaugh (2014).

Photographs of the external features of the new species were taken with a Macropod Pro photomacrography system (Macroscopic Solutions, LLC). Digital images of genitalia were taken with a Nikon light microscope Eclipse N*i*-U supplied with DS-Fi2 camera and DS-LR3 camera control unit. Line drawings of selected body parts were prepared with the help of a camera lucida attached to an Olympus BX 50 compound microscope.

All specimens were measured using the tpsDig 2.17 (Rohlf 2013) software on digital photographs. Measurements for various body parts are coded as follows: **ABL** = apparent body length from clypeus to apex of elytra; **WH** = width of head at level of first orbital setae; **WPm** = maximal width across pronotum; **WPa** = width across anterior angles of pronotum; **WPp** = width across posterior angles of pronotum; **LP** = length of pronotum from base to apex along midline; **WE** = width of elytra at level of 2nd discal setae; **LE** = length of elytra from apex of scutellum to apex of left elytron. ABL measurements are given in mm; others are presented as nine ratios:

mean widths – WH/WPm and WPm/WE; and body parts – WPa/WPp, WPm/WPp, WPm/LP, WE/LE, LP/LE, LE/ABL and WE/ABL. All values are given as mean ± standard deviations.

Taxonomic Part

Order Coleoptera Linnaeus, 1758
Family Carabidae Latreille, 1802
Subfamily Trechinae Bonelli, 1810
Tribe Anillini Jeannel, 1937

Genus Anillinus Casey, 1918

Anillinus Casey, 1918: 167. Type species: *Anillus* (*Anillinus*) *carolinae* Casey, 1918, by original designation.

Micranillodes Jeannel, 1963a: 57. Synonymy established by Bousquet (2012: 699) and confirmed by Sokolov et al (2014: 83). Type species: *Micranillodes depressus* Jeannel, 1963a, by original designation.

Troglanillus Jeannel, 1963b: 147. Synonymy established by Barr (1995: 240). Type species: *Troglanillus valentinei* Jeannel, 1963b, by original designation.

***Anillinus felicianus* sp. nov.**
http://zoobank.org/CA1608B7-D169-418F-9F80-02E88AEBA5B3
Figs 1, 2, 5

Type material. ***Holotype*** male (NMNH), dissected, labeled: \ USA-LA: West Feliciana Par., ~4mi SW Jackson at 30.794°N, 91.254°W, mixed pine-hardwood forest, soil washing/berlese Sokolov I.M. 19–25 Apr 2018 \. ***Paratype*:** one female, labeled as holotype (NMNH); three males and three females labeled: \USA, LA, W. Feliciana Par. Feliciana Preserve Natural Area, Orange Trail, 30.792649°N, 91.253382°W, 29 Oct. 2015 \ Soil washing in hardwood forest B.E. Owens and C.E. Carlton \(LSAM).

Etymology. The name of this species is a Latinized adjective based on the name of Feliciana Preserve, in which this species occurs. Feliciana Preserve is a privately owned nature reserve created by several professors of the Louisiana State University (principal developer Dr. Dorothy Prowell) and located in the Tunica Hills area of southeastern Louisiana.

Type locality. USA, Louisiana, West Feliciana Parish, Tunica Hills, 4 mi SW of Jackson.

Recognition. Adults of *A. felicianus* can be distinguished from those of other subterranean members of *Anillinus* by the combination of smooth pronotum and completely microsculptured head. Males of *A. felicianus* can be also distinguished from those of other congeners by the structure of the median lobe.

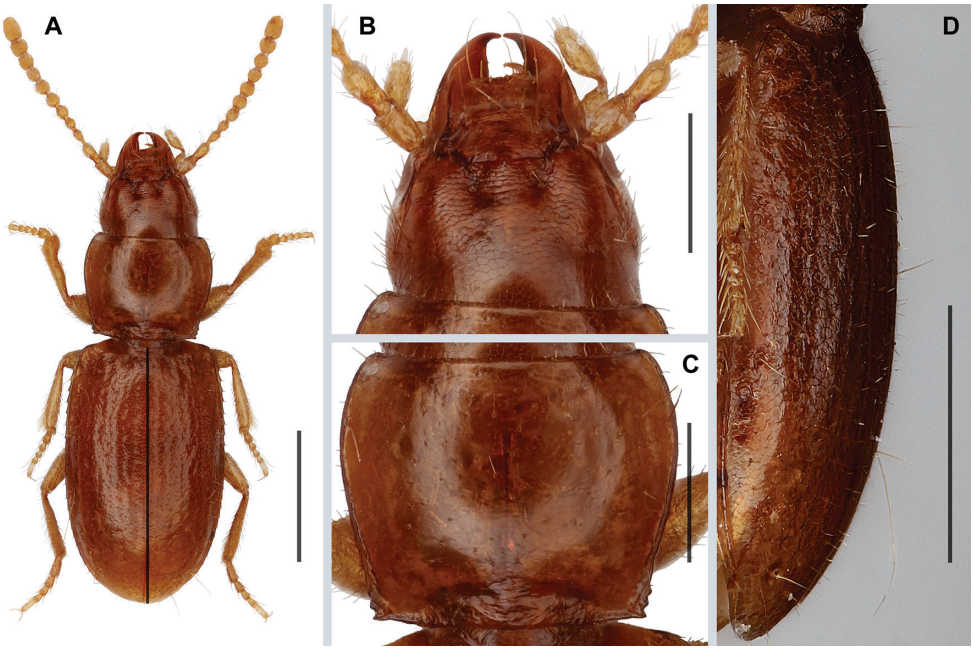

Figure 1. Digital images of external features of *Anillinus felicianus* sp. nov. (male, 4 mi SW of Jackson, West Feliciana Parish, Louisiana) **A** habitus, dorsal aspect **B** head, dorsal aspect **C** pronotum, dorsal aspect **D** elytral vestiture, left lateral aspect. Scale bars: 0.5 mm (**A, D**); 0.2 mm (**B, C**).

Description. Moderate-sized for genus (ABL 1.59–1.68 mm, mean 1.64±0.064 mm, n = 2).

***Habitus*:** Body form (Fig. 1A) moderately convex, subparallel, elongate (WE/ABL 0.36±0.001), head moderately large in comparison to pronotum (WH/WPm 0.77±0.008), pronotum of moderate width in comparison to elytra (WPm/WE 0.82±0.006).

***Integument*:** Body color brunneo-rufous, appendages testaceous. Microsculpture (Fig. 1B–D) present across all head and elytra, where it is represented by isodiametric polygonal sculpticells; and absent from disc of pronotum. Body surface shiny, surface sparsely and finely punctate, covered with sparse, yellowish, short setae. Vestiture of elytra (Fig. 1D) short (~0.3 length of discal setae). Elytral chaetotaxy typical for *Anillinus*, umbilicate series of type A (*sensu* Jeannel 1963a and Giachino and Vailati 2011): nine setae arranged in three groups, subhumeral (3+1), middle (2) and subapical (1+2), with the last two (8th and 9th) pores of umbilicate series "geminate", much closer to each other than 7th pore is to 8th; in subapical group the 8th pore is the longest.

***Prothorax*:** Pronotum (Fig. 1C) moderately convex, of moderate size (LP/LE 0.41±0.010) and moderately transverse (WPm/LP 1.26±0.009), with lateral margins almost rectilinearly and moderately constricted posteriorly (WPm/WPp 1.26±0.009). Anterior angles indistinct, posterior angles slightly obtuse (105–110°). Width between posterior angles equals width between anterior angles (WPa/WPp 0.97±0.001). Basal margin slightly concave in middle.

***Scutellum*:** Externally visible, triangular, with pointed apex.

***Elytra*:** Slightly convex, of average length (LE/ABL 0.58±0.012) and width (WE/LE 0.63±0.015) for genus, with traces of 4–5 striae. Humeri distinct, rounded, in outline forming obtuse angle with longitudinal axis of body. Lateral margins subparallel in middle, slightly convergent at basal fourth, evenly rounded to apex at apical third, with shallow subapical sinuation. Basal margination distinct.

***Legs*:** Protarsi of male with moderately dilated tarsomere 1. Profemora moderately swollen. Metafemora unmodified.

***Male genitalia*:** Median lobe (Fig. 2A) of aedeagus anopic, slightly arcuate and moderately twisted. Shaft dilated in apical two-thirds, with moderately elongate apex, slightly tapered to rounded tip. Ventral margin of median lobe straight, not enlarged, with few poriferous canals, curved downward close to basal orifice. Endophallus with dorsal copulatory sclerites fused to form slightly curved dorsal blade-like structure and straight, apically-pointed ventral plate of moderate length. Spines and scaled membranous folds of endophallus absent. Left paramere (Fig. 2B) of shape common in genus, paramere apex with four setae getting longer toward apex. Right paramere (Fig. 2C) of moderate length, bearing three long setae of approximately same length as paramere.

***Female genitalia*:** Spermatheca (Fig. 2E) unsclerotized, shaped as a question mark, with sharply dilated bean-like distal part. Length of spermathecal gland shorter than length of spermatheca. Spermathecal duct uncoiled. Gonocoxites and laterotergite as in Fig. 2D. Gonocoxite 2 falciform, more than 2 times longer than wide basally, with acute ensiferous setae. Laterotergite with 7–8 setae.

Geographic distribution. This species is known only from the type locality in the Tunica Hills area of West Feliciana Parish, Louisiana (Fig. 5, green circle).

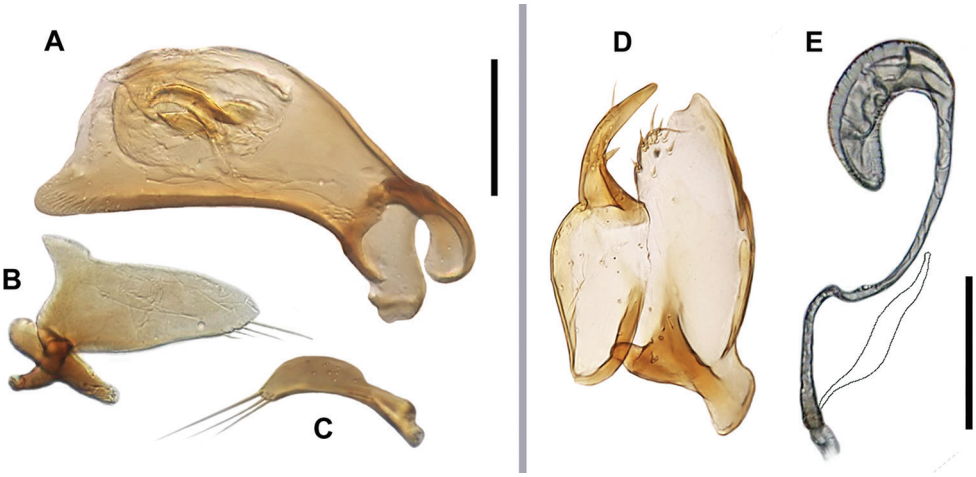

Figure 2. Digital images of male and female genitalia of *A. felicianus* sp. nov. (4mi SW of Jackson, West Feliciana Parish, Louisiana). Male genitalia **A** median lobe, right lateral aspect **B** left paramere, left lateral aspect **C** right paramere, right lateral aspect. Female genitalia **D** ovipositor sclerites **E** spermatheca (spermathecal gland manually restored). Scale bars: 0.1 mm.

Habitat. All specimens of this species were collected from loess soil samples using soil washing techniques (Southwood and Henderson 2000). These samples were taken under forest canopy on the top of a hill between two gullies with temporal creeks. *Anillinus felicianus* is a true endogean species and has never been found in litter samples.

Relationships. The species belongs to group V of endogean species (*sensu* Sokolov et al. 2004), characterized by a combination of a completely microsculptured head and smooth disc of pronotum. Within this group, *A. felicianus* is most closely related to the endogean *A. sinuaticollis* Jeannel (Jeannel 1963b), differing from the latter by a smooth – not microsculptured – base of the pronotum, a bigger size, and details of the pronotum shape and body proportions. The range of *A. sinuaticollis* is confined to Roane County of Tennessee (Fig. 5, green area with vertical line pattern); thus, its range lies about 500 miles north of the type locality of *A. felicianus*.

***Anillinus relictus* sp. nov.**
http://zoobank.org/8F185D84-D2A4-464B-97F9-A5FEDD791B47
Figs 3, 4A–C, 5

Type material. ***Holotype***, one male (CMNH), dissected, labeled: \ ALABAMA: Blount Co., Tidwell Hollow Nature Trail east of Oneonta. T. N. King April 1 1972 \ 4/1/72 o [handwritten] \ THOMAS C. BARR COLLECTION 2011 Acc. No. 38,014 \. ***Paratype***, one female, labeled as holotype (CMNH).

Etymology. The specific epithet is a Latin adjective, *relictus* (from Latin: abandoned, forsaken), in the masculine form, and refers to the geographical isolation of this species from its morphologically closest congeners, as it is believed to be the only remaining eastern representative of an ancestral group once more widespread.

Type locality. USA, Alabama, Blount County, the Oneonta area.

Recognition. Adults of *A. relictus* can be distinguished from those of other members of eastern *Anillinus* by the combination of the large size, completely microsculptured head and pronotum, and, especially, by the long elytral vestiture equals to 0.5–0.7 of length of discal elytral setae.

Description. Large-sized for genus (ABL 2.29–2.42 mm, mean 2.36±0.092 mm, n = 2).

***Habitus*:** Body form (Fig. 3A) moderately convex, ovoid (WE/ABL 0.39±0.012), head of average proportions for genus (WH/WPm 0.71±0.023), pronotum moderately narrow in comparison to elytra (WPm/WE 0.77±0.007).

***Integument*:** Body color piceo-brunneus, appendages testaceous. Microsculpture (Fig. 3B–D) present across all head, pronotum, and elytra, where it is represented by isodiametric polygonal sculpticells. Body surface shiny, surface sparsely and finely punctate, covered with moderately dense, yellowish, long setae. Vestiture of elytra (Fig. 3D) long (0.5–0.7 length of discal setae). Elytral chaetotaxy typical for *Anillinus*, umbilicate series of type A (*sensu* Jeannel 1963a and Giachino and Vailati 2011).

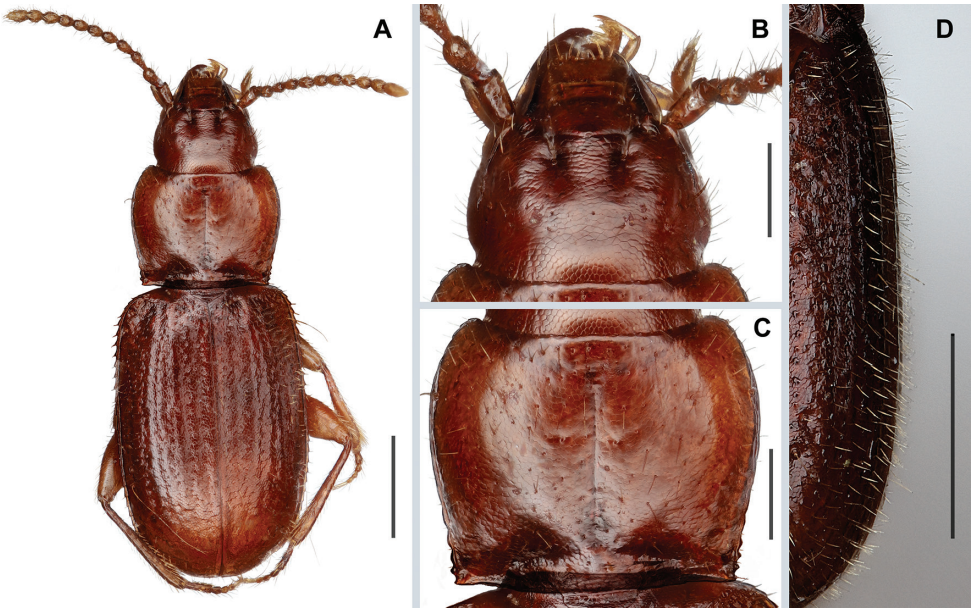

Figure 3. Digital images of external features of *Anillinus relictus* sp. nov. (male, E of Oneonta, Blount County, Alabama) **A** habitus, dorsal aspect **B** head, dorsal aspect **C** pronotum, dorsal aspect **D** elytral vestiture, left lateral aspect. Scale bars: 0.5 mm (**A, D**); 0.2 mm (**B, C**).

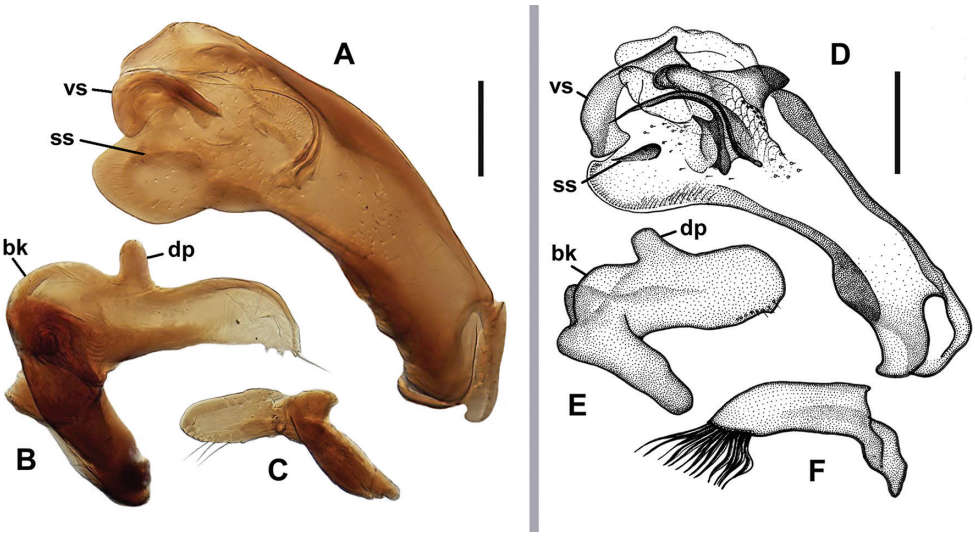

Figure 4. Digital images and line drawings of male genitalia of *Anillinus* species. *A. relictus* (E of Oneonta, Blount County, Alabama) **A** median lobe, right lateral aspect **B** left paramere, left lateral aspect **C** right paramere, right lateral aspect. *A. sinuatus* (Bexar County, Texas) **D** median lobe, right lateral aspect **E** left paramere, left lateral aspect **F** right paramere, right lateral aspect. bk – basal keel, dp – dorsal process, ss – spine-like structure, vs – ventral sclerite. Scale bars: 0.1 mm.

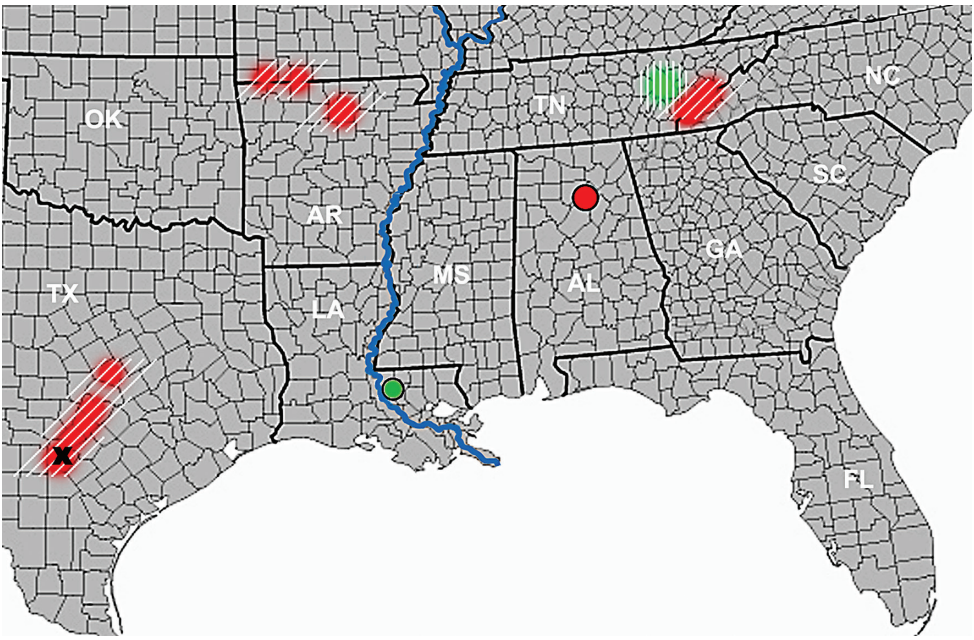

Figure 5. Map of the South of eastern United States, showing positions of locality records for the newly described species of *Anillinus* and the ranges of their presumed relatives (localities of the same color reflect supposed relatedness). *A. felicianus*, green circle; *A. relictus*, red circle. Green area with vertical line pattern – range of *A. sinuaticollis*. Black cross – type locality of *A. sinuatus*. Red areas with diagonal line pattern – ranges of the species of *Anillinus* whose males have a spine-like structure in the endophallus of the median lobe (after Sokolov et al. 2004; Sokolov and Watrous 2008; Sokolov 2011; Sokolov et al. 2014; Sokolov et al. 2017). Blue line – Mississippi River. State abbreviations follow Federal Information Processing Standards (https://www.nlsinfo.org/content/cohorts/nlsy79/other-documentation/codebook-supplement/nlsy79-attachment-102-federal).

***Prothorax*:** Pronotum (Fig. 3C) moderately convex, of moderate size (LP/LE 0.40±0.003) and moderately transverse (WPm/LP 1.26±0.028), with lateral margins almost rectilinearly and slightly constricted posteriorly (WPm/WPp 1.19±0.013). Anterior angles slightly prominent, posterior angles nearly rectangular (95–100°). Width between posterior angles much greater than between anterior angles (WPa/WPp 0.87±0.038). Basal margin slightly concave in middle.

***Scutellum*:** Externally visible, triangular, with rounded apex.

***Elytra*:** Narrowly depressed along suture, of average length (LE/ABL 0.59±0.005) and width (WE/LE 0.66±0.026) for genus, with traces of 6–7 striae. Humeri distinct, rounded, in outline forming obtuse angle with longitudinal axis of body. Lateral margins subparallel in middle, slightly convergent at basal fifth, evenly rounded to apex at apical fourth, with shallow subapical sinuation. Basal margination distinct.

***Legs*:** Protarsi of male with moderately dilated tarsomere 1. Profemora moderately swollen. Metafemora unmodified.

***Male genitalia*:** Median lobe of aedeagus (Fig. 4A) anopic, slightly arcuate and slightly twisted. Basal orifice comparatively short for the genus. Shaft with long subparallel basal part, slightly dilating in apical third. Apical part with enlarged apex in form of rounded parallelogram. Dorsal margin slightly convex and strongly sclerotized at middle. Ventral margin curved near middle, where it is suddenly enlarged right before the apex. Endophallus with dorsal sclerite in form of a semicircular filament-like structure with short basal prolongations. Ventral sclerite located at apical orifice, in form of golf gap wedge plate. Dorsal scaly membranous field present at middle of dorsal sclerite. Enlarged apical area of median lobe with a dark spine-like structure (Fig. 4A, ss). Left paramere (Fig. 4B) modified, with long, subparallel apical half of moderate width with one seta at angulate tip, basally with strong concave keel (bk), and thick basal processes of different length. Right paramere (Fig. 4C) of moderate length, with eight setiferous pores bearing only three long setae (several others might be broken), which are shorter than length of paramere.

***Female genitalia*:** Spermatheca not investigated. Ovipositor sclerites standard for genus with falciform gonocoxite 2 bearing two ensiform setae. Laterotergite with 8–9 setae.

Geographic distribution. This species is known only from the type locality in Blount County, Alabama (Fig. 5, red circle).

Habitat. The label does not contain any habitat information. Presumably, this species is not a cavernicolous species.

Relationships. Based on the structure of the median lobe, *A. relictus* is a sister species to the endogean *A. sinuatus* (Jeannel) (Jeannel 1963a). The latter species is known to occur in Bexar County, Texas, where it was documented by a small series of three specimens extracted from the soil during surveys in peach orchards (Jeannel 1963a; Sokolov et al. 2014). The range of *A. sinuatus* (Fig. 5, black cross) is situated approximately 770 miles southwest of the type locality of *A. relictus*.

The following key to the Alabama *Anillinus* is modified from couplet 2 in Sokolov (2020) to accommodate *A. relictus*:

2(1) Ventral parts of body (meso- and metathorax, abdominal sterna) covered with numerous setae. Spines of endophallus clustered together in a robust plate (Fig. 5G in Sokolov 2012, p. 67) ..... ***A. hirsutus* Sokolov**

2' Ventral parts of body without unusual vestiture. Spines of endophallus either lacking or, if present, scattered inside median lobe and separate from each other **3a**

3a (2') Elytra covered with shorter vestiture. Discal setae approximately 2.5–3.0 times longer than surrounding vestiture. Endophallus of median lobe lacking sclerotized spine-like structure in apical area and with copulatory sclerites merged into one structure **3**

3a' Elytra covered with longer vestiture. Discal setae at most 2 times longer than surrounding vestiture. Endophallus of median lobe with sclerotized spine-like structure in apical area and with two distant copulatory sclerites..... ..... ***A. relictus* Sokolov, sp. nov.**

3(2') [continue following key in Sokolov (2020)].

Discussion

The discovery of two new species extends our knowledge of the *Anillinus* fauna, the relationships within the genus, the distribution patterns of its representatives, and the evolutionary history of species inhabiting the Gulf Coast of the United States, a territory with a much less known fauna of *Anillinus* in comparison with the same fauna of the southern Appalachians.

Especially amazing is the discovery of *A. relictus*, because the immediate relatives of this Alabama species live in Texas. For *A. relictus*, some peculiar characters of the endophallus of the median lobe can be traced in several groups of *Anillinus* species separated geographically. At least three groups of species can be distinguished: (1) all Texan species except *A. depressus* Jeannel and *A. acutipennis* Sokolov and Reddel (whose males are still unknown), (2) both species from the Ozark Mountains, and (3) all three species of the *moseleyae*-group from the high altitudes of the Great Smoky Mountains. All these species have a unique character: the presence of a sclerotized, spine-like structure visible in the apical area of the median lobe (Fig. 4A, D ss). In addition, all species show modifications in the shape of the left paramere (Fig. 4B, E): a long right basal process and strong convex basal keel (bk), whose convexity shifts the position of the dorsal process (dp) of the paramere distally from its standard position. The eastern species of the *moseleyae*-group and *A. aleyae* Sokolov & Watrous from Missouri are closer to each other in having only one dorsal copulatory sclerite in the endophallus, an evenly-curved ventral margin, and the shorter shaft of the median lobe (Sokolov and Watrous 2008; Sokolov 2011). The Texan species and *A. alleni* Sokolov & Carlton, contrary to the members of the previous subgroup, have a longer shaft, often with a strong dorsal sclerotization, and more than one copulatory sclerite in the endophallus of the median lobe (Sokolov et al. 2014, 2017). Of these, *A. relictus* is morphologically closer to the Texan species and *A. alleni*, thus being the only representative of this subgroup east of the Mississippi River. Especially striking is the similarity in the structures of the median lobes between *A. relictus* and the endogean *A. sinuatus*. Similarities can be seen in the general proportion and the shape of the median lobe, in the similar dorsal sclerotization, and in the position and shape of the ventral sclerite (cf. Fig. 4A, D vs). Convergence in such a number of details within the male genitalia seems less probable than structural similarity due to the common origin of these two species. If this is correct, we can assume that at a certain point in time, their ancestor occupied a vast territory from the southern edges of the Cumberland Plateau westward to the Edwards Plateau. During glacial cycles, most migration routes in eastern North America followed the north-south direction, because of the local topography, especially that of the Appalachian Mountains, characterized by a series of parallel north-east to south-west trending valleys and ridges (Howden 1969; Gonzales et al. 2008). The directionality of glacial drainages was similar, and together, this topography slowed down the latitudinal migrations, brought genetic discontinuity, and formed east-west phylogeographical patterns in the southeastern USA (Liu et al. 2006; Pauly et al. 2007;

Gonzales et al. 2008). This presumably prevented the formation of latitudinal ranges. Hence, it is reasonable to suppose that such a latitudinal range of the wingless ancestor of *A. sinuatus* and *A. relictus* likely arose before the Quaternary glaciations. Thus, the assemblage of species with a sclerotized, spine-like structure in the endophallus of the median lobe represents one of the ancient lineages of *Anillinus*.

The discovery of a new species of *Anillinus* in Louisiana is of biogeographical significance, because Louisiana is the only Gulf state in which anillines had previously never been recorded; thus, this record fills a gap in the distribution of *Anillinus* in the territories around the Gulf of Mexico. Speculating about the possible ways *A. felicianus* could have arisen in the territory of Louisiana, it is worth paying attention to the history of the Tunica Hills, the area where the species was discovered. Interestingly, many northern disjuncts of plants have been recorded to occur in this area (Delcourt and Delcourt 1996). It was once considered as an isolated "island" refugium for plant species, which presumably had migrated southward during the glaciation cycles (Braun 1950). The majority of these plants now occur within north-central United States and in the Appalachian Mountains (Delcourt and Delcourt 1975). Thus, during the glacial cycles, some of the Appalachian plant communities probably reached the Tunica Hills area. Evidently, other living organisms associated with plant communities could have migrated synchronously. The recent discoveries of the eastern *Bembidion* (*Hirmoplataphus*) *nigrum* Say (Bousquet 2012) and *Batrisodes dorothae* Ferro & Carlton (Ferro and Carlton 2014) in the Tunica Hills may constitute a strong evidence in support of this assumption. Therefore, the external similarity between *A. felicianus* and the Appalachian endogean *A. sinuaticollis* was, in fact, not unexpected. Unfortunately, the males of *A. sinuaticollis* are still unknown, making it impossible to examine male genitalia of this species. However, many of the characters of the male genitalia of *A. felicianus*, including its blade-like dorsal sclerite with a basally attached ventral plate of the endophallus of the median lobe, can be found in the median lobes of another group of Appalachian *Anillinus* – the litter members of the *langdoni*-group (Sokolov et al. 2007). Both of these facts unequivocally point to the Appalachian origin of *A. felicianus*. It is likely that, contrary to *A. relictus*, the speciation of *A. felicianus* happened comparatively late, presumably during the Quaternary glacial cycles, although the details remain obscure. Given its external morphology, the closest relative of the endogean *A. felicianus* should be the endogean *A. sinuaticollis*, not the litter species of the *langdoni*-group. In contrast to the litter representatives of the *langdoni*-group, both endogean species lack the microsculpture on the pronotal disc and have slightly different body proportions. Whether these characters are adaptive and repeatedly evolve each time the litter species developed adaptations to living in a subterranean environment is not clear. Currently, both scenarios of the arising of *A. felicianus* should be considered as equally possible: (1) an allopatric origin after splitting the range of migrated endogean species, or (2) a sympatric origin from migrated litter species, whose adaptations to an endogean lifestyle gave birth to a new species, while the ancestral litter form subsequently became extinct due to unknown, possibly ecological factors.

Acknowledgements

I would like to express special thanks to Christopher E. Carlton (Professor and former Director of Louisiana State Arthropod Museum, LSU, Baton Rouge), who kindly shared information about finding *Anillinus* in Louisiana, and Dorothy Prowell (Faculty Emeritus and Professor of Conservation Biology of the Louisiana State University) for permission to collect beetles in Feliciana Preserve. I am also grateful to Robert L. Davidson (former Curator of the Carnegie Museum of Natural History, Pittsburg, Pennsylvania) who lent me the material of *Anillinus* from the museum collection in his care. I greatly appreciate the valuable help with digital imaging provided by Alex S. Konstantinov (Systematic Entomology Laboratory-USDA, Washington, DC, USA).

The mention of trade names or commercial products in this publication is solely for the purpose of providing specific information and does not imply recommendation or endorsement by the USDA; the USDA is an equal opportunity provider and employer.

References

Barr TC (1995) Notes on some anillines (Coleoptera, Carabidae, Bembidiinae) from southeastern United States, with description of a new genus and two new species. Special Bulletin Japanese Society of Coleopterology 4: 239–248.

Bonelli FA (1810) Observations entomologiques. Première partie (cicindélètes et portion des carabiques) [with the "Tabula synoptica exhibens genera carabicorum in sectiones et stirpes disposita"]. Turin, 58 pp. [+ 1 table]

Bousquet Y (2012) Catalogue of Geadephaga (Coleoptera, Adephaga) of America, North of Mexico. ZooKeys 245: 1–1722. https://doi.org/10.3897/zookeys.245.3416

Braun EL (1950) Deciduous Forests of Eastern North America. Blakiston Co., Philadelphia, 596 pp.

Casey TL (1918) Memoirs on the Coleoptera. VIII. The New Era Printing Company, Lancaster, PA, 727 pp. https://doi.org/10.5962/bhl.title.1159

Delcourt HR, Delcourt PA (1975) The Blufflands: Pleistocene pathway into the Tunica Hills. The American Midland Naturalist 94: 385–400. https://doi.org/10.2307/2424434

Delcourt PA, Delcourt HR (1996) Quaternary paleoecology of the Lower Mississippi Valley. Engineering Geology 45: 219–242. https://doi.org/10.1016/S0013-7952(96)00015-4

Ferro ML, Carlton CE (2014) Two new species of *Batrisodes* Reitter (Coleoptera: Staphylinidae: Pselaphinae) from eastern North America. Insecta Mundi 0380: 1–21.

Giachino PM, Vailati D (2011) Review of the Anillina of Greece (Coleoptera, Carabidae, Bembidiini). Biodiversity Journal, Monograph 1: 1–112.

Gonzales E, Hamrick JL, Chang SM (2008) Identification of glacial refugia in south-eastern North America by phylogeographical analyses of a forest understorey plant, *Trillium cuneatum*. Journal of Biogeography 35: 844–852. https://doi.org/10.1111/j.1365-2699.2007.01834.x

Howden HF (1969) Effects of the Pleistocene on North American insects. The Annual Review of Entomology 14: 39–56. https://doi.org/10.1146/annurev.en.14.010169.000351

Jeannel R (1937) Les Bembidiides endogés (Col. Carabidae). Revue française d'Entomologie 3: 241–339.

Jeannel R (1963a) Monographie des "Anillini", Bembidiides endogés [Coleoptera Trechidae]. Mémoires du Muséum National d'Histoire Naturelle, Série A, Zoologie 28: 33–204.

Jeannel R (1963b) Supplément à la monographie des Anillini. Sur quelques espèces nouvelles de l'Amérique du Nord. Revue Française d'Entomologie 30: 145–152.

Latreille PA (1802) Histoire naturelle, générale et particulière des crustacés et des insectes. Ouvrage faisant suite à l'histoire naturelle générale et particulière, composée par Leclerc de Buffon, et rédigée par C.S. Sonnini, membre de plusieurs sociétés savantes. Familles naturelles des genres. Tome troisième. F. Dufart, Paris, 467 pp. https://doi.org/10.5962/bhl.title.15764

Linnaeus C (1758) Systema naturae per regna tria naturae, secundum classes, ordines, genera, species, cum characteribus, differentiis, synonymis, locis. Editio decima, reformata. Tomus I. Laurentii Salvii, Holmiae, [4 +] 823 [+ 1] pp. https://doi.org/10.5962/bhl.title.542

Liu F-GR, Moler PE, Miyamoto MM (2006) Phylogeography of the salamander genus *Pseudobranchus* in the southeastern United States. Molecular Phylogenetics and Evolution 39: 149–159. https://doi.org/10.1016/j.ympev.2005.09.015

Pauly GB, Piskurek O, Shaffer B (2007) Phylogeographic concordance in the southeastern United States: the flatwoods salamander, *Ambystoma cingulatum*, as a test case. Molecular ecology 16: 415–429. https://doi.org/10.1111/j.1365-294X.2006.03149.x

Rohlf FJ (2013) tpsDig2 version 2.17. Department of Ecology and Evolution, State University of New York at Stony Brook, New York.

Sokolov IM (2011) Five new species of *Anillinus* Casey from the southern Appalachian Mountains and the Piedmont Plateau of eastern U.S.A. (Coleoptera: Carabidae: Trechinae: Bembidiini). Insecta Mundi 164: 1–14.

Sokolov IM (2020) Four new species of the genus *Anillinus* Casey (Coleoptera, Carabidae, Anillini) from Alabama, U.S.A., with a revised key to the Alabama species. Zootaxa 4808: 547–559. https://doi.org/10.11646/zootaxa.4808.3.9

Sokolov IM, Carlton CE, Cornell JF (2004) Review of *Anillinus* with descriptions of 17 new species and a key to soil and litter species (Coleoptera: Trechinae: Bembidiini). The Coleopterists Bulletin 58: 185–233. https://doi.org/10.1649/611

Sokolov IM, Carlton CE, Watrous LE, Robison HW (2017) *Anillinus alleni* Sokolov and Carlton (Coleoptera: Carabidae: Trechinae: Bembidiini), a new species from the Ozark Interior Highlands of Arkansas, USA. The Coleopterists Bulletin 71: 289–297. https://doi.org/10.1649/0010-065X-71.2.289

Sokolov IM, Kavanaugh DH (2014) The *integripennis* species group of *Geocharidius* Jeannel, 1963 (Carabidae, Bembidiini, Anillina) from Nuclear Central America: a taxonomic review with notes about biogeography and speciation. ZooKeys 443: 61–118. https://doi.org/10.3897/zookeys.443.7880

Sokolov IM, Sokolova YY, Carlton CE (2007) New species of *Anillinus* Casey (Carabidae: Trechinae: Bembidiini) from Great Smoky Mountains National Park, U.S.A. and phyloge-

ography of the *A. langdoni* species group. Zootaxa 1542: 1–20. https://doi.org/10.11646/zootaxa.1542.1.1

Sokolov IM, Reddell JR, Kavanaugh DH (2014) Life beneath the surface of the central Texan Balcones Escarpment: genus *Anillinus* Casey, 1918 (Coleoptera, Carabidae, Bembidiini): new species, a key to the Texas species, and notes about their way of life and evolution. ZooKeys 417: 71–101. https://doi.org/10.3897/zookeys.417.7733

Sokolov IM, Watrous LE (2008) A new species and the first record of the genus *Anillinus* (Carabidae: Trechinae: Bembidiini) from the Ozark region. The Coleopterists Bulletin 62: 537–543. https://doi.org/10.1649/1114.1

Southwood TRE, Henderson PA (2000) Ecological Methods (3rd Edn.). Blackwell Science, Oxford, 575 pp.

ZooKeys 1016: 77–141 (2021)
doi: 10.3897/zookeys.1016.59699
https://zookeys.pensoft.net

RESEARCH ARTICLE

A peer-reviewed open-access journal
ZooKeys
Launched to accelerate biodiversity research

Taxonomic revision of grass frogs (Ptychadenidae, *Ptychadena*) endemic to the Ethiopian highlands

Sandra Goutte[1]*, Jacobo Reyes-Velasco[1]*, Xenia Freilich[2], Abeje Kassie[3,4], Stephane Boissinot[1]

1 *New York University Abu Dhabi, Saadiyat Island, Abu Dhabi, UAE* **2** *Department of Biology, Queens College, City University of New York, Flushing, New York, USA* **3** *Ethiopian Biodiversity Institute, Addis Ababa, Ethiopia* **4** *Addis Ababa University, Addis Ababa, Ethiopia*

Corresponding author: Sandra Goutte (sandra.goutte@nyu.edu); Stephane Boissinot (stephane.boissinot@nyu.edu)

Academic editor: A. Crottini | Received 17 October 2020 | Accepted 20 December 2020 | Published 11 February 2021

http://zoobank.org/A462DE73-4428-4857-973C-BCFD17294D15

Citation: Goutte S, Reyes-Velasco J, Freilich X, Kassie A, Boissinot S (2021) Taxonomic revision of grass frogs (Ptychadenidae, *Ptychadena*) endemic to the Ethiopian highlands. ZooKeys 1016: 77–141. https://doi.org/10.3897/zookeys.1016.59699

Abstract

Frogs of the genus *Ptychadena* that inhabit the Ethiopian highlands serve as a model system to understand biogeography, diversification, and adaptations to high elevations. Despite recent studies focusing on the systematics of this group, the taxonomy of the *Ptychadena neumanni* species complex remains only partially resolved, owing largely to the morphological resemblance of its members. Here, the taxonomy of this historically problematic group of frogs is revised by integrating morphological and molecular analyses on both century-old type specimens and more recently collected material. Based on these multiple lines of evidence, the *P. neumanni* species complex is shown to be more speciose than previously thought and four new species are described. With the aim of clarifying and stabilizing the taxonomy of the group, six species are also re-described and morphological and acoustic identification keys are provided. This study also establishes species distribution maps and reveals important differences in range size between the members of the *P. neumanni* complex, calling for adapted conservation measures across the Ethiopian highlands.

Keywords

Bioacoustics, herpetology, integrative taxonomy, linear morphometrics, phylogeny, species complex

* These authors contributed equally.

Table of contents

Introduction

The grass frog genus *Ptychadena* Boulenger, 1917 currently contains 56 recognized species found throughout sub-Saharan Africa (Frost 2020). Some members of this group have dispersed to islands of the Indian (Madagascar, the Seychelles Islands and the Mascarene Islands) and Atlantic Oceans (Bioko island, Sao Tome; Vences et al. 2004; Measey et al. 2007), while others have invaded the Ethiopian highlands and can occur

at elevations above 3000 meters. The genus *Ptychadena* is notorious for its highly conserved morphological features and the difficulty to distinguish closely related species and has thus baffled taxonomists for decades (e.g., Poynton 1970; Bwong et al. 2009; Dehling and Sinsch 2013). In particular, resolving the taxonomy of *Ptychadena* inhabiting the Ethiopian highlands has proven to be extremely challenging for a number of reasons, including the morphological resemblance among species, their inter- and intra-populations morphological variation, and confusing original descriptions (Ahl 1924). Thus, species misidentifications and taxonomic errors have accumulated throughout the literature (Perret 1980, 1994; Largen 2001; Smith et al. 2017a, b; Reyes-Velasco et al. 2018) and engendered confusion on the species' ecology and distribution.

Six species of *Ptychadena* from the Ethiopian highlands were originally described based only on morphology: *P. neumanni* (Ahl, 1924), *P. erlangeri* (Ahl, 1924), *P. cooperi* (Parker, 1930), *P. nana* Perret, 1980, *P. harenna* Largen, 1997, and *P. wadei* Largen, 2000. A seventh species, *P. largeni*, was described by Perret (1994), but later synonymized with *P. neumanni* by Largen (2001). These species, except for *P. wadei*, form a monophyletic group, hereafter referred to as the *P. neumanni* complex (Freilich et al. 2014).

Most of the confusion regarding the taxonomy of the Ethiopian *Ptychadena* arose from the original descriptions of *P. neumanni* and *P. erlangeri*, described by Ahl (1924) in the same article. While the description of *P. erlangeri* was based on a single female, the description of *P. neumanni* was based on 35 syntypes originating from four distinct localities. Perret (1980) showed that the type series of *P. neumanni* in fact contained multiple species, restricted *P. neumanni* to three males within the original type series and designating them as syntypes. Due to the sexual dimorphism present in the group, comparing the two species based on the morphological characters of their type specimens (one female versus three males) became very challenging, and numerous species misidentification occurred in the following studies (e.g., Perret 1994; Largen 2001; Smith et al. 2017a; Reyes-Velasco et al. 2018). For example, the distribution maps of *P. erlangeri* and *P. neumanni* published by Largen (2001) and later Largen and Spawls (2010) each contained individuals of both species, as well as additional ones (Fig. 1, Suppl. material 3: Table S6). Because of the difficulty to identify the different species, some subsequent authors relied on these maps to assign names to the populations they encountered (e.g., Smith et al. 2017a) and taxonomic confusion grew further.

Molecular analyses using both mitochondrial and nuclear loci revealed that *Ptychadena neumanni sensu* Largen (2001) in fact comprised five distinct taxa, which did not form a monophyletic group (Freilich et al. 2014). Freilich et al. (2014) did not describe the potential new species they identified because they were not able to compare their specimens with the type specimens of previously described taxa. A subsequent publication reproduced Freilich and colleagues' molecular analysis with a few additional samples and assigned names to these new taxa, but without any comparison with type specimens of previously described species and little morphological analysis (Smith et al. 2017a, b). Smith and colleagues thus assigned names of previously described species based solely on the locality of the few specimens they collected (Smith et al. 2017a, b), thereby adding to the general confusion regarding the taxonomy of this group (Suppl. material 3: Table S6).

In order to resolve the taxonomy of the *Ptychadena neumanni* species complex, we examined the type series of *P. neumanni*, *P. largeni*, *P. erlangeri*, and *P. nana*, and compared them morphologically to recently collected specimens for which molecular data was available (Reyes-Velasco et al. in review). We also sequenced mitochondrial DNA of the type specimens of these four species and included them in a phylogenetic analysis, which included recently sampled specimens as well as the type specimens of the species described by Smith and colleagues (2017a, b) (Fig. 2; Reyes-Velasco et al. in review). We recovered all the clades found in previous molecular phylogenetic analyses (Freilich et al. 2014; Smith et al. 2017a, b; Reyes-Velasco et al. 2018) and were able to determine the phylogenetic relationships of the historical type specimens relative to recently collected material, which allowed us to assign taxonomically correct names to these clades.

Our analyses grouped together the holotypes of *P. largeni* and *P. erlangeri*, showing that *P. largeni* was a junior synonym of *P. erlangeri* (Fig. 2). Additionally, these specimens grouped with the population designated as *P.* cf. *neumanni 2* by Freilich et al. (2014). The type specimen of *P. neumanni* grouped with the population considered as *P. erlangeri* by multiple authors since Largen (1997) (Suppl. material 3: Table S6). The population assigned to *P. neumanni* by Smith et al. (2017a, b) (*P.* cf. *neumanni 1* in Freilich et al. 2014), however, represented a new species. Finally, we showed that the type specimens of *P. nana* grouped with the population found in the Didda plateau, and that the individuals found on the east Arussi plateau (east of the Bale Mountains) represented a new species (Fig. 2; Reyes-Velasco et al. in review).

Based on molecular and morphological analyses, we describe four new species and re-describe six species of the *P. neumanni* complex with the goal of clarifying and stabilizing the taxonomy of the group. We also describe the advertisement calls of eleven species of the complex, and provide morphological and acoustic identification keys (Suppl. material 1: Appendix S1 and Suppl. material 2: Appendix S2). We did not include *Ptychadena wadei* in the current study, as this species is more distantly related to and readily distinguishable from other *Ptychadena* species from the Ethiopian highlands (Mengistu 2012). We also excluded *P. cooperi* and *P. harenna* from this revision, as their original descriptions are sufficiently complete to distinguish them from other species of the complex, however, we have included these three species in our identification key.

Materials and methods

Sampling

Methods of sampling are discussed in detail in Freilich et al. (2014) and Reyes-Velasco et al. (2018). In brief, we collected individuals of the *Ptychadena neumanni* species complex from the highlands of Ethiopia between 2011 and 2019 (Fig. 3, Suppl. material 3: Table S1). Our study was approved by the relevant Institutional Animal Care and Use Committee at Queens College and New York University School of Medicine (IACUC; Animal Welfare Assurance Number A32721–01 and laboratory animal protocol 19–0003). Frogs were sampled according to permits DA31/305/05,

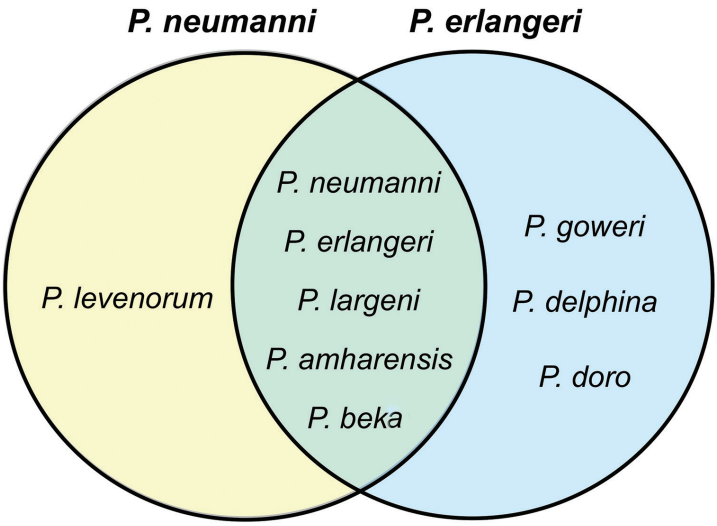

Figure 1. Species included under the names *Ptychadena neumanni* and *P. erlangeri* in previous studies. Species names within the circles correspond to the revised taxonomy. Left (yellow) and right (blue) circles contains all species identified as *P. neumanni* and *P. erlangeri*, respectively, since their original descriptions Ahl (1924). Species at the intersection of the two circles were identified as both species either in different studies (e.g., Largen 2001; Freilich et al. 2014; Smith et al. 2017a, b; Reyes-Velasco et al. 2018) or within the same study (e.g., Largen 2001). The full taxonomic history of the group is summarized in Suppl. material 3: Table S6.

DA5/442/13, DA31/454/07, DA31/192/2010, DA31/230/2010, DA31/7/2011 and DA31/02/11 provided by the Ethiopian Wildlife Conservation Authority. We photographed individuals in life and euthanized them by ventral application of 20% benzocaine gel. We extracted tissue samples and stored them in RNAlater or 95% ethanol. Adult individuals were fixed in 10% formalin for 24 to 48 hours, and then transferred to 70% ethanol. After preservation, we took additional photographs of all individuals. All specimens were deposited at the Zoological Natural History Museum (**ZNHM**), Addis Ababa, Ethiopia. Tissue samples are deposited at the Vertebrate Tissue Collection, New York University Abu Dhabi (**NYUAD**). Species distribution maps for the 12 species of the complex are shown in Figs 3–5.

Phylogenetic analyses

We describe the extraction of genomic DNA from fresh samples in Freilich et al. (2014) and Reyes-Velasco et al. (2018) and of mitochondrial genome of the type specimens of *Ptychadena neumanni*, *P. erlangeri*, *P. largeni*, and *P. nana* in Reyes-Velasco et al. (in review). Genetic data was already available for the type specimens of the more recently described species in the group (*P. amharensis*, *P. goweri*, and *P. levenorum*), so we did not re-sequence those type specimens. Fig. 2 reproduces the phylogeny obtained by Reyes-Velasco et al. (in review) based on the 12s rRNA, 16s rRNA and Cytochrome C oxidase I (COX1) mitochondrial genes for the type specimens as well as for recently collected specimens. GenBank accession numbers are given in Suppl. material 3: Table S2.

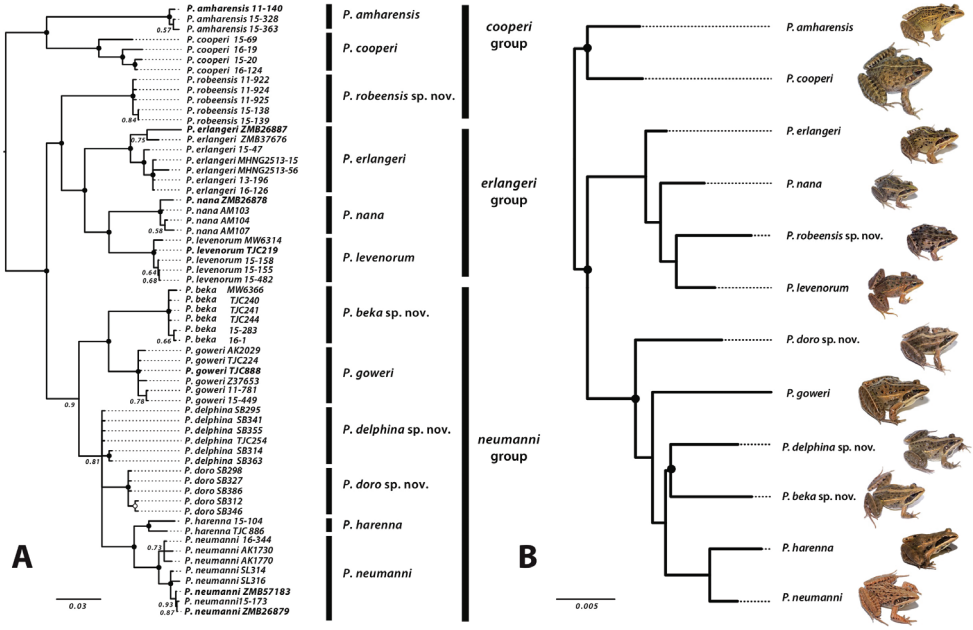

Figure 2. Phylogeny of the *Ptychadena neumanni* species complex **A** bayesian phylogenetic inference based on the concatenated sequences of the mitochondrial loci 12S and 16S rRNA as well as the protein-coding gene COX1. Black circles represent nodes with a posterior support of 1. Type specimens are indicated in bold **B** maximum Likelihood estimate (ML) of phylogenetic relationships in the *Ptychadena neumanni* species complex, inferred from a concatenated SNP dataset obtained using ddRAD sequencing. Black circles represent nodes with > 95% bootstrap support. Inset images represent members of each species: frogs are illustrated to the same scale. Modified from Reyes-Velasco et al. 2018.

Morphometric measurements

We measured individuals that were collected in recent years as well as type specimens for all taxa in the *Ptychadena neumanni* species complex, including the species described by Smith et al (2017a, b), using a SPI dial caliper, model #31-415-3 (accuracy ± 0.0015 mm). We measured type specimens at the following institutions: Zoological Natural History Museum, Addis Ababa University, Ethiopia (**ZNHM**), The Natural History Museum (formerly British Museum, Natural History; **NHMUK**), Muséum d'Histoire Naturelle, Geneva, Switzerland (**MHNG**) and the Museum für Naturkunde Berlin, Germany (**ZMB**). We took 19 linear morphometric measurements for each specimen (Fig. 6, Table 1, Suppl. material 3: Table S3), which are defined in Watters et al. (2016) and were shown to be useful for morphological differentiation of anurans.

List of abbreviations:

ED	eye diameter;	**FinDW**	longest finger disc width;
EN	eye-nostril distance;	**FL**	foot length;
ETD	eye-tympanum distance;	**FLL**	forearm length;

GRV	great rift valley;	**SL**	snout length;
HAL	hand length;	**SVL**	snout-vent length;
HL	head length;	**THL**	thigh length;
HW	head width;	**TD**	tympanum diameter;
IND	inter-nares distance;	**TL**	tibia length;
IOD	inter-orbital distance;	**Toe4DW**	fourth toe disc width;
MTL	metatarsal tubercle length;	**UEW**	upper eyelid width.
NS	snout-nostril distance;		

Statistical analyses of linear morphometric measurements

We analyzed males and females separately due to sexual size dimorphism. We used the R package *FactoMineR* (Lê et al. 2008). Because of shrinkage due to variable conditions of fixation and long-term preservation of type specimens, we ran discriminant analyses on recently collected individuals only, in order to select the measurements best discriminating between species (removing the types of *Ptychadena neumanni*, *P. erlangeri*, *P. largeni*, and *P. nana*). We then compared type specimens to the results.

To determine the best discriminating morphometric measurements, we first split the 12 species into groups based on their body size using the snout-vent length (SVL): we ran an ANOVA followed by a Tukey Honest Significant Differences (Tukey HSD) test on log-transformed SVL measurements of the 12 species, of males and females separately. Species that were not significantly different in body size in both sexes were placed in the same group. We then ran discriminant analyses sepa-

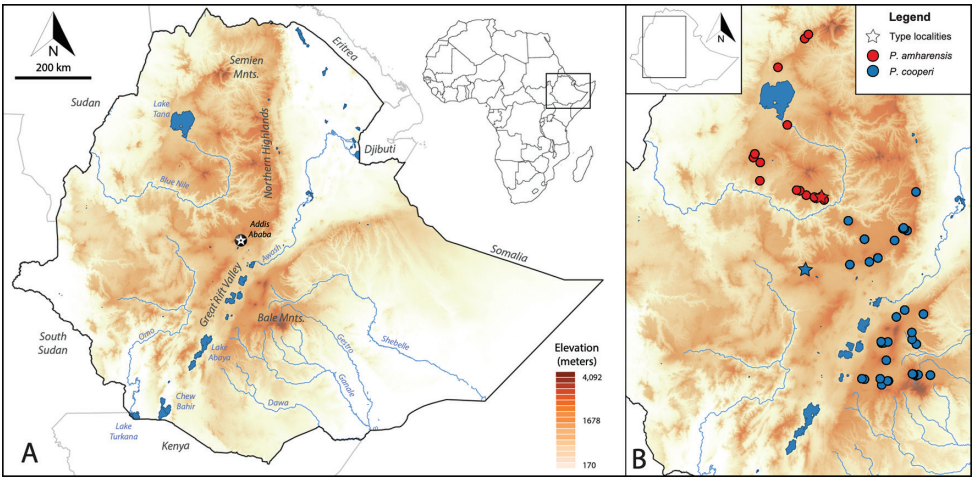

Figure 3. Distribution map of members of the *cooperi* species group in the highlands of Ethiopia **A** map of Ethiopia showing some of the most important geographic features of the country **B** distribution maps of members of the *cooperi* species group: *Ptychadena cooperi* (blue circles) and *P. amharensis* (red circles). Type localities for each species are indicated with a star.

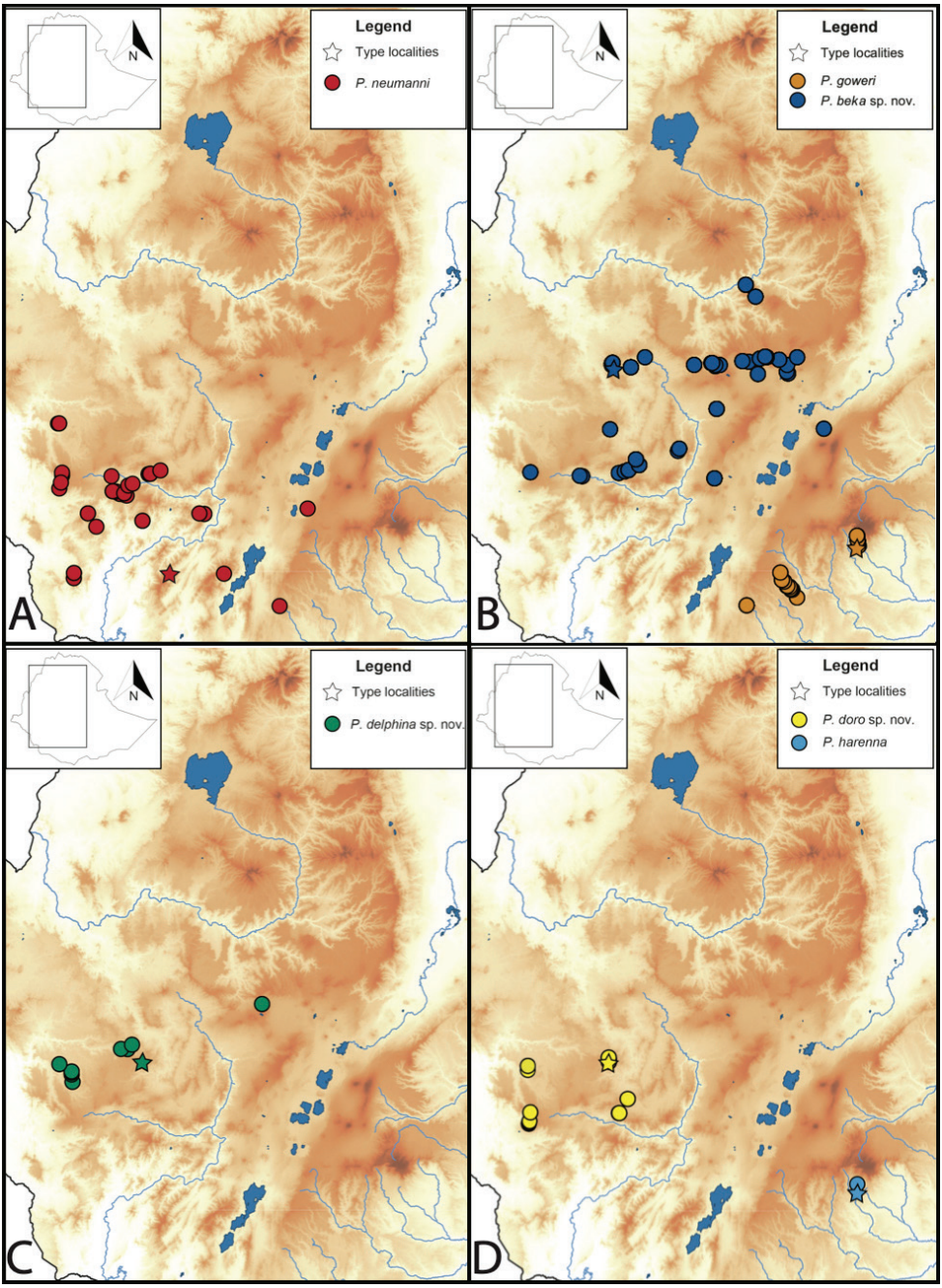

Figure 4. Distribution maps of members of the *neumanni* species group **A** *Ptychadena neumanni sensu stricto* (red circles) **B** *Ptychadena beka* sp. nov. (blue circles) and *P. goweri* (orange circles) **C** *Ptychadena delphina* sp. nov. (green circles) **D** *Ptychadena doro* sp. nov. (yellow circles) and *P. harenna* (light blue circles). Type localities for each species are indicated with a star.

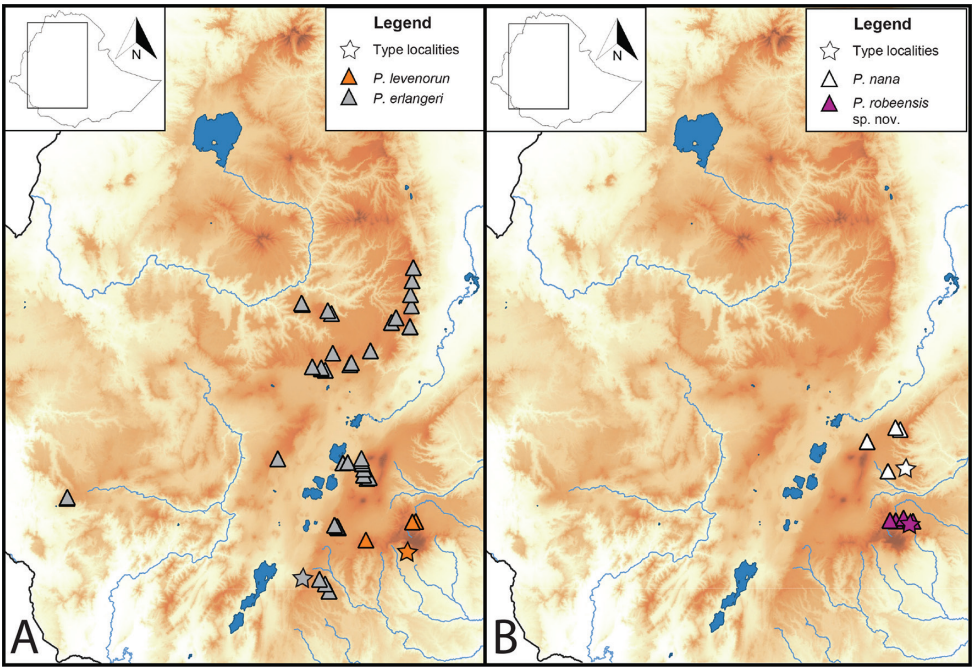

Figure 5. Distribution maps of members of the *erlangeri* species group **A** *Ptychadena erlangeri sensu stricto* (gray triangles) and *P. levenorum* (orange triangles) **B** *Ptychadena robeensis* sp. nov. (purple triangles) and *P. nana* (white triangles). Type localities for each species are indicated with a star.

rately to select the best discriminating measurements in each of these groups, and an ANOVA followed by a Tukey HSD on these variables for each of these groups. Suppl. material 3: Tables S4, S5 show the results of statistical analyses on linear morphometric measurements.

Morphometric measurements were all log-transformed prior to analysis in order to approach normality. In order to correct for body size in our measurements, we used ratios of measurements / SVL. We did not use other adjustment method such as the one proposed by Lleonart et al. (2000) and used by others (e.g., Onn et al. 2018) to correct for allometric growth, because this method relies on coefficients calculated on populations and therefore artificially segregates individuals in a priori-determined groups. In addition, this method requires to measure multiple individuals of a given population before calculating the adjusted variables, which is not always possible in the field. Given that our species are found in sympatry and that our goal here is to define characters that may be used for species identification without any a priori, we chose to resort to a size correction only based on the individual's own mensuration. Additionally, when comparing both correction methods on barcoded individuals, we found only marginal differences in the results and the ratios method proved to be more conservative.

Recording and analysis of advertisements calls

Spontaneously calling males were located acoustically or visually at night between 18:00 and 05:00. The call type most often heard from single males was considered as the advertisement call. Other call types produced by conspecific males, often heard when males were close to each other or physically engaged were considered as aggressive or release calls (Bogert 1960) and were disregarded. We recorded advertisement calls in situ at a distance of 0.5–2 meters to avoid near-field effect (Rossing 2007) or excessive attenuation or distortion of the sound. We used a Sennheiser ME66 directional microphone with a Sennheiser K6 powering module and an Olympus LS-100 or a Marantz PMD661 MKII recorder at a sampling rate of 44.1 kHz at 16 bits. Comments were recorded at the end of each recording using a Sennheiser ME62 microphone. For each recording, the maximum Sound Pressure Level (SPL) of the call was measured with a Galaxy Audio CM-170 SPL meter on A-weighting (precision: 1 dB at 1 kHz). The exact distance between the microphone and the calling male was measured with a Leica E7100i laser meter (precision: 3 mm) subsequent to the capture of the frog.

When possible, video recordings were taken simultaneously with an infrared camcorder (SONY DCR-SR85) and custom-made Colorado Para Tech infrared lights to ensure the identity of the focal individual. Videos were subsequently used to select the focal male's calls in recordings containing vocalizations of multiple individuals.

Advertisement calls were analyzed using Avisoft SAS (Sprecht 2017). We use a note-centered terminology scheme as described in Köhler et al. (2017), where the call constitutes a coherent unit and may contain one or several sub-units (notes), which, in turn, may contain distinct or indistinct pulses. We extracted 12 temporal and four spectral acoustic traits from our audio recordings: call duration, number of notes per call, note duration, inter-note interval duration (when applicable), note repetition rate (when applicable), number of pulses per note (when applicable), pulse duration (when applicable), inter-pulse interval duration (when applicable), pulse rate (when applicable), number of pulse groups per note (when applicable), number of pulses per pulse group (when applicable), relative time of peak amplitude, call peak frequency, call frequency bandwidth, minimal and maximal call frequencies. We did not extract values for call repetition rate or inter-call interval duration as these variables were highly dependent on the number of acoustically active individuals, and as such, are not taxonomically relevant characters.

Notes, pulses, and pulse groups were labelled semi-automatically using the pulse train analysis function and subsequently adjusting labels by eye. Sampling frequency was adjusted to 22050 Hz. Spectral traits were extracted from the spectrogram using the automatic parameter measurement function on spectrograms using a Fast Fourier Transformation (FFT) length of 512, Hamming windowing, 50% frame size, and 99.43% overlap between contiguous windows. All values were exported and averaged per individual and then per species in the R environment (R Core Team 2020). Spectrograms and oscillograms of the calls were plotted using the R package *seewave* (Sueur et al. 2008; Figs 7, 8).

Results

Phylogenetic analysis

The sampled populations of highland Ethiopian *Ptychadena* represent 12 distinct species grouped in three species groups, in agreement with previous studies (Freilich et al. 2014; Reyes-Velasco et al. 2018; Reyes-Velasco et al. in review). The *cooperi* species group comprises *P. cooperi* and *P. amharensis*. Although the two species are morphologically distinct, they share call traits which distinguish them from the other species of the *P. neumanni* complex: their calls are composed of a few, rapidly repeated pulsed note, which presents an ascending frequency modulation and indistinct pulses (Figs 7, 8). The *neumanni* species group comprises six species: *P. neumanni*, *P. harenna*, *P. goweri*, *P. beka* sp. nov., *P. delphina* sp. nov., and *P. doro* sp. nov. Members of this group are generally larger and have longer hindlimbs and larger tympanums than members of the *erlangeri* species group. Sexual dimorphism is also more marked in this group (Fig. 6). Advertisement calls of the members of this group are very diverse and encompass all call types found in the *P. neumanni* species complex. The *erlangeri* species group comprises four species: *P. nana*, *P. erlangeri*, *P. levenorum*, and *P. robeensis* sp. nov. The members of the *erlangeri* species group are generally smaller and have shorter hind limbs, head, and snout than the members of the *cooperi* and the *neumanni* species groups (Fig. 6). They

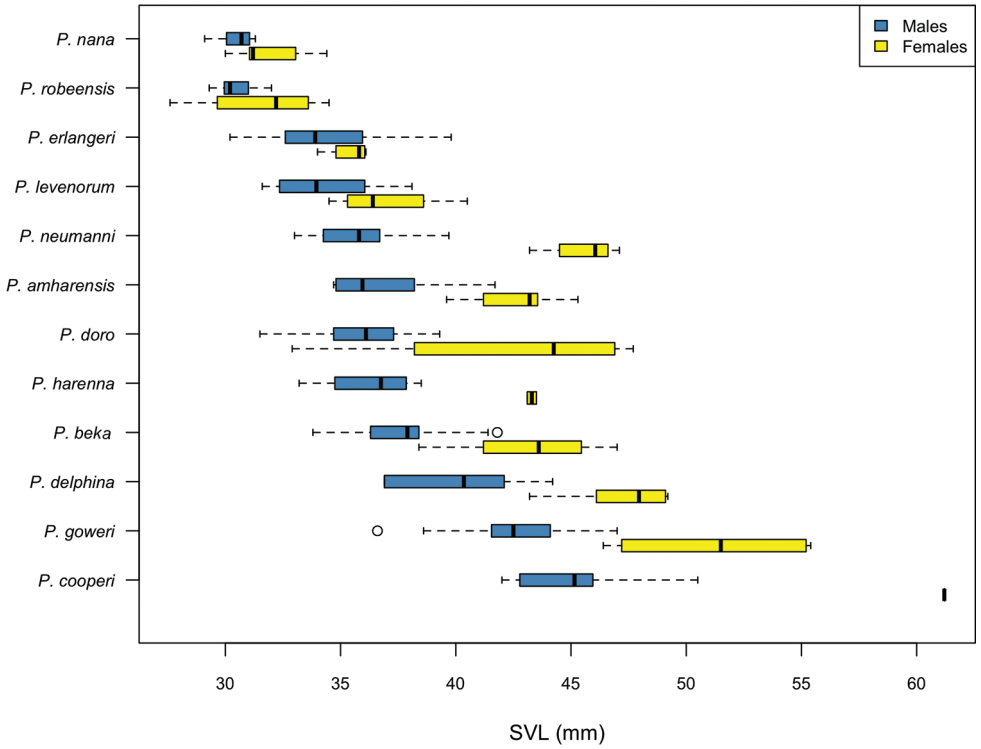

Figure 6. Snout-vent length (mm) of adult males and females of the *Ptychadena neumanni* complex.

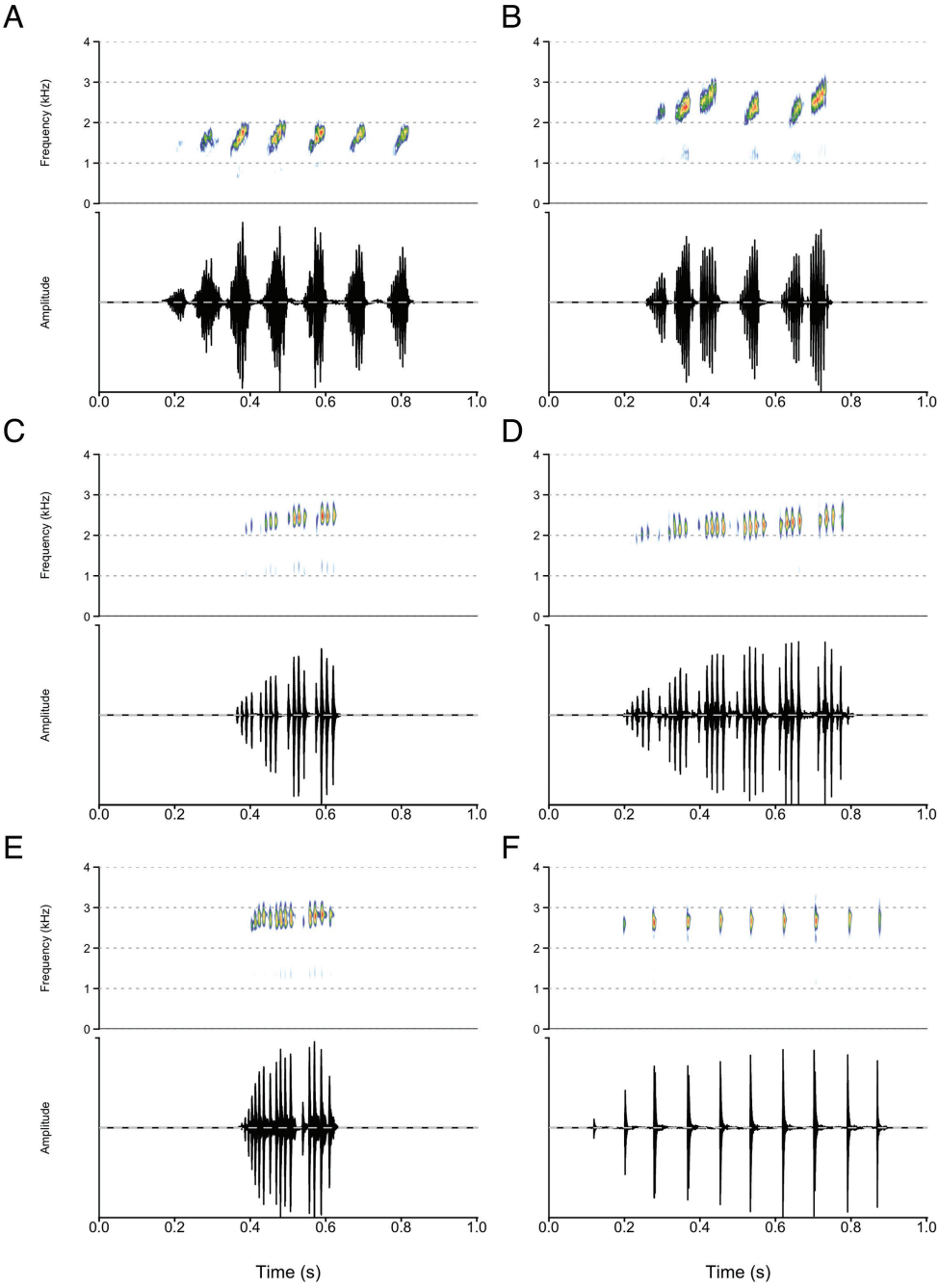

Figure 7. Spectrograms and oscillograms of calls of the *cooperi* and *erlangeri* species groups **A** *P. cooperi* **B** *P. amharensis* **C** *P. erlangeri* **D** *P. levenorum* **E** *P. nana* **F** *P. robeensis* sp. nov.

generally have smaller eyes and a shorter inter-nares distance and a smaller tympanum than the members of the other two species groups (Table 1). The sexual dimorphism is not as marked in this group as in the *neumanni* and *cooperi* species groups, with fe-

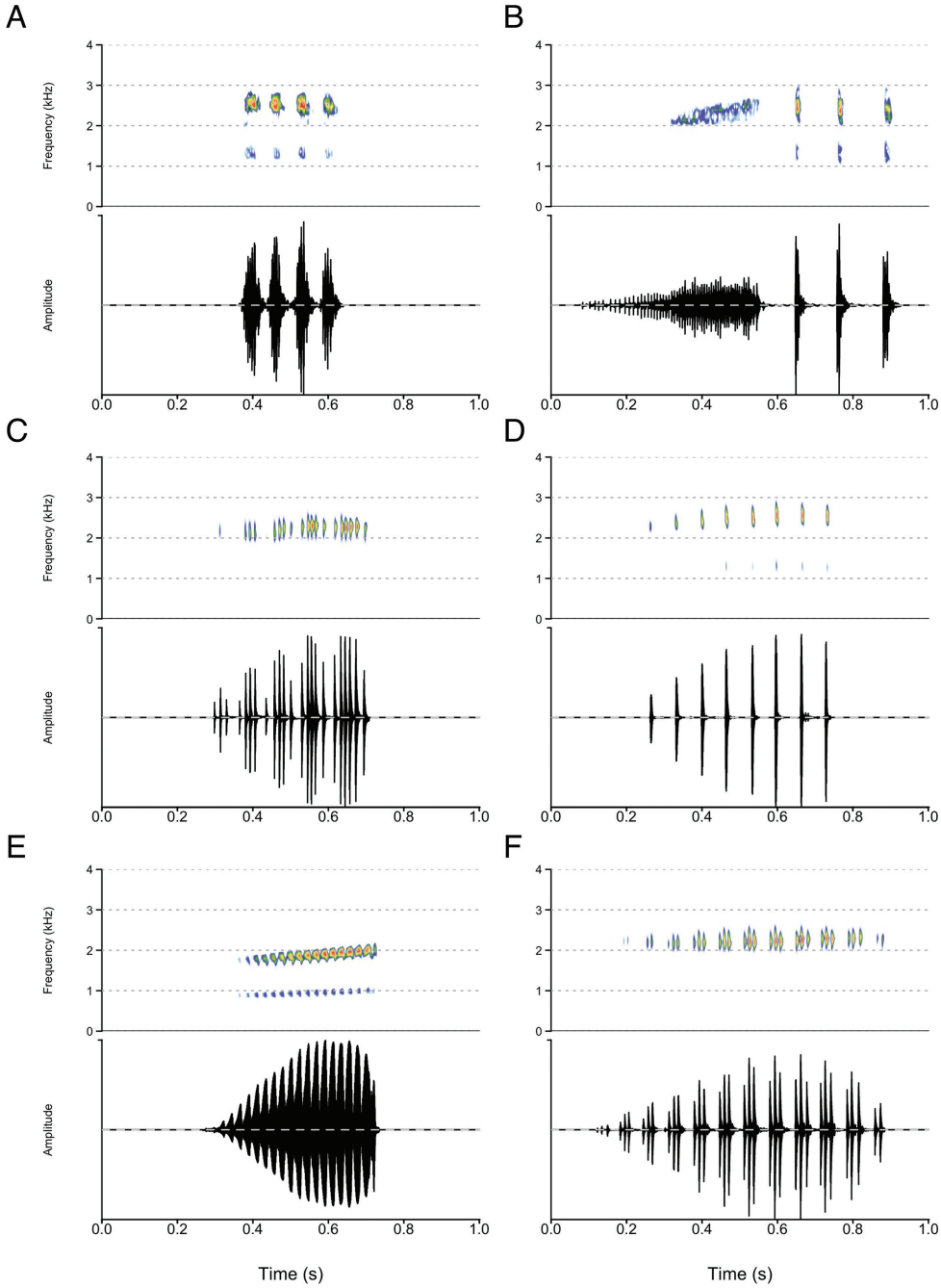

Figure 8. Spectrograms and oscillograms of calls of the *neumanni* species group **A** *P. neumanni* call type **A, B** *P. neumanni* call type **B, C** *P. beka* sp. nov. **D** *P. delphina* sp. nov. **E** *P. doro* sp. nov. **F** *P. goweri*.

males' body size range largely overlapping males' body size range (Fig. 6). Members of this group present an important level of color polymorphism compared to the other species groups, with individuals of the same species presenting either brown, bright

green, yellow or dark red background coloration or patterns. The vertebral stripe is also polymorphic in all species of this group, and can be absent, thin, medium, or wide. Advertisement calls of the members of the *erlangeri* species group are single notes composed of distinct pulses that may or may not be grouped within the note. Within *P. erlangeri*, two subclades emerge in molecular phylogenetic analyses, corresponding to the populations west and east of the GRV, respectively (Freilich et al. 2016).

Linear morphometrics

Based on body size, we split the 12 species into three groups: small (*P. nana*, *P. robeensis* sp. nov., *P. levenorum* and *P. erlangeri*), large (*P. cooperi*, *P. goweri* and *P. delphina* sp. nov.), and medium to large (*P. amharensis*, *P. levenorum*, *P. erlangeri*, *P. beka* sp. nov., *P. doro* sp. nov., *P. neumanni*, *P. harenna*, and *P. goweri*). Certain species were placed in two groups because of the important body size variation within their range. Overall, males generally showed more significant differences than females, which may in some cases be due to low sample size for females. Results of the analyses are provided Suppl. material 3: Tables S4, S5. An identification key is provided as Suppl. material 1: Appendix S1.

Small size group: *P. erlangeri*, *P. levenorum*, *P. nana*, and *P. robeensis* sp. nov.

Within the *small* group, male *P. erlangeri* differed from all three other species in having significantly longer hind limbs (TL, THL, and FL/TL; Suppl. material 3: Table S3). They further differed from *P. nana* and *P. robeensis* males in SVL, FL, HAL, TD, and ED. Male and female *P. levenorum* differed from *P. nana* and *P. robeensis* sp. nov. in a larger body size and longer tibias. Male *P. levenorum* differed from *P. erlangeri* in head shape (SL, EN, IOD) and hind limbs (TL, THL, FL/TL, FL/THL). Female *P. levenorum* also had longer metatarsal tubercles than all other three species (Table 1).

Ptychadena nana and *P. robeensis* sp. nov. were the most similar and challenging to distinguish based on morphometry alone. We therefore ran an additional analysis including only the two species. Males showed differences in head shape (HL, HW/HL, TD) and limb sizes (FL, HAL, FL/THL). Females showed differences in head shape (TD/ED, IND/IOD, IOD/ED) and forearm length (Suppl. material 3: Table S3).

Large size group: *P. cooperi*, *P. delphina* sp. nov., and *P. goweri*

Male *Ptychadena cooperi* differed in head shape (HW, NS, NS/SL) from *P. goweri* and *P. delphina* sp. nov. males (Table 1, Suppl. material 3: Table S3). They also differed in hand length (HAL), snout length (SL) and eye-tympanum distance (ETD) from *P. delphina* sp. nov. and head shape (HW/HL and TD) and forearm length (FLL) from *P. goweri*. *Ptychadena cooperi* was significantly larger than *P. delphina* sp. nov. in both males and females. Male *P. delphina* sp. nov. differed from *P. cooperi* and *P. goweri* in hind limb proportions (TL, MTL, Toe4DW). They further differed from *P. goweri* in hind limbs morphology (THL, TL, FL) and interorbital distance (IOD). Foot (FL)

Table 1. Morphometric measurements (average ± standard deviation) of the *Ptychadena neumanni* complex.

Species	Sex	N	SVL	HW	HL	SL	NS	IND	EN	IOD	ETD	TD	ED	UEW	FLL	HAL	FinDW	THL	TL	FL	Toe4DW	MTL
P. amharensis	M	6	36.9±2.7	13.9±1.4	13.2±0.6	5.5±0.3	2.8±0.2	2.9±0.3	2.5±0.3	2.1±0.2	1.2±0.2	2.9±0.3	4.2±0.6	2.7±0.4	6.8±0.3	8.3±0.5	0.6±0.1	17.4±1.2	18.8±1.3	18.9±0.9	0.6±0.1	1.6±0.3
	F	7	42.5±2	13.9±0.9	14.2±0.9	6.1±0.3	3±0.5	3.3±0.2	2.6±0.3	2.4±0.3	1.5±0.3	2.9±0.3	4.3±0.4	2.9±0.2	7.6±0.6	8.5±0.5	0.6±0.1	19.2±1.3	21.2±1.3	21.1±1.3	0.5±0.2	1.7±0.2
P. beka	M	9	37.9±2.6	14.5±1	14.2±1.3	5.7±0.4	2.9±0.4	3±0.2	2.6±0.3	2.7±0.3	1.1±0.4	2.9±0.2	4±0.5	2.6±0.4	6.7±0.5	8.3±0.5	0.6±0.1	17.6±1.2	19.5±1	19.5±1	0.6±0.1	1.7±0.2
	F	8	43.2±2.9	14.7±1.2	15.6±1.3	6.7±0.5	3.4±0.4	3.7±0.3	3.2±0.3	3.2±0.5	1.5±0.2	3.2±0.3	4.5±0.7	2.9±0.3	8±0.7	9.5±0.5	0.6±0.1	20.9±1.8	24.7±1.9	23.6±1.4	0.7±0.2	1.9±0.1
P. cooperi	M	8	45±2.7	17.7±1.1	16.5±1.5	7.3±0.5	4.2±0.5	3.3±0.4	2.9±0.4	2.9±0.5	1.7±0.3	3.6±0.4	4.9±0.5	3±0.3	9.7±1.1	11.5±1.2	0.7±0.2	22.5±2.7	26.4±1.5	25.3±1.5	0.7±0.1	1.9±0.2
	F	1	61.2	19.9	20.7	7.6	3.8	4	3.1	3.4	2.2	4.6	5.8	4.8	11.4	12.6	0.9	29.4	31.9	31.1	1	2.5
P. delphina	M	6	40.1±2.9	14.7±0.4	14.3±0.8	6.2±0.3	3±0.2	3.2±0.4	2.8±0.6	2.5±0.3	1.3±0.2	3±0.4	4.2±0.6	2.9±0.2	8.1±0.5	8.9±0.9	0.6±0.1	18.8±0.8	21.4±1.5	21.6±2.6	0.5±0	1.5±0.2
	F	6	47.2±2.3	15.9±1.4	16.3±0.8	6.9±0.4	3.3±0.3	3.4±0.2	3.2±0.2	3.2±0.3	1.6±0.2	3.4±0.3	5.2±0.4	3.3±0.3	9.3±0.7	10.1±0.6	0.6±0.1	22.9±1.9	25.9±2.2	25.7±1.6	0.7±0.1	1.8±0.1
P. doro	M	13	35.8±2.2	12.6±0.8	13.1±1.1	5.6±0.4	2.7±0.3	3.1±0.2	2.5±0.2	2.8±0.4	1.1±0.2	2.5±0.3	4±0.4	2.5±0.2	7.1±0.5	8.5±0.7	0.6±0.2	17.5±1.6	20.7±1.4	21.1±2.2	0.5±0.1	1.5±0.3
	F	6	42.4±5.7	14.2±0.9	15±0.4	6.7±0.5	3.4±0.5	3.5±0.4	2.8±0.5	3.2±0.5	1.3±0.3	2.9±0.4	4.6±0.4	3±0.4	8.9±0.9	10.4±1	0.6±0.1	22.6±2.4	26.6±1.1	26.9±1.6	0.8±0.2	1.8±0.3
P. erlangeri	M	35	34.1±2.5	11.7±1	12.2±1.3	5±0.5	2.6±0.3	2.7±0.3	2.2±0.2	2.5±0.4	1±0.2	2.4±0.3	3.5±0.4	2.4±0.4	6.3±0.6	7.2±0.7	0.6±0.1	15.8±1.3	17.9±2	18.3±1.8	0.5±0.1	1.4±0.3
	F	10	34.6±1.7	11.6±1	12.2±1.3	5.2±0.5	2.7±0.3	2.9±0.2	2.5±0.2	2.5±0.4	1±0.2	2.3±0.3	3.6±0.5	2.4±0.3	6.2±0.5	7.5±0.8	0.5±0.1	16.9±2.1	18.7±2.5	19.2±1.8	0.5±0.1	1.4±0.3
P. goweri	M	15	42.4±2.7	15.7±0.9	16.2±1.4	6.7±0.5	3.1±0.3	3.5±0.4	3.1±0.4	3.2±0.4	1.5±0.2	3.1±0.4	4.3±0.7	2.9±0.2	8.5±0.9	10.2±0.8	0.7±0.2	21.9±1.5	25.4±1.5	25.7±1.2	0.7±0.1	2±0.3
	F	6	51.2±4.2	17.6±2	18.6±2.1	7.5±0.4	3.7±0.3	3.9±0.5	3.5±0.3	3.5±0.4	1.8±0.3	3.5±0.4	5±0.5	3.3±0.2	9.8±1	11.8±1	0.7±0.1	25.7±2.7	30.4±2.3	29.4±2	0.8±0.1	2.5±0.3
P. harenna	M	4	36.3±2.3	13.6±1.2	14.2±1.6	5.8±0.3	3.1±0.2	3.4±0.5	2.4±0.3	2.4±0.5	1.2±0.4	3.1±0.6	4.8±0.6	2.8±0.5	7.6±0.4	8.1±0.5	0.6±0.1	18.4±2	20.6±1.3	20.7±1.7	0.5±0.1	1.4±0.1
	F	2	43.3±0.3	15.4±1.2	16±0.8	7±0.4	3.4±0.3	3.8±0.1	3±0.1	4.2±0.2	1.4±0.1	3.1±0.4	4.7±0.1	2.7±0.6	7.8±0.5	9.8±0.6	0.8±0.4	21.8±0.4	24.9±0.4	24±0.5	0.8±0.3	2±0.5
P. levenorum	M	8	34.3±2.3	11.7±1.3	11.9±1.1	4.6±0.5	2.4±0.3	2.4±0.3	1.8±0.4	2.2±0.3	1±0.3	2.2±0.2	3.2±0.4	2.2±0.4	6.5±1	7±0.7	0.6±0.1	14.2±1.4	16.9±1.8	18±2	0.5±0.1	1.6±0.2
	F	4	37±2.5	12.2±0.9	12.1±0.5	4.8±0.5	2.5±0.3	2.7±0.4	2.1±0.2	2.6±0.3	1.3±0.2	2.4±0.4	3.5±0.6	2.5±0.4	6.6±0.8	7.5±0.5	0.5±0.2	16±1.6	18.9±2.1	20.1±2.4	0.6±0.1	1.8±0.2
P. nana	M	12	28.3±3.3	10.2±1.4	10.1±0.7	4.2±0.4	2.2±0.2	2.3±0.2	1.8±0.2	2.2±0.3	0.9±0.1	1.8±0.2	2.9±0.5	2±0.3	5±0.6	5.6±0.6	0.5±0.1	11.7±1.4	12.7±0.9	13.8±1	0.5±0.1	1.2±0.2
	F	12	29.6±3.2	9.5±1.3	10±0.8	4.2±0.4	2.3±0.3	2.5±0.3	1.9±0.2	2±0.4	1±0.2	1.8±0.2	3.2±0.4	2.1±0.4	4.9±0.3	5.8±0.6	0.5±0.1	12.2±1.2	12.9±1.1	14.3±1.2	0.5±0.1	1.2±0.2
P. neumanni	M	20	34.6±2	12±1.2	13.6±0.8	5.6±0.4	2.8±0.4	3.2±0.3	2.6±0.3	3.1±0.3	1±0.1	2.7±0.4	3.9±0.2	2.3±0.4	6.8±0.4	8.1±0.6	0.6±0.2	17.9±1.2	20.1±1.1	20.6±1.4	0.6±0.1	1.4±0.2
	F	8	45.6±1.4	15.2±1.1	16.7±1.6	7.1±0.4	3.6±0.1	4±0.4	3.2±0.3	3.6±0.4	1.5±0.3	3.4±0.4	4.7±0.5	3±0.4	8.3±0.7	9.8±0.7	0.7±0.2	21.8±1.5	26.1±0.8	26.4±1.4	0.7±0.2	1.9±0.3
P. robeensis	M	13	30.3±0.7	10.7±0.7	11.1±0.8	4.3±0.2	2.2±0.2	2.4±0.2	1.9±0.1	2.4±0.3	1.1±0.1	2±0.2	3±0.4	2.1±0.2	5.4±0.5	6.4±0.4	0.6±0.2	12.4±0.8	13.6±0.8	15.1±1	0.5±0.1	1.2±0.3
	F	4	31.6±2.9	11.1±0.6	10.9±0.2	4.3±0.4	2.2±0.5	2.5±0.2	2±0.1	2.5±0.4	1.1±0.2	2±0.2	3.3±0.1	2±0.3	5.5±0.5	6.5±0.5	0.5±0.1	12.2±1.1	13.9±0.8	15.4±1.2	0.6±0.1	1.3±0.2

Table 2. Call variables for pulsed calls. Durations are given in ms; frequencies, frequency bandwidths, and pulse rates are given in Hz (s^{-1}).

Species	N individuals	N calls	Call duration	Number of notes	Pulse duration	Pulses per note	Overall Inter-pulse duration	Overall pulse rate	Groups per note	Group duration	Pulses per group	inter-pulse duration within groups	Pulse rate within group	Peak frequency	Min frequency	Max frequency	Fequency bandwidth	Relative time of peak amplitude
P. beka	5	128	410±113	1±0	3±0	24.5±5.7	14±4	62.4±14.1	10.5±2.6	21±17	3.7±1.9	9±1	210.8±129.7	2482±142	2169±118	2529±150	742±66	258±77
P. delphina	4	33	504±92	1±0	5±1	8.4±1.4	64±8	16.8±2.4	–	–	–	–	–	2327±147	1982±161	2366±166	736±94	384±129
P. erlangeri	5	226	290±35	1±0	4±0	16.5±1.6	15±1	57.1±4.1	4.3±0.8	37±17	4.1±2.5	11±2	123.8±92.7	2343±454	1709±383	2600±297	1138±767	230±14
P. goweri	4	32	634±74	1±0	3±0	33.5±2.9	17±3	53.6±8.4	14.1±2.3	20±14	3.3±1.5	9±2	231.6±182.1	2318±86	1934±57	2356±88	838±156	404±65
P. levenorum	2	30	465±98	1±0	3±0	23.5±4.3	17±3	51.1±5.6	7.1±1.5	36±25	4.1±1.5	12±2	172.7±142.6	2223±90	1840±51	2286±73	864±40	345±34
P. nana	5	56	205±47	1±0	4±0	16.9±2.8	9±2	84±10.2	2.3±0.8	76±49	7.2±4.7	9±2	123±71.3	2801±52	2461±26	2845±53	751±63	136±31
P. robeensis	5	101	534±53	1±0	4±0	9.8±1	57±5	18.5±1.8	–	–	–	–	–	2876±74	2397±40	2896±78	853±97	292±19

Table 3. Call variables for calls composed of several notes.

Species	N individuals	N calls	Call duration	Number of notes	Note duration	Inter-note duration	Note rate	Peak frequency	Min frequency	Max frequency	Frequency bandwidth	Relative time of peak amplitude
P. cooperi	3	54	393±126	4.5±1.2	42±8	58±11	11.7±0.8	1653±64	666±267	1687±62	1547±494	235±82
P. amharensis	4	47	355±276	5±3.5	43±15	37±12	14.7±3.6	2224±158	1535±274	2247±177	1282±176	169±44
P. doro	3	21	411±41	1±0	411±41	–	–	1966±105	1752±87	1999±93	415±31	295±39

Table 4. Call variables for *P. neumanni* two call types.

Species	N (individual)	Call type	N calls	Call duration	Note type	Number of notes	Note duration	Inter-note duration	Note rate	Peak frequency	Min frequency	Max frequency	Frequency bandwidth	Relative time of peak amplitude
P. neumanni	3	A	78	307±149	a	5.8±2.4	32±14	28±11	19.1±3.5	2406±339	2088±274	2408±332	703±119	19±8
	1	B	13	437±54	b	1±0	437±54	–	–	2207±129	1440±578	2369±178	1392±692	346±74
				244±67	c	3±0.6	19±5	94±5	12.6±1.3	2337±191	1975±263	2336±187	744±179	6±2

and metatarsal tubercle lengths (MTL) also differed between female *P. delphina* sp. nov. and *P. goweri* (Suppl. material 3: Table S3).

Medium size group: *P. amharensis*, *P. beka* sp. nov., *P. doro* sp. nov., *P. erlangeri*, *P. goweri*, *P. harenna*, *P. levenorum*, and *P. neumanni*

Male *Ptychadena levenorum* significantly differed from all other species in THL and EN (Suppl. material 3: Table S3). Additionally, they differed from all other species except *P. erlangeri* in snout shape (IND and SL). *Ptychadena goweri* males were larger than all other species except for *P. delphina* sp. nov. and had longer thighs than all species except for *P. delphina* sp. nov. and *P. harenna*. Males of *P. goweri* further differed from all other species, except *P. beka* sp. nov. and *P. doro* sp. nov., in their IOD. Finally, *P. goweri* differed from all species except *P. doro* sp. nov. and *P. harenna* in hind limb size (TL and FL), and all species but *P. beka* sp. nov. in their Toe4DW (Suppl. material 3: Table S3).

Ptychadena neumanni males differed from *P. amharensis*, *P. erlangeri*, *P. harenna*, *P. levenorum* and *P. delphina* sp. nov. in IOD. *Ptychadena neumanni* also differed from *P. goweri* in ETD, FLL, and MTL. *Ptychadena neumanni* also differed from *P. levenorum* and *P. erlangeri* in TD, from *P. goweri* and *P. levenorum* in HAL, and from *P. levenorum* in ED and THL (Suppl. material 3: Table S3). *Ptychadena erlangeri* males differed from *P. doro* sp. nov., *P.goweri*, *P. harenna* and *P. delphina* sp. nov. in FLL. They had a narrower head than *P. amharensis*, *P. beka* sp. nov., *P. goweri*, *P. delphina* sp. nov., and further differed in SL from *P. beka* sp. nov., *P. doro* sp. nov., *P. goweri*, *P. harenna* and *P. delphina* sp. nov. Finally, they differed from *P. doro* sp. nov. and *P. goweri* in HAL and FL. *Ptychadena beka* sp. nov. differed from *P. doro* sp. nov. in HW and hindlimbs length (TL and FL), from *P. amharensis* in IOD, from *P. delphina* sp. nov. in FLL (Suppl. material 3: Table S3).

Few significant differences were found between the morphometric measurements of males *P. harenna*, *P. delphina* sp. nov., *P. doro* sp. nov. and *P. amharensis* (Suppl. material 3: Table S5). We therefore ran an additional analysis on these four species alone. *Ptychadena amharensis* males differed from *P. doro* sp. nov., *P. harenna* and *P. delphina* sp. nov. in TL. They also differed from *P. harenna* and *P. delphina* sp. nov. in FLL, from *P. doro* sp. nov. in head shape (HW, IOD, IOD/ED, HW/HLW) and FL, and from *P. delphina* sp. nov. in SL. Female *P. amharensis* differed from *P. doro* sp. nov., *P. harenna* and *P. delphina* sp. nov. in IOD, from *P. doro* sp. nov. in limb length (TL, FL, HAL, FLL) and SL, from *P. delphina* sp. nov. in ED.

Head shape differed between males of *Ptychadena harenna* and of *P. doro* sp. nov. (TD, ED, IOD/ED; Suppl. material 3: Table S3) and females of *P. harenna* and of *P. delphina* sp. nov. (IOD and IOD/ED; Suppl. material 3: Table S3). Finally, *P. doro* sp. nov. males differed from *P. delphina* sp. nov. in SVL, HW, and TL (Suppl. material 3: Table S3).

Acoustic analyses

Advertisement calls of the species of the *P. neumanni* complex were diverse (Figs 7, 8) and provided useful discriminant characters. Species of the group are thus more easily

identified by their advertisement calls than their morphology. An identification key based on spectral and temporal call traits is provided as Suppl. material 2: Appendix S2. Three major types of advertisement calls are produced by the species of the *P. neumanni* complex: a group of a few short notes with indistinct pulses, a single note with partly fused pulses, and a single note comprising distinct pulses.

Ptychadena cooperi, *P. amharensis*, and *P. neumanni* produce calls composed of a few pulsed notes, somewhat resembling human laughter. The call of *P. neumanni* (call type A) differs from those the *P. cooperi* species group in that it does not contain any frequency modulation. The call of *P. cooperi* can be distinguished from the call of *P. amharensis* by its lower average dominant frequency, reflecting a larger body size.

Ptychadena doro sp. nov. produces an advertisement call very distinctive within the group, reminiscent of the sound produced by a chicken. It is a relatively long, single note with partly fused pulses and an increase of the dominant frequency along the note.

Most species of the *P. neumanni* complex (*P. erlangeri*, *P. levenorum*, *P. nana*, *P. robeensis* sp. nov., *P. beka* sp. nov., *P. delphina* sp. nov., and *P. goweri*) produce single-note calls containing distinct pulses. *Ptychadena robeensis* sp. nov. and *P. delphina* sp. nov. are distinct from the other species in that their pulses are evenly and well-spaced, while the other species calls contain multiple pulse groups. The size difference between the two species is reflected in the peak frequency of their calls, with *P. robeensis* sp. nov. calling at a higher frequency *than P. delphina* sp. nov. *Ptychadena goweri* produces the longest (634 ± 74 ms), while *P. nana* produces the shortest call (205 ± 47 ms) of the subgroup. The calls of *Ptychadena beka* sp. nov., *P. erlangeri* and *P. levenorum* can be distinguished based on the number of pulse groups and the number of pulses within each pulse group: the call of *P. beka* sp. nov. in composed of 8–13 pulses groups containing 2–6 pulses each, while *P. levenorum* produces calls with 5–9 pulse groups of 10–33 pulses each. *Ptychadena erlangeri* pulse structure is variable, with 3–6 pulses groups containing 3–21 pulses each, but can be distinguished from *P. levenorum* but a shorter call duration (< 325 ms versus > 370 ms for the call of *P. levenorum*).

Finally, *Ptychadena neumanni* produces a second call type (type B), containing a long, pulsed note followed by a short series of distinct pulses. This call type is unique within the *P. neumanni* species complex, and we believe that it may be an aggressive call. However, our data are insufficient to attribute the function of this second call type with certainty.

Integrative taxonomy

Our analysis distinguishes 12 species in the *Ptychadena neumanni* complex, in agreement with previous molecular phylogenetic studies (Freilich et al. 2014; Reyes-Velasco et al. 2018). For eight of these species, names are available, while four are new species. Our previous molecular and morphometric analyses, including type specimens, demonstrated that the specimens designated as *P. erlangeri* by Largen 2001; Freilich et al. 2014; Smith et al. 2017a, b and Reyes-Velasco et al. 2018 belong to *P. neumanni* Ahl, 1924 (Reyes-Velasco et al. in review). Similarly, our results show that *P. largeni* described by Perret in 1994 is a junior synonym of *P. erlangeri* Ahl, 1924, and not of

P. neumanni as stated by Largen (2001), nor a proper species as considered by Smith et al. 2017a, b (Reyes-Velasco et al. in review).

Smith et al. (2017a, b) assigned *P. neumanni* to the population designated as *P.* cf. *neumanni 1* in Freilich et al. (2014) without comparing the sequenced specimens to the type series of *P. neumanni*. Our results show that *P.* cf. *neumanni 1* constitutes in fact a new species, which we name *Ptychadena beka* sp. nov. and describe hereafter. The three new species described in Smith et al (2017a, b), *P. amharensis*, *P. goweri* and *P. levenorum*, based on molecular evidence constitute valid species names. However, no useful diagnostic character other than molecular data was provided in the original descriptions. We therefore re-describe those three species below.

Systematic accounts

Ptychadena amharensis Smith, Noonan & Colston, 2017

Type material. ***Holotype.*** by original designation. A juvenile (XF140) collected on 18 July 2011 by X. Freilich and S. Boissinot in Dejen, Amhara region, Ethiopia (10.1908°N, 38.140°E, 2425 m a.s.l.). ***Paratypes.*** Three adult females (XF141, XF142, XF143) collected by X. Freilich and S. Boissinot on the same date and location. All type specimens and material examined are deposited at ZNHM.

Material examined. In addition to the type series, we examined one male (15–313) collected on 17 August 2015 by X. Freilich, J. Reyes-Velasco and S. Boissinot southeast of Debre Markos (10.2745°N, 37.8564°E, 2261 m a.s.l.), one female (15–367) collected on 19 August 2015 by X. Freilich J. Reyes-Velasco and S. Boissinot southwest of Debarq (13.0359°N, 37.799°E, 2583 m a.s.l.), one female (16–175) collected on 15 July 2016 by X. Freilich, J. Reyes-Velasco and S. Boissinot in Debre Markos (10.35195°N, 37.7414°E, 2803 m a.s.l.), one female (SB580) collected on 8 July 2018 by S. Goutte and Y. Bourgeois north-west of Debre Markos (10.3566°N, 37.6571°E, 2589 m a.s.l.), one female (SB584) collected on 8 July 2018 by S. Goutte and Y. Bourgeois in Debre Markos (10.35195°N, 37.7414°E, 2388 m a.s.l.) and five males (SB591, SB592, SB593, SB597 and SB606) collected on 9 July 2018 by S. Goutte and Y. Bourgeois in Debre Markos (10.3520°N, 37.7414°E, 2388 m a.s.l.).

Diagnosis. Medium-sized species (male (6) SVL 36.9 ± 2.7 mm, female (7) SVL 42.5 ± 2.0 mm) of the *cooperi* species group (Fig. 9). It differs from other members of the *Ptychadena neumanni* species complex by the following combination of characters: (1) tibia half of the snout-vent length, (2) eye close to one another (male IOD/HW 0.16 ± 0.02, female IOD/HW 0.17 ± 0.02), (3) vertical light stripe on the tympanum, (4) vocal sacs are light grey to cream, sometimes mottled with light grey, (5) adult males' bodies covered in small warts.

Comparison. *Ptychadena amharensis* is smaller than *P. cooperi* and larger than *P. nana* and *P. robeensis* sp. nov. It has shorter hindlimbs than *P. doro* sp. nov., *P. neumanni*, *P. goweri*, and *P. harenna*. *Ptychadena amharensis* has a shorter head than *P. beka*

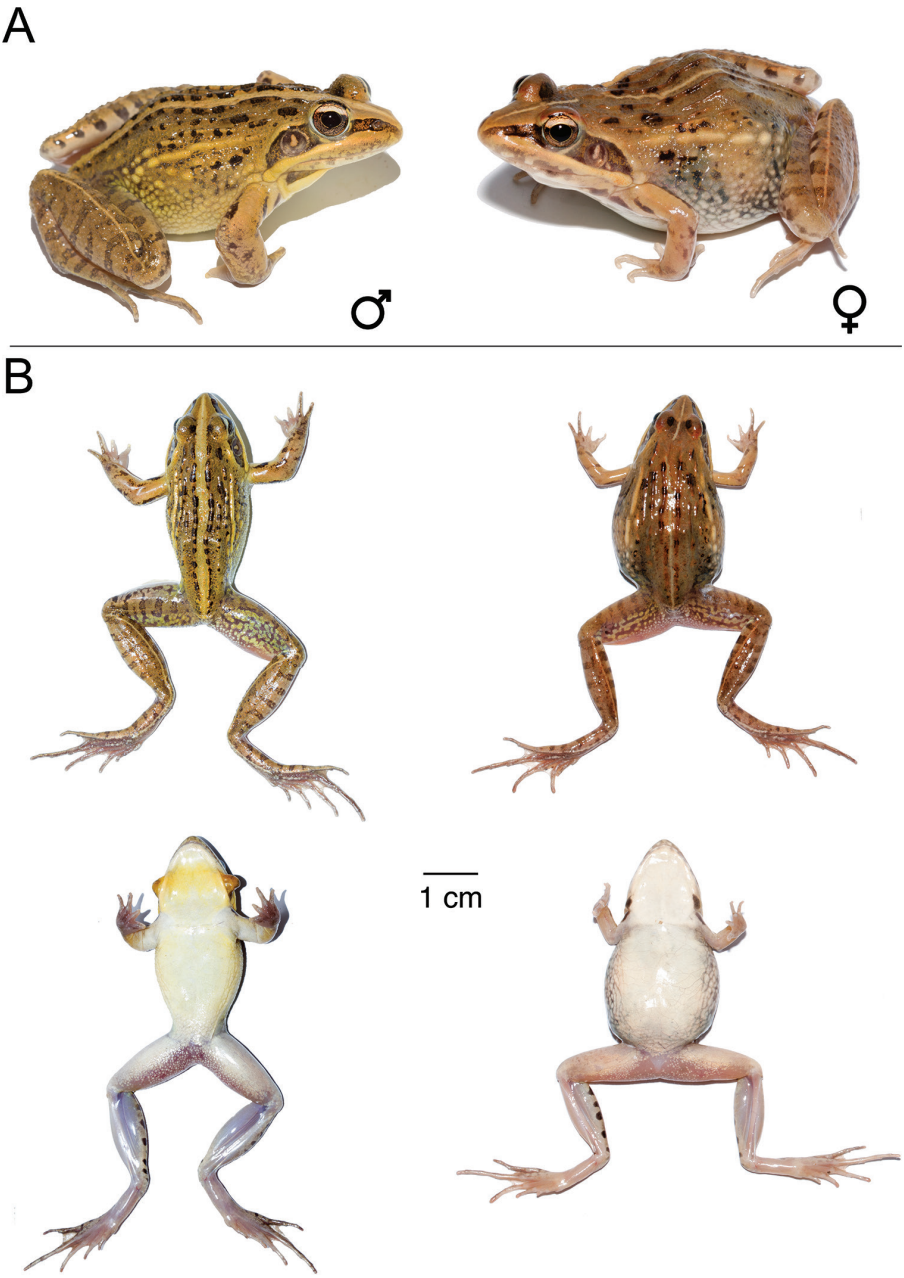

Figure 9. *Ptychadena amharensis* **A** live male (SB593; left) and female (SB580, right) **B** dorsal and ventral views of the same individuals (male left, female right) after euthanasia and before fixation.

sp. nov., *P. neumanni*, *P. harenna* and *P. goweri*. The species' interorbital distance is shorter than in *P. doro* sp. nov., *P. delphina* sp. nov., *P. erlangeri*, *P. levenorum*, *P. goweri*, *P. nana*, *P. neumanni*, and *P. robeensis* sp. nov.

Description of the holotype. Juvenile, in poor condition (Fig. 10). Right hind limb missing. No visible ridges or coloration on the back due to the poor condition of the specimen. Finger formula: 1<2<4<3, hand free of webbing. Toe formula: 1<2<5<3<4. Toe webbing indistinguishable. Tongue bifurcated and free for half is length. Maxillary and premaxillary teeth present, vomerine teeth not visible. Throat cream.

Measurements of the holotype (mm): SVL 21.4, HW 8.8, HL 9.3, SL 3.7, NS 2.1, IND 2.1, EN 1.8, IOD 1.6, ETD 0.9, TD 1.6, ED 2, UEW 1.1, FLL 3.9, HAL 4.9, F4DW 0.3, THL 9.6, TL 9.7, FL 10.1, T4DW 0.3, MTL 0.9.

Coloration of the holotype in preservative. Dorsal background color is grey, with almost completely faded away dark grey markings in between the eyes and on the upper part of the dorsum. Dark brown canthal stripe from the tip of the snout to the back of the jaw. No vertical stripe or blotch on the tympanum. Upper lip, throat, and posterior part of flanks cream. Irregular dark brown markings on the anterior third of the flanks. Ventrum, ventral side of the thighs and tibias uniformly cream. Faint dark brown bars on the tibia. Thighs posteriorly dark brown with large cream spots.

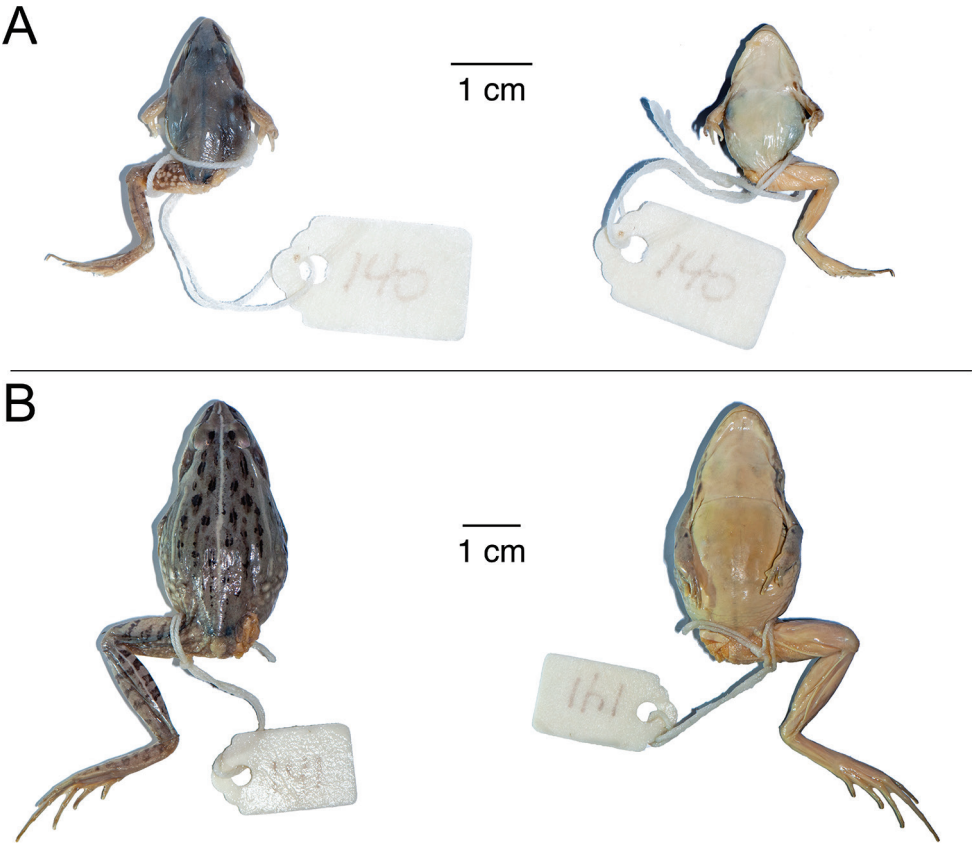

Figure 10. Type specimens of *Ptychadena amharensis* **A** dorsal and ventral views of the juvenile holotype (XF140) **B** dorsal and ventral views of one of the three adult female paratypes (XF141).

Variations. In life, background coloration varies from dark orange to light olive or yellowish brown. Small, more or less distinct, dark brown blotches distributed on the dorsal ridges and on the antero-dorsal part of the flanks. Cream or sand-colored thin or wide vertebral stripe present in all examined specimens.

Iris bicolored, with the upper third silver to sand color, and the lower two thirds brown or copper to dark brown. Upper and lower jaws with light brown irregular markings. Dark brown canthal stripe from the tip of the snout to the back of the upper jaw. More or less distinct cream-colored vertical stripe or blotch on the tympanum. Light thin stripe on the tibia, extending over the lower third of the thigh. Back thighs light yellowish grey to greenish yellow reticulated with dark grey. Ventrum white to light yellow, throat white to bright yellow. Vocal sacs cream or light grey sometimes molted with light grey. Dorsum and hindlimbs of adult males covered in small warts.

Habitat, distribution, and natural history. *Ptychadena amharensis* is found in the Amhara plateau, at elevations ranging from 1824 m to 2642 m a.s.l. This species is found notably around Debre Markos, Enjebara, Bahar Dar and Gondar. The northern-most individuals were found just south of Debarq (13.1098°N, 37.8637°E), while the southernmost individuals were found around Dejen (10.1908°N, 38.1401°E), just North of the Blue Nile. This species has not been found south of the Blue Nile.

Males are found calling at night from flooded grass fields, sometimes aggregating in important numbers, in sympatry with *Ptychadena wadei* and *Ptychadena pumilio* south of Bahar Dar.

Advertisement call. *Ptychadena amharensis* males produce calls (4 males, 47 calls) of 355 ± 276 ms duration, containing 4 ± 3.5 pulsed notes. Each note is 43 ± 15 ms in duration and pulses are indistinct. Call rate is highly dependent of the social context as *P. amharensis* tends to call in large choruses and their motivation to call is linked to the number of acoustically active conspecific males in their direct surroundings. Call dominant frequency is 2224 ± 158 Hz. Notes are frequency modulated, with an increase in dominant frequency within each note.

Within the *P. neumanni* complex, the call of *P. amharensis* can be distinguished from those of *P. erlangeri*, *P. levenorum*, *P. nana*, *P. robeensis* sp. nov., *P. beka* sp. nov., *P. delphina* sp. nov., *P. goweri*, and *P. neumanni* call type 2 by the indistinct pulses of its notes. It is distinct from *P. doro* sp. nov. by having calls composed of multiple notes, a higher dominant frequency and wider frequency bandwidth. The call of *P. amharensis* is distinguishable from *P. neumanni* call type 1 by having frequency-modulated notes and note groups and longer notes. The call of *P. amharensis* resemble most the call of its closely related *P. cooperi*, although with a higher peak frequency, reflective of the smaller size of the species, and notes grouped within each call while the notes of *P. cooperi* calls are regularly spaced.

Remarks. Neither the holotype designated by Smith et al. (2017a), which is a juvenile in poor condition with one missing leg, nor the diagnosis provided in the original description provide characters allowing the distinction between *P. amharensis* and

other species of the *P. neumanni* complex. The SVL values given for males and females in Smith et al. (2017a, b) do not correspond to measurements taken on the type series (holotype: juvenile SVL 21.8 mm, paratypes: adult females, SVL 40.2, 43.3, 43.8 mm) and were taken from a summary table (table 4 in Freilich et al. 2014) with no acknowledgement of the original data, and specimens of the type series have evidently not been examined by the authors. The altitudinal range for the species was taken from the same table, but values were rounded in Smith et al. (2017a, b).

Ptychadena erlangeri **(Ahl, 1924)**

Rana erlangeri Ahl, 1924: 4.
Ptychadena erlangeri – Perret 1980: 151–168.
Rana (*Ptychadena*) *erlangeri* – Dubois 1981: 233.
Ptychadena (*Ptychadena*) *erlangeri* – Dubois 1992: 316.
Ptychadena largeni Perret 1994: 67.

Type material. ***Holotype.*** A gravid female (ZMB–26887) collected by C. von Erlanger in December 1900 at lake Abaya, Ethiopia (likely the eastern shore of the lake, 1300 m a.s.l., see remarks below).

Material examined. Except for the type specimen and the type series of *P. largeni*, all the material examined is deposited at ZNHM. One female (15–47) collected by X. Freilich, J. Reyes-Velasco and S. Boissinot south of Assela (7.9068°N, 39.1238°E, 2520 m a.s.l.), one male (15–400) collected by X. Freilich, J. Reyes-Velasco and S. Boissinot on 22 August 2015 north of Fitche (9.7877°N, 38.6974°E, 2821 m a.s.l.), two males (15–417 and 15–420) collected by X. Freilich, J. Reyes-Velasco and S. Boissinot on 26 August 2015 north (6.3844°N, 38.5927°E, 2655 m a.s.l.) and south (6.3256°N, 38.6645°E, 2684 m a.s.l.) of Bore, respectively, one male (16–6) collected by J. Reyes-Velasco and S. Boissinot on 4 July 2016 between Addis Ababa and Ambo, eight males (16–6, 16–10, 16–11, 16–12, 16–14, 16–16, 16–17 and 16–24) collected by J. Reyes-Velasco and S. Boissinot on 5 July 2016 south of Assela (7.7776–7.8431°N, 39.1384–39.1529°E, 2553–2637 m a.s.l.), one female (16–131) and six males (16–99, 16–106, 16–112, 16–113, 16–114 and 16–118) collected by J. Reyes-Velasco and S. Boissinot on 12 July 2016 southeast of Mehal Meda (9.9894–10.3316°N, 39.7452–39.8092°E, 3017–3394 m a.s.l.), one female (16–142) and one male (16–155) collected by J. Reyes-Velasco and S. Boissinot on 13 July 2016 north of Debre Birhan (9.6822–9.6979°N, 39.5505–39.5628°E, 2833–2837 m a.s.l.), one male (16–166) collected by J. Reyes-Velasco and S. Boissinot on 14 July 2016 south of Fitche (9.7502°N, 38.7445°E, 2726 m a.s.l.), one female (SB231) and one male (SB232) collected by S. Goutte and J. Reyes-Velasco on 23 April 2018 south of Gumer (7.9125°N, 38.0644°E, 2831 m a.s.l.), two males (SB552 and SB553) collected by S. Goutte and Y. Bourgeois on 3 July 2018 east of Mehal Meda (10.3247°N, 39.8092°E, 2795 m a.s.l.), one male (SB562) collected by S. Goutte and Y. Bourgeois on 4 July

2018 east of Mehal Meda (10.3247°N, 39.8092°E, 2795 m a.s.l.), three males (SB570, SB571 and SB577) collected by S. Goutte and Y. Bourgeois on 7 July 2018 north of Gebre Guracha (9.8818°N, 38.3660°E, 2558 m a.s.l.), one male (SB615) collected by S. Goutte and Y. Bourgeois on 14 July 2018 near Holeta (9.0692°N, 38.5214°E, 2397 m a.s.l.), *P. largeni* male holotype (MHNG–2513.31), *P. largeni* male paratypes (MHNG–2513.38, MHNG–2513.42, MHNG–2513.44, MHNG–2513.45, MHNG–2513.49, MHNG–2513.52), *P. largeni* female paratypes (MHNG–2513.56, MHNG–2513.57, MHNG–2513.58, MHNG–2513.59 and MHNG–2513.60) collected by M. Largen on 12 June 1977 in Addis Ababa, Shewa (Shoa) (9.03°N, 38.75°E, 2500 m a.s.l.).

Diagnosis. A medium-sized (male (35) SVL 34.1 ± 2.5 mm, female (10) SVL 34.6 ± 1.7 mm) member of the *erlangeri* species group (Fig. 11). *Ptychadena erlangeri* differs from other members of the *P. neumanni* complex by the following combination of characters: (1) relatively short hind limbs (male TL/SVL 0.53 ± 0.04, female TL/SVL 0.54 ± 0.05), (2) tympanum translucent, without any light bar or blotch, (3) vocal sacs light in color, from cream to light grey, very rarely with a bit of grey, (4) adult males with robust forelimbs, (5) adult males often covered in small warts.

Comparison. Species very variable in body size across its range, but always smaller than *P. cooperi*, *P. goweri* and larger than *P. nana* and *P. robeensis* sp. nov. *Ptychadena erlangeri* can be distinguished from *P. beka* sp. nov., *P. delphina* sp. nov., *P. doro* sp. nov., *P. amharensis*, *P. neumanni*, and *P. robeensis* sp. nov. by the absence of light bar or blotch on the tympanum. Furthermore, adult males can be distinguished by their cream or light-yellow vocal sac from *P. beka* sp. nov., *P. neumanni*, *P. robeensis* sp. nov., *P. doro* sp. nov., and *P. delphina* sp. nov. *Ptychadena erlangeri* has a shorter snout than *P. amharensis*, *P. harenna*, *P. beka* sp. nov., *P. delphina* sp. nov., *P. goweri*, *P. cooperi*, and *P. doro* sp. nov. Finally, *P. erlangeri* can be distinguished from *P. levenorum* by longer eye-nostril and inter-orbital distances and longer hind limbs.

Description of the holotype. Medium sized (SVL 37.6 mm), slender, gravid female with long hind limbs (TL/SVL 0.63, Fig. 12, Suppl. material 3: Table S1). Head longer than wide (HW/HL 0.94). Snout pointed, projecting beyond the lower jaw. Interorbital distance 0.58 × eye diameter. Nostril half-way between the tip of the snout and the eye. Internarial distance 1.2 × interorbital distance. Tympanum 0.61 × eye diameter. Finger tips not expanded but rounded, with moderate subarticular tubercles. Finger formula: I<II<IV<III. Hand free of webbing. Hindlimbs elongated, with tibia length 0.63 × snout-vent length. Rounded white warts irregularly spread on the dorsal side of tibia. Foot as long as thigh and almost as long as tibia (FL/TL 0.98). Toe tips rounded. Subarticular tubercles small and round. Inner metatarsal tubercle present, external absent. Toe formula: I<II<III<V<IV (right foot) and I<II<VIII<IV (left foot). Foot webbing formula (toe internal/external sides, number of phalanges webbed): Ie(1), IIi/e(1–2), IIIi/e(2–2), IVi/e(2–2), Vi(2). Two light, continuous lateral ridges, four interrupted dorsal ridges. No vertebral nor sacral ridges. Note that we did not see the nasal ridges that Perret (1980) noted as the single major diagnostic character for the species.

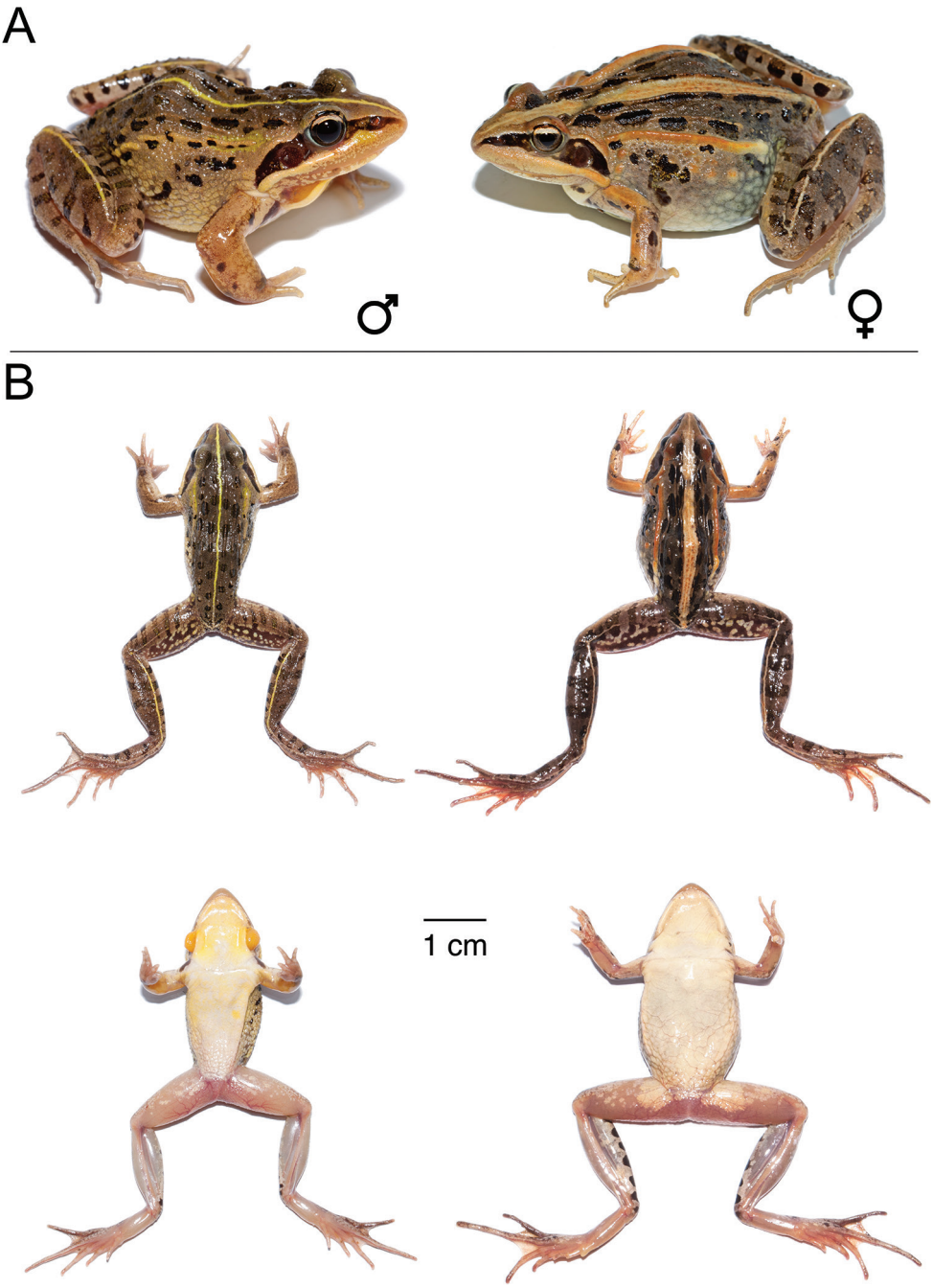

Figure 11. *Ptychadena erlangeri* **A** live male (SB571; left) and female (SB548, right) **B** dorsal and ventral views of the same individuals (male left, female right) after euthanasia and before fixation.

Coloration of the holotype in preservative. Although the holotype is in overall very good condition, the coloration seems to have faded away with time and some dark markings noted by Ahl (1924) in the original description and Perret (1980) are

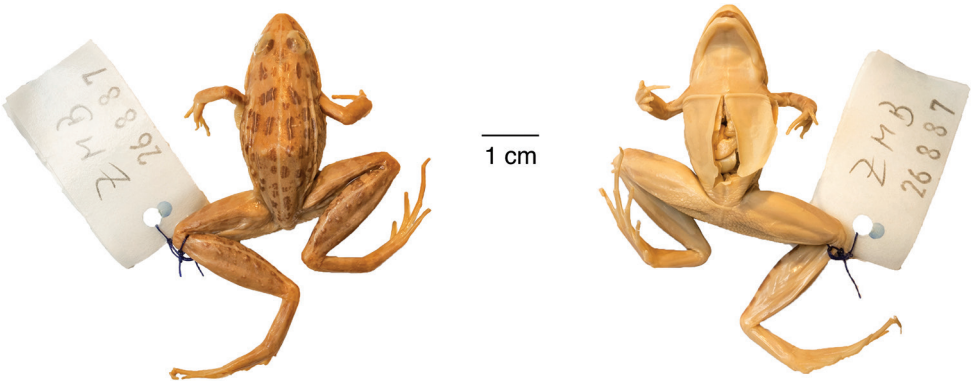

Figure 12. Holotype of *Ptychadena erlangeri*. Dorsal and ventral views of the female holotype (ZMB–26887).

now barely visible or have vanished altogether. Dorsal ground color light brown with irregular oval dark brown blotches symmetrically distributed on the dorsolateral ridges. Thin, cream vertebral stripe from the tip of the snout to the vent. Dark brown canthal stripe from the tip of the snout to the back of the jaw. Upper lip and flanks cream. The dark markings on the upper and lower lips noted by Ahl (1924) are no longer visible. Throat, ventrum, ventral side of the thighs, and tibias uniformly cream without any melanization. A thin, cream longitudinal stripe on the tibias and half of the thighs. Dark brown bars on the tibias and brown markings on the thighs.

Variations. *Ptychadena erlangeri* shows important variations in body size, morphology, and coloration across its large distribution range. South of the GRV, individuals of *P. erlangeri* are generally larger (male (9) SVL 36.8 ± 1.9 mm, female (1) SVL 35.6) than north of the GRV (male (17) SVL 33.5 ± 1.9 mm, female (3) SVL 35.4 ± 1.2). Morphometric variations are summarized in Table 1.

In life, dorsum coloration varies from dark brown to grey-brown, olive and golden, sometimes with irregular green blotches. All specimens examined had small dark brown or black blotches distributed symmetrically on the dorsal ridges. A few additional dark brown or black blotches are found in the anterior part of the flanks. A vertebral stripe is always present, either thin or wide and may be white, cream, or green.

Iris bicolored, the upper third silver and lower two thirds dark brown. Upper and lower jaws featuring irregular light grey or brown markings but no barring. All specimens examined featured a dark brown canthal stripe from the tip of the snout to the back of the upper lip, with the tympanum uniformly colored and lacking any light stripe of blotch. A thin cream longitudinal stripe on the tibia extends to a fifth to the whole length of the thigh. Tibias, thighs, and feet more or less regularly barred with dark brown. Thighs posteriorly marbled with dark brown and yellowish brown. Ventrum and throat uniformly cream to yellow. Vocal sacs cream, yellowish or light grey, very rarely with a bit of grey. Small warts over the body and forelimbs present in 80% of adult males examined.

Habitat, distribution, and natural history. *Ptychadena erlangeri* has a wide distribution range extending on both sides of the Great Rift Valley (6.23–10.33°N, 38.06–39.81°E). It is restricted to higher altitudes, from 2387 m to 3394 m a.s.l. (based on 156 barcoded individuals). West of the Great Rift Valley, its range is limited by the Blue Nile valley and specimens have been found just north of Gebre Guracha. Its northernmost locality is Mehal Meda. Southeast of the GRV, populations have been found near Assela, Kofele and Irba Moda. A few individuals have been found in the southwest, between Tippi and Gech'a, and at lower elevation than any other population (7.4512°N, 35.3992°E, 2270 m a.s.l.). GPS coordinates for all examined specimens are given in Suppl. material 3: Table S1. *Ptychadena erlangeri* is found in syntopy with *P. beka* sp. nov. at the lower end of its altitudinal range, notably near Fitche, Holeta, between Ambo and Wonchi, and possibly near Assela. It is also found in sympatry with *P. cooperi* across its range.

Males are found calling in shallow puddles, flooded grasslands, or agricultural fields. Males can be found vocalizing very close to one another, sometimes in important numbers. Calling activity depends on rainfall and is highest during rainy months. Calling usually starts after 22:00, and sometimes as late as 02:00 in dry weather, and ceases before dawn. Numerous, small bicolored eggs are laid in the same water body.

Advertisement call. The call of *Ptychadena erlangeri* (5 males, 226 calls) is composed of a single pulsed note of 290 ± 35 ms in duration, containing 46.5 ± 1.6 pulses. Within calls, pulses are grouped, with 4.1 ± 2.5 pulses per group and the first pulse typically notably lower in amplitude than the other pulses of the pulse group. Amplitude of the call increases gradually during most of the call, peaking at 230 ± 14 ms, and decreases abruptly afterwards. Call dominant frequency is 2343 ± 454 Hz.

The call of *P. erlangeri* can be differentiated from those of *P. cooperi*, *P. amharensis*, *P. doro* sp. nov. and *P. neumanni* (type A and B) by the distinguishable pulses composing the calls. It is also distinct from the calls of *P. delphina* sp. nov. and *P. robeensis* sp. nov. by its short inter-pulse intervals. The call of *P. erlangeri* differs from the calls of *P. delphina* sp. nov., *P. robeensis* sp. nov., *P. levenorum*, *P. beka* sp. nov. and *P. goweri* by its short duration. Finally, the call of *P. erlangeri* differs from the call of *P. nana* by its longer duration and lower pulse rate.

Remarks. Confusion and difficulty to distinguish *P. erlangeri* from *P. neumanni* arose from the original descriptions of the species themselves, both published by Ahl in 1924 in the same article. The original description of *P. neumanni*, based on 35 syntypes, most likely contained three distinct species (Perret 1980), while *P. erlangeri* was described based on a single gravid female. Perret (1980) restricted *P. neumanni* to three male syntypes. Comparing the two closely related species was thus rendered near impossible due to the low sample size and the fact that each species was represented by specimens of different sexes. Adding to the confusion, in 1994, Perret described *Ptychadena largeni* from 30 specimens from Addis Ababa, Shewa (Shoa) sent to him by Largen as *Ptychadena erlangeri.* Largen (1997) then considered that the morphological diagnostic characters found by Perret in the 30 specimens were due to

conservation artefacts as these individuals were fixed in alcohol rather than in formalin, and subsequently synonymized *P. largeni* with *P. neumanni* in 2001, even though he had originally considered those specimens to belong to *P. erlangeri*. Recently, molecular phylogenetic analyses grouped the holotype of *P. largeni* with that of *P. erlangeri* (Reyes-Velasco et al. in review).

Largen (2001) thus included a population of *P. erlangeri* (*P. largeni*) in *P. neumanni*, along with specimens from Debre Markos, Gondar, the Bale Mountains, etc. and included specimens from the Harenna forest and Debre Markos in *P. erlangeri.* The two groupings thus comprised specimens of several species, many of which placed in both groups (Fig. 1). As a result, Largen (2001) failed to give satisfactory diagnostic characters distinguishing *P. erlangeri* from *P. neumanni* as all the given characters largely overlapped, and later authors relied heavily on the distribution ranges given by Largen to assign species names to the populations they sampled. Notably, the photos presented in Largen and Spawls (2010) for *P. erlangeri* is in fact most likely a *P. goweri* (Yadot River, close to Dolo Mena described as the "large" form occurring in Bale Mountain by Largen 1997), and the specimens presented as *P. neumanni* are in fact *P. erlangeri*.

Ptychadena levenorum Smith, Noonan & Colston, 2017

Type material. ***Holotype.*** Male, TJC219, collected in Katcha, Bale Moutains National Park, Ethiopia (6.7165°N, 39.7248°E, 2326 m a.s.l.) by T. Colston on 8 December 2012. ***Paratypes.*** XF923 and XF927, collected by X. Freilich and S. Boissinot on the 9 August 2011 west of Dinsho (7.1112°N, 39.7430°E, 3024 m a.s.l.). All type specimens and material examined are deposited at ZNHM.

Material examined. Beside the male holotype (TJC219) we examined one female (15–155) and one male (15–158) collected by X. Freilich, J. Reyes-Velasco, and S. Boissinot on 9 August 2015 east of Dinsho (7.1061°N, 39.8181°E, 3058 m a.s.l.), one female (15–482) collected by X. Freilich, J. Reyes-Velasco and S. Boissinot on 3 October 2015 south of Dodola (6.8465°N, 39.1933°E, 3404 m a.s.l.), one female (16–89) and one male (16–90) collected by J. Reyes-Velasco and S. Boissinot on 10 July 2016 east of Dinsho (7.1065°N, 39.8184°E, 3065 m a.s.l.), one male (SB43) collected by S. Goutte and J. Reyes-Velasco on 6 April 2018 south of Dodola (6.8632°N, 39.1948°E, 3260 m a.s.l.), two males (SB66 and SB67) collected by S. Goutte and J. Reyes-Velasco on 8 April 2018 south of Dinsho, one female (SB85) and two males (SB90 and SB94) collected by S. Goutte and J. Reyes-Velasco on 9 April 2018 east of Dinsho.

Diagnosis. A small species (male (8) SVL 34.3 ± 2.3 mm, female (4) SVL 37.0 ± 2.5 mm) of the *erlangeri* species group (Fig. 13) with variable coloration, distinguished by the following combination of characters: (1) short hindlimbs (male TL/SVL 0.49 ± 0.06, female TL/SVL 0.51 ± 0.04), (2) head as long as wide, (3) snout short (male SN/SVL 0.13 ± 0.02, female SN/SVL 0.13 ± 0.01), (4) vocal sacs cream, light grey, or bicolored cream and grey.

Comparison. Smaller than *P. goweri*, *P. delphina* sp. nov., and *P. cooperi* and larger than *P. nana* and *P. robeensis* sp. nov. Snout shorter than all species of the *P. neumanni* complex

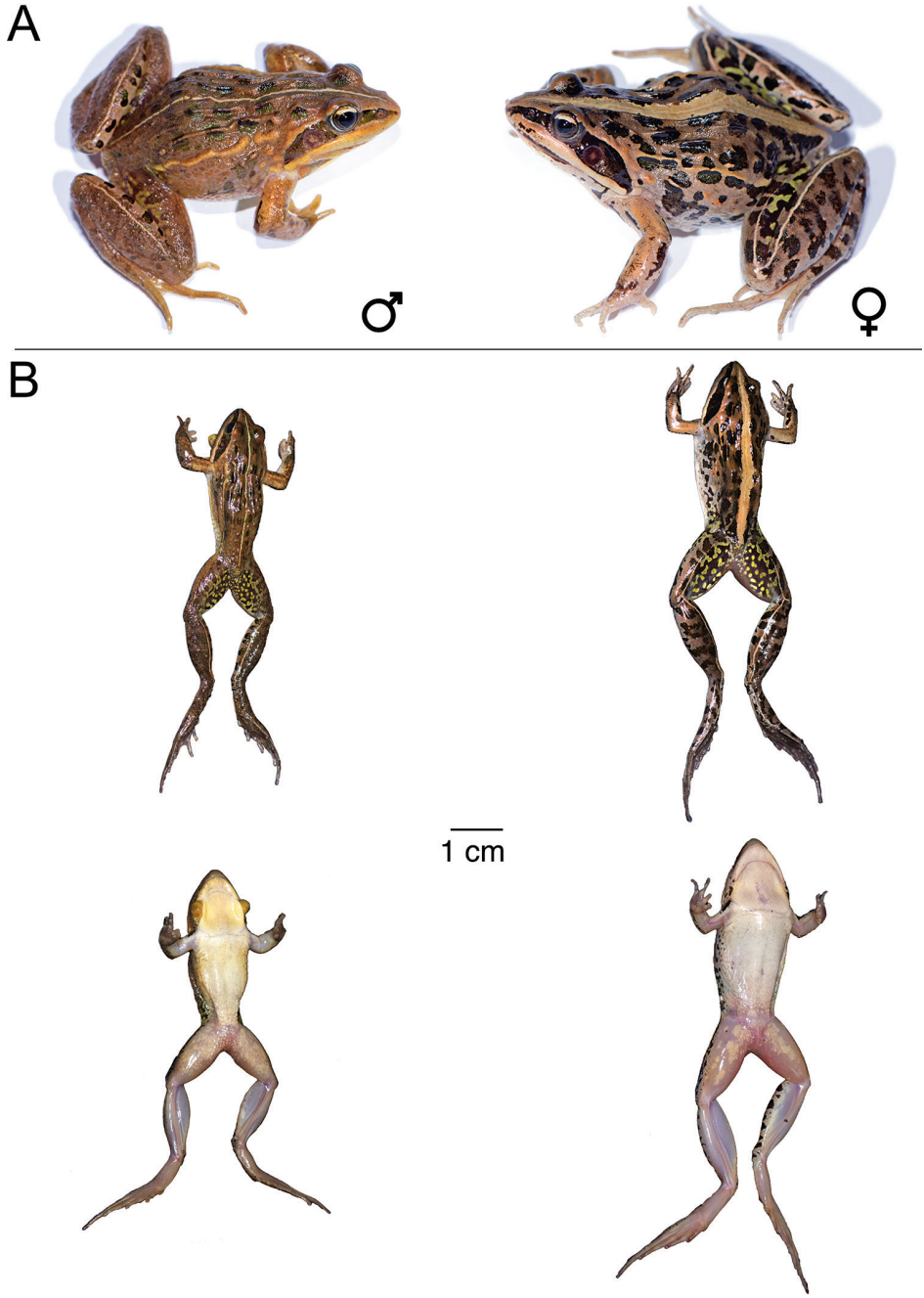

Figure 13. *Ptychadena levenorum* **A** live male (SB90; left) and female (SB85, right) **B** dorsal and ventral views of the same individuals (male left, female right) after euthanasia and before fixation.

except for *P. nana*, *P. robeensis* sp. nov., and *P. erlangeri.* Inter-orbital and eye-nostril distances shorter than *P. erlangeri*. Thigh and tibia of *P. levenorum* are shorter than those *P. erlangeri*, *P. doro* sp. nov., *P. harenna*, *P. goweri*, and *P. neumanni*, and longer than those

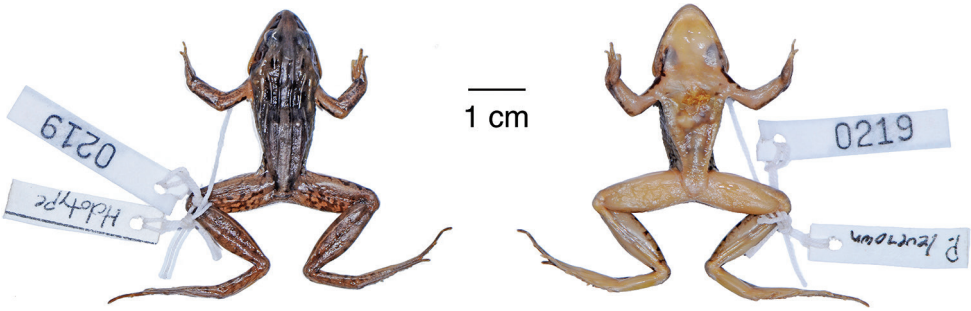

Figure 14. Holotype of *Ptychadena levenorum*. Dorsal and ventral views of the male holotype (TJC219).

of *P. nana* and *P. robeensis* sp. nov. Shorter feet than *P. neumanni* and *P. doro* sp. nov. Shorter hands than *P. amharensis*. Tympanum larger than in *P. nana* and *P. robeensis* sp. nov.

Description of the holotype. Small sized (SVL 33.3 mm) male (Fig. 14). Head longer than wide (HW/HL 0.93). Snout slightly rounded, projecting beyond the lower jaw. Interorbital distance shorter than eye diameter (IOD/ED 0.78) and internarial distance (IOD/IND 0.93). Nostril closer to the eye than the tip of the snout. Tympanum 0.72 × eye diameter. Finger tips not expanded but rounded. Finger formula: I<II<IV<III. Hand free of webbing. Hindlimbs moderately long, with tibia length 0.54 × snout-vent length. Thigh shorter than tibia. Foot 1.3 × tibia length. Toe tips rounded. Inner metatarsal tubercle present, outer absent. Toe formula: I<II<V<III<IV. Foot webbing formula (toe internal/external sides, number of phalanges webbed): Ie(1), IIi/e(1–1.5), IIIi/e(1.5–2), IVi/e(2–2), Vi(2). Four discontinuous dorsal ridges and two discontinuous cream lateral ridges.

Coloration of the holotype in preservative. Dorsal ground color brown with few small irregular oval dark brown blotches symmetrically distributed on the dorsolateral ridges. Very faint wide light grey-brown vertebral stripe from the tip of the snout to the vent. One faint interrupted dorsolateral cream ridge on each side. Dark brown canthal stripe from the tip of the snout to the back of the jaw. Upper lip cream dusted with brown and with irregular dark brown markings. Flanks cream with a few large and irregular dark brown spots. Throat, ventrum, ventral side of the thighs and tibias uniformly cream without any melanization, except for a couple of small irregular brown blotches on the upper ventrum. Barely visible dark brown bars on the tibias and feet. Irregular dark brown markings on the thighs, arms and forearms. Back of the thighs light brown marbled dark brown. Tympanum uniformly dark brown. Vocal sacs cream with some grey markings.

Variations. *Ptychadena levenorum* shows important variations in coloration. In life, dorsum coloration varies from light yellowish brown to dark reddish brown, dark brown and bright green. All specimens examined had black blotches distributed symmetrically on the dorsal ridges, and for some of them the blotches were black with a green iridescence. A few additional dark brown or black blotches are found in the anterior part of the flanks. A vertebral stripe is always present, either thin, medium, or wide and may be cream, yellow, pale brown or bright green.

Iris bicolored, the upper third silver to golden and lower two thirds dark brown. Upper and lower jaws white to golden with few irregular light grey or brown markings but no barring. All specimens examined featured a dark brown or iridescent green canthal stripe from the tip of the snout to the back of the upper lip. Tympanum dark brown, sometimes with golden-iridescent green undefined blotch or dusting. A thin cream or green longitudinal stripe on the tibia is present in some individuals and may extend to the foot and to part or the entire length of the thigh. Tibias, thighs and feet more or less visibly barred with dark brown. Thighs posteriorly dark brown marbled with yellow. Ventrum and throat uniformly white to light yellow. Vocal sacs cream or light grey, very rarely with a bit of grey anteriorly. Small warts over the body and forelimbs present in 40% of adult males examined.

Habitat, distribution, and natural history. The relatively restricted distribution range of *Ptychadena levenorum* extends on both the northern and southern sides of the Sanetti plateau (6.72–9.42°N, 38.66–39.82°E), although there is no record of its presence on the plateau itself. This species occurs mostly at elevation higher than 3000 m a.s.l. (3015 to 3404 m a.s.l.), except for the population living at the type locality Katcha (6.72°N, 39.72°E, 2410 m a.s.l.). The westernmost population was found south of Dodola, near Garamba (6.86°N, 39.19°E, 3260 m a.s.l.).

Individuals have been found, generally in small numbers, calling at night from shallow puddles in grassy meadows or forest clearings. Within the genus, this species is found in sympatry with *Ptychadena cooperi* and *P. robeensis* sp. nov. in the northern part of its range, and *Ptychadena harenna* and *P. goweri* at the type locality. Genetic analyses have shown that *P. levenorum* and *P. robeensis sp. nov*. hybridize where their ranges overlap.

Advertisement call. The call of *Ptychadena levenorum* (2 males, 30 calls) is composed of a single pulsed note of 465 ± 98 ms in duration, containing 23.5 ± 4.3 pulses. Within a call, pulses are grouped, with 4.1 ± 1.5 pulses per group and sometimes with a lower-amplitude single pulse between pulse groups. The duration of inter-pulse intervals within pulse groups is 12 ± 2 ms. Call peak frequency is 2223 ± 90 Hz.

The call of *P. levenorum* differs from those of *P. cooperi*, *P. amharensis*, *P. doro* sp. nov. and *P. neumanni* (type A and B) by the distinguishable pulses composing the calls. Grouped pulses and short inter-pulses intervals distinguish the call of *P. levenorum* from those of *P. robeensis* sp. nov. and *P. delphina* sp. nov. The call of *P. levenorum* can be further distinguished from those of *P. nana* and *P. erlangeri* by a longer duration and from *P. goweri* by a shorter duration and fewer pulses.

Ptychadena nana **Perret, 1980**

Ptychadena nana Perret, 1980: 160.
Rana (*Ptychadena*) *nana* – Dubois 1981: 233.
Ptychadena (*Ptychadena*) *nana* – Dubois 1992: 316.

Type material. ***Holotype.*** A female (ZMB–26878 H) collected by O. Neumann and C. von Erlanger between June and mid-August 1900 (see Neumann 1902) in

"Somaliland", which corresponds to Didda, East Arussi plateau, Ethiopia, 2000–3000 m a.s.l. according to Largen and Perret (Largen 1975, 1977; Perret 1980) [Coordinates estimated by Largen (1997): 7.83°N, 39.50°E]. ***Paratypes.*** From the 20 paratypes included in the original description (Perret 1980), 16 specimens (ZMB–26877, ZMB–57185 up to and including ZMB–57199) collected by O. Neumann and C. von Erlanger at the same time and location are in the collections of the Berlin Museum and four have either been lost or placed in another collection.

Material examined. Except for the type series, all the material examined is deposited at ZNHM. Beside the female holotype (ZMB–26878 H), we examined four female paratypes (ZMB–57189, ZMB–57190, ZMB–57193, ZMB–57199) and four male paratypes (ZMB–26877, ZMB–57191, ZMB–57192, ZMB–57195) collected by C. von Erlanger and O. Neumann in 1900 likely between June and mid-August in Didda, East Arussi plateau, one female (SB488) and two males (SB486, SB487) collected by S. Goutte and Y. Bourgeois on 26 June 2018 west of Ch'ange (8.1303°N, 39.3985°E, 2357 m a.s.l.), one female (SB493) and two males (SB494, SB495) collected by S. Goutte and Y. Bourgeois on 27 June 2018 between Robé and Sedika (7.7307°N, 39.7133°E, 2377 m a.s.l.), five females (SB508, SB510, SB512, SB515, SB516) and four males (SB523, SB524, SB525, SB526) collected by S. Goutte and Y. Bourgeois on 29 June 2018 southeast of Ch'ange (8.1086°N, 39.4486°E, 2573 m a.s.l.).

Diagnosis. The smallest species (male (12) SVL 28.3 ± 3.3 mm, female (12) SVL 29.6 ± 3.2 mm) of the *P. neumanni* complex (Fig. 15), distinguished by the following combination of characters: (1) short hind limbs (male TL/SVL 0.45 ± 0.03, female TL/SVL 0.44 ± 0.03), (2) short hands (HAL/SVL 0.20 ± 0.02), (3) short feet (male FL/SVL 0.49 ± 0.04, female FL/SVL 0.48 ± 0.04), (4) reduced foot webbing, (5) no stripe or blotch on the tympanum, (6) adult males almost always covered in small warts during the breeding season.

Comparison. Distinguished from all Ethiopian *Ptychadena*, except for *P. robeensis* sp. nov., by a considerably smaller size. Very similar to *P. robeensis* sp. nov., *P. nana* has relatively shorter hand, shorter head, a shorter eye-tympanum distance and shorter feet than *P. robeensis* sp. nov. The tympanum lacks any light marking, as opposed to *P. robeensis* sp. nov. Small warts almost always present in males, whereas they are absent in *P. robeensis* sp. nov.

Description of the holotype. Small sized (SVL 26.9 mm) gravid female with short hind limbs (TL/SVL 0.43, Fig. 16, Suppl. material 3: Table S1). Head longer than wide (HW/HL 0.95). Snout rounded, slightly projecting beyond the lower jaw. Interorbital distance 0.58 × eye diameter. Nostril half-way between the tip of the snout and the eye. Internarial distance 1.4 × interorbital distance. Tympanum 0.65 × eye diameter. Finger tips not expanded but rounded. Finger formula: III<IV<III. Hand free of webbing. Hindlimbs short, with tibia length 0.42 × snout-vent length. Foot 1.2 × tibia length and 1.3 thigh length. Toe tips rounded. Outer metatarsal tubercle absent. Toe formula: I<II<V<III<IV. Foot webbing formula (toe internal/external sides, number of phalanges webbed): Ie(1), IIi/e(1–1), IIIi/e(1–2), IVi/e(2–2), Vi(2). Ridges hardly distinguishable due to the state of preservation of the specimen.

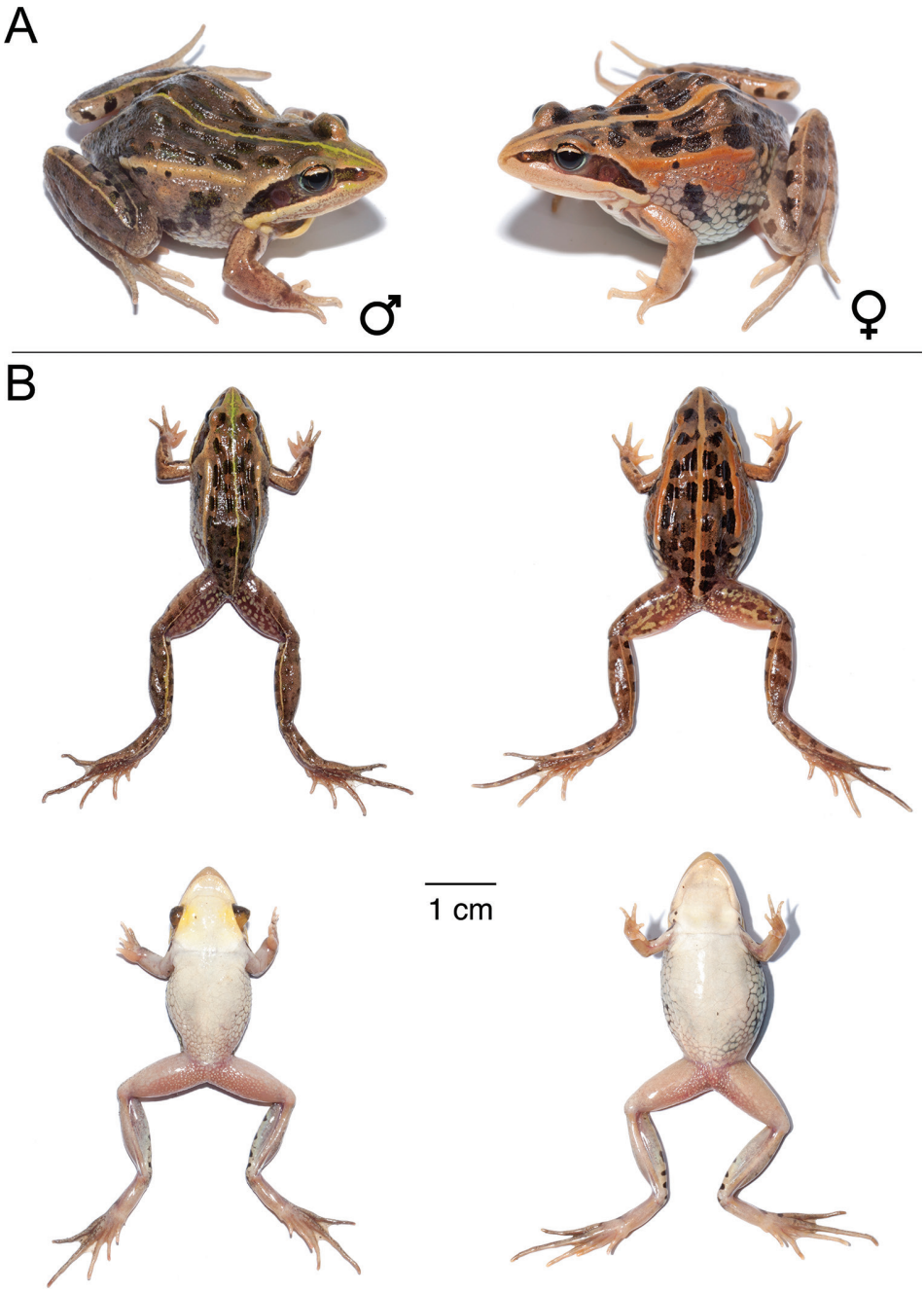

Figure 15. *Ptychadena nana* **A** live male (SB494; left) and female (SB488, right) **B** dorsal and ventral views of the same individuals (male left, female right) after euthanasia and before fixation.

Coloration of the holotype in preservative. Dorsal ground color brown with irregular oval dark brown blotches symmetrically distributed, presumably on the dorsolateral ridges. One dark brown blotch on each upper eyelid. No vertebral stripe. One

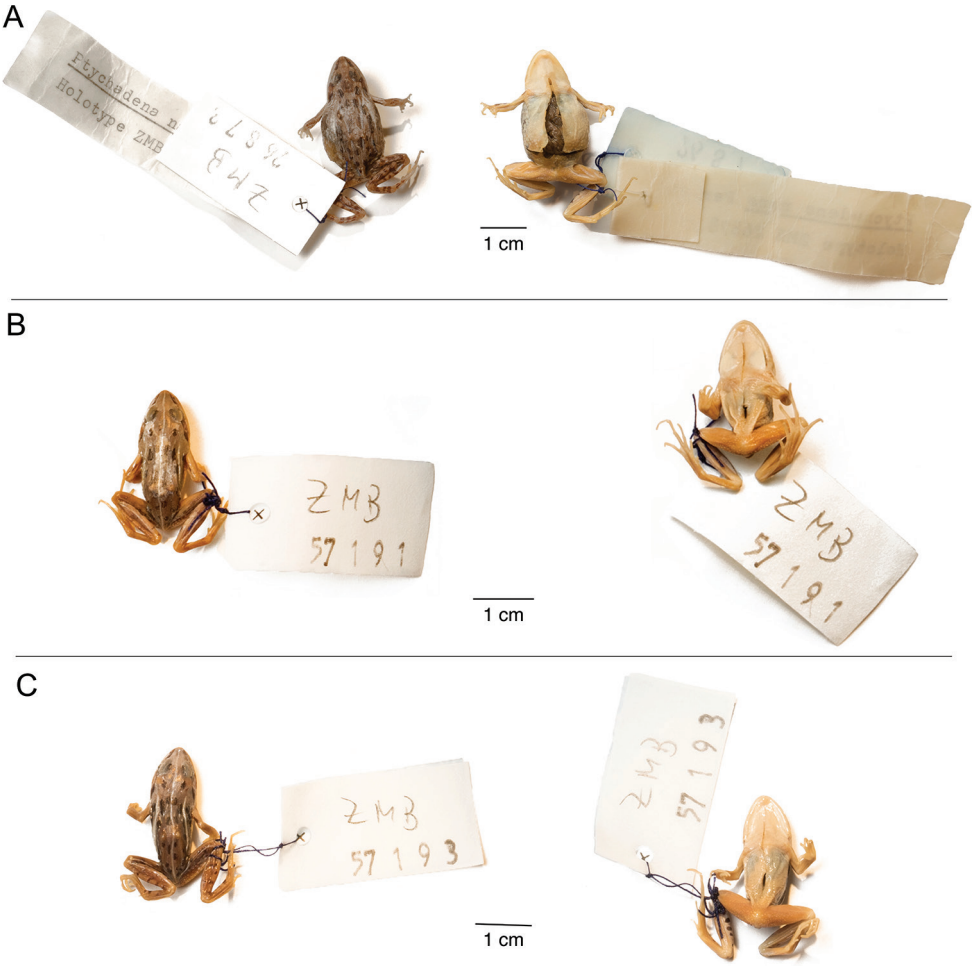

Figure 16. Type specimens of *Ptychadena nana*. Dorsal and ventral views of three specimens from the type series **A** female holotype (ZMB–26878 H) **B** male paratype (ZMB–57191) **C** female paratype (ZMB–57193).

fainted dorsolateral cream ridge on each side. Dark brown canthal stripe from the tip of the snout to the back of the jaw. Upper lip cream. Flanks brown to dark brown with numerous cream spots which merge ventrally. Throat, ventrum, ventral side of tibias uniformly cream without any melanization. Ventral side of the thighs light brown. Dark brown bars on the thighs, tibias and feet. Back of the thighs brown marbled with cream. Dark brown irregular markings on the arms and forearms. No stripe or blotch on the tympanum.

Variations. As the other members of the *Ptychadena erlangeri* species group, *Ptychadena nana* shows color polymorphism. In life, dorsum coloration varies from light grey to sand and brown. The dark blotches disposed more or less symmetrically on the dorsum vary in size and number, sometimes covering more than half the dorsum. Their colors vary from olive-brown, with some green iridescence, to black. One or several blotches of the same color, sometimes fused into a large irregular shape,

were present on the anterior part of the flank in all examined specimens. The vertebral stripe, when present, may be thin, medium or wide and cream, light brown or bright green. Some individuals lack any vertebral stripe.

Iris bicolored, the upper third silver to golden and lower two thirds brown to dark brown. Upper and lower jaws cream, golden or light brown, often with irregular light grey or light brown markings but no barring. All specimens examined featured a dark brown canthal stripe from the tip of the snout to the back of the upper lip, sometimes dusted with small green spots. Tympanum uniformly colored and lacking any light stripe of blotch. A thin cream or light green longitudinal stripe on the tibia extending the complete length of the thigh is present in some individuals. Barring on the tibias, thighs, and feet may be very distinct or almost completely absent. Thighs posteriorly marbled with dark brown and yellow or cream. Ventrum uniformly white. Throat white in females and pale yellow to deep yellow in adult males. Vocal sacs bicolored grey anteriorly and cream posteriorly, rarely completely grey. Small warts over the body and forelimbs present in 90% of adult males examined.

Habitat, distribution, and natural history. *Ptychadena nana* is found on the eastern half of the Arussi plateau (7.64–8.30°N, 39.39–39.87°E, Oromia, Ethiopia from 2380 to 2850 m a.s.l. In the south, its range is limited by the Shebelle River, while in the northeast it is bordered by the Great Rift Valley. The westernmost individuals were found around four kilometers west of Ch'ange. The steep terrain just east of Huruta may serve as geographic barrier for dispersal in this species, as it has not been found further southeast. In the southwest end of its range, *P. nana* has been found just north of Dibe, but presumably occurs all the way down to Barbari as there is no physical barrier that would prevent its dispersal on this side of the plateau.

Males are found calling at night in large numbers from shallow roadside puddles, usually overgrown by grass. Within the genus, *P. nana* is found in sympatry with *Ptychadena cooperi*.

Advertisement call. The call of *Ptychadena nana* (5 males, 56 calls) is composed of a single pulsed note of 205 ± 47 ms in duration, containing 16.9 ± 2.8 pulses. Inter-pulses intervals are very short (9 ± 2 ms) and irregular, forming few irregular pulse groups and resulting in a high pulse rate (84 ± 10.2 pulses s^{-1}). Call peak frequency is 2461 ± 26 Hz.

The call of *P. nana* can be differentiated from those of *P. cooperi*, *P. amharensis*, *P. doro* sp. nov. and *P. neumanni* (types A and B) by the distinguishable pulses composing the calls. It is also distinct form the calls of *P. delphina* sp. nov. and *P. robeensis* sp. nov. by its short inter-pulse intervals. Finally, the call of *P. nana* differs from the calls of *P. delphina* sp. nov., *P. robeensis* sp. nov., *P. erlangeri*, *P. levenorum*, *P. beka* sp. nov., and *P. goweri* by its short duration and high pulse rate.

***Ptychadena robeensis* sp. nov.**
http://zoobank.org/C43EB165-5CC3-4489-8B07-AACA17E30367

Type material. ***Holotype.*** Adult male (SB81) collected on 9 April 2018 by S. Goutte and J. Reyes-Velasco between Robe and Ali (7.2111°N, 39.9672°E, 2374 m a.s.l.).

Paratypes. Three males (15–139, 15–140 and 15–147) and one female (15–138) collected on 8 August 2015 northwest of Robe (7.1720°N, 39.9722°E; 2431 m a.s.l.), one male (15–163) collected on 9 August 2015 east of Dinsho (7.1061°N, 39.8182°E; 3058 m a.s.l.), one male (16–92) and one female (16–77) collected by J. Reyes-Velasco and S. Boissinot 10 July 2016 east of Dinsho (7.1065°N, 39.8184°E, 3065 m a.s.l.), one male (SB65) collected by J. Reyes-Velasco and S. Goutte on 8 April 2018 south of Dinsho (7.0915°N, 39.7834°N, 3079 m a.s.l.), three males (SB82, SB83, SB84) collected by J. Reyes-Velasco and S. Goutte on 9 April 2019 between Robe and Ali (7.2111°N, 39.9672°E, 2374 m a.s.l.), three males (SB88, SB92, SB93) and two females (SB87, SB89) collected by J. Reyes-Velasco and S. Goutte on 9 April 2019 east of Dinsho (7.1056°N, 39.8168°E, 3015 m a.s.l.). All specimens are deposited at ZNHM.

Diagnosis. Small species (male (13) SVL 30.3 ± 0.7 mm, female (4) SVL 31.6 ± 2.9 mm) of the *erlangeri* species group (Fig. 17), distinguishable from other species of the *P. neumanni* complex by the following combination of characters: (1) short hind limbs (male TL/SVL 0.45 ± 0.0.03, female TL/SVL 0.44 ± 0.02), (2) short forearms (male FLL/SVL 0.18 ± 0.02, female FLL/SVL 0.18 ± 0.00), (3) short feet (male FL/SVL 0.5 ± 0.03, female FL/SVL 0.49 ± 0.05), (4) reduced foot webbing, (5) a vertical cream or golden stripe or blotch on the tympanum (sometimes faint), (6) warts absent in adult males during the breeding season.

Comparison. Distinguished from all Ethiopian *Ptychadena*, except for *P. nana*, by a considerably smaller size. Compared to *P. nana*, it has relatively longer hands, greater eye-tympanum distance and longer feet. *Ptychadena robeensis* sp. nov. also presents a more or less distinct cream or golden blotch on the tympanum, which is absent in *P. nana*. Finally, the bodies of adult male *P. robeensis* sp. nov. are not covered in warts as opposed to *P. nana*.

Description of the holotype. Small sized (SVL 29.3 mm) male with short hind limbs (TL/SVL 0.45, Fig. 17, Suppl. material 3: Table S1). Head longer than wide (HW/HL 0.96). Snout slightly rounded, projecting beyond the lower jaw. Interorbital distance equal to the eye diameter and to the internarial distance. Nostril half-way between the tip of the snout and the eye. Tympanum 0.77 × eye diameter. Finger tips not expanded but rounded. Finger formula: I<II<IV<III. Hand free of webbing. Hindlimbs short, with tibia length 0.45 × snout-vent length. Tibia and thigh lengths equal. Foot 1.3 × tibia length. Toe tips rounded. Inner metatarsal tubercle present, outer absent. Toe formula: I<II<V<III<IV. Foot webbing formula (toe internal/external sides, number of phalanges webbed): Ie(1), IIi/e(1–1), IIIi/e(1–1), IVi/e(1–1), Vi(1). Four continuous dorsal ridges and one faint cream lateral ridge, interrupted on one side and continuous on the other.

Coloration of the holotype in life. Dorsal ground color grey with a few, elongated dark brown blotches symmetrically distributed on the dorsolateral ridges. Thin cream stripe on the dorsum from the tip of the snout to the vent, on the foot, tibia, and half of the thigh. Dark olive brown canthal stripe from the tip of the snout to the back of the jaw. Small cream blotch on the otherwise dark brown tympanum. Upper and lower lip cream to light brown towards the tip of the snout with irregular small brown markings.

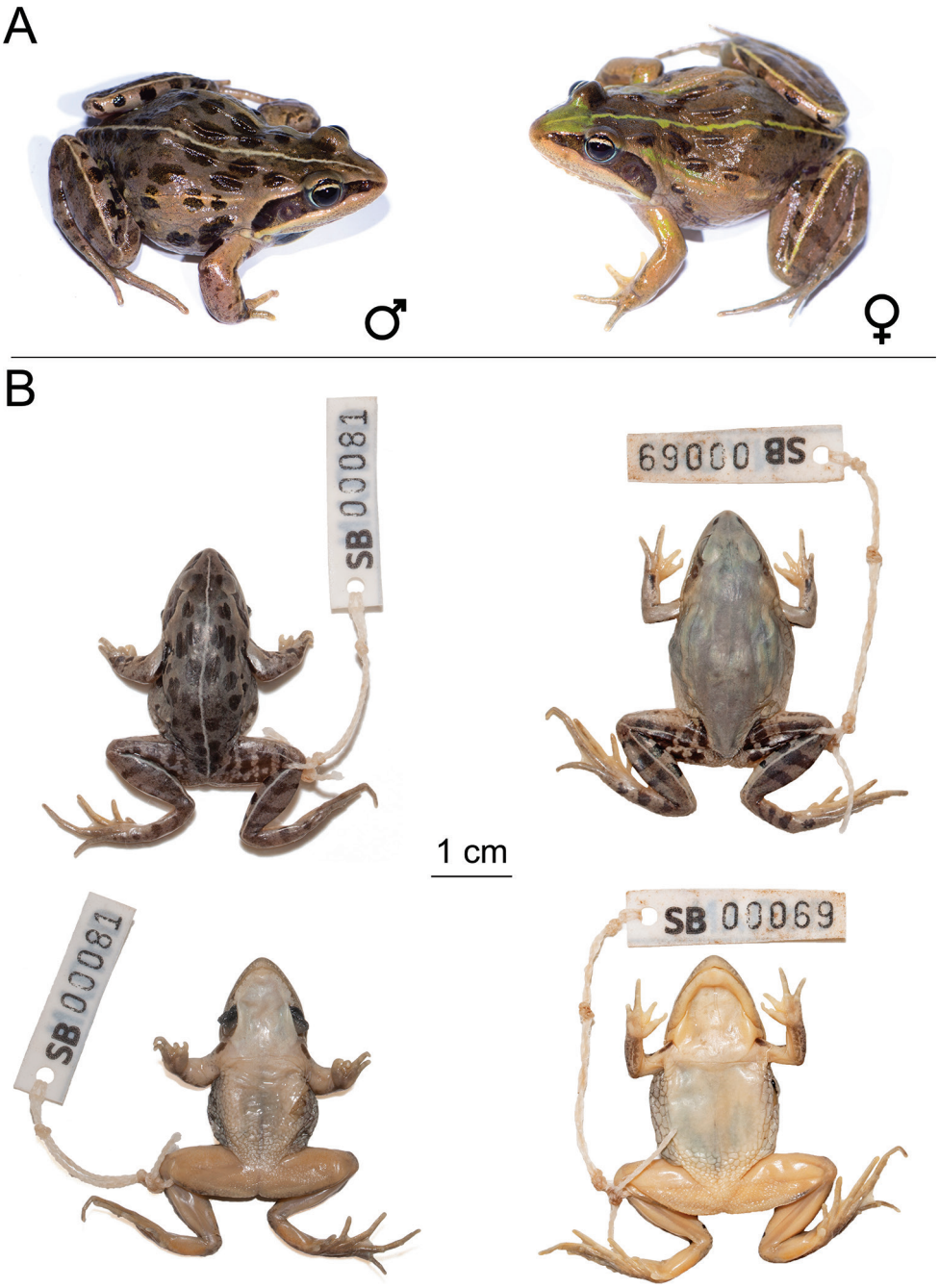

Figure 17. *Ptychadena robeensis* sp. nov. **A** live male holotype (SB81; left) and female paratype (SB89, right) **B** dorsal and ventral views of the male holotype (SB81; left) and a female (SB69; right) after fixation. The female SB69, green in life, lacks any melanization on the dorsum, a rare phenotype that has been encountered in a few individuals only.

Iris bicolored, with upper third light cream, and the lower two thirds dark brown with golden freckles. Irregular dark brown blotches on the flanks. Ventrum cream, reticulated with light brown on its lower part. Throat light yellow. Two small symmetrical dark brown blotches on the antero-ventral side of the shoulders. Hind limbs brown with dark brown bars over the thighs, tibias and feet. A few very small round white dots around the groin. Back of the thighs dark brown irregularly molted with yellow. Vocal sacs dark grey anteriorly and light grey posteriorly.

Coloration of the holotype in preservative. Dorsal ground color grey with a few large oval black blotches symmetrically distributed on the dorsolateral ridges. Thin cream vertebral stripe from the tip of the snout to the vent. Dark brown canthal stripe from the tip of the snout to the back of the jaw. Faint vertical stripe on the otherwise brown tympanum. Upper lip and lower lips cream dusted with light grey. Flanks light with a few irregular small dark brown blotches. Throat, ventrum, ventral side of the thighs and tibias uniformly cream. Two symmetrical brown blotches on the ventral side of the shoulders. Faint, thin longitudinal stripe on the tibia, foot and half of the thigh. Foot, tibia and thigh barred with brown. Back of thighs molted light grey and brown. Vocal sacs dark grey anteriorly and light grey posteriorly. Nuptial pads cream.

Variations. As the other members of the *erlangeri* species group, *Ptychadena robeensis* sp. nov. shows color polymorphism. In life, dorsum coloration varies from grey-brown to reddish or yellowish brown, or bright lime green. The dark blotches disposed more or less symmetrically on the dorsum vary in size and number and are either dark brown or black. A few individuals completely lack melanization on the dorsum, resulting in an almost uniform light brown or bright lime green coloration. The limbs of these individuals, however, have melanization patterns comparable to other individuals.

One or a few dark blotches is present on the anterior part of the flank of some individuals.

The vertebral stripe, when present, may be thin or wide and cream, sand, yellow or bright lime green. Wide stripes may be doubled with a thin, lighter line. Some individuals lack any vertebral stripe and individuals lacking dorsal melanization generally have a barely visible thin light vertebral stripe.

Iris bicolored, the upper third cream, silver or golden and lower two thirds brown to dark brown. Upper and lower jaws cream, golden or light green, often with irregular light grey or light brown markings but no barring. Most individuals feature a dark brown canthal stripe from the tip of the snout to the back of the upper lip, sometimes dusted with small green spots. Individuals lacking dorsal melanization have a golden canthal stripe covered with small dark grey spots. Interestingly, the nostrils of these individuals are outlined in black. Tympanum dark brown with a more or less defined cream to golden vertical blotch. A thin cream or light green longitudinal stripe on the tibia extending to half or the whole length of the thigh is present in some individuals. Barring on the tibias, thighs and feet may be very distinct or almost completely absent. Thighs posteriorly marbled with dark brown and light brown, yellow or light green. Ventrum uniformly white. Throat white or very pale yellow in females and pale to deep

yellow in adult males. Vocal sacs dark grey in 70% of examined specimens, bicolored dark grey anteriorly and light grey posteriorly in some individuals, and rarely light grey. Warts were absent from all adult males examined.

Etymology. The specific name refers to the town of Robe, near the type locality.

Habitat, distribution and natural history. *Ptychadena robeensis* sp. nov. occupies a very small range (7.05–7.23°N, 39.78–39.98°E) around the town of Robe, Bale zone, Oromia, Ethiopia. It is found at elevations ranging from 2375 m to 3120 m a.s.l. The westernmost individuals were found near Dinsho, which is also the highest elevation point of the species range. In the south, *P. robeensis* sp. nov. is found between Robe and Goba, while it is known up to just west of Ali in the north. The species presumably occurs further north on the plateau as elevation and habitat seem rather homogeneous up to the Shebelle River.

Males are found calling at night from shallow grassy puddles or flooded cultivated fields. Calling activity typically starts after 22:00, even though males may be at calling sites earlier. Males have been found calling in syntopy with *P. cooperi* and *P. levenorum*. Genetic analyses have shown that *P. levenorum* and *P. robeensis* sp. nov. hybridize where their ranges overlap.

Advertisement call. The call of *Ptychadena robeensis* sp. nov. (5 males, 101 calls) is composed of a single pulsed note of 534 ± 53 ms in duration, containing 9.8 ± 1 regularly-spaced pulses. Pulse amplitude increases gradually until 292 ± 19 ms, after what it decreases. Call peak frequency is 2876 ± 74 Hz with a slight increase in frequency within the call.

The call of *P. robeensis* sp. nov. can be distinguished from the calls of all other members of the *P. neumanni* complex, except for *P. delphina* sp. nov., by its regularly spaced pulses and long inter-pulses intervals (57 ± 5 ms). A higher frequency allows discriminating the calls of *P. robeensis* sp. nov. and *P. delphina* sp. nov.

***Ptychadena beka* sp. nov.**

http://zoobank.org/CCF36B05-F7FC-436B-8858-765B6F682127

Type material. ***Holotype.*** Adult male (SB291) collected by S. Goutte and J. Reyes-Velasco on 5 June 2018 southwest of Nekemte (8.9950°N, 36.4955°E, 2213 m a.s.l.). ***Paratypes.*** one male (15–5) collected by X. Freilich, J. Reyes-Velasco and S. Boissinot on 3 August 2015 west of Holeta Genet (9.0508°N, 38.4312°E, 2433 m a.s.l.), one male (15–283) collected by X. Freilich, J. Reyes-Velasco and S. Boissinot on 14 August 2015 southwest of Nekemte (8.9742°N, 36.4906°E, 2243 m a.s.l.), one female (16–1) collected by J. Reyes-Velasco and S. Boissinot on 4 July 2016 west of Holeta Genet (9.05078°N, 38.4312°E, 2386 m a.s.l.), one female (SB268) collected by S. Goutte and J. Reyes-Velasco on 3 June 2018 northwest of Bonga (7.5085°N, 36.0637°E, 2038 m a.s.l.), 3 females (SB270, SB272 and SB276) collected by S. Goutte and J. Reyes-Velasco on 3 June 2018 south of Ambo (8.9671–8.9922°N, 37.7951–37.8471°E, 1945–2170 m a.s.l.), one female (SB282) collected by S. Goutte and J. Reyes-Velasco

on 4 June 2018 southwest of Nekemte (8.9950°N, 36.4955°E, 2213 m a.s.l.), one female (SB287) and one male (SB292) collected by S. Goutte and J. Reyes-Velasco on 5 June 2018 southwest of Nekemte (8.9950°N, 36.4955°E, 2213 m a.s.l.), one male (SB387) collected by S. Goutte and J. Reyes-Velasco on 11 June 2018 south of Gech'a (7.5544°N, 35.4148°E, 1936 m a.s.l.), one male (SB471) collected by S. Goutte and Y. Bourgeois on 21 June 2018 east of Iteya (8.1275°N, 39.2732°E, 2138 m a.s.l.), one female (SB566) collected by S. Goutte and Y. Bourgeois north of Gohatsion (10.01967°N, 38.2494°E, 2448 m a.s.l.), one male (SB576) collected by S. Goutte and Y. Bourgeois on 7 July 2018 north of Gebre Guracha (9.8664°N, 38.3758°E, 2596 m a.s.l.), two males (SB614, SB617) collected by S. Goutte and Y. Bourgeois on 14 July 2018 east of Holeta Genet (9.0682°N, 38.5214°E, 2397 m a.s.l.). All specimens are deposited at ZNHM.

Diagnosis. A medium-sized species (male (9) SVL 37.9 ± 2.6 mm, female (8) SVL 43.2 ± 2.9 mm) of the *neumanni* species group (Fig. 18), distinguished by the following combination of characters: (1) relatively short hind limbs (male TL/SVL 0.51 ± 0.03, female TL/SVL 0.57 ± 0.03), (2) tympanum with a light vertical bar, (3) medium or wide vertebral stripe always present, (4) vocal sacs of most males are bicolored, from light to dark grey posteriorly and from yellow to cream anteriorly, rarely, they are light grey, (5) forearms of adult males not thickened.

Comparison. *Ptychadena beka* sp. nov. is smaller than *P. cooperi* and *P. goweri* and larger than *P. nana* and *P. robeensis* sp. nov. Hand, feet, tibias, thighs and snout are of similar dimensions than *P. amharensis* and shorter than those of *P. delphina* sp. nov. and *P. goweri*. *Ptychadena beka* sp. nov. can be distinguished from *P. amharensis* by a wider inter-orbital distance. It can be distinguished from *P. erlangeri* by a larger tympanum, the light stripe or blotch on the tympanum and the bicolored vocal sacs in adult males. *Ptychadena beka* sp. nov. differs from *P. levenorum* by longer thighs, larger tympanum and longer snout. The head is wider and the tibias are longer than in *P. doro* sp. nov.

Description of the holotype. A medium-sized (SVL 36.3 mm) adult male (Fig. 18). Head slightly wider than long. Snout projecting beyond the lower jaw. Interorbital distance 0.62 × the eye diameter. Internarial distance 1.12 × interorbital distance. Tympanum 0.67 × eye diameter. Finger tips not expanded but rounded, with very small subarticular tubercles. Finger formula: I<II<IV<III. Hand free of webbing, palmar tubercle absent. Nuptial pads light grey. Hindlimbs moderately elongated, with tibia length 0.51 × snout-vent length. Foot as long as thigh and shorter than tibia (FL/TL0.97). Toe tips rounded. Subarticular tubercles extremely small. Inner metatarsal tubercle present, external absent. Toe formula: I<II<V<III<IV. Foot webbing formula: Ie(1), IIi/e(1–1), IIIi/e(1–2), IVi/e(2–2), Vi(2). Two light brown, continuous lateral ridges, two continuous and four interrupted dorsal ridges. No vertebral nor sacral ridges. No warts on the body. Small and round light brown warts on tibias and thighs.

Coloration of the holotype in life. Dorsal ground color brown with a few small, elongated dark brown blotches symmetrically distributed on the dorsolateral ridges. Wide light brown vertebral stripe, doubled with a thin, clearer line from the tip of the

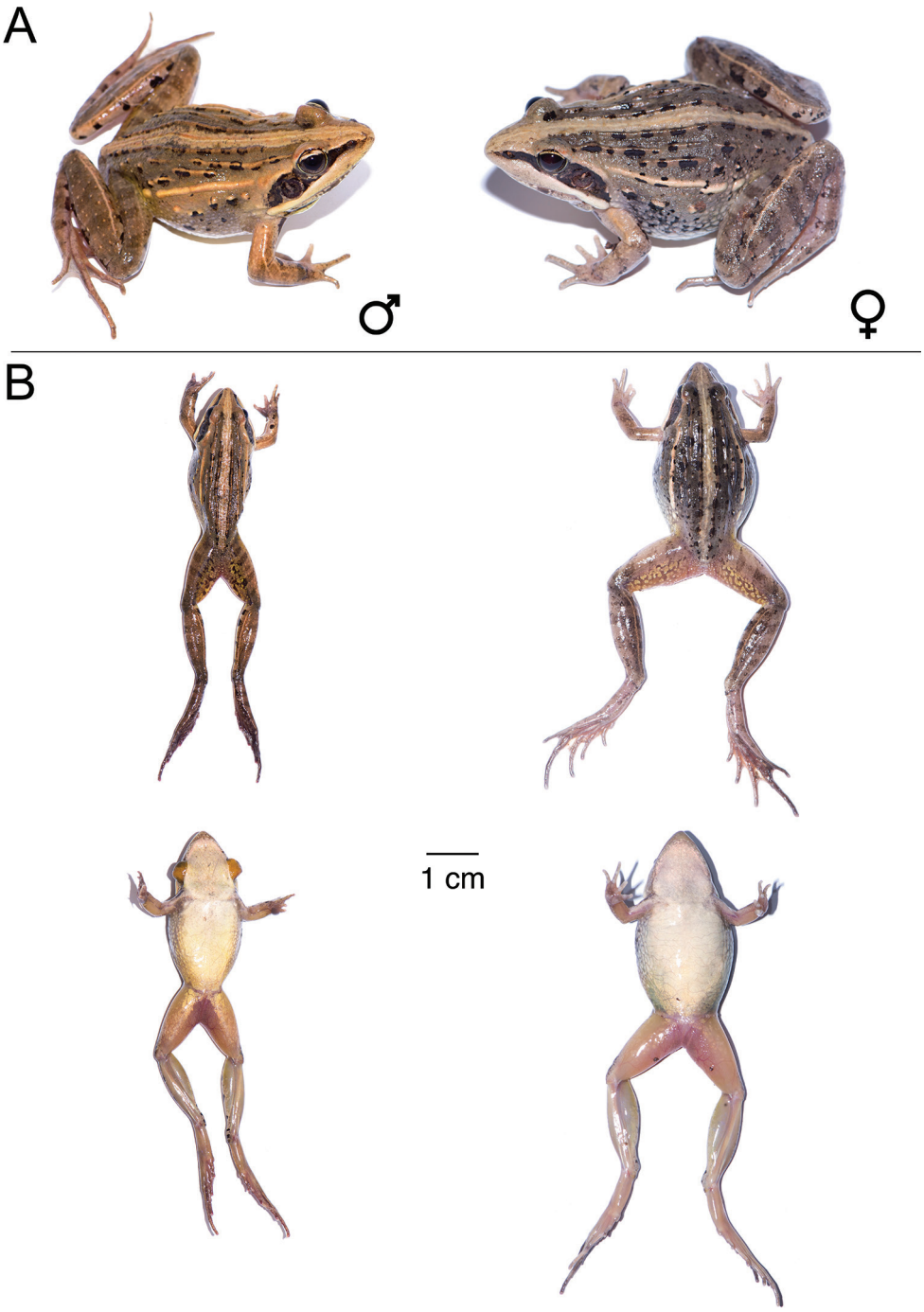

Figure 18. *Ptychadena beka* sp. nov. **A** live male holotype (SB291; left) and female paratype (SB270, right) **B** dorsal and ventral views of the same individuals (male left, female right) after euthanasia and before fixation.

snout to the vent. Dark brown canthal stripe from the tip of the snout to the back of the jaw. Faint light vertical stripe on the otherwise brown tympanum. Upper and lower lip cream with irregular brown markings.

Iris bicolored, with upper third light silver-grey, and the lower two thirds dark brown. Small irregular dark olive brown blotches on greyish flanks. Throat and chest cream, ventrum, ventral sides of the thighs and of the tibias light yellow. Two small symmetrical dark brown blotches on the antero-ventral side of the shoulders. Thin, light longitudinal stripe on the tibias. Few white round warts on the tibias. Hind limbs brown with dark olive bars over the thighs, tibias, and feet. A few very small round white dots around the groin. Back of the thighs dark brown irregularly molted with yellow. Vocal sacs dark grey anteriorly, yellow posteriorly.

Coloration of the holotype in preservative. Dorsal ground color grey with a few oval dark brown blotches symmetrically distributed on the dorsolateral ridges. Wide light brown vertebral stripe, doubled with a lighter thin line from the tip of the snout to the vent. Dark brown canthal stripe from the tip of the snout to the back of the jaw. Faint vertical stripe on the otherwise brown tympanum. Upper lip and lower lip cream heavily blotched with grey. Flanks brown with a few black blotches underlined with a cream bar. Throat, ventrum, ventral side of the thighs and tibias cream, with the chest and throat dusted with grey. Two symmetrical dark brown blotches on the ventral side of the shoulders. Faint, thin longitudinal stripe on the tibias. Faint brown bars on the thigh and tibia. A few small round white spots forming a line on the posterior side of tibia and foot. Back of thighs molted light and dark brown. Vocal sacs dark grey anteriorly, cream posteriorly. Nuptial pads light grey.

Variations. In life, background color varies from yellowish brown to greyish brown. Dorsal ridges vary in number and definition. In all examined specimens, median ridges were continuous from the back of the head to the groin. Postpalpebral fold usually interrupted in the middle of the back, sometimes continuing on the lower back by a ridge or multiple aligned warts. Short latero-dorsal fold almost always present, sometimes fractioned. Lateral ridges, briefly interrupted in a few specimens, most often continuous, from orange-brown to cream. All specimens examined had small dark brown or black blotches distributed symmetrically on the dorsal ridges, in very few specimens, those blotches were very small or barely visible. All examined individuals have a wide, generally around a lighter thin stripe. The light blotch on the tympanum is generally small and more conspicuous in some specimens than in others. The thin cream longitudinal stripe on the tibia may be more or less conspicuous and extended to half of the thigh in some individuals. Tibias, thighs and feet posteriorly barred with more or less defined brown or light brown markings. Yellow and brown marbling on the posterior side of the thighs more or less contrasted and almost absent in some individuals. Ventrum and throat uniformly white to light yellow. Vocal sacs grey, bicolored cream to yellow and light grey to grey. Small warts over the back and flanks in ca. 10% of adult males examined.

Etymology. The specific name corresponds to the translation of the word "enough" or "that's it" in Amharic (በቃ), in reference to the controversial taxonomic history of the group that we hope has come to an end. It is an invariable noun used in apposition.

Habitat, distribution, and natural history. *Ptychadena beka* sp. nov. has a wide distribution range extending both sides of the Great Rift Valley, although most records were made west of the GRV (6.14–10.01°N, 35.41–39.27°E). It is restricted to moderate altitudes, from 1695 m to 2596 m a.s.l. (based on 106 barcoded individuals). In the north, its range is limited by the Blue Nile valley and the northernmost specimens have been found just north of Gohatsion. The westernmost population has been found in Gech'a. Two populations have been found southeast of the GRV, near Iteya and south of Irba Muda. GPS coordinates for all examined specimens are given in Suppl. material 3: Table S1. *Ptychadena beka* sp. nov. is found in syntopy with *P. erlangeri* at the higher end of its altitudinal range, notably near Fitche, Holeta, between Ambo and Wonchi, and possibly near Assela. Within the genus, *P. beka* sp. nov. is also sympatric with *P. neumanni*, *P. delphina*, and *P. doro* in the west.

Males are found calling at in shallow roadside puddles or agricultural fields. Males can be found vocalizing very close from one another, sometimes in important numbers. Calling activity depends on rainfall and is highest during rainy months. Calling usually starts after 22:00, and sometimes as late as 02:00 in dry weather, and ceases before dawn. Numerous, small bicolored eggs are laid in the same water body.

Advertisement call. The call of *Ptychadena beka* sp. nov. (5 males, 128 calls) is composed of a single pulsed note of 447 ± 112 ms in duration, containing 31 ± 10.6 pulses. Within calls, pulses are grouped by 3–5 pulses, with the first and the last pulses of each pulse group notably lower in amplitude than the other pulses. Low-amplitude single pulses are sometimes present between pulse groups. Amplitude increases gradually during the call, peaking at 266 ± 78 ms, after which it drops. Call dominant frequency is 2491 ± 129 Hz.

The call of *P. beka* sp. nov. can be distinguished from those of *P. cooperi*, *P. amharensis*, *P. doro* sp. nov., and *P. neumanni* (type A and B) by the distinguishable pulses composing the calls. It is also distinct from the calls of *P. delphina* sp. nov. and *P. robeensis* sp. nov. by its short inter-pulse intervals. The call of *P. beka* sp. nov. differs from the calls of *P. delphina* sp. nov., *P. erlangeri*, *P. levenorum*, and *P. goweri* by its higher dominant frequency. Finally, the call of *P. beka* sp. nov. differs from the call of *P. nana* and *P. erlangeri* by its longer duration.

***Ptychadena delphina* sp. nov.**

http://zoobank.org/8BFAD046-6E3B-4622-B488-D4483FA2BE31

Type material. ***Holotype.*** Adult male (SB310) collected on 7 June 2018 by S. Goutte and J. Reyes-Velasco between Dembi and Gechi, Oromia, Ethiopia (8.2195°N, 36.446°E, 2064 m a.s.l.). ***Paratypes.*** One female (16–242) and one male (16–241) collected 22

July 2016 by X. Freilich, J. Reyes-Velasco and S. Boissinot west of Bedele (8.3746°N, 36.2596°E, 1876 m a.s.l.), one female (SB295) collected on 6 June 2018 by S. Goutte and J. Reyes-Velasco west of Bedele (8.4330°N, 36.3176°E, 1942 m a.s.l.), two males (SB313 and SB314) collected on 7 June 2018 by S. Goutte and J. Reyes-Velasco between Dembi and Gechi (8.2195°N, 36.4460°E, 2064 m a.s.l.), one female (SB341) collected on 9 June 2018 by S. Goutte and J. Reyes-Velasco west of Gore (8.1769°N, 35.3627°E, 1612 m a.s.l.), 3 females(SB355, SB356 and SB357) and two males (SB354 and SB363) collected on 10 June 2018 by S. Goutte and J. Reyes-Velasco south of Gore (8.0802°N, 35.5239°E, 1903 m a.s.l.). All specimens are deposited at ZNHM.

Diagnosis. Large member (male (6) SVL 40.1 ± 2.9 mm, female (6) SVL 47.2 ± 2.3 mm) of the *neumanni* species group (Fig. 19) distinguished by the following combination of characters: (1) moderately long hind limbs (male TL/SVL 0.53 ± 0.02, female TL/SVL 0.55 ± 0.03), (2) long forearms (FLL/SVL 0.20 ± 0.01), (3) eye close to one another (male IOD/HW 0.17 ± 0.02, female IOD/HW 0.20 ± 0.03), (4) light vertical stripe on the tympanum, (5) vocal sacs are dark grey or dark grey posteriorly and lighter anteriorly.

Comparison. *Ptychadena delphina* sp. nov. is smaller than *P. cooperi* and larger than *P. nana*, *P. erlangeri*, *P. levenorum*, and *P. robeensis* sp. nov. This species has shorter hind limbs and feet than *P. goweri* but longer than *P. beka* sp. nov. and *P. amharensis* (see Suppl. material 3: Table S2). The length of its forearms is also greater than in *P. beka* sp. nov. and *P. amharensis*. *Ptychadena delphina* sp. nov. can be distinguished from *P. goweri* by shorter hands, shorter snout, and pigmented vocal sacs in adult males. Eyes are closer to one-another than *P. goweri*, but further apart than in *P. amharensis*. Tympanum larger than *P. doro* sp. nov.

Description of the holotype. Relatively large (SVL 44.2 mm) male (Fig. 19). Head wider than long (HL/HW 0.87). Snout projecting beyond the lower jaw. Interorbital distance 0.54 × eye diameter. Internarial distance 1.68 × interorbital distance. Tympanum 0.71 × eye diameter. Finger tips not expanded but rounded, with small subarticular tubercles.

Finger formula: I<II<IV<III. Hand free of webbing. Hindlimbs elongated, with tibia length 0.55 × snout-vent length. Foot longer than thigh (FL/THL 1.27) and slightly longer than tibia (FL/TL 1.02). Toe tips rounded. Subarticular tubercles small and round. Inner metatarsal tubercle present, external absent. Fourth toe on the left foot amputated. Toe formula: I<II<V<III<IV. Foot webbing formula: Ie(minimal), IIi/e(minimal–1), IIIi/e(2–2), IVi/e(2–2), Vi(2). Two light lateral ridges, continuous on the right side and discontinuous on the left side. Two continuous dorsal ridges and two interrupted dorsolateral ridges. No vertebral nor sacral ridges. Body and eyelids covered with minute transparent warts. Nuptial pad developed along finger I. Tongue longer than wide, free for half of its length, bifurcated at the end. Vomerine, maxillary and premaxillary teeth present.

Coloration of the holotype in life. Dorsal ground color brown with elongated dark brown blotches symmetrically distributed on the dorsal ridges. Wide light

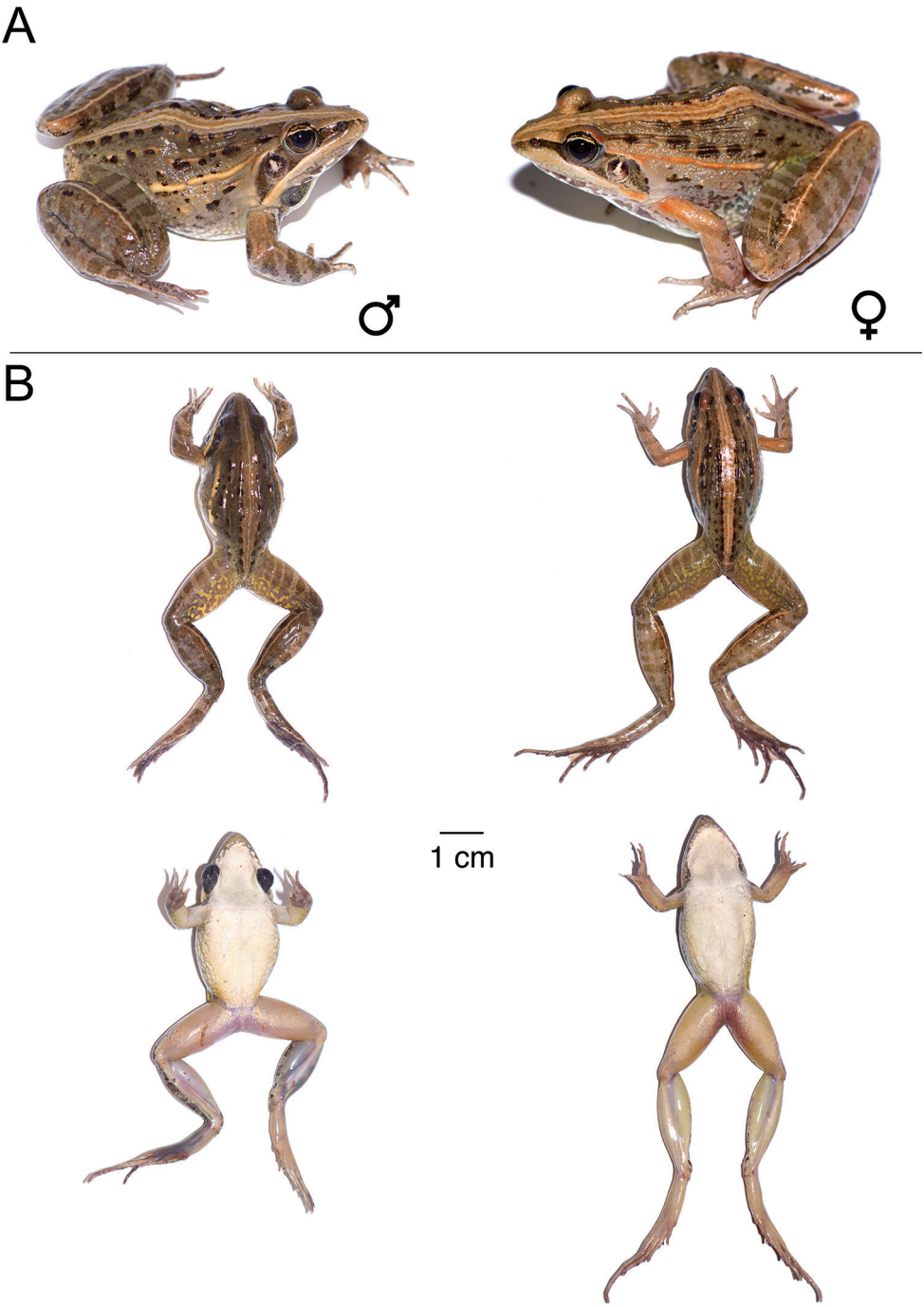

Figure 19. *Ptychadena delphina* sp. nov. **A** live male holotype (SB310; left) and female paratype (SB341, right) **B** dorsal and ventral views of the same individuals (male left, female right) after euthanasia and before fixation.

grey-brown vertebral stripe, doubled with a thin, clearer stripe from the tip of the snout to the vent. Dark brown canthal stripe from the tip of the snout to the back of the jaw. Light vertical blotch on the otherwise brown tympanum. Upper and lower lip cream to light brown with irregular brown markings. Iris dark brown on the lower two thirds, light golden brown above, separated by a cream horizontal stripe.

A few irregular dark brown blotches on the light grey flanks. Throat and ventrum cream with a few small light grey dots under the chin. Two small symmetrical dark brown blotches on the antero-ventral side of the shoulders. Thin light longitudinal stripe on the tibias and lower half of the thighs. Hind limbs brown with dark bars over the thighs, tibias, and feet. A few small round white dots around the groin. Back of the thighs dark brown irregularly molted with yellow. Vocal sacs uniformly dark grey.

Coloration of the holotype in preservative. Dorsal ground color dark brown with a few small, oval dark brown blotches symmetrically distributed on the dorsolateral ridges. Wide lighter brown vertebral stripe, doubled with a thin, clearer line from the tip of the snout to the vent. Dark brown canthal stripe from the tip of the snout to the back of the jaw. Light vertical stripe on the otherwise brown tympanum. Upper lip grey on the anterior half and cream on posterior half. Lower lip grey with irregular cream spots. Flanks brown with a few irregular small dark brown blotches. Throat, ventrum, ventral side of the thighs and tibias uniformly cream with the throat and chest lightly dusted with grey. Two symmetrical dark brown blotches on the ventral side of the shoulders. Thin, light longitudinal stripe on the tibias. Faint brown bars on the thighs. Back of thighs molted light grey and brown. Vocal sacs dark grey. Nuptial pads cream.

Variations. In life, background color varies from light to dark brown. Dorsal ridges vary in number and definition. Median ridges may be continuous from eye level to the groin, or interrupted and be present only along half the back. Postpalpebral fold interrupted in the middle of the back, sometimes continuing on the lower back. Short laterodorsal fold almost always present. Lateral ridges generally non-interrupted until the lower third of the back and from orange to cream. All specimens examined had small dark brown or black blotches distributed symmetrically on the dorsal ridges. Inguinal area more or less conspicuously yellow. Vertebral stripe may be thin or wide, generally around a lighter thin stripe. Tympanum blotch may be more or less conspicuous depending on the individual.

The thin cream longitudinal stripe on the tibia may be extended to the thigh or half of the thigh and the foot in some individuals. Tibias, thighs, and feet posteriorly barred with more or less defined brown or light brown markings. Thighs posteriorly marbled with light to dark brown and yellow. Ventrum and throat uniformly white to light yellow. Vocal sacs grey to dark grey or bicolored cream and grey. Small warts over the back and flanks in ca. 20% of adult males.

Etymology. The specific name originates from the Latin *delphinus*, dolphin, in reference to the advertisement call of the species resembling a dolphin's clicking sound. We have Latinized *delphinus* into the adjective *delphina* to be in accordance with the gender of genus *Ptychadena*. The advertisement call best distinguishes *P. delphina* sp. nov. from *P. doro* sp. nov.

Habitat, distribution, and natural history. The distribution range of *Ptychadena delphina* sp. nov. is mostly restricted to mid-elevation forests (1612 to 2064 m a.s.l.), west of the GRV and north of the Geba River (tributary of the Baro River). However, two individuals (XF13–283 and XF13–285) collected in 2013 by X. Freilich and S. Boissinot in Asgori, between Addis Ababa and Ambo (8.9799°N, 38.0241°E, 2370 m a.s.l.) clustered with *Ptychadena delphina* in phylogenetic analyses based on four molecular markers (Freilich et al. 2016). If the molecular results are not caused by introgression between *P. delphina* sp. nov. and *P. beka* sp. nov, which occurs in the area, and if these two individuals represent a real population, this is the easternmost and highest known population of *P. delphina* sp. nov. The habitat at this locality is also quite different from the rest of *P. delphina* sp. nov. distribution range, as it is composed of open agricultural fields and not forest. No other individual of the species was collected in the multiple sampling campaigns subsequently conducted, and this population remains to be confirmed. Beside these two individuals, the easternmost populations have been found south of Bedele, while, in the west, Individuals have been collected by Uka, west of Gore. The southernmost individuals were found in Bichano, just north of the Geba River.

Males of *P. delphina* sp. nov. call at night in flooded grassland ponds or puddles, or in rainwater-filled holes on the road. Within the genus, *P. delphina* sp. nov. is found in sympatry with *P. beka* sp. nov., *P. doro* sp. nov., and *P. neumanni*. Males of *P. delphina* sp. nov. have been found calling jointly with *P. doro* sp. nov.

Advertisement call. To the human ear, the call of *Ptychadena delphina* sp. nov. (4 males, 33 calls) resembles a dolphin's series of clicks. It is composed of a single note of 504 ± 92 ms in duration, containing 8.4 ± 1.4 pulses, which are clearly distinct and at regular intervals. Amplitude increases regularly within the note until 384 ± 129 ms, where it decreases. As in other Ethiopian *Ptychadena* species, call repetition rate is highly variable and dependent of the social context. Call dominant frequency is 2327 ± 147 Hz, with a gradual increase in dominant frequency within the call.

The call of *Ptychadena delphina* sp. nov. is easily distinguishable from the calls of all other *Ptychadena* from the Ethiopian highland by its well defined and regularly spaced pulses, except for the call of *P. robeensis*, which presents a similar structure. The call *P. robeensis* can however be distinguished by its higher dominant frequency (2876 ± 74 Hz), related to the species' smaller body size. It is worth noting that the call of the closely related syntopic species *P. doro* sp. nov. is remarkably different both in temporal and spectral features, while the two species are morphologically extremely similar. The two species were thus named after their respective calls, which constitute their most distinguishable traits.

***Ptychadena doro* sp. nov.**
http://zoobank.org/CA0740EE-5B73-479B-8202-E61F1C29788A

Type material. ***Holotype.*** An adult male (SB328) collected on 8 June 2018 by S. Goutte and J. Reyes-Velasco between Dembi and Gechi, Oromia, Ethiopia (8.2195°N,

36.446°E, 2064 m a.s.l.). ***Paratypes.*** 14 males: one male (15–260) collected on 15 August 2015 by X. Freilich, J. Reyes-Velasco and S. Boissinot south of Gech'a (7.4213°N, 35.3993°E, 2316 m a.s.l.), two males (16–198, 16–200) collected on 17 July 2016 by J. Reyes-Velasco and S. Boissinot northwest of Jimma (7.7307°N, 36.6926°E, 2218 m a.s.l.), two females (16–344, 16–350) and 3 males (16–352, 16–353, 16–361) collected on 21 July 2016 by J. Reyes-Velasco and S. Boissinot south of Gech'a (7.4212°N–7.4393°N, 35.3992–35.4047°E, 2240–2304 m a.s.l.), one male (SB247) collected on 24 April 2018 by S. Goutte and J. Reyes-Velasco west of Jimma (7.5449°N, 36.582°E, 2272 m a.s.l.), two females (SB298, SB309) and 3 males (SB299, SB311, SB312) collected on 7 June 2018 by S. Goutte and J. Reyes-Velasco between Dembi and Gechi (8.2195–8.2524°N, 36.446–36.4465°E, 2064–2198 m a.s.l.), one female (SB327) collected on 8 June 2018 by S. Goutte and J. Reyes-Velasco between Dembi and Gechi (8.2195°N, 36.446°E, 2064 m a.s.l.), one female (SB346) collected on 9 June 2018 by S. Goutte and J. Reyes-Velasco west of Gore (8.1645°N, 35.3819°E, 1654 m a.s.l.), one male (SB386) collected on 11 June 2018 by S. Goutte and J. Reyes-Velasco south of Gech'a (7.5544°N, 35.4148°E, 1936 m a.s.l.), one male (SB408) collected on 13 June 2018 by S. Goutte and J. Reyes-Velasco south of Gech'a (7.5532°N, 35.4158°E, 1940 m a.s.l.). All specimens are deposited at ZNHM.

Diagnosis. Moderately large (male (13) SVL 35.8 ± 2.2 mm, female (6) SVL 42.4 ± 5.7 mm) member of the *neumanni* species group (Fig. 20) distinguished by the following combination of characters: (1) long hind limbs (male TL/SVL 0.58 ± 0.03, female TL/SVL 0.64 ± 0.11), (2) long hands (male HAL/SVL 0.24 ± 0.02, female HAL/SVL 0.25 ± 0.05), (3) long snout (male SL/SVL 0.16 ± 0.01, female SL/SVL 0.16 ± 0.02), (4) relatively small tympanum (male TD/ED 0.64 ± 0.09, female TD/ED 0.63 ± 0.1), (5) light vertical stripe on the tympanum, (6) vocal sacs are grey or dark grey posteriorly and lighter anteriorly,

Comparison. *Ptychadena doro* sp. nov. can be distinguished from all medium sized Ethiopian *Ptychadena* by its long feet and smaller tympanum. It can be further distinguished from *P. beka* sp. nov. by a narrower head and longer tibias. Snout is longer, inter-nares distance is greater and hands are longer than in *P. erlangeri* and *P. levenorum*. It can be distinguished from *P. amharensis* and *P. levenorum* by its larger inter-orbital distance. *Ptychadena doro* sp. nov. can be distinguished from *P. delphina* sp. nov. by a smaller body, a narrower head and shorter inter-orbital distance.

Description of the holotype. A medium-sized (SVL 36.4 mm) adult male with long hind limbs (TL/SVL 0.58; Fig. 20, Suppl. material 3: Table S1). Head as long as wide. Snout projecting beyond the lower jaw. Interorbital distance 0.60 × the eye diameter. Internarial distance 1.08 × interorbital distance. Tympanum 0.63 × eye diameter. Finger tips not expanded but rounded, with very small subarticular tubercles. Finger formula: I<II<IV<III. Hand free of webbing, palmar tubercle absent. Nuptial pads light grey to cream, extending dorsally to the second finger. Hindlimbs elongated, with tibia length 0.57 × snout-vent length. Foot longer than thigh and slightly longer than tibia (FL/THL 1.20, FL/TL 1.01). Toe tips rounded. Subarticular tubercles extremely

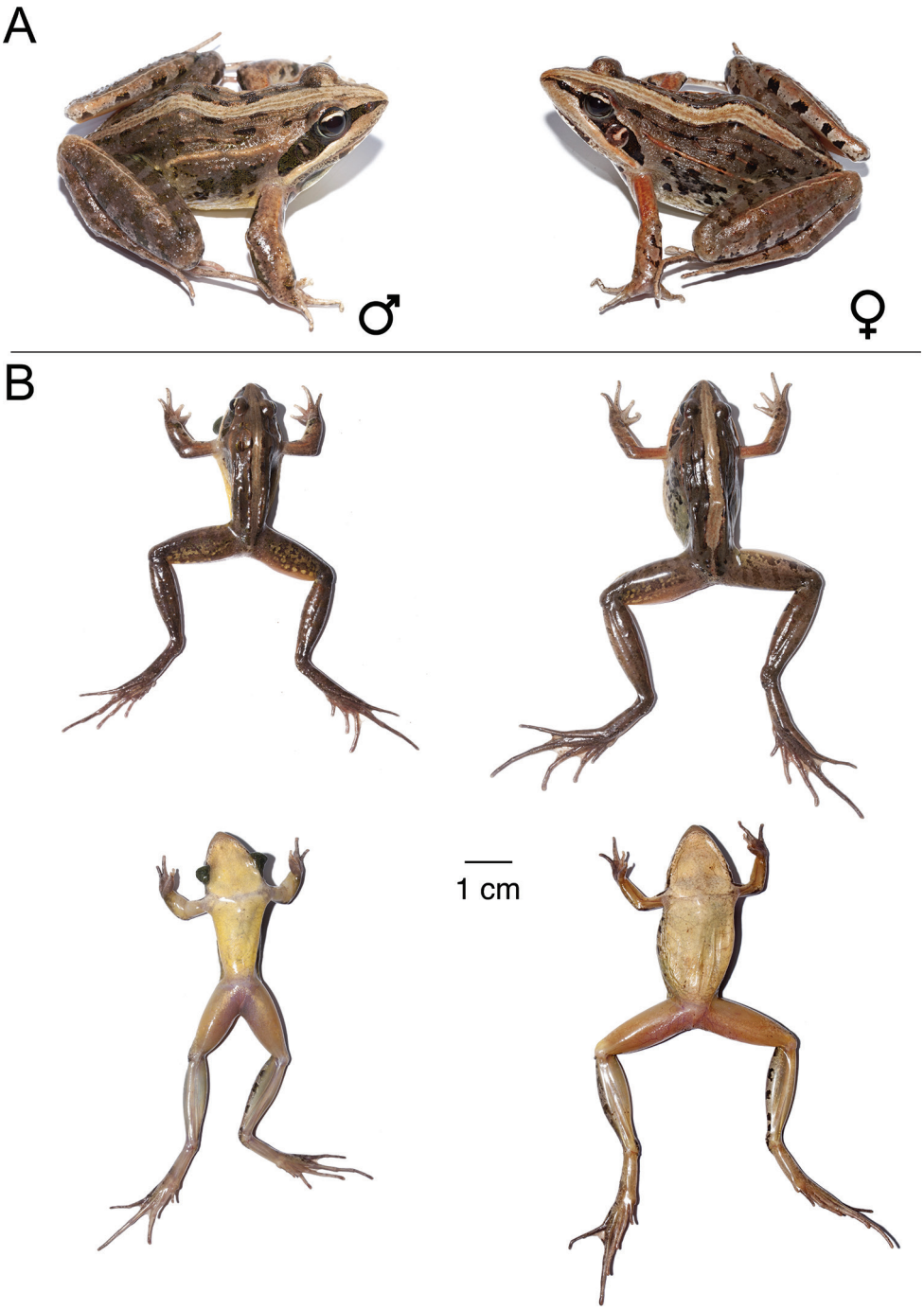

Figure 20. *Ptychadena doro* sp. nov. **A** live male holotype (SB328; left) and female paratype (SB327, right) **B** dorsal and ventral views of the same individuals (male left, female right) after euthanasia and before fixation.

small. Inner metatarsal tubercle present, external absent. Toe formula: I<II<V<III<IV. Foot webbing formula: Ie(1), IIi/e(1–1), IIIi/e(1–2), IVi/e(2–2), Vi(2). Two light brown, continuous lateral ridges, two continuous and four interrupted dorsal ridges. No vertebral nor sacral ridges. Very small, translucent warts on the body and small round warts on tibias and feet. Tongue free for half of its length, bifurcated at the end. Vomerine, maxillary and premaxillary teeth present.

Coloration of the holotype in life. Dorsal ground color brown with a few elongated dark brown blotches symmetrically distributed on the dorsolateral ridges. Wide light grey-brown vertebral stripe, doubled with a thin, clearer stripe from the tip of the snout to the vent. Dark olive brown canthal stripe from the tip of the snout to the back of the jaw. Light vertical stripe on the otherwise brown tympanum. Upper and lower lip cream to light brown with irregular brown markings.

Iris bicolored, with upper third light silver-grey, and the lower two thirds dark brown. Irregular dark olive brown blotches fused into a large undefined mark on the flanks. Throat, ventrum, ventral side of the thighs and tibias uniformly light yellow. Two small symmetrical dark brown blotches on the antero-ventral side of the shoulders. Thin, barely visible, light longitudinal stripe on the tibias. Few white round warts on the tibias. Hind limbs brown with dark olive bars over the thighs, tibias, and feet. A few very small round white dots around the groin. Back of the thighs dark brown irregularly molted with yellow. Vocal sacs uniformly dark grey.

Coloration of the holotype in preservative. Dorsal ground color grey with a few oval dark brown blotches symmetrically distributed on the dorsolateral ridges. Wide lighter brown vertebral stripe from the tip of the snout to the vent. Dark brown canthal stripe from the tip of the snout to the back of the jaw. Faint vertical stripe on the otherwise brown tympanum. Upper lip and lower lips cream heavily blotched with grey. Flanks brown with a few irregular small dark brown blotches. Throat, ventrum, ventral side of the thighs and tibias uniformly cream. Two symmetrical grey blotches on the ventral side of the shoulders. Faint, thin longitudinal stripe on the tibias. No distinct bars on the thighs or tibias. A few small round white spots forming a line on the posterior side of tibias. Back of thighs molted yellowish cream and brown. Vocal sacs dark grey. Nuptial pads light grey.

Variations. In life, background color varies from yellowish brown to dark brown. Dorsal ridges vary in number and definition. In all examined specimens, median ridges were continuous from eye level to the groin. Postpalpebral fold usually interrupted in the middle of the back, sometimes continuing on the lower back by a ridge or multiple aligned warts. Short laterodorsal fold almost always present, sometimes fractioned. Lateral ridges generally briefly interrupted once or twice and from orange to cream. All specimens examined had small dark brown or black blotches distributed symmetrically on the dorsal ridges. Inguinal area yellowish in some individuals. Most individuals have a wide, generally around a lighter thin stripe, some individuals have a thin vertebral stripe only. All examined specimens had a very conspicuous cream blotch on the tympanum.

The thin cream longitudinal stripe on the tibia may be more or less conspicuous and extended to the thigh or half of the thigh and the foot in some individuals. Tibias, thighs,

and feet posteriorly barred with more or less defined brown or light brown markings. Yellow and brown marbling on the posterior side of the thighs almost absent in some individuals. Ventrum and throat uniformly light yellow, sometimes very lightly dusted with light grey on the throat. Vocal sacs grey, bicolored cream and grey in some individuals, and rarely light grey. Small warts over the back and flanks in ca. 50% of adult males.

Etymology. The species name is the Amharic translation of chicken (ዶሮ), in reference to the advertisement call of the species resembling a chicken's song. The advertisement call distinguishes best *Ptychadena doro* sp. nov. from the syntopic species *P. delphina* sp. nov.

Habitat, distribution, and natural history. The distribution range of *Ptychadena doro* sp. nov. is restricted to mid-elevations (1654 to 2318 m a.s.l.), west of the GRV. The easternmost populations have been found around Jimma and south of Bedele. Individuals have been collected west of Metu and between Metu and Tippi. Males of *P. doro* sp. nov. call at night in flooded grassland ponds or puddles, or in rainwater-filled holes on the road. Within the genus *Ptychadena*, *P. doro* sp. nov. is found in sympatry with *P. beka* sp. nov., *P. delphina* sp. nov. and *P. neumanni*. Males of *P. doro* sp. nov. have been found calling jointly with males of *P. delphina* sp. nov.

Advertisement call. The call of *Ptychadena doro* sp. nov. (3 males, 21 calls) is reminiscent of a chicken call. It is composed of a single, pulsed note of 411 ± 41 ms in duration. Pulses are partly fused without any silent intervals between them. Amplitude increases during most of the note (peak amplitude at 295 ± 39 ms) and decreases abruptly at the end of the note. As in other Ethiopian *Ptychadena* species, call repetition rate is highly variable and dependent of the social context. Call dominant frequency is 1966 ± 105 Hz, with a gradual increase in frequency within the note. Frequency bandwidth is remarkably narrower than that of the calls of the other species of the *P. neumanni* complex (415 ± 31 Hz), resulting in a more tonal sound. The call of *P. doro* sp. nov. is easily distinguishable from the call of all other species of the *P. neumanni* complex by its single note, tonal call composed of indistinct pulses.

Ptychadena goweri Smith, Noonan & Colston, 2017

Type material. ***Holotype.*** An adult male (TJC224) collected on 10 December 2012 by T. J. Colston in Katcha, Bale National Park, Ethiopia (6.71779°N, 39.72572°E, 2375 m a.s.l.). ***Paratypes.*** Three juveniles (XF781, XF782, XF783) collected 7 August 2011 by X. Freilich and S. Boissinot north of Hagere Mariam, Oromia, Ethiopia (5.8027°N, 38.2705°E, 2323 m a.s.l.). All type specimens and examined material are deposited at ZNHM.

Material examined. In addition to the holotype, we examined one male (TJC218) collected by T. J. Colston , one female (15–85) and two males (15–103, 15–105) collected on 7 August 2015 by X. Freilich, J. Reyes-Velasco and S. Boissinot in the Harenna forest (6.5866°N, 39.7417°E, 1778 m a.s.l.), one male (15–121) collected on 7 August 2015 by X. Freilich, J. Reyes-Velasco and S. Boissinot in the Harenna forest

(6.6634°N, 39.7302°E, 2002 m a.s.l.), one female (15–425) and two males (15–426, 15–427) collected on 27 September 2015 by X. Freilich, J. Reyes-Velasco and S. Boissinot northwest of Kibre Mengist (5.9055–6.04546°N, 38.837–38.9334°E, 1745–2238 m a.s.l.), two males (15–448, 15–449) collected on 28 September 2015 by X. Freilich, J. Reyes-Velasco and S. Boissinot in Harenna forest (6.71925 N, 39.7202 E), two males (SB99 and SB100) collected on 10 April 2018 by S. Goutte and J. Reyes-Velasco in the Harenna forest (6.6634°N, 39.7302°E, 2440 m a.s.l.), two females (SB158, SB159) and two males (SB160, SB161) collected on 17 April 2018 by S. Goutte and J. Reyes-Velasco northwest of Kibre Mengist (6.0093°N, 38.8576°E, 2105 m a.s.l.), one female (SB807) collected on 7 May 2019 by S. Goutte in the Harenna forest (6.6640°N, 39.7301°E, 1992 m a.s.l.), one female (SB808) collected on 10 May 2019 by S. Goutte in the Harenna forest (6.7164°N, 39.7257°E, 2375 m a.s.l.).

Diagnosis. Large species (male (15) SVL 42.4 ± 2.7 mm, female (6) SVL 51.2 ± 4.2 mm) from the *neumanni* species group (Fig. 21) distinguished by the following combination of characters: (1) long hind limbs (male TL/SVL 0.60 ± 0.05, female TL/SVL 0.59 ± 0.02) , (2) long feet (male FL/SVL 0.61 ± 0.05, female FL/SVL 0.58 ± 0.02), (3) long hands (male HAL/SVL 0.24 ± 0.03, female HAL/SVL 0.23 ± 0.01), (4) long head (male HL/SVL 0.38 ± 0.04, female HL/SVL 0.36 ± 0.04), (5) long snout (male SL/SVL 0.16 ± 0.02, female SL/SVL 0.15 ± 0.01), (6) vocal sacs light grey, cream or yellow, sometimes mottled with light grey, (7) male skin smooth.

Comparison. Except for *P. cooperi*, the largest species of the *Ptychadena neumanni* complex. Body size alone distinguishes *Ptychadena goweri* from *P. nana*, *P. robeensis* sp. nov., *P. levenorum*, *P. erlangeri*, and *P. doro* sp. nov. Compared to the larger *Ptychadena* species of Ethiopian highlands, it has longer thigh, tibia, feet, hands, head, snout, and inter-orbital distance than *P. delphina* sp. nov., *P. beka* sp. nov., and *P. amharensis*. The light-colored vocal sacs of adult males distinguish *P. goweri* from *P. beka* sp. nov., *P. delphina* sp. nov., and *P. neumanni* and *P. cooperi*. The almost complete dorsal ridges distinguish further *P. goweri* from *P. cooperi*, which presents rows of short glandular folds on the dorsum.

Description of the holotype. Relatively large (SVL 41.9 mm) male (Fig. 22) with long hind limbs (TL/SVL 0.58, Suppl. material 3: Table S3). Head as long as wide. Snout projecting beyond the lower jaw. Interorbital distance almost equal to the eye diameter. Internarial distance 0.88 × interorbital distance. Tympanum 0.85 × eye diameter. Finger tips not expanded but rounded, with moderate subarticular tubercles. Finger formula: I<II<IV<III. Hand free of webbing. Hindlimbs elongated, with tibia length 0.58 × snout-vent length. Foot slightly longer than thigh and tibia (FL/THL 1.14, FL/TL 1.05). Toe tips rounded. Subarticular tubercles small and round. Inner metatarsal tubercle present, external absent. Toe formula: I<II<V<III<IV. Foot webbing formula: Ie(1), IIi/e(1–1.5), IIIi/e(1.5–2), IVi/e(2–2), Vi(2). Two continuous lateral ridges, brown anteriorly and light brown posteriorly, barely visible, six interrupted dorsal ridges. No vertebral, nor sacral ridges. No wart on body or limbs. Tongue free for less than a third of its length, divided in two lobes. Vomerine, maxillary and premaxillary teeth present.

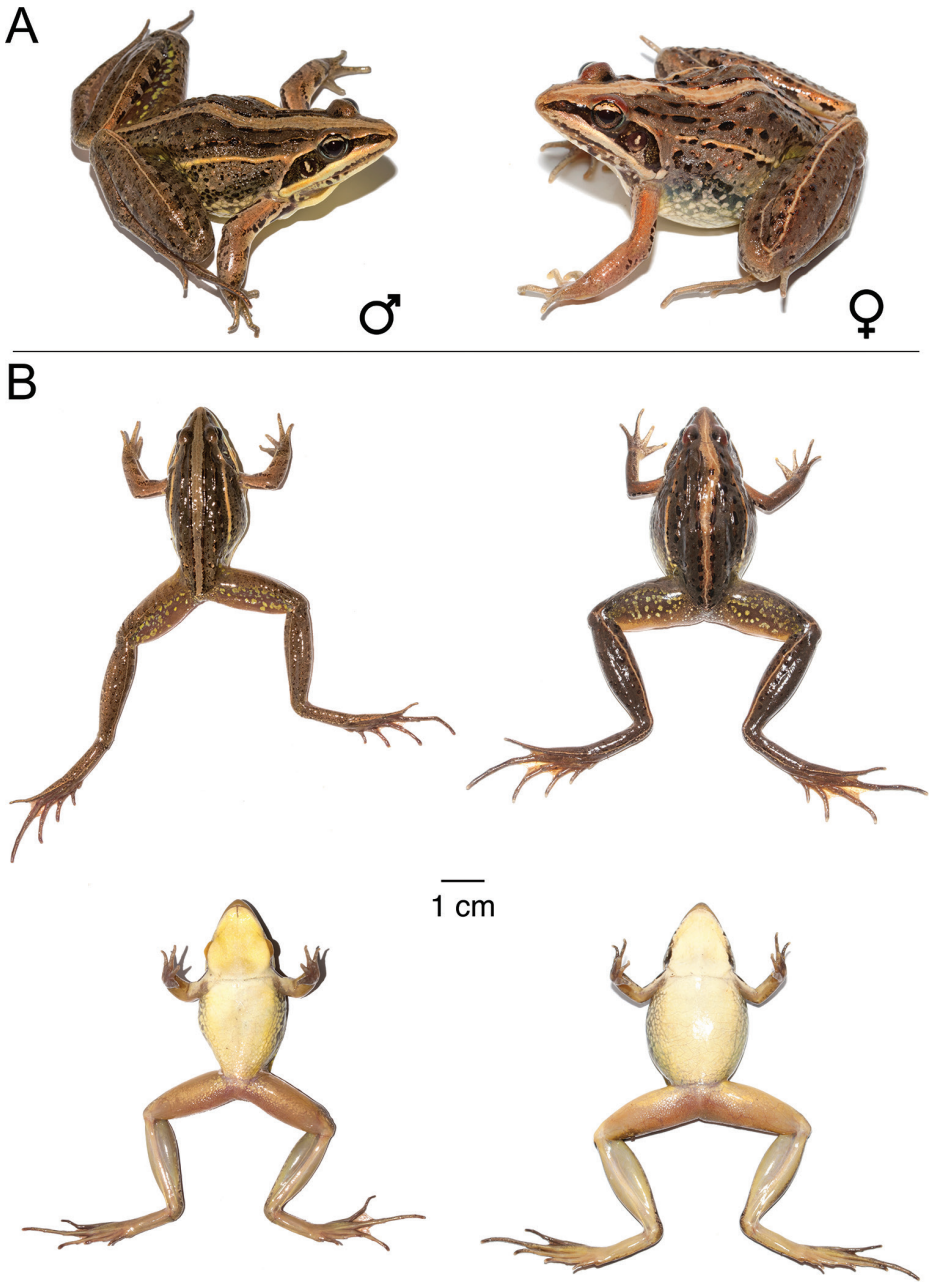

Figure 21. *Ptychadena goweri* **A** Live male (SB99; left) and female (SB5807, right) **B** dorsal and ventral views of the same individuals (male left, female right) after euthanasia and before fixation.

Coloration of the holotype in preservative. Dorsal ground color brown with a few small, irregular oval dark brown blotches symmetrically distributed on the dorsolateral ridges. Wide light brown vertebral stripe, doubled with a thin, clearer stripe

Figure 22. Holotype of *Ptychadena goweri*. Dorsal and ventral views of the male holotype (TJC224).

from the tip of the snout to the vent. Dark brown canthal stripe from the tip of the snout to the back of the jaw. Light vertical stripe on the otherwise brown tympanum. Upper and lower lip brown with irregular dark brown molting. Flanks grey anteriorly to light brown posteriorly with irregular dark brown blotches on the anterior half. Throat, ventrum, ventral side of the thighs and tibias uniformly cream with very light grey dusting on the throat. Two symmetrical dark brown blotches on the ventral side of the shoulders. Thin, barely visible, light longitudinal stripe on the tibias. Irregular and undefined brown markings on the thighs, tibias, and feet. Back of thighs molted light grey and brown. Vocal sacs mostly white, with slight grey dusting posteriorly.

Variations. In life, background coloration varies from light brown, olive grey to dark brown. The vertebral stripe may be thin or wide doubled with a thin lighter stripe within it, and from cream to grey and light yellowish brown. The dark brown to black blotches on the dorsum vary in size and number but are always organized along the dorsal ridges. Some individuals present small, irregular black markings in between ridges. Dark markings on the flanks are quite variable between individuals, from a few large dark blotches to a multitude of smaller ones, covering mostly the antero-dorsal part of the flank. Dorsolateral ridges can be discontinued once or twice and can be cream, yellow, or brown-orange. Some individuals present a reddish-brown marking on top of the eyelid.

Iris bicolored, with upper third silver to golden and lower two thirds dark golden to dark brown. Cream or golden vertical blotch on the dark brown tympanum always present. The thin stripe on the tibia may extend on the thigh in some individuals. Forearms, thighs, tibias and feet are more or less clearly marked with dark brown bars. Vocal sacs always light in color (yellow, cream, or light grey), more or less dusted with grey on their dorsoposterior sides. Dorsal ridges may be more or less discontinuous.

Habitat, distribution, and natural history. The distribution range of *Ptychadena goweri* is restricted to the southeast of the GRV, at elevation ranging from 1745 m to 2550 m a.s.l. The species is found in clearings in the Harenna forest, south of the Sanetti plateau, from Kibre Mengist to Irba Muda, and north of Hagere Mariam (5.8027–6.7193°N, 28.2705°E). Males are found calling at night in shallow puddles in clearings or grassy meadows. Within the genus, *Ptychadena goweri* is found in sympatry with *P. harenna*, *P. levenorum*, *P. neumanni*, and *P. erlangeri.*

Advertisement call. The call of *Ptychadena goweri* (4 males, 32 calls) is composed of a single pulsed note of 634 ± 74 ms in duration, containing 33.5 ± 2.9 pulses. Pulses are grouped by 3.3 ± 1.5 pulses within each note and increase in amplitude up to 404 ± 65 ms, after what the amplitude decreases. Within pulses groups, the first pulse has the lowest, while the second pulse has generally the greatest amplitude. Call repetition rate is highly variable and dependent on the social context. The individuals we recorded produced calls in "bursts", where several males were forming a short chorus, spaced by long silent intervals. Call dominant frequency is 2318 ± 86 Hz with a slight increase in frequency within notes.

Within the *P. neumanni* complex, the call of *P. goweri* can be distinguished from those of *P. cooperi*, *P. amharensis*, *P. doro* sp. nov., and *P. neumanni* (type A and B) by the distinguishable pulses composing the calls. Grouped pulses and short inter-pulses intervals (9 ± 2 ms within pulse groups) distinguish the call of *P. goweri* from those of *P. robeensis* sp. nov. and *P. delphina* sp. nov. The call of *P. goweri* can be further distinguished from those of *P. nana* and *P. erlangeri* by a longer duration.

Ptychadena neumanni **(Ahl, 1924)**

Rana neumanni Ahl, 1924: 4.
Ptychadena neumanni – Perret 1980: 157.
Rana (*Ptychadena*) *neumanni* – Dubois 1981: 233.
Ptychadena (*Ptychadena*) *neumanni* – Dubois 1992: 316.

Lectotype by present designation. One adult male (ZMB26879–1) collected on 2 February 1901 by Oscar Neumann in Gadat (Gofa), south Ethiopia. [Coordinates estimated by Largen (2001): 6.33°N, 36.83°E, 2000 m a.s.l., but see remarks below]. ***Paralectotypes.*** Two adult males (ZMB–57183 = ZMB26879–2 and ZMB–57184 = ZMB26879–3) collected by Oscar Neumann on the same date and location as the lectotype (ZMB26879–1).

Material examined. Except for the type series, all examined specimens are deposited at ZNHM. In addition to the type series, we examined one male (15–173) collected by X. Freilich, J. Reyes-Velasco and S. Boissinot on 9 August 2015 in Wondo Genet (7.0833°N, 38.6381°E, 1896 m a.s.l.), one female (15–181) and four males (15–183, 15–191, 15–208, 15–209) collected by X. Freilich, J. Reyes-Velasco and S. Boissinot on 12 August 2015 northwest of Bonga (7.3076°N, 36.1226°E, 1861 m a.s.l.), one female (16–203) collected on 18 July 2016 by J. Reyes-Velasco and S. Boissinot southwest of Bonga (7.2542°N, 36.2628°E, 1963 m a.s.l.), one female (16–302) and two males (16–303, 16–305) collected on 19 July 2016 by J. Reyes-Velasco and S. Boissinot north of Maji (6.2365°N, 35.5712°E, 1936 m a.s.l.), one female (16–326) and one male (16–313) collected on 20 July 2016 by J. Reyes-Velasco and S. Boissinot northeast of Machi (6.3780°N, 35.6659°E, 2063 m a.s.l.), two males (16–327, 16–329) collected on 20 July 2016 by J. Reyes-Velasco and S. Boissinot northeast of Mizan Teferi (7.0203°N,

35.7545°E, 2449 m a.s.l.), two females (SB333, SB334) collected on 9 June 2018 by S. Goutte and J. Reyes-Velasco northwest of Gore (8.2014°N, 35.3772°E, 1666 m a.s.l.), one male (SB388) collected on 11 June 2018 by S. Goutte and J. Reyes-Velasco south of Gech'a (7.5544°N, 35.4148°E, 1936 m a.s.l.), one female (SB405) collected on 13 June 2018 by S. Goutte and J. Reyes-Velasco south of Gech'a (7.5185°N, 35.4163°E, 1917 m a.s.l.), one female (SB462) collected on 20 June 2018 by S. Goutte and J. Reyes-Velasco northeast of Shebe (7.5423°N, 36.5732°E, 2240 m a.s.l.).

Diagnosis. Medium-sized species (male (20) SVL 35.7 ± 2 mm, female (8) SVL 45.6 ± 1.4 mm) of the *neumanni* species group (Fig. 23) distinguished by the following combination of characters: (1) long hind limbs (male TL/SVL 0.58 ± 0.02, female TL/SVL 0.57 ± 0.01), (2) vertical cream bar on the tympanum, (3) vocal sacs uniformly dark grey.

Comparison. Smaller than *P. cooperi* and *P. goweri* and larger than *P. nana* and *P. robeensis* sp. nov. Head wider than *P. erlangeri* and *P. levenorum* but narrower than *P. beka* sp. nov., Head and snout longer than *P. erlangeri* and *P. levenorum*. Wider inter-orbital distance than *P. doro* sp. nov., *P. beka* sp. nov., *P. erlangeri*, *P. levenorum*, and *P. amharensis*. Wider inter-nares distance and longer eye-nostril distance than *P. erlangeri* and *P. levenorum*. Tympanum larger than *P. doro* sp. nov., *P. erlangeri*, and *P. levenorum*. Larger hands than *P. erlangeri* and *P. levenorum*. Longer thighs and feet than *P. erlangeri*, *P. levenorum*, *P. amharensis*, and *P. beka* sp. nov.

Description of the lectotype. The lectotype is very desiccated (Fig. 24A) and the description of some characters is hindered by the state of conservation of the specimen. Medium sized (SVL 32.2 mm), slender adult male. Snout pointed, projecting beyond the lower jaw. Interorbital distance 0.83 × eye diameter. Head longer than wide (HW/HL 0.80). Nostril half-way between the tip of the snout and the eye. Internarial distance 1.1 × interorbital distance. Tympanum 0.64 × eye diameter. Finger tips not expanded but rounded, with moderate subarticular tubercles. Finger formula: I<II<IV<III. Hand free of webbing. Hindlimbs elongated, with tibia length 0.57 × snout-vent length. Foot longer than thigh (FL/THL 1.1) and as long as tibia. Toe tips rounded. Subarticular tubercles small and round. Inner metatarsal tubercle present, external absent. Toe formula: I<II<III<V<IV. Foot webbing formula: Ie(1), IIi/e(1–2), IIIi/e(2–2), IVi/e(2–2), Vi(2). Two light, continuous lateral ridges, six dorsal ridges difficult to see due to preservation of the specimen. No vertebral nor sacral ridges. Small warts on the body. No sacral, femoral, or crural folds.

Coloration of the lectotype in preservative. Coloration has faded away with time and some patterns are now hardly distinguishable. Dorsal background color is brown, with irregular elongated dark brown blotches distributed along the dorsal ridges and on the antero-dorsal part of the flanks. A wide light vertebral line from snout to vent is present. Dark brown canthal stripe from the tip of the snout to the back of the jaw. Vocal sacs dark grey. Upper lip, throat, and posterior part of flanks cream. Ventrum, ventral side of the thighs and tibias uniformly cream in type 1. Barely distinguishable irregular dark brown bars on the tibias and on the thighs.

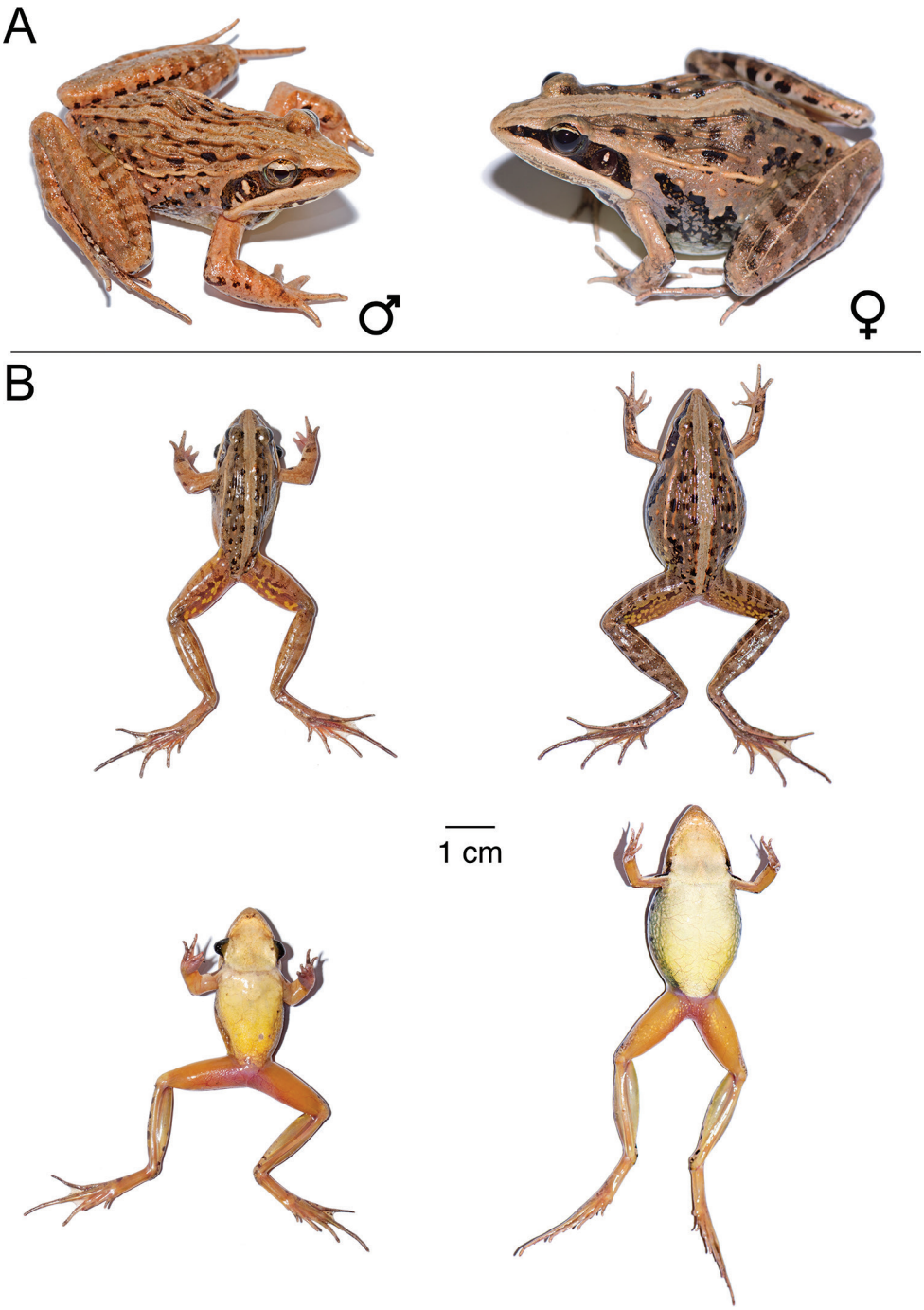

Figure 23. *Ptychadena neumanni* **A** Live male (SB393; left) and female (SB388, right) **B** dorsal and ventral views of a male (SB333, left) and a female (SB388, right) after euthanasia and before fixation.

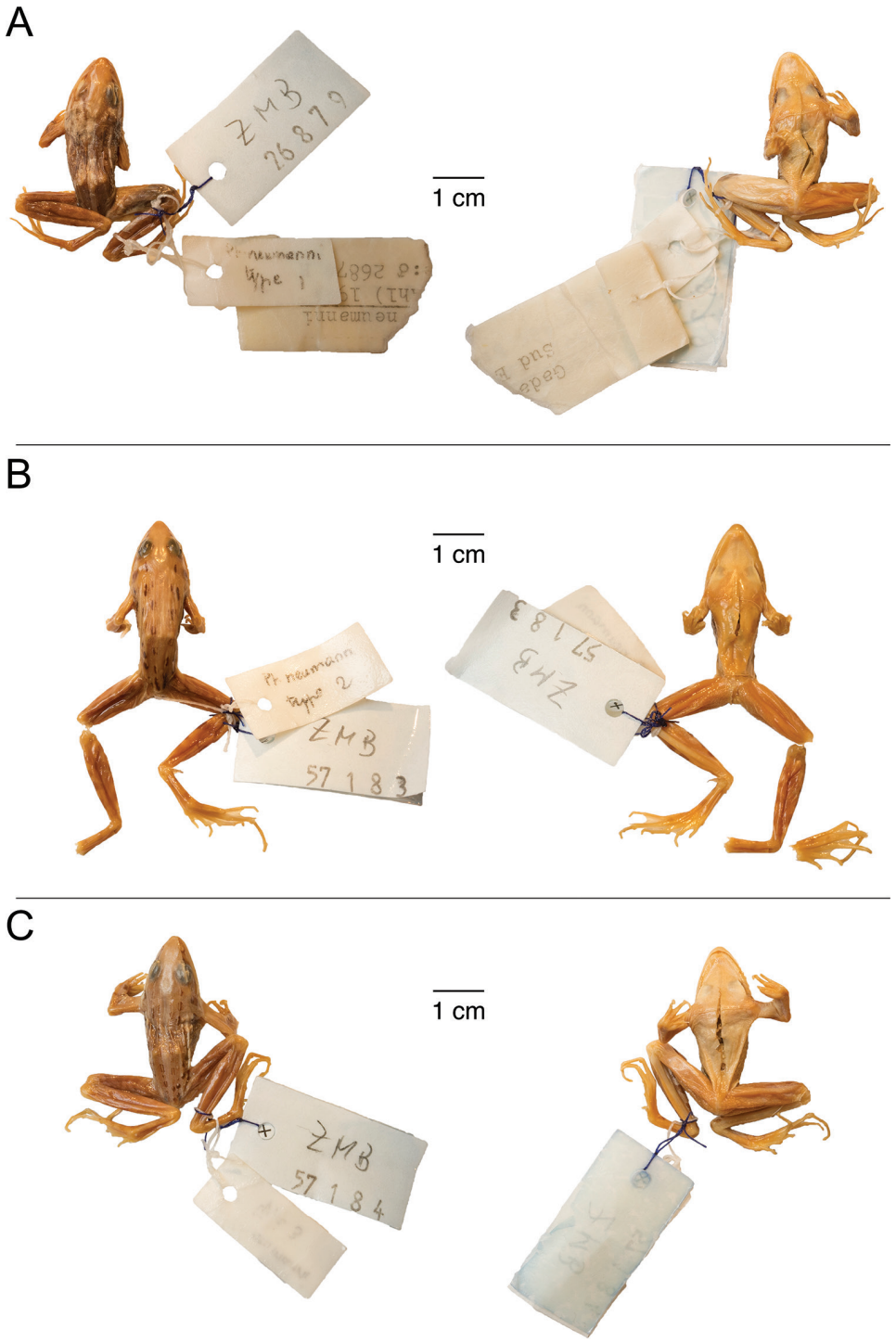

Figure 24. Type specimens of *Ptychadena neumanni*. Dorsal and ventral views of three male type specimens **A** ZMB26879–1, lectotype **B** ZMB–57183 = ZMB26879–2, paralectotype **C** ZMB–57184 = ZMB26879–3, paralectotype.

Variations. In life, background color varies from light to dark brown. Dorsal ridges vary in number and definition. Lateral ridges may be sand or dark orange. All specimens examined had small dark brown or black blotches distributed symmetrically on the dorsal ridges. Flanks more or less heavily colored with black or dark brown blotches. Vertebral stripe absent in some individuals. When present, the vertebral stripe may be thin or wide, sand-color or brown-orange.

Iris bicolored, the upper third silver and lower two thirds dark brown sometimes marbled with light yellow or copper on the bottom half. Upper jaw cream, lower jaws featuring irregular light grey or brown markings but no barring. All specimens examined featured a dark brown canthal stripe from the tip of the snout to the back of the upper jaw and a with a cream vertical stripe. A thin cream longitudinal stripe on the tibia present in some individuals. Tibias, thighs, and feet posteriorly barred with more or less defined brown or light brown markings. Some individuals have dark irregular markings on the posterior side of the arms and anteroventral sides of the thighs and tibias. Thighs posteriorly marbled with dark brown and yellowish brown. Ventrum and throat uniformly cream to yellow. Vocal sacs grey to dark grey. Small warts over the back and flanks in adult males.

Habitat, distribution, and natural history. *Ptychadena neumanni* is found on both sides of the Great Rift Valley (GRV) and limited to the south and southwestern highlands of Ethiopia (5.80–8.20°N, 35.36–38.64°E). This species is found at elevations ranging from 1409 m to 2449 m a.s.l. The southernmost individuals were found north of Hagere Mariam (east of the GRV) and Maji (west of the GRV). In the west, populations are found west of Gore, Gech'a, Bonga and Jimma. *Ptychadena neumanni* has also been found between Sodo and Bonga. East of the GRV it has been found in the vicinity of Wondo Genet. In the southwest, *P. neumanni* is found in syntopy with multiple *Ptychadena* species: *P. doro* sp. nov., *P. delphina* sp. nov., *P. beka* sp. nov., and the lowland species *P. anchietae*. In the southeast, it is found in sympatry with *P. goweri.* Males are found calling at night in shallow puddles on or beside the road, or in flooded grassy meadows.

Advertisement call. *Ptychadena neumanni* produces two types of call, hereafter referred to as call type A and call type B. Based on our video recordings and observations in the field, we believe that call type A corresponds to the advertisement call, while call type B may be a territorial call. Notably, while calling in chorus, males were producing call type A, whereas call type B seem to be employed in two-individuals vocal battles. However, our data are insufficient to categorize with confidence these two calls with regard to their respective function and we describe both call types below. The call type and call rate produced is highly dependent on the social context.

Ptychadena neumanni call type A (3 males, 78 calls) is 307 ± 149 ms long and contains 5.8 ± 2.4 pulsed notes. Notes are 32 ± 14 ms in duration and are produced at regular intervals (19.1 ± 3.5 notes s^{-1}) within each call. Amplitude modulation is very low within the call. Call type A's dominant frequency is 2406 ± 339 Hz, with no frequency modulation within notes or calls.

Ptychadena neumanni call type B (1 male, 13 calls) is composed of one initial long (437 ± 54 ms) pulsed note (note B1), followed by 3 ± 0.6 distinct pulses (note B2). The peak frequency of note B1 is 2207 ± 129 Hz while note B2 has a dominant frequency of 2337 ± 191 Hz.

Call type A of *P. neumanni* can be distinguished from those of all other species of the P. neumanni complex, except for *P. cooperi* and *P. amharensis*, by its composition of multiple pulsed notes with indistinguishable pulses. It differs from the call of *P. cooperi* and *P. amharensis* by the absence of frequency modulation, shorter notes, and shorter inter-note intervals.

Call type B of *P. neumanni* is unique within the *P. neumanni* complex in its composition of two different types of notes and can easily be distinguished from those of all other species of the group.

Remarks. Ahl (1924) described *Rana neumanni* based on 35 syntypes collected in Didda (one specimen), Somaliland (23 specimens), Gadat (Gofa) (three specimens), and Uba (eight specimens). Perret (1980) examined the type series, split the collection, and assigned the specimens to three distinct species. Perret designated the three specimens from Gadat (ZMB–26879 type 1, ZMB–26879 type 2 and ZMB–26879 type 3) as syntypes of *Ptychadena neumanni* (sensu stricto) as they were the only specimens with individual tags. Additionally, those specimens were the only ones of the original type series to have a collection date: 2 February 1901. Gadat (Gofa), south Ethiopia thus became Terra typica restricta of *Ptychadena neumanni*. Perret (1980) then revised the description of the species and gave measurement values for the three syntypes. When we examined the type series in the collection of the Museum of Berlin, we realized that the syntypes 2 and 3 had been attributed new collection numbers: ZMB–57183 (ZMB–26879 type 2) and ZMB–57184 (ZMB–26879 type 3) and the jar containing ZMB–26879 type 1 bears the label "*lectotypus*". To our knowledge, no designation of ZMB–26879 type 1 as lectotype for *P. neumanni* has been published. Given that the original description of the species by Ahl (1924) included 35 syntypes and that the restriction by Perret (1980) is not valid according to the Code as it does not designate an individual specimen, we hereby designate ZMB–26879 (type 1) as a lectotype according to Article 74 of the International Zoological Code of Nomenclature (ICZN 1999). The specimens ZMB–57183 (ZMB–26879 type 2) and ZMB–57184 (ZMB–26879 type 3) thus become paralectotypes.

Discussion

The recent efforts made towards a biological inventory of Ethiopia demonstrate how species diversity in the Ethiopian highlands is likely to be largely underestimated (e.g., Goutte et al. 2019; Koppetsch 2020; Kostin et al. 2020; Soultan et al. 2020) and taxonomic revision of multiple groups is urgently needed to truly appreciate the ecological importance of this region. Describing the diversity of groups such as the genus *Ptychadena* is, however, challenged by the morphological resemblance of the species. In this study, we combined morphometrics, bioacoustics, and genetics to untangle the diversity of *Ptychadena* in the highlands of Ethiopia. Our integrative analysis distinguished a total of 12 species in the *Ptychadena neumanni* complex, four of which are new to science.

As in any taxonomic work, an important step in resolving the nomenclatural issues of the *P. neumanni* complex was the comparison of the newer material with the type

series of the previously described species of the group. Although in the case of Ethiopian *Ptychadena* we were able to extract DNA from formalin-preserved type specimens and include those sequences in phylogenetic analyses (Reyes-Velasco et al. in review), this is not always possible. A careful morphological examination of all the material available thus often remains the only way to compare century-old specimens to more recently collected material and should not be overlooked.

As in other studies on African grass frogs of the genus *Ptychadena*, advertisement calls provided better discriminant characters than morphometry (e.g., Bwong et al. 2009; Dehling and Sinsch 2013). In the field, syntopic species may not be readily distinguishable morphologically (e.g., *P. delphina* sp. nov. and *P. doro* sp. nov.), however, their advertisement calls easily allow their identification. We therefore provide an acoustic key to the *Ptychadena* of Ethiopian highlands in the hope that it will be used by ecologists and conservationists as a cost-effective, non-invasive identification tool.

Information on species' distribution patterns is essential in designing relevant conservation measures. The split of several species (e.g., *P. nana*, *P. neumanni*, and *P. erlangeri*) often resulted in splitting their distribution ranges. Our results also revealed important differences in sizes of the distribution range among species of the *P. neumanni* complex. For example, *P. robeensis* sp. nov. occupies a very reduced area (20 × 20 km, Fig. 5B), while *P. erlangeri* occurs on both sides of the Great Rift Valley (Fig. 5A; Freilich et al. 2016). These distribution patterns thus call for conservation measures spread across the Ethiopian highlands rather than a focus on only a few hotspots.

Acknowledgements

We would like to thank the Ethiopian Wildlife Conservation Authority and the Ethiopian Biodiversity Institute for providing us with collecting and export permits for the samples. We are very grateful to Yann Bourgeois, Marcin Falis, Yejie Yun, and Paula Mora Rojas who helped with the acoustic recordings in the field. Fieldwork in Ethiopia would not have been possible if not for the invaluable assistance of Megersa Kelbessa, Itbarek, and Samuel Woldeyes of Rock Hewn Tours. This work could not have been possible without the assistance of many curators and collection managers from numerous institutions, including Bezawork Afework Bogale and M. Ketema, Natural History Collection, Addis Ababa University, Ethiopia; Jeff Streicher, The Natural History Museum, London; Andreas Schmitz, Museum d'Histoire Naturelle, Geneva; and Mark-Oliver Rödel and Frank Tillack, Museum für Naturkunde Berlin. We thank Yann Bourgeois and Sebastian Kirchhof who helped with measuring specimens and Marcin Falis and Kole Utzinger who helped with lab work. We are in debt with Marc Arnoux and Nizar Drou from the Genome Core Facility and the Bioinformatics group at NYUAD. Finally, we thank the subject editor and the two reviewers for their valuable comments which helped improving this manuscript. The NYUAD Sequencing Core is supported by NYUAD Research Institute grant G1205A to the NYUAD Center for Genomics and Systems Biology. This research was supported by New York University Abu Dhabi Research Funds AD180 (to SB).

References

Ahl E (1924) Über eine froschsammlung aus Nordost-Afrika und Arabien. Mitteilungen aus dem Zoologischen museum in Berlin 11: 1–12. https://doi.org/10.1002/mmnz.4830110102

Bwong BA, Chira R, Schick S, Veith M, Lötters S (2009) Diversity of Ridged Frogs (Ptychadenidae: *Ptychadena*) in the easternmost remnant of the Guineo-Congolian rain forest: an analysis using morphology, bioacoustics and molecular genetics. Salamandra 45: 129–146.

Dehling JM, Sinsch U (2013) Diversity of Ridged Frogs (Anura: Ptychadenidae: *Ptychadena* spp.) in wetlands of the upper Nile in Rwanda: Morphological, bioacoustic, and molecular evidence. Zoologischer Anzeiger – A Journal of Comparative Zoology 253: 143–157. https://doi.org/10.1016/j.jcz.2013.08.005

Dubois A (1981) Liste des genres et sous-genres nominaux de Ranoidea (Amphibiens Anoures) du monde, avec identification de leurs espèces types; consequences nomenclaturales. Monitore Zoologico Italiano. Nuova Serie, Supplemento. Firenze 15: 225–284. https://doi.org/10.1080/03749444.1981.10736637

Dubois A (1992) Notes on the classification of Ranidae (Amphibia, Anura). Bulletin Mensuel de la Société Linnéenne de Lyon 61: 305–352. https://doi.org/10.3406/linly.1992.11011

Freilich X, Tollis M, Boissinot S (2014) Hiding in the highlands: Evolution of a frog species complex of the genus *Ptychadena* in the Ethiopian highlands. Molecular Phylogenetics and Evolution 71: 157–169. https://doi.org/10.1016/j.ympev.2013.11.015

Freilich X, Anadón JD, Bukala J, Calderon O, Chakraborty R, Boissinot S, Calderon D, Kanellopoulos A, Knap E, Marinos P, Mudasir M, Pirpinas S, Rengifo R, Slovak J, Stauber A, Tirado E, Uquilas I, Velasquez M, Vera E, Wilga A, Evolutionary Genetics – Class of 2013 (2016) Comparative Phylogeography of Ethiopian anurans: impact of the Great Rift Valley and Pleistocene climate change. BMC Evolutionary Biology 16: e206. https://doi.org/10.1186/s12862-016-0774-1

Frost DR (2020) Amphibian species of the world: an online reference. Version 6.0. http://research.amnh.org/herpetology/amphibia/index.html [accessed 5 December 2020]

Goutte S, Reyes-Velasco J, Boissinot S (2019) A new species of puddle frog from an unexplored mountain in southwestern Ethiopia (Anura, Phrynobatrachidae, *Phrynobatrachus*). ZooKeys 824: 53–70. https://doi.org/10.3897/zookeys.824.31570

ICZN (1999) International code of zoological nomenclature. 4th ed. The International Trust for Zoological Nomenclature, London. https://www.iczn.org/the-code

Köhler J, Jansen M, Rodríguez A, Kok PJR, Toledo LF, Emmrich M, Glaw F, Haddad CFB, Rödel M-O, Vences M (2017) The use of bioacoustics in anuran taxonomy: theory, terminology, methods and recommendations for best practice. Zootaxa 4251: 1–124. https://doi.org/10.11646/zootaxa.4251.1.1

Koppetsch T (2020) A new species of *Trachylepis* (Squamata: Scincidae) from the Amhara Region, Ethiopia, and a key to the Ethiopian *Trachylepis*. Zootaxa 4859: 113–126. https://doi.org/10.11646/zootaxa.4859.1.4

Kostin DS, Martynov AA, Komarova VA, Alexandrov DY, Yihune M, Kasso M, Bryja J, Lavrenchenko LA (2020) Rodents of Choke Mountain and surrounding areas (Ethiopia): the Blue Nile gorge as a strong biogeographic barrier. Journal of Vertebrate Biology 69: 1–12. https://doi.org/10.25225/jvb.20016

Largen M, Spawls S (2010) Amphibians and Reptiles of Ethiopia and Eritrea. Edition Chimaira, Serpent's Tale NHBD, Frankfurt am Main, 687 pp.

Largen MJ (1975) The Status of the Genus *Kassina* (amphibia Anura Hyperoliidae) in Ethiopia. Monitore Zoologico Italiano, Supplemento 6: 1–28. https://doi.org/10.1080/03749444.1975.10736806

Largen MJ (1977) The Status of the Genus *Leptopelis* (amphibia Anura Hyperoliidae) in Ethiopia, Including Descriptions of Two New Species. Monitore Zoologico Italiano. Supplemento 9: 85–136. https://doi.org/10.1080/03749444.1977.10736845

Largen MJ (2001) The status of the genus *Phrynobatrachus* Günther 1862 in Ethiopia and Eritrea, including description of a new species (Amphibia Anura Ranidae). Tropical Zoology 14: 287–306. https://doi.org/10.1080/03946975.2001.10531158

Measey GJ, Vences M, Drewes RC, Chiari Y, Melo M, Bourles B (2007) Freshwater paths across the ocean: molecular phylogeny of the frog *Ptychadena newtoni* gives insights into amphibian colonization of oceanic islands. Journal of Biogeography 34: 7–20. https://doi.org/10.1111/j.1365-2699.2006.01589.x

Mengistu AA (2012) Amphibian diversity, distribution and conservation in the Ethiopian highlands: morphological, molecular and biogeographic investigation on *Leptopelis* and *Ptychadena* (Anura). Ph.D. thesis. https://core.ac.uk/reader/18256268

Neumann O (1902) From the Somali Coast through Southern Ethiopia to the Sudan. The Geographical Journal 20: 373–398. https://doi.org/10.2307/1775561

Onn CK, Abraham RK, Grismer JL, Grismer LL (2018) Elevational size variation and two new species of torrent frogs from Peninsular Malaysia (Anura: Ranidae: *Amolops* Cope). Zootaxa 4434: 250–264. https://doi.org/10.11646/zootaxa.4434.2.2

Perret J-L (1980) Sur quelques *Ptychadena* (Amphibia Ranidae) d'Ethiopie. Monitore Zoologico Italiano, Supplemento 13: 151–168. https://doi.org/10.1080/00269786.1980.11758552

Perret J-L (1994) Description de *Ptychadena largeni* n. sp. (Anura, Ranidae) d'Ethiopie. Bulletin de la Société Neuchâteloise des Sciences Naturelles 117: 67–77.

Poynton JC (1970) Guide to the *Ptychadena* (Amphibia: Ranidae) of the southern third of Africa. Annals of the Natal Museum 20: 365–375.

R Core Team (2020) R: A language and environment for statistical computing. R Foundation for Statistical Computing, Vienna. http://www.R-project.org/

Reyes-Velasco J, Manthey JD, Bourgeois Y, Freilich X, Boissinot S (2018) Revisiting the phylogeography, demography and taxonomy of the frog genus *Ptychadena* in the Ethiopian highlands with the use of genome-wide SNP data. PLoS ONE 13: e0190440. https://doi.org/10.1371/journal.pone.0190440

Reyes-Velasco J, Goutte S, Freilich X, Boissinot S (in review) On the use of type specimens in the age of genomics.

Smith ML, Noonan BP, Colston TJ (2017a) The role of climatic and geological events in generating diversity in Ethiopian grass frogs (genus *Ptychadena*). Royal Society Open Science 4: 170021. https://doi.org/10.1098/rsos.170021

Smith ML, Noonan BP, Colston TJ (2017b) Correction to 'The role of climatic and geological events in generating diversity in Ethiopian grass frogs (genus *Ptychadena*). Royal Society Open Science 4(10): 171389. https://doi.org/10.1098/rsos.171389

Soultan A, Wikelski M, Safi K (2020) Classifying biogeographic realms of the endemic fauna in the Afro-Arabian region. Ecology and Evolution 10: 8669–8680. https://doi.org/10.1002/ece3.6562

Sprecht R (2017) Avisoft-SASlab Pro. Avisoft Bioacoustics, Berlin. http://avisoft.com/index.html

Sueur J, Aubin T, Simonis C (2008) Seewave, a free modular tool for sound analysis and synthesis. Bioacoustics. The International Journal of Animal Sound and Its Recording 18: 213–226. https://doi.org/10.1080/09524622.2008.9753600

Vences M, Kosuch J, Rödel M-O, Lötters S, Channing A, Glaw F, Böhme W (2004) Phylogeography of *Ptychadena mascareniensis* suggests transoceanic dispersal in a widespread African-Malagasy frog lineage. Journal of Biogeography 31: 593–601. https://doi.org/10.1046/j.1365-2699.2003.01031.x

Supplementary material 1

Appendix S1

Authors: Sandra Goutte, Jacobo Reyes-Velasco, Xenia Freilich, Abeje Kassie, Stephane Boissinot

Data type: identification key

Explanation note: Key to the species of Ptychadena in the Ethiopian highlands.

Link: https://doi.org/10.3897/zookeys.1016.59699.suppl1

Supplementary material 2

Appendix S2

Authors: Sandra Goutte, Jacobo Reyes-Velasco, Xenia Freilich, Abeje Kassie, Stephane Boissinot

Data type: call identification key

Explanation note: Key to the calls of the Ptychadena neumanni species complex.

Link: https://doi.org/10.3897/zookeys.1016.59699.suppl2

Supplementary material 3

Tables 1–6

Authors: Sandra Goutte, Jacobo Reyes-Velasco, Xenia Freilich, Abeje Kassie, Stephane Boissinot

Data type: excel file

Explanation note: **Table S1.** Morphometric measurements and localities of all examined individuals. **Table S2.** GenBank accession numbers. **Table S3.** Morphometric measurements ratios (average ± standard deviation) of the Ptychadena neumanni complex. **Table S4.** Results of discriminant analyses based on linear morphometric measurements of recently sampled specimens of the P. neumanni complex. **Table S5.** Summary table presenting the results of the Tukey HSD pairwise tests based on linear morphometrics of the Ptychadena neumanni complex. **Table S6.** Taxonomic history of the Ptychadena neumanni species complex.

Link: https://doi.org/10.3897/zookeys.1016.59699.suppl3

ZooKeys 1016: 143–161 (2021)
doi: 10.3897/zookeys.1016.51866
https://zookeys.pensoft.net

RESEARCH ARTICLE

A peer-reviewed open-access journal
ZooKeys
Launched to accelerate biodiversity research

Revealing the biodiversity of Chilean birds through the COI barcode approach

Nelson Colihueque[1], Alberto Gantz[2], Margarita Parraguez[3]

1 *Laboratorio de Biología Molecular y Citogenética, Departamento de Ciencias Biológicas y Biodiversidad, Universidad de Los Lagos, Avenida Alcalde Fuchslocher 1305, Casilla 933, Osorno, Chile* **2** *Laboratorio de Ecología, Departamento de Ciencias Biológicas y Biodiversidad, Universidad de Los Lagos, Osorno, Chile* **3** *Laboratorio de Genética, Acuicultura y Biodiversidad, Universidad de Los Lagos, Osorno, Chile*

Corresponding author: Nelson Colihueque (ncolih@ulagos.cl)

Academic editor: G. Sangster | Received 9 March 2020 | Accepted 20 December 2020 | Published 11 February 2021

http://zoobank.org/CAC90F3A-268B-41B0-B8BA-AC7BAA310D09

Citation: Colihueque N, Gantz A, Parraguez M (2021) Revealing the biodiversity of Chilean birds through the COI barcode approach. In: Spence J, Casale A, Assmann T, Liebherr J, Penev L (Eds) Systematic Zoology and Biodiversity Science: A tribute to Terry Erwin (1940–2020). ZooKeys 1016: 143–161. https://doi.org/10.3897/zookeys.1016.51866

Abstract

The mitochondrial cytochrome c oxidase subunit I (COI) gene is an effective molecular tool for the estimation of genetic variation and the identification of bird species. This molecular marker is used to differentiate among Chilean bird species by analyzing barcodes for 76 species (197 individuals), comprising 28 species with no previous barcode data and 48 species with sequences retrieved from the BOLD and GenBank databases. The DNA barcodes correctly identified 94.7% of the species analyzed (72 of 76 species). Mean intraspecific K2P distance was 0.3% (range 0–8.7%). Within the intraspecific divergence range, three species, *Phrygilus gayi*, *Sephanoides sephanoides* and *Curaeus curaeus*, showed relatively high intraspecific divergence (1.5–8.7%), possibly due to the presence of a species complex or geographic isolation of subpopulations. Mean interspecific K2P distance was 24.7% (range 1.3–43.5%). Consequently, the intraspecific K2P distance showed limited overlap with interspecific K2P distance. The mean intraspecific divergence in our study was similar to that found in temperate regions of South America (0.24%). However, it was approximately one order of magnitude lower than values reported for bird species in tropical regions of northern South America (1.8–2.13%). This result suggests that bird species from Chile show low levels of genetic structure and divergence. The small overlap between intra- and inter-specific distances implies that COI barcodes could be used as an effective tool to identify nearly all the Chilean bird species analyzed.

Keywords

Aves, biodiversity, COI, genetic variation, Neotropical birds, taxonomy

Introduction

Birds are among the animal groups that have been subjected to extensive DNA barcoding. Currently, DNA barcodes are publicly available for 41% of known bird species in the world, with data for nearly 4300 species from 37 of 39 recognized avian orders (Barreira et al. 2016). The reported accuracy of species-level DNA barcoding is 93%–99% for birds, confirming its efficacy in discriminating among avian species and its potential as a tool for assigning unknown avian individuals to a species. The accuracy of this method in birds is attributable to fact that the maximum intraspecific distance is typically smaller than the minimum interspecific distance in these species. This so-called barcode gap (Meyer and Paulay 2005) means that the COI gene has the power to delineate species boundaries.

In recent years, a number of DNA barcoding studies have assessed the efficacy of using COI data to identify South American birds. Analyses of hundreds of bird species from countries in this region, such as Argentina (Kerr et al. 2009), Brazil (Chaves et al. 2015), and Ecuador and French Guiana (Milá et al. 2012), have shown that COI sequences are highly accurate for species-level identification (93–98%). Findings for birds from other geographic areas show similar levels of accuracy (Barreira et al. 2016). Moreover, these studies reveal deep intraspecific genetic divergence in Neotropical birds, likely associated with a more complex pattern of regional divergence than in the North American avifauna (Tavares et al. 2011; Milá et al. 2012). Thus, in some birds, intraspecific differences overlap with interspecies differences, especially in populations that include multiple sub-species or in samples from large geographic areas, ecoregions, or areas of endemism (Tavares et al. 2011). Therefore, the current taxonomy likely underestimates the biodiversity of the Neotropical avifauna. Given the complex genetic divergence patterns reported in this region, likely associated with a high incidence of non-monophyletic species, the general utility of DNA barcoding across different biogeographic regions of South America merits further attention.

The Chilean avifauna comprises of 443 species, if we only consider species that are residents or regular visitors (Couve et al. 2016), or those that meet the criteria of at least five records in the national territory (Martínez-Piña and González-Cifuentes 2017). These birds belong to 65 families distributed across broad altitudinal (0–6000 m) and latitudinal (18°S–56°S) gradients in various ecoregions of the country. This avifauna represents around 13% of all Neotropical bird species, estimated at 3370 species (Newton 2003). The Chilean avifauna is characterized by a fusion of South American relic elements (e.g., *Pygarrhichas* and Furnariidae) of Cenozoic origin with North American elements (e.g., members of the genus *Phrygilus*) that arose during the Pleistocene (Díaz 2005; González and Wink 2008; Álvarez-Varas et al. 2015). During this period, glacial cycles profoundly affected species distribution and gene flow patterns in populations throughout the world (Shepard and Burbrink 2009). Some studies have shown that Pleistocene climate fluctuations may have altered the distributions, sizes, and genetic structures of avian populations (Lovette 2005; van

Els et al. 2012; Lougheed et al. 2013). Most of the elements that compose the Chilean avifauna originated during the Pleistocene, due to population differentiation events that occurred in paleorefuges in the Altiplano, central Chile, Patagonian temperate forests, and other areas (Cracraft 1985; Vuilleumier 1991; Díaz 2005; Masselo et al. 2011). These geological processes, along with the geographic isolation of Chile imposed by geographic barriers such as the Andes, the Pacific Ocean, and the northern desert, resulted in depleted species richness and a high level of endemism in relation to the size of this geographic area (Kelt et al. 2016). For example, around of 2.3% of terrestrial avifauna of Chile are endemic species (Kelt et al. 2016) that are largely restricted to certain ecoregions such as the Atacama Desert, Mediterranean forests, Valdivian temperate rain forests, Patagonian steppe, and dry Puna (Jaramillo 2014). Of note is that natural selection and local adaptation mechanisms associated with this geographic isolation seem to have also played an important role in the diversification of Chilean avifauna along the Andes mountains (Campagna et al. 2011; Álvarez-Varas et al. 2015).

Little is known about the population structure and genetic diversity of the taxa that currently compose the diversity of birds in Chile (Colihueque and Gantz 2019). Recent molecular studies of Chilean birds using COI sequences have provided insight into phylogenetic, phylogeographic and taxonomic issues (Masello et al. 2011; González 2014; Álvarez-Varas et al. 2015; Colihueque et al. 2015). This molecular tool also offers the opportunity for an in-depth evaluation of the genetic differentiation within and between Chilean bird species and to test its species-level resolution for bird identification. The particular evolutionary history of Chilean birds, associated with glacial events and isolation imposed by strong geographic barriers, has likely affected the gene flow and genetic variability of many species. Therefore, this approach may provide clues that would clarify, for example, the taxonomic status of various species, divergence patterns across different ecoregions, and the speciation process in Chile. Here, we examine the pattern of barcode divergence in a significant proportion of Chilean bird species, based on new COI sequences and sequences previously published in the Barcode of Life Data Systems (BOLD) (http://www.barcodinglife.org/) and GenBank databases.

Materials and methods

Sampling

We obtained samples from across central and southern Chile, mainly from the Cachapoal (34°S) and Osorno, Ranco, and Valdivia provinces (40°–41°S). Samples corresponded to dead birds found along the highways which were collected between 2012 and 2019 by volunteers and the authors; date and site of collection (at least at province level) were recorded immediately. Collection sites were georeferenced using Google Earth based on locality names. Information about vouchers and collection sites

is available in Suppl. material 2: Table S1. The author A. Gantz, given his broad expertise in ornithology, performed the species identification according to standard diagnostic criteria based on morphology and feather coloration. Identification guides of Chilean birds (Jaramillo 2014; Couve et al. 2016) were also used to assist in the identification task. After identification, the specimens were photographed, and deposited in the bird collection of the Laboratorio de Biología Molecular y Citogenética of the Universidad de Los Lagos (ULA), Osorno, Región de Los Lagos, under identification numbers 1160ULA, 1161ULA, 1163ULA, 1164ULA, 1165ULA, 1167ULA, 1194ULA, 1195ULA, 1200ULA, 1201ULA, 1214ULA–1217ULA, 1235ULA–1237ULA, 1245ULA, 1249ULA, 1277ULA, 1278ULA, 1280ULA–1283ULA, 1295ULA, 1309ULA–1314ULA, 1316ULA, 1318ULA, 1320ULA, 1329ULA, 1332ULA–1334ULA, 1338ULA, 1339ULA, 1346ULA, 1347ULA, 1350ULA, 1354ULA, 1385ULA, 1388ULA, 1389ULA, 1391ULA, 1392ULA, 1395ULA, 1397ULA, 1400ULA, 1401ULA, 1403ULA, 1405ULA, 1460ULA, 1465ULA–1473ULA,1506ULA and 1507ULA (Suppl. material 2: Table S1). These specimens are publicly available for further investigation. A set of photographs of representative analyzed specimens is provided in Suppl. material 1. Tissue samples were taken mainly from the pectoral and femoral muscles as the size of these muscles facilitates dissection. Tissue samples were then fixed in 80% ethanol. DNA was extracted from the fixed muscle tissue using the phenol-chloroform method, as described in Taggart et al. (1992). Extracts were standardized at 100 ng/μL using Tris-EDTA buffer, pH 8.0. To obtain COI sequences of birds from Chile, we searched the BOLD Public Data Portal using the search terms [Aves Chile]. Subsequently, the recovered records were assessed for correct collection site (i.e., Collected in: Chile) and also by checking the correct geographic coordinates within Chile using Google Earth. The same verification process was used for COI sequences recovered from GenBank. The addition of these sequences enhances assessment of COI gene variability at the intraspecific and interspecific levels. Based on the location of collection sites, some species cover a wide latitudinal range across Chile. For example, *Thinocorus orbignyianus* covers a range from Tarapaca (20°S) to Santiago (33°S) (ca. 1700 km), and *Vanellus chilensis* from Santiago (33°S) to Magallanes (53°S) (ca. 2200 km). Species nomenclature follows the Clements et al. (2016) taxonomy. We analyzed 116 individuals from 42 species. In total we obtained sequences from 68 individuals of 32 species, including 28 species not previously barcoded. Lists of the newly sequenced specimens with those from BOLD and GenBank, as well as information about vouchers and collection sites, are available in Suppl. materials 2 (Table S1) and 3 (Table S2), respectively.

PCR and sequencing

The primer pairs BirdF1 (5'-TTCTCCAACCACAAAGACATTGGCAC-3') and BirdR1 (5'-ACGTGGGAGATAATTCCAAATCCTG-3'), as well as BirdF1 and BirdR2 (5'-ACTACATGTGAGATGATTCCGAATCCAG-3') (Hebert et al. 2004), were used for COI amplification. Resulting amplicons had a length of ca. 700 bp. When PCR failed, possibly due to degraded DNA, alternative M13-tailed primer

pairs were used, following Ivanova et al. (2007): FishF2_t1 (5'-GTAAAACGACGGC-CAGTCGACTAATCATAAAGATATCGGCAC-3') and FishR2_t1 (5'-CAGGAAA-CAGCTATGACACTTCAGGGTGACCGAAGAATCAGAA-3'). In addition, when FishF2_t1 and FishR2_t1 also failed the internal primer pairs AvMiF1 (5'-CCCC-CGACATAGCATTCC-3') and AvMiR1 (5'-ACTGAAGCTCCGGCATGGGC-3') in conjunction with BirdF1 and BirdR1 were used. PCR amplification was carried out in 15 µL using a reaction mix composed of 3 µL Taq polymerase buffer (1×), 2 µL of enhancer (0.7×), 0.3 µL of dNTPs (0.2 mM), 0.45 µL of $MgCl_2$ (1.5 mM), 0.3 µL of each primer (0.2 µM), 0.06 µL of Taq DNA polymerase (0.02 U/ µL) (Kapa Biosystems), 3 µL of template DNA (20 ng/µL), and 5.59 µL of DNAse/RNAse free distilled water (Gibco). Thermal cycling was performed as follows: initial denaturation at 94 °C for 2 min followed by 40 cycles of 94 °C for 45 s, annealing temperature of 52 or 58 °C, depending on the primer pairs, for 45 s, 72 °C for 45 s, and a final extension step at 72 °C for 5 min. PCR products were visualized on 2% agarose gels and cleaned prior to sequencing with an QIA quick gel extraction kit (Qiagen). PCR products were bi-directionally sequenced on an Applied Biosystems ABI377 automated sequencer. Sequence records were assembled from forward and reverse reads using GENEIOUS 4.0.2 software (Biomatters Ltd.). We checked for potential amplifications of pseudogenes (NUMTs) by translating the COI sequence into amino acid sequences using mitochondrial vertebrate genetic code. When unexpected stop codons, frameshifts, or unusual amino acidic substitutions were observed, the sequence was discarded from the analysis. All sequences were deposited in GenBank (accession numbers MG263831 to MG263870 and MN986932 to MN986959).

Data analyses

The sequences obtained were aligned and edited using GENEIOUS 4.0.2 software (Biomatters Ltd.). Base substitution saturation, a phenomenon that may decreases the amount of phylogenetic information contained in a sequence dataset, was tested based on the index of substitution saturation (ISS) (Xia et al. 2003), which assumes a critical index of substitution saturation (ISSc) that defines a threshold for significant saturation in the data. This analysis was performed using DAMBE v. 5.3.105 (Xia 2013). For all sequence comparisons, the Kimura 2-parameter distance model (K2P) (Nei and Kumar 2000) was used. This metric was chosen because its performance for species identification is equivalent to other models (Collins et al. 2012). This genetic distance was calculated using MEGA 5.05 software (Tamura et al. 2011). Pairwise sequence divergence was calculated separately for intraspecific and interspecific distances as well as for intrageneric comparisons. Mean intraspecific distances were calculated for species that were represented by at least two specimens. Intrageneric K2P genetic distances were calculated based on at least two species for a particular genus. The best-fit nucleotide substitution model was determined using jModelTest 2.1. (Darriba et al. 2012) based on Bayesian Information Criterion (BIC). The best model was then used with maximum likelihood (ML) analyses to construct a ML tree. The consistency of topolo-

gies (nodal support) was estimated using a bootstrap approach with 1000 bootstrap replications (Felsenstein 1985). Phylogenetic trees were rooted with one representative of Great Tinamu (*Tinamus major*). To include all sequences developed in this study and as many as sequences as possible from BOLD and GenBank, we used 443-bp sequence length alignments. A species was considered distinguishable by DNA barcode if: a) it was monophyletic (i.e., the species formed a single cluster) and b) it did not share a barcode with any other species.

Results

Sequences dataset and model of nucleotide substitution

Barcodes were analyzed for a total of 76 unique species (197 individuals), including 32 species sequenced in this study (68 individuals) and 48 species (129 individuals) from BOLD and GenBank (see Suppl. material 2, 3 – respectively). These sequences represent 17.2% (76/443) of known species from Chile. This dataset comprised 36 families. The COI sequences of new specimens ranged in size from 464 to 750 bp, with a mean length of 655.3 bp. The average number of sequences per species was 2.6 (range 1–17), with 43 species (56.6%) presenting between 2 and 17 sequences. After aligning the 197 sequences, a dataset of 443-pb sequence length were obtained. For this alignment, 193 variable positions and 182 parsimony-informative sites were found. Overall nucleotide frequencies were: A (24.7%), T (26.5%), C (33.3%) and G (15.4%). The best fit-model of nucleotide substitution was Hasegawa-Kishino-Yano model (HKY) with a fraction of invariable sites and gamma distribution (HKY+I+G) (BIC value = 22738.5785). No evidence of base saturation was found, since the ISS value (0.219) was significantly lower ($T = 15.4$, d.f. = 443, $P < 0.0001$) than the observed ISS.c value (0.696).

Species identification

The COI barcode correctly identified 94.7% of the species studied (72 of 76 species). That is, these 72 species had unique DNA barcodes that did not overlap with the barcodes of any other species. Interspecific K2P distance ranged from 1.3 to 43.5% (mean 24.7%). In most cases, the ML tree, as shown in Figure 1, reflected a relatively low within-species divergence as compared to between-species divergence. Most of the terminal groups included specimens of the same species in a single cluster, as expected for samples of the same species in a monophyletic group. Bootstrap values were above 80, except for *Curaeus curaeus*, *Phrygilus gayi* and *Phrygilus plebejus* (Figure 1). The phylogenetic analysis showed a close phylogenetic relationship in the *Phalacrocorax* and *Spheniscus* genera, i.e., some species clustered together within the same branch. For example, *P. atriceps* clustered together with *P. magellanicus* and *S. humboldti* grouped in the same cluster with *S. magellanicus*. In addition, these species pairs exhibited a

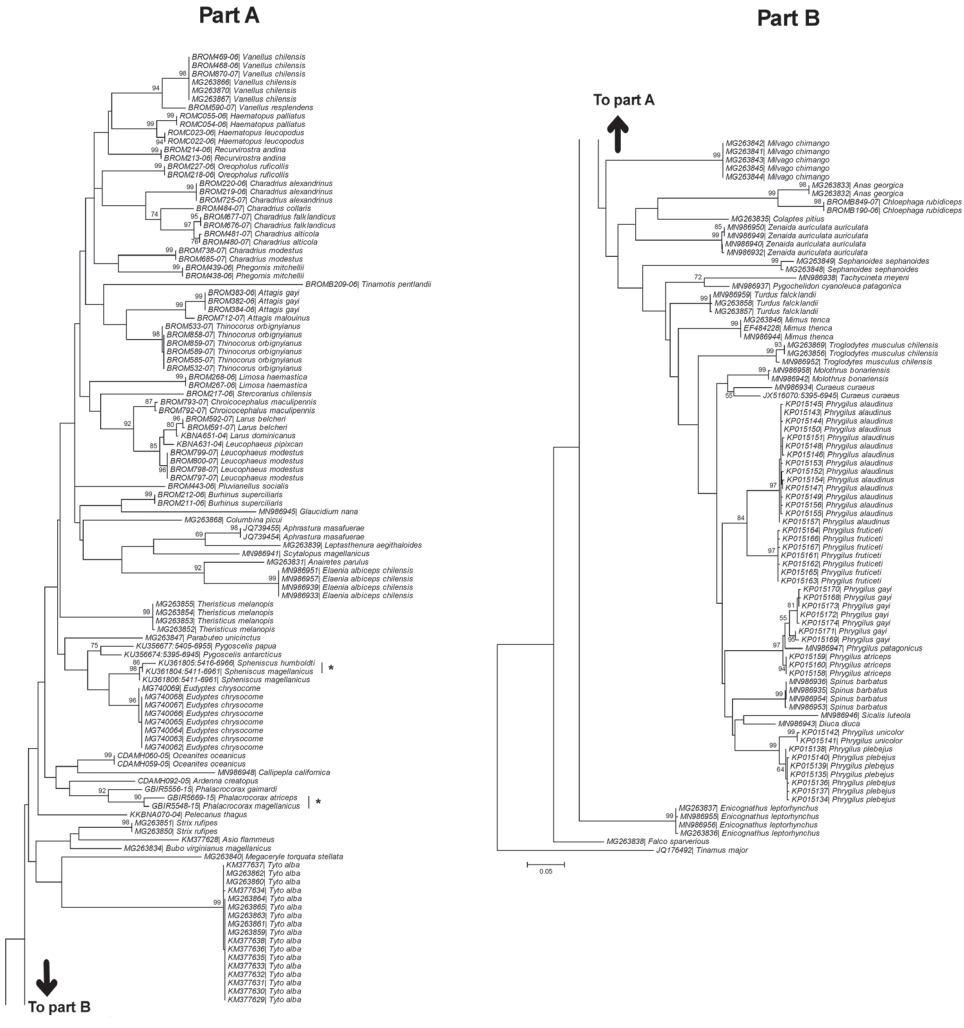

Figure 1. Maximum likelihood (ML) tree derived from the analysis of COI sequences for 76 bird species from Chile. The numbers at the nodes represent the percentage of bootstrap support. GenBank or BOLD accession number for each specimen are shown. Scale indicates the sequence divergence estimated from the number of nucleotide substitutions per site. The asterisk indicates the contradictory clusters found in the tree. *Charadrius alexandrinus* is currently known as *Charadrius nivosus*.

very similar COI barcode given that the K2P distance was relatively low (3.8% and 2.2%, respectively). These clusters were relatively well-supported (86–90% bootstrap support), we considered that this result may suggest the occurrence of reciprocal non-monophyly. However, this conclusion should be treated with caution due to the low number of COI sequences analyzed and, therefore, further analysis of additional samples will be necessary to support this result.

Table 1. Comparisons of K2P-pairwise distances at two taxonomic levels for 76 species of birds from Chile. Intraspecific distance was calculated for species which two or more sequences were available.

Taxonomic level	Number of individuals	Number of taxa	Number of comparisons	Genetic distances (%)			
				Mean	SE	Minimum	Maximum
Intraspecific	164	43	448	0.3	0.0	0.0	8.7
Interspecific	197	76	2850	24.7	0.1	1.3	43.5

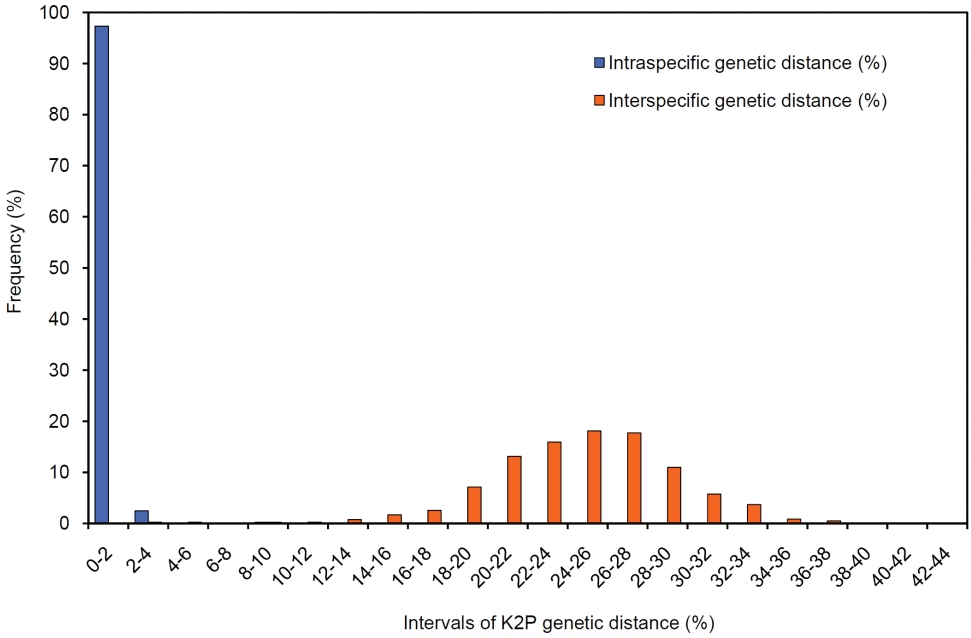

Figure 2. Histogram showing the distribution of K2P-pairwise genetic distances based on the COI gene of 76 bird species from Chile. Intraspecific distances are indicated with blue bars and interspecific distances, excluding within-species comparisons, are shown with red bars.

Intra- and interspecific divergence

The between-species differences in COI sequences were greater than the within-species differences. Mean intraspecific K2P distance was 0.3% (range 0–8.7%), while mean interspecific K2P distance was ca. two orders of magnitude larger, at 24.7% (range 1.3–43.5%) (see Table 1). Consequently, the intraspecific K2P distance showed limited overlap with interspecific K2P distance (Figure 2). In fact, only 22 of 2850 species-pair comparisons (0.77%) showed a divergence level below the maximum intraspecific K2P distance (8.7%), such as were recorded for *Larus dominicanus* and *Larus belcheri* (1.3%), *Charadrius falklandicus* and *Charadrius alticola* (2.1%), and *Phrygilus atriceps* and *Phrygilus gayi* (2.9%). Three species had a relatively high intraspecific divergence that overlapped with the minimum interspecific distance, namely, *Curaeus curaeus* (mean K2P = 8.7%), *Phrygilus gayi* (mean K2P = 1.5%) and *Sephanoides sephanoides*

Table 2. Intraspecific K2P genetic distances for 43 species of birds from Chile, calculated when two or more sequences were available. Bold face indicates species with high mean intraspecific divergence that overlapped the minimum interspecific distance (> 1.3%). ‡ Currently known as *Charadrius nivosus.*

Species or subspecies	Number of individuals	Genetic distances (%)			
		Mean	SE	Minimum	Maximum
Anas georgica	2	0.0	0.0	0.0	0.0
Aphrastura masafuerae	2	0.0	0.0	0.0	0.0
Attagis gayi	3	0.0	0.0	0.0	0.0
Burhinus supercialiaris	2	0.0	0.0	0.0	0.0
Charadrius alexandrinus‡	3	0.0	0.0	0.0	0.0
Charadrius alticola	2	0.2	0.2	0.2	0.2
Charadrius falklandicus	2	0.0	0.0	0.0	0.0
Charadrius modestus	2	0.2	0.2	0.2	0.2
Chloephaga rubidiceps	2	0.0	0.0	0.0	0.0
Chroicocephalus maculipennis	2	0.5	0.3	0.5	0.5
Curaeus curaeus	**2**	**8.7**	**1.7**	**8.7**	**8.7**
Elaenia albiceps chilensis	4	0.0	0.0	0.0	0.0
Enicognathus leptorhynchus	4	0.2	0.2	0.0	0.5
Eudyptes chrysocome	8	0.1	0.1	0.0	0.5
Haematopus leucopodus	2	0.0	0.0	0.0	0.0
Haematopus palliatus	2	0.0	0.0	0.0	0.0
Larus belcheri	2	0.2	0.2	0.2	0.2
Leucophaeus modestus	4	0.0	0.0	0.0	0.0
Limosa haemastica	2	0.0	0.0	0.0	0.0
Milvago chimango	5	0.0	0.0	0.0	0.0
Mimus thenca	3	0.0	0.0	0.0	0.0
Molothrus bonariensis	2	0.2	0.2	0.2	0.2
Oceanites oceanicus	2	0.0	0.0	0.0	0.0
Oreopholus ruficollis	2	0.0	0.0	0.0	0.0
Phegornis mitchelli	2	0.0	0.0	0.0	0.0
Phrygilus alaudinus	15	0.5	0.1	0.0	0.9
Phrygilus atriceps	3	0.0	0.0	0.0	0.0
Phrygilus fruticeti	7	0.3	0.1	0.0	0.5
Phrygilus gayi	**7**	**1.5**	**0.4**	**0.2**	**3.2**
Phrygilus plebejus	7	0.3	0.1	0.0	0.5
Phrygilus unicolor	2	0.2	0.2	0.2	0.2
Recurvirostra andina	2	0.0	0.0	0.0	0.0
Sephanoides sephanoides	**2**	**2.2**	**0.7**	**2.2**	**2.2**
Spheniscus magellanicus	2	0.5	0.3	0.5	0.5
Spinus barbatus	4	0.1	0.1	0.0	0.2
Strix rufipes	2	0.0	0.0	0.0	0.0
Theristicus melanopis	4	0.1	0.1	0.0	0.2
Thinocorus orbignyianus	6	0.1	0.1	0.00	0.2
Troglodytes musculus chilensis	3	1.1	0.4	0.0	1.7
Turdus falcklandii	3	0.3	0.2	0.2	0.5
Tyto alba	17	0.1	0.1	0.0	0.5
Vanellus chilensis	6	0.0	0.0	0.0	0.0
Zenaida auriculata auriculata	4	0.4	0.2	0.0	0.7

(mean K2P = 2.2%) (Table 2). Mean intrageneric K2P distance varied widely, from 1.3 to 16.1% (see Table 3 and Figure 3). This distance was low in *Larus* (1.3%), *Spheniscus* (2.2%), *Leucophaeus* (3.2%), *Attagis* (4.3%) and *Haematopus* (4.3%) genera, reflecting a pattern of low genetic divergence among these closely related species. The greatest intrageneric divergence levels were observed in *Charadrius* (16.1%) and *Phrygilus* (14.3%).

Table 3. Intrageneric K2P genetic distances. Genetic distances within species were excluded.

Genera	Number of taxa	Genetic distances (%)			
		Mean	SE	Minimum	Maximum
Attagis	2	4.3	0.0	4.3	4.3
Charadrius	5	16.1	1.1	1.9	24.3
Haematopus	2	4.3	0.0	4.3	4.3
Larus	2	1.3	0.1	1.2	1.4
Leucophaeus	2	3.2	0.0	3.2	3.2
Phalacrocorax	3	8.5	2.4	3.8	11.4
Phrygilus	7	14.3	0.1	2.4	19.4
Pygoscelis	2	8.4	0.0	8.4	8.4
Spheniscus	2	2.2	0.3	1.9	2.4
Vanellus	2	7.7	0.0	7.7	7.7

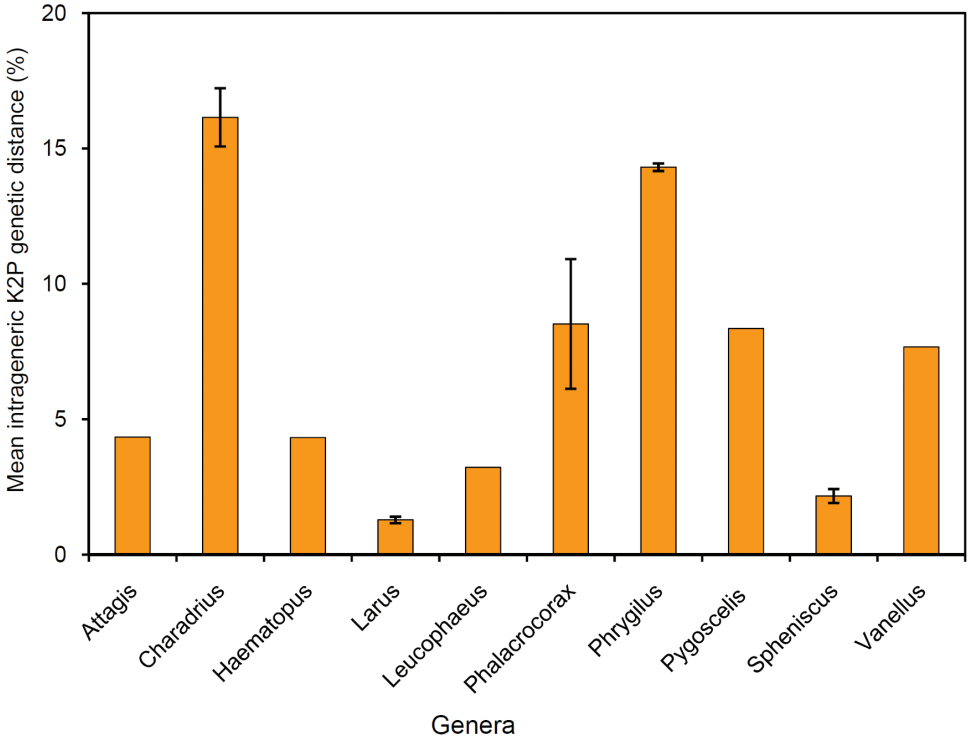

Figure 3. Mean intrageneric K2P genetic distance of ten genera of birds from Chile. Error bars represent the standard error of the mean.

Comparisons with previous studies on Neotropical birds

The mean intraspecific divergence in our study (0.3%) was ca. one order of magnitude lower than values reported for bird species in tropical regions of northern South America (1.8 and 2.13%), reported by Chaves et al. (2015) and Milá et al. (2012), respectively. The mean intraspecific divergence in our study was also approximately one-third lower than the value reported by Tavares et al. (2011) (0.9%) for birds

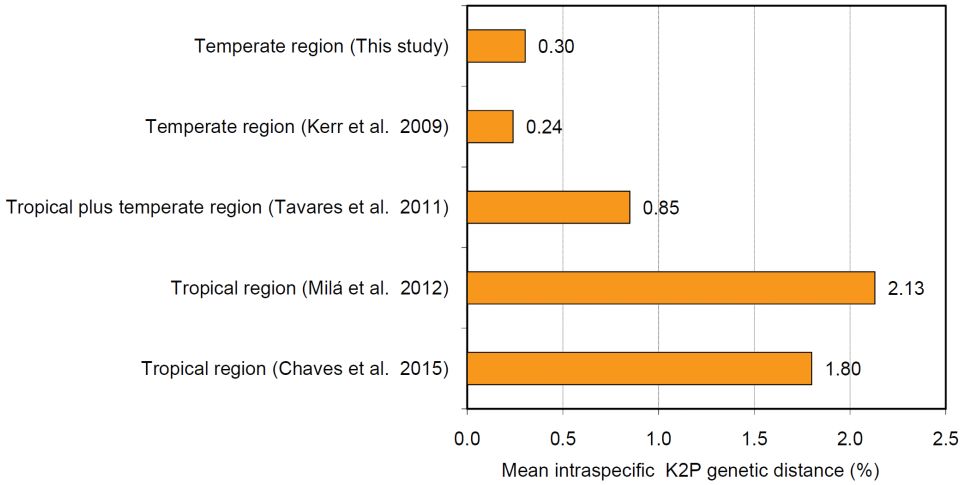

Figure 4. Histogram showing the mean intraspecific genetic distances in bird species from temperate and tropical areas of South America, reported by different research groups.

distributed throughout South America, including temperate areas of Argentina. However, as shown in Figure 4 our result was similar to the value reported for birds in temperate regions of South America, particularly from Argentina (0.24%) (Kerr et al. 2009). Moreover, our analysis revealed that only 7% of the intraspecific K2P distances exceeded 1.5% K2P, similar to reported findings for Argentine birds, in which 5.4% of species analyzed had a maximum intraspecific distance above 1.5% (Kerr et al. 2009). However, the proportion of species with intraspecific divergence above 1.5% recorded in this study was lower than that reported for birds distributed throughout South America (18.6%) (Tavares et al. 2011).

Discussion

The mean intraspecific distances recorded in this analysis of Chilean birds (0.3%, based on 43 species) are largely consistent with other reported values for birds in temperate regions of South America, particularly Argentina (0.24%) (Kerr et al. 2009). However, this value was approximately one order of magnitude lower than those found for bird species in tropical regions of northern South America, such as in Brazil (1.8%) (Chaves et al. 2015) and in Ecuador and French Guiana (2.13 %) (Milá et al. 2012). Thus, our results, along with those of Kerr et al. (2009), indicate that birds in temperate regions of South America show less intraspecific genetic variation than birds from tropical regions of the continent. As in other studies, in our case the COI sequence was highly accurate for species-level identification of birds (94.7%), due to a marked barcoding gap. This figure is consistent with previous data indicating that this mitochondrial DNA marker can typically identify 93% or more of the bird species distributed throughout the world,

including birds in South America and the northern hemisphere (Barreira et al. 2016). This level of resolution represents a good performance for a single genetic marker. Therefore, the COI sequence may provide a cost-effective tool for screening of biodiversity.

DNA barcoding studies of birds from temperate regions of South America have reported that a relatively small number of species show deep divergence. For instance, Kerr et al. (2009) reported that only 21 of 389 species from Argentina (5.4% of the species studied) showed a maximum intraspecific distance above 1.5%. On the other hand, bird species from tropical regions of South America show substantial genetic divergence. For example, Chaves et al. (2015) reported that 11.6% of Brazilian species had an intraspecific distance above 8.1%. Milá et al. (2012) observed that 75% of species from northern South America had a mean intraspecific divergence above 1%, and more than 50% of species had intraspecific lineage distances above 3%. In our case, few of the species studied (7%) showed a mean intraspecific distance higher than 1.5%. Given that divergence analyses may be affected by various factors such as incomplete or geographically restricted sampling (Meyer and Paulay 2005), further analysis is needed to corroborate our results. Nevertheless, our data are consistent with a previous report on birds from temperate regions of South America (Kerr et al. 2009), supporting the notion that bird species in these regions show low levels of genetic structure and divergence as compared to those from tropical regions. Previous COI studies of Chilean birds that focused on phylogenetic relationships also have also produced evidence of limited intraspecific divergence. For example, three species from different orders exhibited only slight intraspecific genetic divergence, such as *Cyanoliseus patagonus* (Masello et al. 2011), *Aphrastura masafuerae* (González 2014), and *Tyto alba* (Colihueque et al. 2015). Studies based on different molecular markers (ISSR markers) have found similar patterns; *Aphrastura spinicauda*, for instance, showed low levels of genetic diversity among populations distributed across the country (González and Wink 2010).

The limited numbers of bird species with deep divergence in temperate regions of South America may reflect distinct a pattern of regional biodiversity in comparison with tropical avifauna. Alternatively, as noted by Weir and Schluter (2007), the divergence pattern of birds distributed throughout the Americas may reflect a general latitudinal gradient in species diversity. Under this scenario, it would be expected that birds throughout the continent at higher latitudes (toward the poles) would tend to show lower levels of intraspecific divergence than those at lower latitudes (toward the equator). Factors involved in this divergence pattern may include different extinction and speciation rates in the two regions (Weir and Schluter 2007) and greater intraspecific genetic variation in tropical regions (Smith et al. 2017). Thus, the low level of genetic divergence recorded in our study could be related to a general pattern for birds that inhabit the temperate regions of South America. However, it should also be noted that southern South America (above 38°S) was affected by strong glaciation processes in the Quaternary (Hulton et al. 2002). The occurrence of these processes is thought to have impacted various species in southern Chile, including the avifauna (Vuilleumier 1991), by fragmenting their geographical distribution (Villagrán 1990). Therefore, the incidence of local phenomenon related to such climatic fluctuations may also be

involved. During glaciation, species survived in refuges and then recolonized sites after resolution of glacial events. As a result, genetic drift, founder effect, or selection may have modified the genetic structure of many species. In the boreal avifauna, the literature suggests that repeated Pleistocene glaciations events may have produced a rapid rate of diversification (Weir and Schluter 2004). Although little is known about the glaciation process associated with the genetic variation of the Chilean avifauna, recent studies suggest that glaciation impacted the genetic structure of specific bird species such as ovenbirds (González and Wink 2010). This notion is based on the finding that within this species, populations currently inhabiting paleorefuge sites show greater genetic variation than populations located in regions that were covered by ice sheets during the Last Glacial Maximum 21,000–14,000 years ago (González and Wink 2010). In addition, the varied genetic patterns of *Phrygilus* species are also consistent with the environmental history of southern South America, including vicariant events and climate changes (Campagna et al. 2011; Álvarez-Varas et al. 2015). Further sampling from a wider latitudinal range will be necessary to produce a more complete view of the genetic structuring and divergence pattern of the bird species analyzed in this work, especially those that include a southern or Patagonian distribution. However, the low levels of genetic variation observed in some species with Patagonian distributions, such as *Vanellus chilensis* and *Charadrius alexandrinus* (currently known as *Charadrius nivosus*) would reveal a genetic structure shaped by glaciation. This conclusion is concordant with the evolutionary history of several Patagonian bird species, whose speciation processes were closely associated with Pleistocene glaciations (Vuilleumier 1991).

A practical utility of DNA barcoding lies in the use of divergence values as a preliminary screening of taxonomic diversity, for example, to screen for within-species divergence. Future work can follow up by examining unusual cases, especially species that show deep divergence. This approach may be useful in understanding the genetic structure of *Curaeus curaeus*, *Phrygilus gayi* and *Sephanoides sephanoides*, as these two species showed the largest intraspecific distances among the species analyzed (above 1.3%). A possible interpretation of this result is that these distances reflect a species complex. In fact, the maximum likelihood tree indicated that *P. gayi* individuals formed at least 3 clusters rather than a cohesive unit, suggestive of different lineages. Álvarez-Varas et al. (2015) have also noted this type of divergence pattern in this species, characterized by genetic clusters associated with different distribution ranges among northern Chilean populations (lowlands vs. Altiplano or highlands). Deep intraspecific divergence in birds may be attributable to the dispersal capacity of the species and/or the presence of barriers to gene flow and environmental heterogeneity. In the case of *P. gayi*, the available evidence indicates that its genetic structure appears to be attributable to ecological factors and a limited dispersal capacity of this species than to geographical factors *per se*, as compared to other species of *Phrygilus* (Álvarez-Varas et al. 2015). For *S. sephanoides*, our finding contrasts with data from a phylogenetic study of the species based on a different set of molecular markers (*Cyt b* and *ND2*) (Roy et al. 1998), which reported non-significant genetic differentiation, estimated as a homogeneity of haplotypes, among north-central and Juan Fernández Islands popu-

lations. The misidentification of specimens of this species could be an explanation of for this strong genetic divergence. However, given that samples analyzed showed the typical diagnostic characteristics related to specimen size, feather coloration pattern and other features, this is unlikely. For example, both sequenced specimens show similar feather coloration (upper head and back of metallic green and whitish belly with iridescent green at flank) and body length (ca. 10 cm), which was concordant with the diagnostic criteria reported in ornithology guides of Chile (Jaramillo 2014; Couve et al. 2016). This set of characteristics yields a well-differentiated phenotype as compared to other sympatric species of hummingbirds, such as *Patagona gigas* (Jaramillo 2014). Therefore, it would be difficult to confuse this species with *S. sephanoides*. In sum, there is little doubt as to the conspecificity of the samples. Further analyses with new samples will help to confirm the marked level of divergence observed in *S. sephanoides*. However, given that the individuals analyzed were sampled from distant locations of the country (central and southern Chile, separated by a distance of ca. 800 km), it seems likely that the high level of divergence found in *S. sephanoides* may be related to isolation-by-distance.

The finding that the greatest intrageneric divergence was found in *Charadrius* (16.1%) and *Phrygilus* (14.3%) is noteworthy. In the case of the *Phrygilus* genus this divergence pattern has been interpreted in the context of a marked phylogeographic structure, which is associated with broad altitudinal and latitudinal distributions of species across the Andean mountains (Campagna et al. 2011; Álvarez-Varas et al. 2015). For instance, some species of this group, such as *P. alaudinus*, *P. atriceps* and *P. unicolor*, show a genetic differentiation mediated by allopatric mechanisms in response to specific geographic barriers. In contrast, some genera studied in this work showed low levels of genetic divergence, such as *Larus* (1.3%) and *Spheniscus* (2.2%). Although there is no genetic data for the *Larus* genus in Chile, our results are consistent with data reported for other Laridae species in the northern hemisphere, which show scarce genetic divergence. In fact, the lack of genetic differentiation within this group, reflected in a high sequence similarity (99.8%), gives rise to overlapping barcode clusters with one or more related species (Johnsen et al. 2010). In the case of *Spheniscus*, the evidence obtained in Chile indicate that this genus exhibit lower genetic divergence among species than other penguin genus (e.g., *Pygoscelis*, ca. three fold less variation), based on the analysis of complete mtDNA genomes of a small sample size (Ramos et al. 2018). Future studies in *Spheniscus* with more comprehensive sample sizes will be required to better support the interspecific genetic variation registered in this study based on COI sequence.

In conclusion, this study indicates that DNA barcoding with COI markers is highly accurate for identifying Chilean bird species, as the barcode sequence for nearly every species studied was markedly distinct from that of any other species. Our analysis identified significant interspecific divergence, roughly two orders of magnitude higher than the intraspecific values observed, reflecting a clear barcode gap. In addition, most of the species analyzed showed low intraspecific divergence. This pattern is consistent with data for birds from other temperate regions of southern South America but

contrasts with studies on birds from tropical regions of South America, which often show deep intraspecific divergence. Thus, these data reflect the existence of different evolutionary patterns associated with specific regions within the continent. We hope that this step-by-step effort focused on obtaining and assessing the DNA barcodes of the Chilean avifauna, will be useful for increasing knowledge of national biodiversity. This approach may also facilitate the establishment of a dataset of avian barcodes from Chile, enhancing the scope of local studies.

Acknowledgements

We would like to thank Soraya Sade, Oscar González, Jaime Rau, and Cristina Parraguez for providing samples. The suggestions and constructive comments of all those who helped to improve the final version of this manuscript are gratefully acknowledged, in particular the efforts of the editor and reviewers, which greatly improved the quality and clarity of the work. We dedicate this paper to the memory of Roberto Schlatter, an outstanding researcher of the birds of Chile, who passed away in October 2016.

References

Álvarez-Varas R, González-Acuña D, Vianna JA (2015) Comparative phylogeography of co-distributed *Phrygilus* species (Aves, Thraupidae) from the Central Andes. Molecular Phylogenetics and Evolution 90: 150–63. https://doi.org/10.1016/j.ympev.2015.04.009

Barreira AS, Lijtmaer DA, Tubaro PL (2016) The multiple applications of DNA barcodes in avian evolutionary studies. Genome 59: 899–911. https://doi.org/10.1139/gen-2016-0086

Cracraft J (1985) Historical biogeography and patterns of differentiation within the south american avifauna: areas of endemism. Ornithological Monograph 36: 49–84. https://doi.org/10.2307/40168278

Campagna L, Geale K, Handford P, Lijtmaer DA, Tubaro PL, Lougheed SC (2011) A molecular phylogeny of the Sierra-Finches (*Phrygilus*, Passeriformes): Extreme polyphyly in a group of Andean specialists. Molecular Phylogenetics and Evolution 61: 521–533. https://doi.org/10.1016/j.ympev.2011.07.011

Chaves BRN, Chaves A V, Nascimento ACA, et al (2015) Barcoding Neotropical birds: assessing the impact of nonmonophyly in a highly diverse group. Molecular Ecology Resources 15: 921–31. https://doi.org/10.1111/1755-0998.12344

Clements JF, Schulenberg TS, Iliff MJ, Billerman SM, Fredericks TA, Sullivan BL, Wood CL (2016) The eBird/Clements checklist of birds of the world: v2016. https://www.birds.cornell.edu/clementschecklist/download/

Colihueque N, Gantz A, Rau JR, Parraguez M (2015) Genetic divergence analysis of the Common Barn Owl *Tyto alba* (Scopoli, 1769) and the Short-eared Owl *Asio flammeus* (Pontoppidan, 1763) from southern Chile using COI sequence. ZooKeys 146: 135–46. https://doi.org/10.3897/zookeys.534.5953

Colihueque N, Gantz A (2019) Molecular genetic studies of Chilean avifauna: an overview about current progress. Neotropical Biology and Conservation 14: 459–477. https://doi.org/10.3897/neotropical.14.e48588

Collins RA, Boykin LM, Cruickshank RH, Armstrong KF (2012) Barcoding's next top model: an evaluation of nucleotide substitution models for specimen identification. Methods in Ecology and Evolution 3: 457–465. https://doi.org/10.1111/j.2041-210X.2011.00176.x

Couve E, Vidal CF, Ruiz J (2016) Aves de Chile, sus islas oceánicas y península Antártica. FS Editorial, Punta Arenas, Chile, 549 pp.

Darriba D, Taboada GL, Doallo R, Posada D (2012) jModelTest 2: more models, new heuristics and parallel computing. Nature Methods 9: e772. https://doi.org/10.1038/nmeth.2109

Díaz IA (2005) Historia natural, diversidad y conservación de las aves en bosques de la Cordillera de la Costa de la Región de Los Lagos, Chile. In: Smith-Ramírez C, Armesto JJ, Valdovinos C (Eds) Historia, biodiversidad y ecología de los bosques costeros de Chile. Editorial Universitaria, Santiago de Chile, Chile, 456–476.

Felsenstein J (1985) Confidence limits on phylogenies: an approach using the bootstrap. Evolution 39: 783–791. https://doi.org/10.1111/j.1558-5646.1985.tb00420.x

González J (2014) Phylogenetic position of the most endangered Chilean bird: the Masafuera Rayadito (*Aphrastura masafuerae*; Furnariidae). Tropical Conservation Science 7: 677–689. https://doi.org/10.1177/194008291400700407

González J, Wink M (2010) Genetic differentiation of the Thorn-tailed Rayadito *Aphrastura spinicauda* (Furnariidae: Passeriformes) revealed by ISSR profiles suggests multiple palaeorefugia and high recurrent gene flow. Ibis 152: 761–774. https://doi.org/10.1111/j.1474-919X.2010.01060.x

Hebert PDN, Stoeckle MY, Zemlak TS, Francis CM (2004) Identification of birds through DNA barcodes. PLOS Biology 2: e312. https://doi.org/10.1371/journal.pbio.0020312

Hulton NRJ, Purves RS, McCulloch RD, Sugden DE, Bentley MJ (2002) The Last Glacial Maximum and deglaciation in southern South America. Quaternary Science Reviews 21: 233–241. https://doi.org/10.1016/S0277-3791(01)00103-2

Ivanova N V, Zemlak TS, Hanner RH, Hebert PDN (2007) Universal primer cocktails for fish DNA barcoding. Molecular Ecology Notes 7: 544–548. https://doi.org/10.1111/j.1471-8286.2007.01748.x

Jaramillo A (2005) Aves de Chile (1st ed.). Lynx ediciones, Barcelona, Spain, 240 pp.

Johnsen A, Rindal E, Ericson PGP, Zuccon D, Kerr KCR, Stoeckle MY, Lifjeld JT (2010) DNA barcoding of Scandinavian birds reveals divergent lineages in trans-Atlantic species. Journal of Ornithology 151: 565–578. https://doi.org/10.1007/s10336-009-0490-3

Kelt DA, Cofré H, Cornelius C, Engilis Jr. A, Gutiérrez JR, Marquet PA, Medel R, Meserve PL, Quirici V, Samaniego H, Vásquez RA (2016) The avifauna of Bosque Fray Jorge National Park and Chile's Norte Chico. Journal of Arid Environments 126: 23–36. https://doi.org/10.1016/j.jaridenv.2015.06.018

Kerr KCR, Lijtmaer DA, Barreira AS, Hebert PDN, Tubaro PL (2009) Probing evolutionary patterns in Neotropical birds through DNA barcodes. PLoS ONE 4: e4379. https://doi.org/10.1371/journal.pone.0004379

Lougheed SC, Campagna L, Dávila JA, Tubaro PL, Lijtmaer DA, Handford P (2013) Continental phylogeography of an ecologically and morphologically diverse Neotropical songbird, *Zonotrichia capensis*. BMC Evolutionary Biology 13: e58. https://doi.org/10.1186/1471-2148-13-58

Lovette IJ (2005) Glacial cycles and the tempo of avian speciation. Trends in Ecology and Evolution 20: 57–59. https://doi.org/10.1016/j.tree.2004.11.011

Martínez-Piña D, González-Cifuentes G (2017) Aves de Chile. Guía de campo y breve historia natural. Ediciones del Naturalista, Santiago, Chile, 538 pp.

Masello JF, Quillfeldt P, Munimanda GK, Klauke N, Segelbacher G, Schaefer MH, Failla M, Cortés M, Moodley Y (2011) The high Andes, gene flow and a stable hybrid zone shape the genetic structure of a wide-ranging South American parrot. Frontiers in Zoology 8: 1–16. https://doi.org/10.1186/1742-9994-8-16

Meyer CP, Paulay G (2005) DNA Barcoding: error rates based on comprehensive sampling. PLOS Biology 3: e422. https://doi.org/10.1371/journal.pbio.0030422

Milá B, Tavares ES, Muñoz Saldaña A, Karubian J, Smith TB, Baker AJ (2012) A trans-Amazonian screening of mtDNA reveals deep intraspecific divergence in forest birds and suggests a vast underestimation of species diversity. PLoS ONE 7: e40541. https://doi.org/10.1371/journal.pone.0040541

Nei M, Kumar S (2000) Molecular evolution and phylogenetics. Oxford University Press, New York, 352 pp.

Newton I (2003) The speciation and biogeography of birds (1st ed.). Academic Press, New York, 656 pp.

Ramos B, González-Acuña D, Loyola DE, Johnson WE, Parker PG, Massaro M, Dantas GPM, Miranda MD, Vianna JA (2018) Landscape genomics: natural selection drives the evolution of mitogenome in penguins. BMC Genomics 19: e53. https://doi.org/10.1186/s12864-017-4424-9

Roy MS, Carlos J, Hertel F (1998) Evolution and history of hummingbirds (Aves: Trochilidae) from the Juan Fernandez Islands, Chile. Ibis 140: 265–273. https://doi.org/10.1111/j.1474-919X.1998.tb04388.x

Shepard DB, Burbrink FT (2009) Phylogeographic and demographic effects of Pleistocene climatic fluctuations in a montane salamander, *Plethodon fourchensis*. Molecular Ecology 18: 2243–2262. https://doi.org/10.1111/j.1365-294X.2009.04164.x

Smith BT, Seeholzer GF, Harvey MG, Cuervo AM, Brumfield RT (2017) A latitudinal phylogeographic diversity gradient in birds. PLOS Biology 15: e2001073. https://doi.org/10.1371/journal.pbio.2001073

Taggart JB, Hynes RA, Prodohl PA, Ferguson A (1992) A simplified protocol for routine total DNA isolation from salmonid fishes. Journal of Fish Biology 40: 963–965. https://doi.org/10.1111/j.1095-8649.1992.tb02641.x

Tamura K, Peterson D, Peterson N, Stecher G, Nei M, Kumar S (2011) MEGA5: Molecular evolutionary genetics analysis using maximum likelihood, evolutionary distance, and maximum parsimony methods. Molecular Biology and Evolution 28: 2731–2739. https://doi.org/10.1093/molbev/msr121

Tavares ES, Gonçalves P, Miyaki CY, Baker AJ (2011) DNA barcode detects high genetic structure within Neotropical bird species. PLoS ONE 6: e28543. https://doi.org/10.1371/journal.pone.0028543

Van Els P, Cicero C, Klicka J (2012) High latitudes and high genetic diversity: Phylogeography of a widespread boreal bird, the gray jay (*Perisoreus canadensis*). Molecular Phylogenetics and Evolution 63: 456–465. https://doi.org/10.1016/j.ympev.2012.01.019

Villagrán C (1990) Glacial climates and their effects on the history of the vegetation of Chile: A synthesis based on palynological evidence from Isla de Chiloé. Review of Palaeobotany and Palynology 65: 17–24. https://doi.org/10.1016/0034-6667(90)90052-K

Vuilleumier F (1991) A quantitative survey of speciation phenomena in Patagonian birds. Ornitología Neotropical 2: 5–28.

Weir JT, Schluter D (2004) Ice sheets promote speciation in boreal birds. Proceedings of the Royal Society London B 271: 1881–1887. https://doi.org/10.1098/rspb.2004.2803

Weir JT, Schluter D (2007) The latitudinal gradient in recent speciation and extinction rates of birds and mammals. Science 315: 1574–1576. https://doi.org/10.1126/science.1135590

Xia X, Xie Z, Salemi M, Chen L, Wang Y (2003) An index of substitution saturation and its application. Molecular Phylogenetics and Evolution 26: 1–7. https://doi.org/10.1016/S1055-7903(02)00326-3

Xia X (2013) DAMBE5: A comprehensive software package for data analysis in molecular biology and evolution. Molecular Biology and Evolution 30: 1720–1728. https://doi.org/10.1093/molbev/mst064

Supplementary material 1

Figure S1. Photographs of external morphology of bird specimens collected from Chile, with lateral, dorsal, or ventral views of specimens showing plumage color and overall appearance.

Authors: Nelson Colihueque, Alberto Gantz, Margarita Parraguez

Data type: image

Explanation note: Data on specimen voucher number with size bar to estimate specimen size are provided.

Link: https://doi.org/10.3897/zookeys.1016.51866.suppl1

Supplementary material 2

Tables S1

Authors: Nelson Colihueque, Alberto Gantz, Margarita Parraguez

Data type: molecular data

Explanation note: **Table S1.** List of Chilean birds sequenced in this study for the COI marker, with voucher numbers, collection localities, and with BOLD and GenBank accession numbers. For all specimens, tissue samples from muscle were taken.

Link: https://doi.org/10.3897/zookeys.1016.51866.suppl2

Supplementary material 3

Tables S2

Authors: Nelson Colihueque, Alberto Gantz, Margarita Parraguez

Data type: molecular data

Explanation note: **Table S2.** List of Chilean bird COI sequences obtained from BOLD and GenBank databases, with voucher numbers and collection localities.

Link: https://doi.org/10.3897/zookeys.1016.51866.suppl3